

On the Structure and Dissolution Properties of
Poly(p-phenylene terephthalamide)
Effect of Solvent Composition

aan: Suzanne, Charlotte en Helene

**On the Structure and Dissolution Properties of
Poly(p-phenylene terephthalamide)
Effect of Solvent Composition**

Proefschrift

ter verkrijging van de graad van doctor
aan de Technische Universiteit Delft,
op gezag van de Rector Magnificus prof. dr .ir. J.T.Fokkema,
voorzitter van het College voor Promoties
in het openbaar te verdedigen op vrijdag 11 december 2009 om 12:30 uur

door

Hendrik Pieter WESTERHOF
ingenieur chemische technologie
geboren te Hilversum

Dit proefschrift is goedgekeurd door de promotor:

Prof. dr. S.J. Picken

Samenstelling promotiecommissie:

Rector Magnificus, voorzitter

Prof. dr. S.J. Picken, Technische Universiteit Delft, promotor

Prof. dr. ir. S. van der Zwaag, Technische Universiteit Delft

Prof. dr. E.J.R. Sudhölter, Technische Universiteit Delft

Prof. dr. P.J. Lemstra, Technische Universiteit Eindhoven

Prof. dr. S. Rastogi, Loughborough University

Dr. ing. G.J.M. Koper, Technische Universiteit Delft

Dr. H.C. Zegers, Teijin Aramid

ISBN/EAN 978-94-901-2281-2

Copyright © 2009 by H.P. Westerhof

Printed at Gildeprint drukkerijen, Enschede, The Netherlands.

Contents

Preface	vii
Abstract	x
1 Introduction on Polyaramids	1
1.1 Structure of high performance materials	1
1.2 Processing of polyaramids	7
1.3 Thesis outline	14
2 Theory on the Structure of Polyaramid Solutions	17
2.1 Introduction	17
2.2 Interaction mechanisms	18
2.2.1 Interactions between amides and salts	18
2.2.2 Interactions between polyamides and salts	22
2.2.3 Conclusions	31
2.3 Theories on Liquid Crystalline behaviour	32
2.3.1 Order parameter	32
2.3.2 Maier-Saupe model	36
2.3.3 Onsager model	38
2.4 Structure formation of PpPTA in NMP-CaCl ₂	41
3 Structure, Stability and Kinetics of PpPTA Solutions	43
3.1 Introduction	43
3.2 Solvent and solution preparation	44
3.3 Meta-stability of the PpPTA-NMP-CaCl ₂ solution	44
3.3.1 Phase separation / Aggregate formation	45
3.3.2 Isotropic-Nematic transition	50
3.4 The NMP-CaCl ₂ solvent system	55
3.4.1 Phase diagram of NMP-CaCl ₂	55
3.4.2 NMR on NMP-salt solutions	57
3.4.3 NMR with addition of benzanilide	64
3.4.4 Electrical conductivity of NMP-CaCl ₂ (-PpPTA)	71

3.5	Phase behaviour and structure in NMP-CaCl ₂ -PpPTA	79
3.5.1	Phase behaviour of NMP-CaCl ₂ -PpPTA	80
3.5.2	X-Ray diffraction	82
3.5.3	Structural picture	84
3.6	Conclusions	86
4	Thermodynamics of Polyaramid Solutions	89
4.1	Introduction	89
4.2	The NMP-CaCl ₂ (-benzanilide) system	92
4.2.1	Calorimetric experiments	92
4.2.2	Chemical potentials	93
4.2.3	Free enthalpy of fusion of PpPTA	103
4.3	NMP-salt(-benzanilide) combinations	108
4.4	Group contributions	112
4.4.1	Interchange terms between NMP, LiCl and PpPTA . . .	117
4.5	Group contributions of other salts	120
4.6	Alternative amide-salt(-benzanilide) systems	121
4.7	Effect of immersion of PpPTA in amide salt solvents	123
4.7.1	Immersion of PpPTA in amide and NMP-salt solvents .	123
4.7.2	Immersion of PpPTA in NMF-LiCl and NEF-LiCl . . .	127
4.7.3	Immersion of isomers of PpPTA	129
4.8	The PpPTA-H ₂ SO ₄ -CaF ₂ system	132
4.9	Conclusions	135
5	Modeling of the NMP-Polyaramid System	139
5.1	Introduction	139
5.2	Methods	140
5.2.1	COSMO	140
5.2.2	Molecular dynamics	142
5.2.3	Quantum mechanics	143
5.3	PpPTA in NMP-CaCl ₂	144
5.3.1	Solubility of CaCl ₂ in NMP	147
5.3.2	Molecular dynamics of NMP-CaCl ₂	155
5.3.3	Solubility of PpPTA in NMP-CaCl ₂	158
5.3.4	Molecular dynamics of PpPTA in NMP-CaCl ₂	161
5.4	PpPTA in other solvents	168
5.4.1	PpPTA in NMP-LiCl	168
5.4.2	PpPTA in NMP-HCl	172
5.5	Conclusions	174

6	Modeling of the H₂SO₄-Polyaramid System	179
6.1	Introduction	179
6.2	Protonation of PpPTA	180
6.2.1	Resonance structures	180
6.2.2	Quantum chemistry	181
6.2.3	Crystallographic data	182
6.3	Electrical conductivity measurements in sulphuric acid	183
6.4	Energy effect of proton transfer	192
6.5	Interactions in aromatic amide-H ₂ SO ₄ -H ₂ O systems	194
6.6	Structure of PpPTA dissolved in sulphuric acid	196
6.6.1	Interaction between HCl and aromatic amides	197
6.7	Conclusions	199
7	Hairpin Formation	201
7.1	Introduction	201
7.2	Simulations of hairpin configurations in PpPTA chains	202
7.3	Energy aspects of the observed hairpin structures	204
7.4	Oscillation rheometry measurements	207
7.5	Conclusions	208
8	Concluding Remarks	211
	References	217
A	Thermodynamics of Liquid Mixtures	227
A.1	Binary mixtures	234

Preface

The history of Poly-para-phenylene-terephthalamide (PpPTA), commercially well known under the trade names Twaron[®] and Kevlar[®] is a turbulent one. Its discovery in 1971 in the laboratories of DuPont led to one of the most severe battles between two chemical companies. DuPont, having discovered PpPTA, understood the potential spectacular mechanical properties of fibers made from this polymer, due to its stiff nature (indicated as a rigid rod polymer). Due to this rigidity the strength of a fiber made out of this polymer is five times stronger than steel on weight basis. DuPont therefore developed a production process to manufacture such fibers. As the polymers exhibit a rigid nature they are very hard to process. It can not be melt processed due to degradation. In order to process PpPTA it needs to be dissolved in a suitable solvent. The only appropriate solvents were found to be strong acids and the fiber today is commercially spun out of 100% sulphuric acid.

Before the polymer can be dissolved however, it has to be manufactured and polymerization is not possible in strong acids. DuPont at the time used hexa-methyl-phosphore-triamide (HMPT) as a polymerization medium. This was found to be a carcinogenic substance and its use was forbidden in commercial processing.

In the Akzo Nobel laboratories an alternative polymerization medium, a mixture of N-methyl-pyrrolidone and calcium chloride (NMP-CaCl₂) was found to be suitable for polymerization purposes as well. This situation, one company having the polymer and the other the route to process it, were the ingredients for a harsh clash. Both companies claimed the right to manufacture it. After a long time in court a settlement was reached and both companies were granted the right to manufacture PpPTA fibers. For years the market for PpPTA fibers was shared roughly 50%-50%. Just recently new manufacturers are starting commercial production.

Until today the polymerization is performed in NMP-CaCl₂ and the fiber spinning is done from a sulphuric acid solution, as no good fibers can be spun from a NMP-CaCl₂ solution directly. PpPTA fibers are used in many products e.g. reinforcement in cables, tires, bullet proof applications, composites, as pulp in print boards and brake pads and many more.

In the year 2000 Akzo Nobel sold the PpPTA business to the Japanese company Teijin. Here research showed that under specific conditions it is possible to manufacture PpPTA pulp (not continuous fibers) directly from a NMP-CaCl₂ solution. Commercially this is attractive as dissolution in sulphuric acid is no longer required. Remarkable behaviour of this new solution was observed and not well understood. One of the observations was that

NMP-CaCl₂ does not form a stable solution with PpPTA. This raised the question whether adjustments to the polymerization medium might improve the solubility and thereby increase polymer concentration. Would it be possible to develop a true solvent system in which not only polymerization but also fiber spinning can be done. This was the incentive for a thorough investigation to the characteristics of the NMP-CaCl₂ system and its interactions with PpPTA. In this thesis this research is presented.

Potential new solvent systems have been identified and tested to some extent. Development of a one step process however requires many more hurdles to be overcome besides the dissolution behaviour of PpPTA alone. Many technical challenges are faced. Also economical and safety facts have to be considered before deciding on commercial production. In this thesis these issues will not be addressed, it is limited to the dissolution behaviour of PpPTA. The road to a polymerization medium suitable for fiber spinning is long and difficult, due to subtle interaction balances required to keep the polymer in solution. The result of this work can be used as the starting point from which further development can be realized and offers a possible development strategy for a more optimal process medium for PpPTA.

During the years that I did my research, I have worked closely with many people and I thank them all. I would not have been able to write this thesis without them. Many measurements were key in understanding the meta-stable behaviour of PpPTA in NMP-CaCl₂. I thank the people from the analytical department of Teijin Aramid for their contributions. My supervisor, Stephen Picken who contributed not only in guiding the process but also advised on the structure of this thesis. Bert Gebben and Hanneke Boerstael have contributed in many ways and always made sure that the necessary research could be done. I am grateful to them. In the final stages the "reading committee" devoted much time on the readability of this work and I thank them for their efforts.

Special thanks goes to three people. Peter Hoogerheide who is an experimental wizard. From calorimetry to rheology and from polymerization to electrical conductivity and microscopy. Whenever something needed to be arranged, he was the man for the job. We have had many fruitful ideas from discussing experimental results. Peter, thank you.

Paul Verwer, also a wizard, but in the field of computer modeling. All the beautiful molecular graphics to be presented are based on his work. The results gave us insight into the nature of the interactions between PpPTA and its environment. This resulted in experimental set ups for verification and understanding of other experimental outcomes. Paul I thank you for the discussions we had, not only on modeling but your keen eye on how processes run in an organization is inspiring.

Last but certainly not least I thank Rik Zegers. An expert in the field of thermodynamics, a true scientist and a very pleasurable person. The many, many discussions we had were both inspiring as well as educational for me. Whenever I had a question I could walk up to you and discuss the matter with you over coffee. The results from the calorimetric experiments form the heart of this work. Rik I thank you for your dedication to this subject.

Abstract

Poly-p-phenyleneterephthalamide (PpPTA) is a so called high performance semi flexible polymer. Commercially it is mainly sold in the form of fibers under the trade names Twaron[©] and Kevlar[©].

Semi flexible denotes, in contrast to fully flexible, the polymer chain to exhibit rigid behaviour over some length of the chain extending a monomeric unit. The rigidity of the chain in case of PpPTA is due to the presence of phenyl units in the backbone of the polymer and the limited rotation around the amide unit due to partly double bond character. Moreover, the amide units connecting the phenyl units are capable of hydrogen bond formation between adjacent chains.

Due to these phenomena PpPTA-fibers exhibit extraordinary mechanical properties. Together with good abrasion and heat resistance this explains its application success in the fields of ballistics, high strength cables, heat- and cut protecting clothes, matrix reinforcements and many more.

In the figure the molecular structure of the repeat unit of PpPTA is shown.

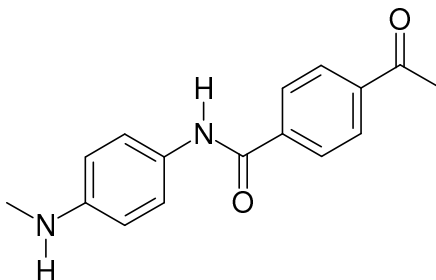


Figure 1: *Structure of PpPTA, the alternation of phenyl rings and amide units is responsible for the excellent mechanical properties.*

Commercially Twaron[©] is produced in a two step process. First a polymerization step is performed in an amide-salt solvent, N-methylpyrrolidone (NMP)-CaCl₂. The polymer is subsequently extracted from this mixture and in a second step dissolved in a strong acid (100% sulphuric acid). From the acid solution fibers can be spun showing these excellent properties.

The purifying of the polymer from the amide-salt solvent and subsequent dissolution in sulphuric acid is tedious and requires many process steps involving corrosion resistant equipment, making it an expensive process. It would therefore be very attractive, economically and technically, if it would be possible to manufacture fibers directly from a polymerization medium. In the current process this is not an option as direct fiber spinning from the polymerization medium (NMP-CaCl₂) results in fibers with very poor mechanical

properties (typical tenacity 0.5 N/tex and tensile modulus 30 N/tex) compared to spinning from sulphuric acid (typical tenacity 2.5 N/tex and tensile modulus 80 N/tex). Direct polymerization from an acid medium is not possible due to protonation of the diamine monomer causing it to become inert to polymerization. This justifies a search for such a one step process.

This thesis provides a basis for the development of such a one step process and is focused on the dissolution behaviour and structure of PpPTA in solvent mixtures. Insight in these phenomena is essential to the potential development of a one step process.

First the dissolution behaviour of PpPTA in amide-salt systems was studied in detail. The currently used polymerization system (NMP-CaCl₂) was found not to be a true solvent. Leading to interesting structures with PpPTA the mixture eventually phase separates. Due to complex formation between salt and amide the maximum PpPTA concentration possible is limited compared to a solution in sulphuric acid. Other amide-salt combinations might be able to possess more polymer and remain processable, or even dissolve PpPTA in the thermodynamic sense and thereby act as a true solvent. Various amide-salt systems were studied aiming to identify which parameters determine the solubility of PpPTA.

The heat effects, occurring due to interactions between different components upon mixing them, were measured. The components were discriminated up to molecular groups of the solvents. The heats of interaction between various amides and several salts were investigated. These heats served as the input for a thermodynamic model to calculate the chemical potentials of the components in the mixture. The lower the chemical potentials of the mixture the better the solvent power. If the solvent power is large enough to overcome the free enthalpy of fusion of PpPTA, a real dissolution would be possible resulting in the individual polymer molecules becoming homogeneously dispersed in the mixture. NMP-CaCl₂ mixtures do not have enough dissolution power to overcome the free enthalpy of fusion of PpPTA and are therefore thermodynamically not stable, however other mixtures will be seen to be able to overcome this free enthalpy of fusion.

Salts were found to be essential during polymerization in order to gain high molecular weight polymer. They show strong interactions with PpPTA and thus greatly enhance the dissolving power. The interaction strength between polymer and salt depends on the specific salt. A large interaction seems beneficial in order to optimize dissolution properties. Strong interaction with the polymer though, may also result in strong interaction with the amide solvent and cause complexation. The optimum therefore needs to be found in balancing interaction strength and maximizing salt solubility, hence preventing

complexation. Charge will be seen to perform a key role in keeping PpPTA dissolved. Due to the strong ability to form hydrogen bonds between polymer chains, repulsive charges are the only forces strong enough to keep them apart and prevent them from crystallization. In the case of strong acids protonation provides the charge on the chains, in non-acidic solvents however salts are needed to provide charged chains.

Computer modeling is used to gain insight on the interactions on a molecular level. The mechanism by which salts perform their task is made visible. It becomes clear that mainly anions interact favourably with the polymer. Water needs to be avoided as much as possible as it binds with the salt and consequently distracts salt from the amide mixture preventing it to perform its task in interacting with the polymer.

Finally, the formation of "hairpin" structures in PpPTA chains were investigated. The chains will be seen to be able to fold back on themselves at relative low energy cost. These hairpins give rise to network formation in a solution and causes the term rigid rod not to be taken too literally.

1. Introduction on Polyaramids

In this chapter some introductory remarks on aromatic polyamides are given. The chemical structure of some common polyaramids as well as other so called rigid rod polymers is presented and their characteristic anisotropic behaviour in solution is discussed. The polymerization and processing of a few polymers is given to illustrate the manufacturing of fibers out of these polymers. At the end an outline of the coming chapters is presented.

1.1 Structure of high performance materials

Polyaramids are among the most important synthetic polymers in the class of high performance materials. They offer excellent physical and chemical properties, thermal stability, flame resistance and superior mechanical properties. Although high performance can be defined in many ways the term is widely used to point out the mechanical properties. These are often characterized by two important characteristics, tenacity and tensile modulus. In figure 1.1 these properties are presented for several commercial available high performance materials, synthetic polymers, E-glass and steel. They are expressed in units of N/tex (tex is a unit of linear density in g/km and is widely used within the fiber community) to compensate for density differences. Due to the anisotropic behaviour of most of the materials the given properties are those measured in the fiber direction. As can be readily seen, the polyaramids (Twaron[®]/Kevlar[®]) and co-polymer Technora[®], polyethylene (UHMWPE) and carbon composites are by far superior to steel and E-glass. This is mainly due to their lower density, which makes these materials excellent for weight saving applications.

Polyamides in general are characterized by the amide group present as the repeating end group as defined by Hill et al. [1]. The amide unit is depicted in figure 1.2.

For aromatic polyamides the nitrogen and carbonyl of each amide unit are directly attached to a carbon atom of an aromatic ring. The resulting

molecule is known as a polyaramid. Many polyaramids have been synthesized in the past. A nice overview is given in the book of Yang [2]. Today the most well known commercially available aromatic amides are the para-aramid *poly(p-phenyleneterephthalamide)* or PpPTA, a homopolymer from *p*-phenylenediamine (PPD) and terephthaloyldichloride (TDC) and the meta-aramid *poly(m-phenyleneisophthalamide)* or PmPTA, a homopolymer from *m*-phenylenediamine (MPD) and terephthaloyldichloride (TDC). The main producers of these aromatic amides are Teijin Co. who sells the para- and meta-aramid respectively under the names of Twaron[®] and Conex[®] and DuPont who sells them respectively under the names of Kevlar[®] and Nomex[®].

Also copolymers of polyaramids are well known and commercially available like *poly(p-phenylene-3,4'-oxydiphenyleneterephthalamide)* to which the monomer 3,4'-diaminodiphenylether (DAPE) is added and sold under the trade name Technora[®] from Teijin Co. Another one to which the monomer diamino-*p*-phenylenebenzamidazole (DAPBI) is added, *poly(n-amidobezamidazole)*, is commercially known as SVM[®] in the case of a

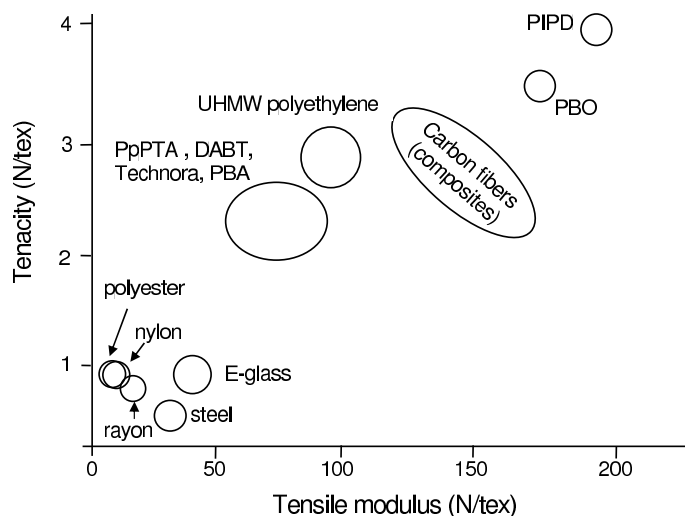


Figure 1.1: Comparison of tenacity and tensile modulus of some high performance materials.

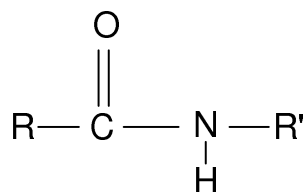


Figure 1.2: The amide repeat unit in polyaramides.

homopolymer and as Armos[©] or Rusar[©] in the case of a random copolymer. The molecular formulas of some polyaramids and co-polymers are given in figure 1.3.

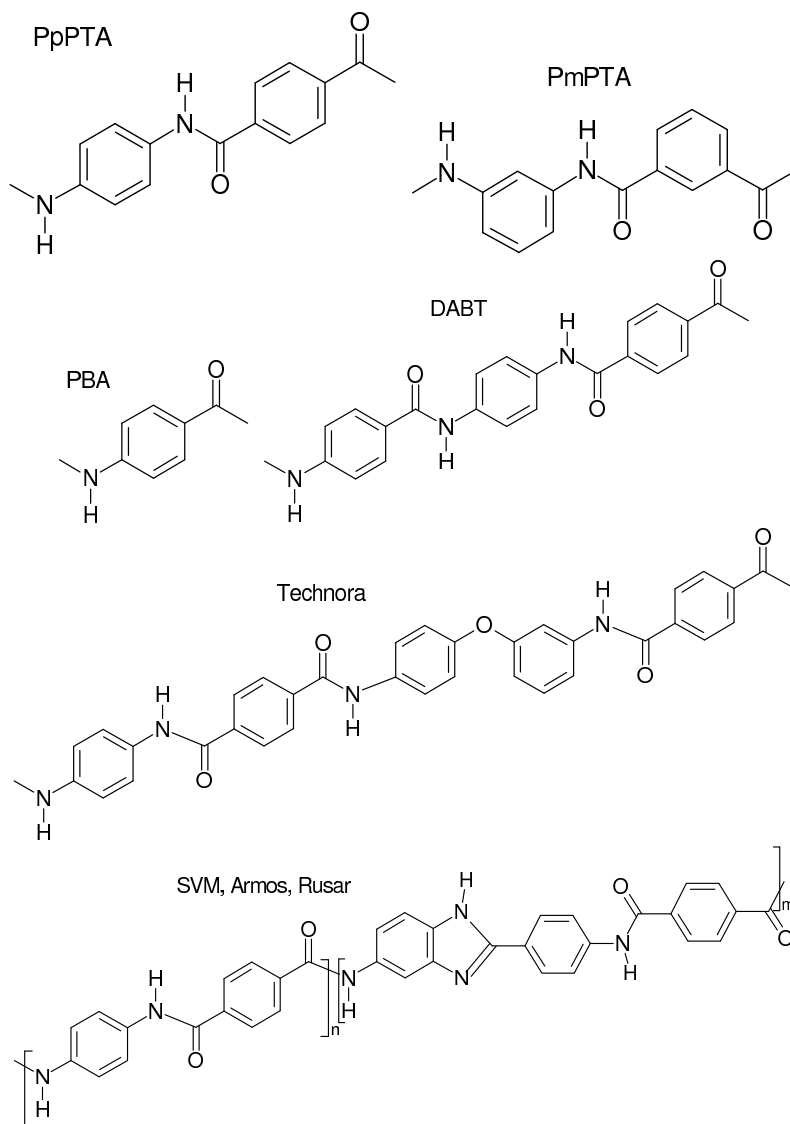


Figure 1.3: Repeat units of some aromatic amides, poly(*p*-phenyleneterephthalamide) (PpPTA), poly(*p*-benzamide), poly(4,4'-diaminobenzanilideterephthalamide) (DABT), poly(*m*-phenyleneisophthalamide) (PmPTA), poly(*p*-phenylene-3,4'-oxydiphenylene terephthalamide) (Technora) and poly(*n*-amidobezamidazole) (SVM, Armos, Rusar).

Besides aromatic amides other molecular structures are known to produce even better mechanical properties such as PBO (Zylon[©]) produced by Toyobo

Co. and PIPD, see figure 1.4. These polymers are even more rigid than polyaramids as they contain ring structures, making them less flexible and possess limited rotation.

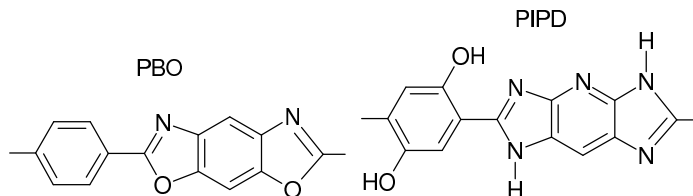


Figure 1.4: Repeat units of poly(*p*-phenylenebenzobisoxazole) (PBO) and poly(pyridobisimidazole) (PIPD).

The polymers existing out of the mentioned repeat units are semi flexible polymers. Due to the presence of phenyl rings their backbones are relatively stiff, resulting in rigid structures with large persistence lengths.

The persistence length is the length over which the polymer can be thought of to be linear and act as a rigid rod. Typical polymers of PpPTA have a molecular weight (M_w) of 30000 g/mol and thus contain in the order of 125 repeat units (two amide units; originating from the monomers TDC and PPD), which results in a contour length of about 1600 Å. In the case of PpPTA the persistence length is determined to be in the range of 175 Å given by Benoit et al. [3] and Arpin et al. [4] up to 240 Å found by Schaeffgen et al. [5], and even higher values (430 Å) were published by Cotts et al. [6]. This large variation is partly due to the limited data, relatively small molecular weight ranges covered and the difficulties in determining molecular weight and radius of gyration by light scattering.

Another approach was used by Ying et al. [7]. They used a method based on the theory of Nagai [8] in which a so called anisotropy factor is determined, which is very sensitive to the persistence length. The anisotropy factor is a type of order parameter based on the polarizabilities along the contour length of the polymer and perpendicular to contour length and is determined by light scattering measurements. They reported a value of 287 Å. In all cases it exceeds the length of the repeat unit, which is ~ 12.9 Å.¹

¹Polymers with extended persistence length are often referred to as rigid rod polymers. This suggests that the physics of these polymers can be addressed using true rods as a basis. The physics of rigid rod behaviour has been described by Doi and Edwards [9]. This description however only holds for limited molecular weight polymer, in the limit of the persistence length. For the superior mechanical properties ascribed to these polymers, molecular weights well above the persistence length are needed and so their physical behaviour deviates significantly from true rigid rod theory and adjustments are necessary like e.g. the Kratky-Porod model [10].

Due to the stiffness of these polymers they show orientational order above a critical concentration. This can be thought of as the aligning of molecules along a common director. This orientational ordering along a common director is expressed in an order parameter, which will be introduced in the next chapter. The resulting ordered phase is an intermediate state between an isotropic liquid and a pure crystal state, known as the nematic phase. In figure 1.5 this is visualized. In this picture the liquid crystalline phase is a nematic phase, meaning there is orientational order in one dimension along a director (\bar{n}).

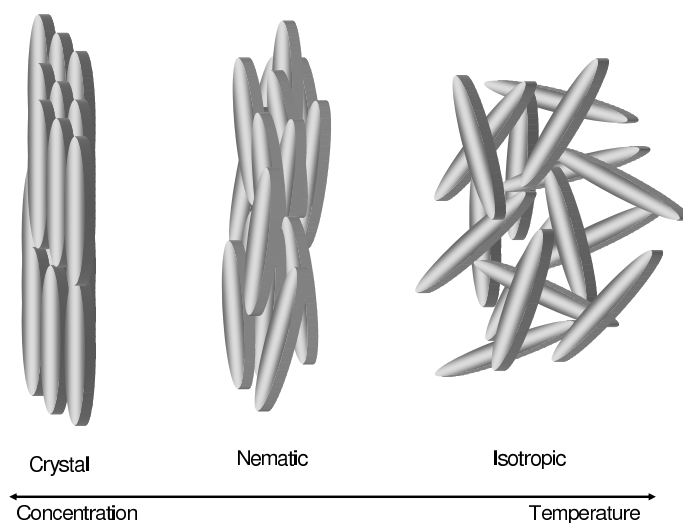


Figure 1.5: *Nematic behaviour due to alignment of the molecules along a common director.*

There are many different ordered phases possible for various rigid polymer systems, depending on their shape and aspect ratio. Picken [11] has determined the orientational order for PpPTA dissolved in sulphuric acid and shows a nematic phase under specific conditions. The isotropic to nematic transition can be seen under the microscope between crossed polarizers by the appearance of birefringent behaviour. In figure 1.6 microscopic images are shown of sulphuric acid (100%) in which different amounts of PpPTA have been dissolved of equal molecular weight. A transition takes place at 8 wt% PpPTA. This transition also has a huge effect on the shear viscosity behaviour. Above the critical concentration it drops dramatically, caused by the aligning of the polymer molecules in a common direction, resulting in a more efficient stacking of these molecules and hence lowering the shear viscosity in the direction of the polymer molecules. Only after further increase of the polymer concentration the viscosity rises again. This effect is depicted in figure 1.7.

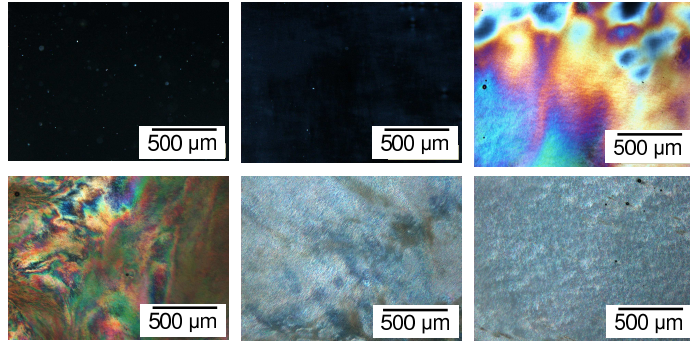


Figure 1.6: Microscopy images between crossed polarizers of solutions of PpPTA ($M_w=30000$ g/mol) in 99.8 wt% sulphuric acid from left to right 4, 6 and 8 wt% (top) 10, 12 and 14 wt% (bottom) at 25°C. Above 8 wt% PpPTA the solutions show birefringence, characteristic for anisotropic behaviour.

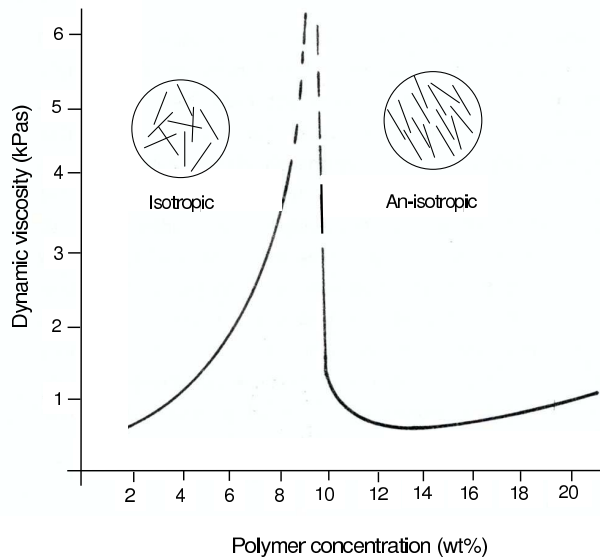


Figure 1.7: Dynamic viscosity of PpPTA in sulphuric acid as a function of its concentration at 88°C, around 8 wt% a sharp drop is observed due to the isotropic-nematic transition.

1.2 Processing of polyaramids

PpPTA

Today in commercial production, the manufacturing of PpPTA fiber is a two step process. In the first step PpPTA is polymerized. This is done in a non-acidic, amide salt solvent, N-methyl-pyrrolidone (NMP)-CaCl₂. Addition of CaCl₂ is necessary to prevent precipitation of the polymer early in the reaction, (the role of salt will be discussed in detail). The reaction itself is a condensation reaction of terephthaloyl chloride (TDC) and p-phenylene diamine (PPD) in which hydrogenchloride is released. The total preparation of PPD and TDC monomers and the polymerization into PpPTA is schematically drawn in figure 1.8.

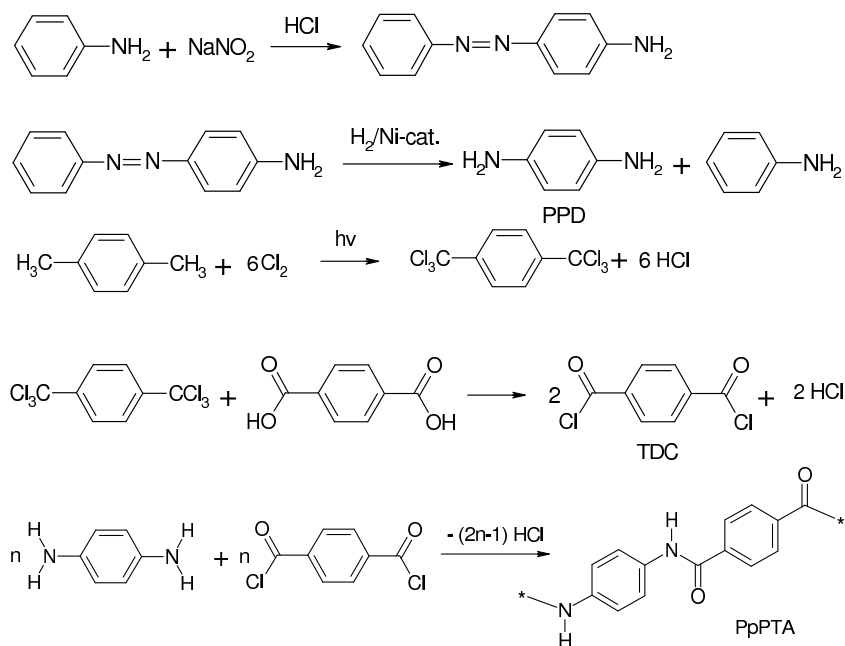


Figure 1.8: Preparation of PPD and TDC followed by the reaction scheme of the condensation polymerization of TDC and PPD resulting in PpPTA.

The end molecular weight is controlled by the ratio of PPD/TDC and by adding water as a stopper to the reacting medium. After polymerization the reaction mixture forms a crumb-like solid phase from which the pure polymer is abstracted by coagulation in water and subsequent drying. In a second step the polymer powder is dissolved in iced sulphuric acid to a concentration of ~ 20 wt% PpPTA. Sulphuric acid is known to be an excellent solvent for PpPTA as well as for other semi flexible polymers. For a thorough overview

of polymerizations, spinning conditions and solvents see the book of Yang [2]. At 20°C the dissolution results in a solid powder solution. This solid solution is then heated to a temperature of 85°C, making it a high viscous fluid which it is pressed through a spinneret. Before the fibres are coagulated in water they are stretched in an airgap to optimize orientational order in the forming fibre. After coagulation the fibres are washed and dried before winding. The process is schematically drawn in figure 1.9.

The two step process requires the purification of the polymer after polymerization in order to dissolve it again for spinning purposes. Commercially it would be beneficial to spin directly from the amide solvent. Up till now spinning from the amide solvent results in poor mechanical properties (typical tenacity 0.5 N/tex and tensile modulus 30 N/tex) compared to spinning from sulphuric acid (typical tenacity 2.5 N/tex and tensile modulus 80 N/tex). One of the major contributors hereto seems to be the maximum amount of PpPTA that can be dissolved in a NMP-CaCl₂ solution and still result in a processable solution. At about 2.5 wt% PpPTA the critical concentration is reached and an isotropic-anisotropic transition takes place. For PpPTA dissolved in sulphuric acid this transition takes place at 8 wt%, figure 1.7. In NMP-CaCl₂ already above 5 wt% PpPTA the solution becomes too viscous for spinning purposes. At elevated temperatures precipitation occurs in contrast to the case for sulphuric acid solutions, where spinnable solutions are obtained up to 20 wt%. Both phenomena will be addressed later on.

Another important application of PpPTA is in the form of pulp. The fiber is cut in small (6 mm) pieces and suspended in water. The suspended chopped fibers are mechanically fibrillated, eventually resulting in pulp. It seems tedious to produce pulp in this way, first manufacture a fiber and consequently "destroy" it mechanically into a pulp. A new production process for pulp material has been developed, see [12] [13] [14] in which the pulp is manufactured directly from an NMP-CaCl₂ solution instead of from the fiber. There are however a number of drawbacks in this process. Next to the mentioned maximum of 5 wt% PpPTA content, the resulting solutions are found to be thermodynamically unstable. Upon heating phase separation occurs. Due to this instable behaviour, the viscosity of the mixture changes in time resulting in processing difficulties. Another characteristic property of these mixtures is that viscosity decreases upon neutralization with CaO by a factor of 10 to 100 at moderate shear rates. This is essential as this causes the mixture to remain liquid-like and suitable for processing purposes up to 5 wt%. This phenomenon is also addressed. In figure 1.10 the influence of neutralization on the shear viscosity is visualized.

The phenomena encountered upon developing this new process, like in-

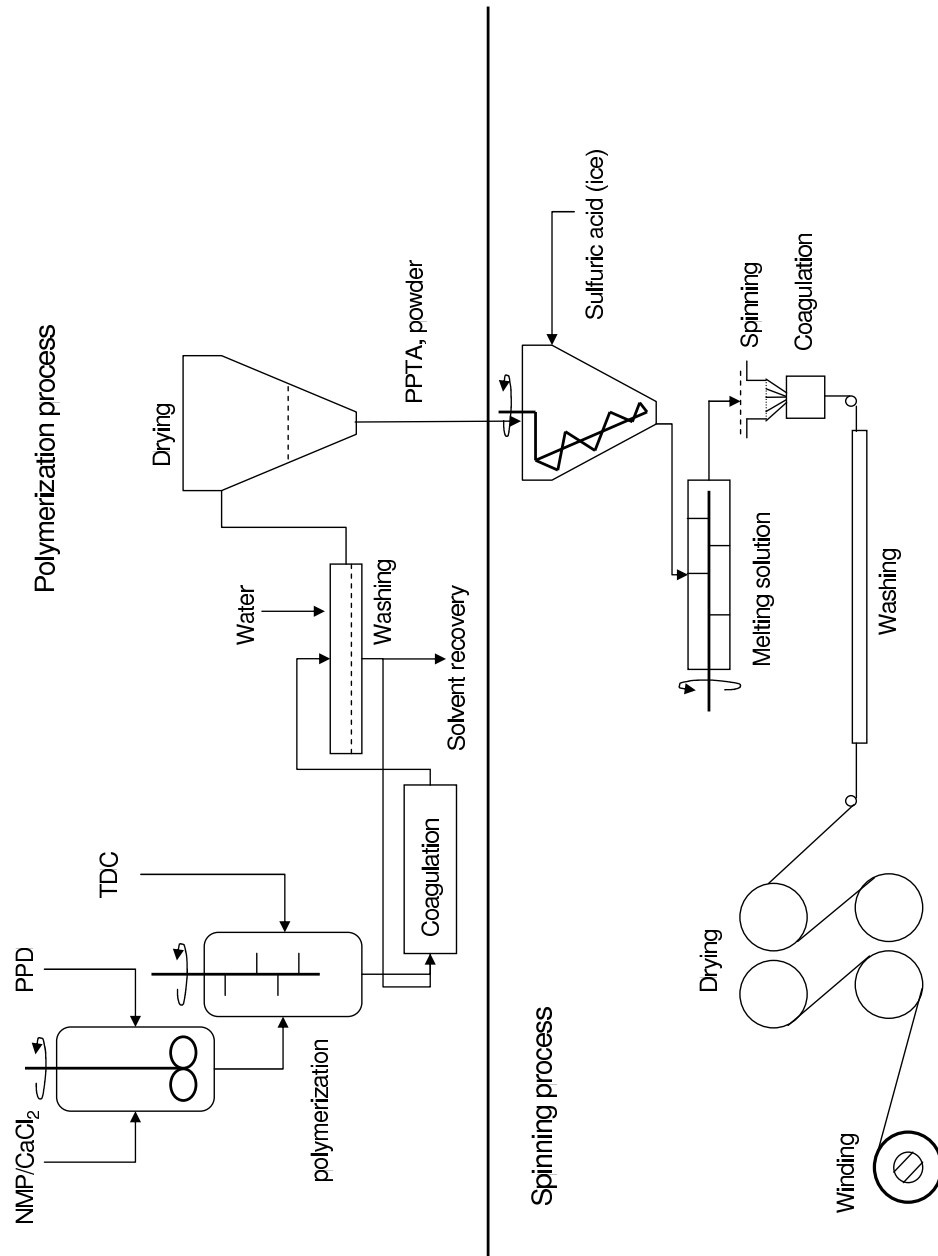


Figure 1.9: Schematic overview of the polymerization and spinning process of PpPTA.

stable phase behaviour leading to phase separation, viscosity variations and structural changes lead to a number of fundamental questions.

- Why does sulphuric acid act as a true solvent for PpPTA and NMP- CaCl_2 does not, what is the dissolving mechanism?
- Is it possible to predict the solvent power of a given solvent? That is the thermodynamic stability of a given solvent containing PpPTA.
- Is it possible to design a solvent system that combines polymerization and spin processing?

These are the questions that lay at the basis of this thesis. The objective is to gain a better and deeper knowledge of the dissolving mechanism and finally provide leads to develop alternative polymerization- and spinning media from which both processes can be optimized and hopefully ultimately combined.

Solubility alone however is certainly not enough to develop a commercial process. To that purpose many other issues need be addressed, to name just a few:

- A potential true solvent must exhibit the required physical properties to make it fit for processing purpose (viscosity-, mass transfer- and recycle properties to name a few).
- The components of this solvent need be non-hazardous and allowed in commercial production.

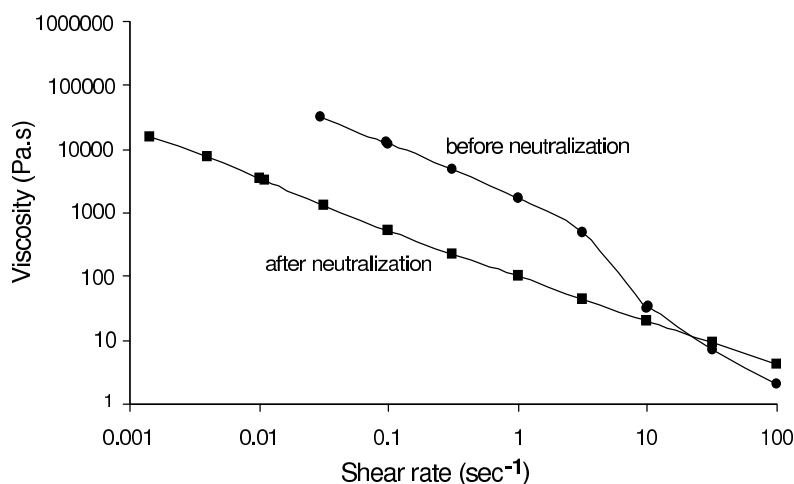


Figure 1.10: Viscosity as a function of shear rate, before and after neutralization of a reactor mixture (4 wt% PpPTA in 4 wt% CaCl_2 -NMP). The drop follows right after adding calciumoxide (CaO) as neutralizing agent.

- The cost price of raw materials must be low enough to make it economical attractive.

The objective of this thesis therefore is not the development of a commercial one step process.

There exists a structural isomer of PpPTA which in contrast to PpPTA can be spun into fibers of good mechanical properties in a one step process from an amide-salt system, poly-p-benzamide (PBA). Its preparation is discussed briefly.

PBA

Kwolek et al. reported fibers with excellent mechanical properties (comparable with those from PpPTA spun from sulphuric acid) when spun from an amide solvent system [15] by a dry spin process. This seems remarkable as PBA is an isomer of PpPTA, differing only in the manner in which the amide units are organized around the phenyl rings, see figure 1.3.

PBA can be polymerized out of sulphonyl-aminobenzoyl chloride [15], which is obtained by reaction of p-aminobenzoic acid with thionyl chloride, in two ways.

The first dissolves pure sulphonyl-aminobenzoyl chloride in ether-HCl to form p-aminobenzoyl chloride hydrogencchloride. The resulting salt can be dissolved in a N,N-dialkylamide, such as dimethylacetamide or tetra-methylurea. The amine group is released from hydrogencchloride and polymerization proceeds to obtain high molecular weight polymer, reaction scheme 1.11.

The second dissolves sulphonyl-aminobenzoyl chloride directly in an amide solvent containing an equivalent of water, reaction scheme 1.12. In both methods addition of lithium base to the amide solvent further promotes the polymerization reaction [16].

It is mentioned by Kwolek [15] that spinning can be either from acids, such as HF or H₂SO₄ or directly from the amide solution. In the case of dry spinning of a 13 wt% PBA from the amide solvent, Tetramethylurea(TMU)-LiCl (6.5 wt%) and heat treated, mechanical properties (tenacity 2 N/tex, modulus 100 N/tex, in the range of Twaron as mentioned in figure 1.1) are obtained comparable to those spun from acid solutions. This in contrast to 5 wt% PpPTA which, wet spun from amide solvent (NMP-CaCl₂), results in poor mechanical properties as mentioned before. 5 wt% PpPTA is the maximum concentration resulting in a spinnable solution. The fact that it is possible to contain 13 wt% PBA in the amide-salt system and still have a processable mixture may very well account for this difference. In chapter

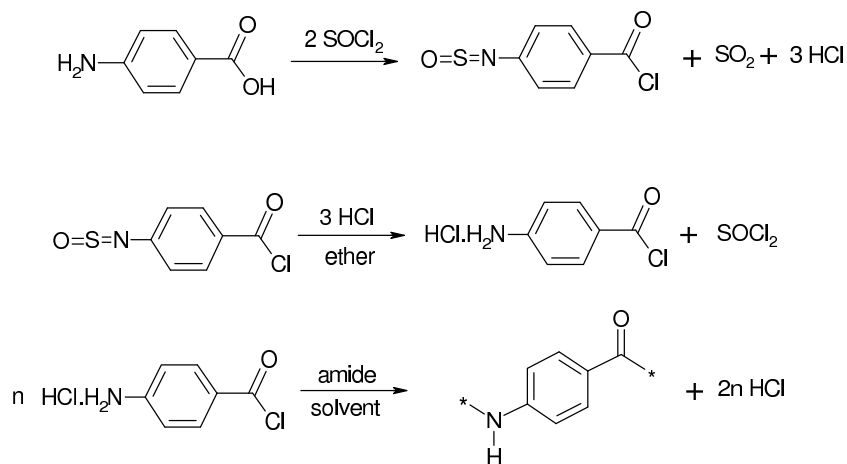


Figure 1.11: Reaction scheme of poly-*p*-benzamide from *p*-aminobenzoyl chloride hydrogenschloride.

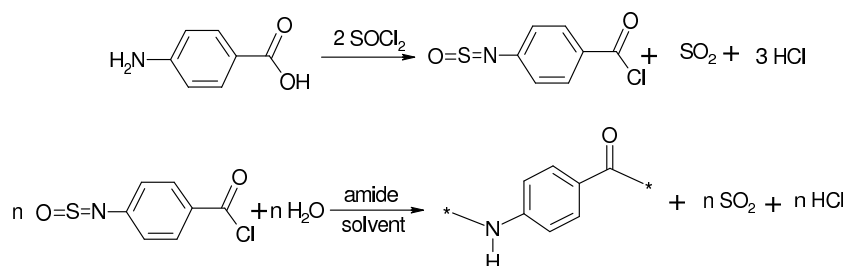


Figure 1.12: Reaction scheme of poly-*p*-benzamide from sulphinyl-aminobenzoyl chloride.

4, at the end of section 4.4 it will become clear after the treatment of dissolution thermodynamics that the PBA-TMU-LiCl mixture is meta-stable also and will eventually phase separate.

DABT

Another isomer, DABT is discussed as it is an intermediate between PpPTA and PBA. Its preparation is schematically given in scheme 1.13. To obtain good mechanical properties also this polymer needs to be spun from a strong acid like sulphuric acid.

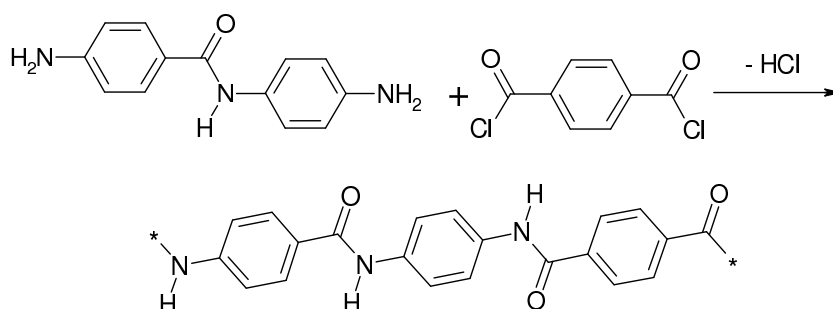


Figure 1.13: Reaction scheme of 4,4'-DABT from 4,4'-diaminobenzanilide and terephthaloyldichloride.

PmPTA, Technora and Russian Aramids

Poly-m-phenyleneisophthalamide (PmPTA) is the meta analogue of Twaron. This polymer is polymerized from the monomers metaphenylenediamine (MPD) and Isophthaledichloride (IDC), both have the substituents at the meta position, in NMP- CaCl_2 and in contrast to PpPTA and PBA, directly spun from the reaction medium out of an isotropic phase. As the monomers are now joined in the meta position the polymer does not form a rigid rod structure and experiences much more chain flexibility and remains isotropic. The same holds for the co-polymers Technora (DAPE/PPD (random co-polymer molar ratio 50/50) and TDC), polymerized in an NMP- CaCl_2 solution and Rusar/Armos (random co-polymer with DAPBI/PPD molar ratio 70/30 and TDC) and SVM (homopolymer) polymerized in a DMA- LiCl solution. Also these polymers are spun from their reaction media out of an isotropic phase. Orientation in all these fibers is obtained by drawing afterward.

Although many of the phenomena encountered in the dissolving process for PpPTA might be applicable to similar molecular systems, the discussion in the coming chapters is limited to PpPTA and some of its isomers.

1.3 Thesis outline

Rigid rod like polymers, like para-aramids, are all spun into fibers from solutions, as melt processing is not possible. These polymers degrade before melting. The nature of the dissolution medium can be quite different, as was shown in the previous section. PpPTA is spun from a strong acid to produce fibers with good mechanical properties, which is not possible when spun from its polymerization medium. Its isomers PBA and PmPTA on the other hand can be spun from an amide-salt system to produce fibers with good mechanical properties. The questions stated before concerning the mechanism of dissolution and how it can be influenced are the main issues addressed. The dissolution behaviour of PpPTA is studied in detail and of its isomers, PmPTA, PBA and DABT to some extent.

In chapter 2 a general overview on the interactions between amides, polyamides and salts, as can be found in literature, is presented. Also in brief the main theories describing liquid crystals are discussed. Successively in chapter 3 experimental evidence on the behaviour of mixtures of PpPTA in NMP- CaCl_2 is discussed. This includes meta-stable behaviour based on rheological, structural and calorimetric data and also the observed isotropic-nematic transition at low PpPTA concentration and the shear viscosity change upon neutralization of the reaction medium.

The phase diagram of NMP- CaCl_2 is cleared up and both ^1H -NMR and ^{13}C -NMR results reveal the nature of the interactions in the liquid phase. Electrical conductivity experiments performed on NMP- CaCl_2 (-PpPTA), are useful in explaining the way in which CaCl_2 is present in NMP(-PpPTA) solutions.

In chapter 4 the thermodynamics of PpPTA solutions are discussed. A quasi lattice thermodynamic model is developed to describe and predict thermal stability of solvent mixtures. In this model an interchange term is introduced as the key parameter to express the interaction between the different components in a mixture. Calorimetric data are used as input to determine the interchange terms between PpPTA, CaCl_2 and NMP as well as between PpPTA and H_2SO_4 . Next, by measuring the interchange terms between the components in various amide-salt systems, group contributions from the amides are calculated. This indicates which molecular groups are most profoundly interacting with PpPTA. Also the influence of different salts is discussed. Not just the interchange term itself but the combination with the maximum solubility of that salt in a solvent is vital in determining its dissolution power of PpPTA.

In chapter 5 results are presented of molecular modeling done on PpPTA

in NMP- CaCl_2 . The simulations show aggregate formation of ions in NMP. For other salts similar results are found. Modeling results of the solubility of CaCl_2 in NMP are found to be in good agreement with experimental data when these aggregates are assumed. In chapter 6 molecular modeling and quantum chemistry on PpPTA in sulphuric acid is discussed. The main issue is to show the protonation of PpPTA under different circumstances. The results agree with the conclusions based on the experimental data from conductivity measurements performed on PpPTA in sulphuric acid. The key role of charge in dissolution power of solvents becomes clear. An explanation for the coagulation of PpPTA dissolved in sulphuric acid, upon adding water, is also presented.

An interesting phenomenon of structural nature is discussed in chapter 7. In spite of what might be expected from the rigid nature of PpPTA it is very well possible that folding back of the chains occurs to form so called hairpins. Simulations show the fold back of a chain due to cis-trans transitions at relative low energy cost. Experimental evidence is found in the oscillation rheology showing a dramatic increase in elastic modulus upon increase of molecular weight. This may be ascribed to entanglement network formation by increasing the number of hairpins per chain. In the final chapter some concluding remarks are given and an outlook, on which solvent systems may be promising for future development, is presented.

2. Theory on Interactions in - and Structure of Polyaramid Solutions

This chapter exists out of two parts. In the first part the interaction mechanisms of amides and polyamides with salts as can be found in literature is presented. In the second part, the theory of molecular alignment is given that describes the formation of anisotropy in solutions of polyaramids. This includes the derivation of the order parameter and two models describing the isotropic-nematic transition. The first model, the Maier-Saupe model is enthalpy based and introduces a nematic potential to predict the conditions under which the isotropic-nematic transition occurs. Secondly, the Onsager model which makes use of the excluded volume principle to predict the transition is described. This model is based purely on entropy.

2.1 Introduction

Upon visual observation of solutions of PpPTA in NMP-CaCl₂ up to 5 wt%, these were found to be meta-stable and appear to phase separate and crystallize. The rate at which such processes take place is very much dependent on solution parameters such as PpPTA concentration and storage temperature and may vary from hours till months. Below 1 wt% however, the mixtures were found to be stable for years.

Between crossed polarizers these solutions were found to show birefringent behaviour, at remarkably low concentration of about 2 wt%. This in contrast to solutions of PpPTA in sulphuric acid (known to be a good solvent) in which birefringence does not appear until 8 wt% PpPTA. Based on similar behaviour found in literature e.g. [17] it is probable that supramolecular structures are formed in the NMP-CaCl₂ solution upon polymerization of PpPTA.

In this chapter the mechanisms of interaction between salt and (poly)amides are discussed in order to understand the role of salt on dissolution behaviour.

Secondly, Maier-Saupe and Onsager theories are presented, these are the limiting theories describing structure formation and phase behaviour in liquid crystalline systems. Maier-Saupe theory is purely enthalpy based and temperature dependent in contrast to Onsager theory, which is purely entropy based and non-temperature dependent.

An important parameter in this respect is the order parameter as indication of the amount of orientational order in a solution. It will be derived briefly and related to the two theories mentioned before.

This chapter ends with a few preliminary remarks on the structural behaviour of PpPTA in NMP- CaCl_2 , for which experimental evidence is presented in the following chapter.

2.2 Interaction mechanisms

2.2.1 Interactions between amides and salts

Many amide-salt systems have been subject of study over the past decades. They are widely used as polymerization media for the production of polyamides and aromatic polyamides. The chemical structure of solvents mentioned in this chapter are depicted in figure 2.1.

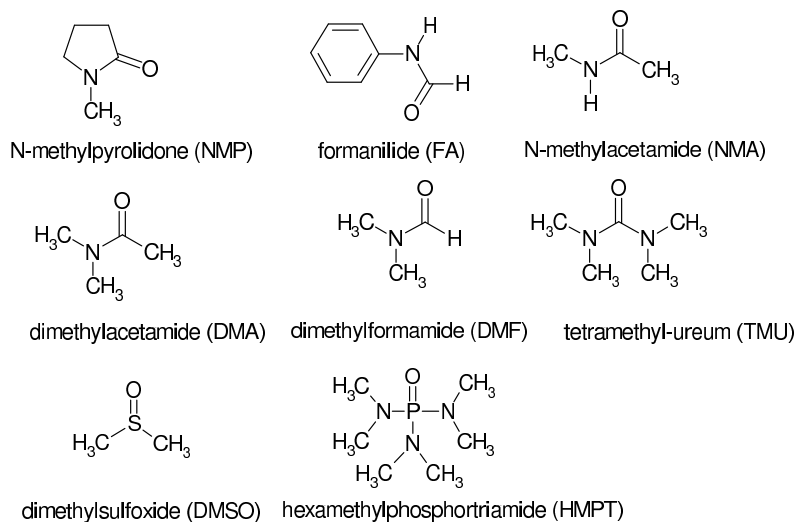


Figure 2.1: *Chemical structure of solvents mentioned in this chapter.*

Alkali and earth-Alkaline metal ions are known to form complexes in interaction with amides. Different techniques have been used to identify the existence of such complexes. Federov et al. [18] studied the solubilities of aromatic amides in various Li-salt/dimethylacetamide (DMA) solvents. A

correlation was established between the anion of the salt and the chemical shift in the infrared spectrum of the amide proton, indicating interaction.

Rao et al. [19] studied the influence of different cations on the peptide unit of benzanilide. Benzanilide is often used as a model compound for PpPTA as it consists of an amide unit between two aromatic rings mimicking the characteristics of a PpPTA amide unit. Also in this thesis it will be used as a model compound in some of the experiments and its chemical structure is depicted in figure 2.2.

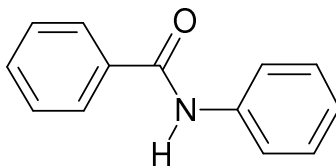


Figure 2.2: Chemical structure of benzanilide.

Rao et al. found a blue shift in the intensity of the double bond character of the $\text{N}=\text{C}$. This was attributed to the interaction of the cation with the carbonyl oxygen of the amide. The shift decreases in the order: $\text{H}^+ > \text{Li}^+ > \text{Ca}^{2+} > \text{Mg}^{2+} > \text{Na}^+$ causing stronger overlap in the π electrons of the $\text{C}=\text{N}$ bond.

Interaction effects have also been measured by use of calorimetry. Balasubramanian et al. [20] measured mixing heats of salts with amides in aqueous solution and found structural changes in ^1H -NMR and infra red spectra. An overview of the heats of interaction of various salts with different ligands was published by the same group [21]. The rate of protonation is a technique used by Cox et al [22]. They found an increase in this rate when lithium salts were added to an amide solution. It was concluded that Li^+ binds strongly to the amide. Other techniques used are viscosity measurements and crystallography.

Bello et al. [23] used these techniques to demonstrate strong interactions of CaCl_2 and LiCl with N-methylacetamide (NMA) and DMA. Stanley et al. [24] demonstrated the existence of complexes of NMP with different salt systems by analysis of the crystalline state using X-ray diffraction.

Other researchers studied the double bond character of the amide when salts were added.

Waghorne et al. [25] studied interactions of DMA with different salts. The rate of rotation and the activation energy of rotation were determined. Except for Ag^+ and Zn^{2+} addition of salt yielded a decrease in rotation rate and an increase of the activation energy of rotation. This was attributed to the increase of the double bond character of the amide group. A linear correlation

with the electrostatic field intensity, \vec{F} , at the surface of the ion was found. In the case of Ag^+ and Zn^{2+} , complex formation with nitrogen was suggested, decreasing double bond character.

The mechanism is proposed that the amide group exists in an intermediate state between single and double bond character, figure 2.3. Interaction of metal ions with the carbonyl oxygen shifts the bond to more double bond character increasing the activation energy (E_A) of rotation. The electrostatic force field \vec{F} at the surface of the ion increases the E_A linearly. Exception is Ag^+ which lowers the E_A . It is proposed that Ag^+ might interact with nitrogen of the amide unit causing more single bond character, however no evidence was given.

Besides experimental evidence also computational techniques have been used to demonstrate salt-amide interactions. Balasubramanian et al. [26] calculated binding energies of Li^+ to the carbonyl oxygen of amides (formanilide (FA), NMA, DMA) using Pople's CNDO/2 method. The stretch frequency of the C-N bond upon interaction and also the rotation barrier was found to increase.

Kawakami et al. [27] performed an ab initio molecular orbital study to the interaction of N-ethyl-1-naphtalenecarboxamine with alkali and earth alkaline metals. In UV absorption spectra a new longer wave length was observed. MO calculation was done to determine a local energy minimum upon metal binding to explain this new wavelength. Several were found, one in which a metal complex was formed with the carbonyl oxygen as well as the nitrogen of the amide unit (bidentate complex) and one in which the metal binds to the carbonyl oxygen and the π electrons of the phenyl. The latter is more stable due to de-localization of the charge of the cation.

In conclusion, the general accepted interaction concept involves the binding of a cation to the carbonyl-oxygen, which is exposed due to the non-acidic medium. The anion then acts as a counter ion for the formed positively charged amide-cation complex. In figure 2.3 a schematic representation of the two possible resonance structures of an amide is given. In figure 2.4 the interaction with a cation and anion is depicted.

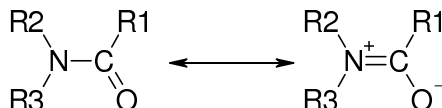


Figure 2.3: *Two resonance structures of an amide.*

Other types of complex formation have been proposed by e.g. Kawakami et al. [27]. They performed an ab initio molecular orbital study of interactions

of amides with different cations. The interaction was not restricted to the carbonyl oxygen only, but may also take place with the aromatic π -electrons, or with the nitrogen forming a bidentate complex. They studied this for the interaction of several cations with a naphthalenecarboxamide moiety, figures 2.5 and 2.6 show these interactions for magnesium. Experimentally it was found to show fluorescence spectral changes upon adding different salts. The largest shifts were found for magnesium salts.

A consequence of the complex formation is a more rigid amide unit, due to an increased double bond character. This phenomenon can be well studied using resonance techniques like ^1H -NMR, ^{13}C -NMR, UV-VIS as well as IR and as heats of interaction.

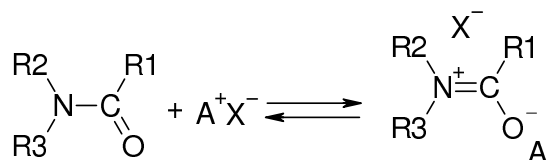


Figure 2.4: Interaction model of salt-ions with an amide.

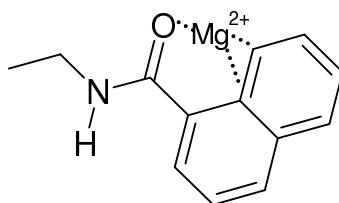


Figure 2.5: Binding model with magnesium ion forming a π -complex with the π -electrons of the ring and the carbonyl-oxygen.

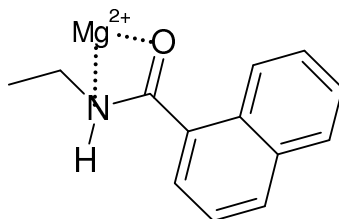


Figure 2.6: Binding model with magnesium ion forming a bridge between the carbonyl-oxygen and the nitrogen, bidentate complex.

2.2.2 Interactions between polyamides and salts

The synthesis of PpPTA was studied in 1970 by Federov et al. [28]. They used N,N-dimethylacetamide(DMA)-LiCl as the polymerization medium. Several interesting features are described, that are also very characteristic for the NMP-CaCl₂ solvent discussed in this thesis.

In the article a study is made of the dependence of the viscosity (as a measure for molecular weight) of PpPTA on the concentration of the monomers and LiCl in solution, on the moisture content, on the nature of the solvent and on reaction time and temperature. The influence on the molecular weight and solubility is discussed.

Molecular weight shows an optimum in the case the amount of LiCl is equivalent to 1 salt molecule per amide unit in the PpPTA chains [29]. This is concluded from a sharp rise in the viscosity in a certain region of the LiCl concentration. A sharp fall in viscosity is observed on introducing small amounts of moisture. This is explained by hydrolysis of TDC and terminal end groups of the growing chains. Temperature has shown little effect in the range -11°C to 20°C. When LiBr is used instead of LiCl precipitation of polymer occurs during the reaction (starting after 15 minutes) resulting in low viscosity, $\eta_{sp}=1.3$ compared to the reaction with LiCl, $\eta_{sp}=2.5$.

(η_{sp} was determined by measuring the relative viscosity using a 0.5 g PpPTA in 100 ml sulphuric acid and by the relation $\eta_{sp} = \eta_{rel} - 1$).

Effect of solvent on molecular weight:

Both solubility and viscosity increase with increasing polarity of the solvent in which the following series was established, hexamethylphosphortriamide (HMPT)>NMP>DMA>tetramethylureum (TMU). Adding salt increases viscosity in all solvents and is more predominant in less polar solvents.

Effect of the nature of the salt on molecular weight:

Molecular weight increases with increasing electro negativity of the anion LiCl>LiNO₃>LiBr>LiSCN>LiI (for lithium as halide) and

CaCl₂>CaBr₂>CaI₂ (for calcium as halide) and decreasing tendency in complex formation of the cation (Alkali, Alkaline metals)

LiCl>CaCl₂>MgCl₂>AlCl₃. When strong complex forming cations, d-metals, are used the molecular weight remains very low, $\eta_{sp} \sim 0.2$ in the case of ZnCl₂, NiCl₂, CdCl₂, CoCl₂, SbCl₃. [30]). In figure 2.7 the relationship between the electro negativity (according to Pauling) of the cation and anion and the viscosity (molecular weight) is shown.

Effect of rigidity of chain on molecular weight:

Various aromatic polyamides, differing in chain rigidity were synthesized in DMA-LiCl.

In order of decreasing chain flexibility [31] these were

Poly-m-Phenyleneisophthalamide (PmPIA),

Poly-p-Phenyleneisophthalamide (PpPIA),

P-m-Phenyleneterephthalamide (PmPTA) and

P-p-Phenyleneterephthalamide (PpPTA).

The more rigid the polymer chain the lower the solubility in pure DMA and the greater the increase in viscosity upon adding LiCl during polymerization.

Dissolution mechanism:

Ample evidence was found to conclude that the addition of salts of the alkali and alkaline groups contribute favourably to the maximum molecular weight obtainable. The polyterephthalamides, due to their high crystallinity, are insoluble in the amide-salt solvents. Therefore to investigate the interactions of salts with the different amide configurations, model compounds were used in dissolving experiments. This can be done since there exists a definite relationship between the solubility of the polymers and the solubility of their corresponding low molecular weight model compounds [32]. Addition of salt increases the solubility of the model compounds. Salt influences not only the solubility of the polymer, but also the solubility of the monomers and reaction kinetics. That is PPD dissolves better when LiCl is added but TDC becomes insoluble.

To elucidate the effect of salt on the solubility of the polymers, NMR, IR and electrical conductivity measurements were performed. The electrical conductivity of the solvent shows an optimum with increasing salt concen-

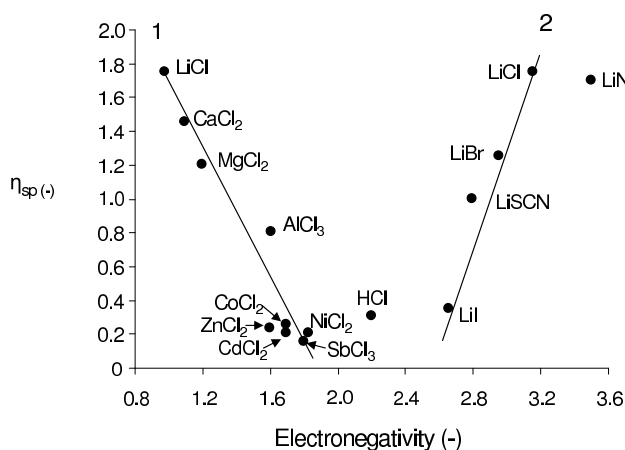


Figure 2.7: Dependence of the specific viscosity of PpPTA on the electronegativity of the cations (1) and anions (2) in the solvent.

tration. This concentration coincides with the maximum viscosity. Further increase in salt content decreases the solubility of the polymer. Apparently ion pair formation occurs reducing the number of ions available and reduce solubility. In chapter 3 evidence of ion pair formation is presented based on NMR experiments of NMP-salt-benzanilide solutions. Increasing the amount of LiCl leads to a reduced hydrodynamic radius of benzanilide indicating less interaction with its environment.

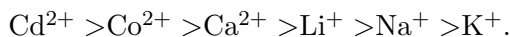
Evidence for the dependence of the molecular weight of the polymer on the concentration of the ions present in solution was found in the following series of metal-chlorides $\text{LiCl} > \text{CaCl}_2 > \text{MgCl}_2 > \text{SrCl}_2 > \text{CdCl}_2$, SbCl_3 , CoCl_2 and ZnCl_2 . This series is in order of decreasing electrical conductivity and also decreasing molecular weight obtainable for PpPTA, see figure 2.7.

It is well known that in polar non-acidic solvents (like DMA) cations are readily dissolved but anions only slightly [33]. It can be expected that hydrogen bonding occurs when a compound with labile hydrogen atoms is dissolved in a non-acidic salt containing solvent. This is discussed in more detail in references [34] and [35].

In other work of Federov [36], the interaction between a number of metal salts and benzanilide, taken as a model compound for PpPTA, in solution of DMA was studied using NMR. It showed that hydrogen bonds were formed between the anions of the salt and the hydrogen of the amide group of benzanilide.

A shift in the NMR spectrum of the amide hydrogen is a measure for the interaction between polymer and solvent. The magnitude of this shift and the solubility show the series $\text{Cl}^- > \text{Br}^- > \text{NO}_3^- > \text{SCN}^- > \text{I}^-$. Hence the increase in the solubility of benzanilide in the presence of salts is due to the formation of hydrogen bonds between the anions and the protons of the amide group, and depends on the strength of these bonds. The dissolved cation influences the chemical shift, as the dissolved cation interacts with the anion associated with the polymer. This shift therefore is an indication of the interaction strength and thus the dissolution power of the solvent. In chapter 5 evidence is presented, based on molecular modeling simulations, that in solutions of NMP- CaCl_2 mainly the anion interacts with the polymer.

Cations may form complexes with the carbonyl-oxygen. Through IR spectroscopy two types of complexes could be distinguished simultaneously, (1) cation bonded to free carbonyl-oxygen electron pair, (2) cation bonded to free carbonyl-oxygen electron pair and anion to amide proton. The first belonging to the complexation with DMA and the second to the complexation with benzanilide. The interaction with benzanilide is stronger than the one with DMA. The strength of the interactions decreases in the series



Comparing this with the results of the synthesis results led to the conclusion that the interactions between polymer and the cation should be minimal to maximize molecular weight.

Inspection of IR spectra led to the conclusion that when the amount of benzanilide is increased, the cations bind more strongly to the benzanilide. The same holds if the salt concentration is increased. If the concentrations of benzanilide and salt are rather low, most of the cations are bonded to the DMA.

This also applies to polymer solutions in which attention needs to be paid to the polymer chain length compared to the model compound. To generalize the above results. When a salt (e.g. LiCl) is added to a solvent (e.g. DMA) a complex of the form as shown in figure 2.8 is formed according to Paul and Sreenathan [37].

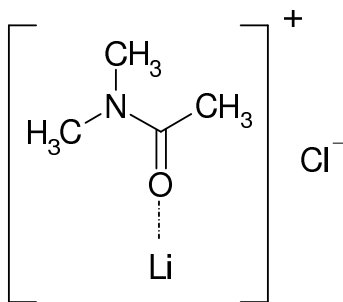


Figure 2.8: *Complexing of lithium with DMA through the carbonyl oxygen, chloride weakly interacting.*

The solvation number of the cation in many salt-solvent combinations is larger than one (in the case of Li^+ in DMA, two to three), Gopal [38], Diorio [39]. The Cl^- is present in a weakly bonded state. Therefore when a polymer containing labile protons, like polyamides, is added, the anion forms hydrogen bonds with it.

When the concentration of polymer and salt are low, the cation preferentially binds to the amide solvent. Probably the solvent in the solvated complex interacts more favourably with the polymer than the pure solvent in the absence of salt. This can explain the observed higher molecular weight polymer formation upon polymerization in amide-salt systems. In addition the complexation of the anion to the polymer through hydrogen bonding prevents aggregation of polymer (due to charge effects) and enhances the solubility. This can schematically be represented as in figure 2.9

When the concentration of either polymer or salt is increased the interaction of the cation with the polymer is also increased. Formation of the complex as indicated in figure 2.10 is more prominent.

These neutral polymer complexes are less able to complex with solvent molecules and hence the solubility is reduced. Also increasing the amount of salt promotes the possibility of ion pair formation and these ion pairs can interact with solvent and polymer.

The described mechanism holds for salts with metal ions that have a low tendency of salt formation (alkali and alkaline earth metals). Obviously it does not apply to metals with a strong salt formation tendency. Such salts interact with a large number of solvent molecules and thus prevent the interaction of polymer with the solvent molecules, hence lowering the solubility.

Diorio et al. [39] mentioned that the introduction of small amounts of

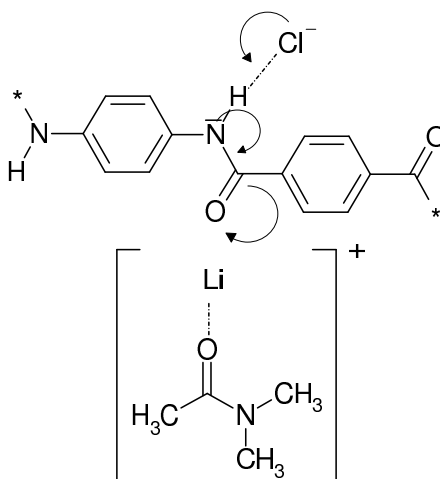


Figure 2.9: *Complexing of lithium with DMA through the carbonyl oxygen and chloride with the polymer through the amide hydrogen.*

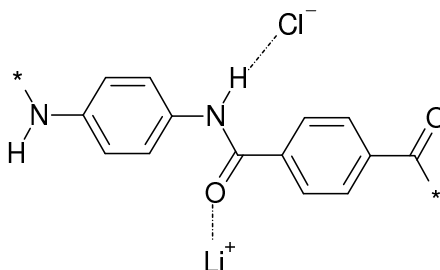


Figure 2.10: *Complexing of both lithium and chloride with polymer through the carbonyl oxygen and amide hydrogen respectively.*

water to a N-methylpropionamide-lithiumperchlorate mixture results in the vanishing of the splitting of the carbonyl band in the IR spectrum (3600 cm^{-1}). This is attributed to the formation of a hydration shell around the Li^+ ions, reducing the effective lithium ion concentration available for bonding with the amide.

Gan et al. [40] have synthesized different aromatic polyamides, among which PpPTA, in DMA-HMPT-LiCl. To keep 2-3 % PpPTA in solution 5% LiCl is required. Lower concentrations of LiCl resulted in higher M_w but the solution gels in time or upon stirring. In the ^1H -NMR spectrum a down shift in the amide-proton was clearly seen and it was concluded that Li^+ binds to the carbonyl oxygen while Cl^- binds to the amide proton.

Dibrova et al. [41] found the solubility of aromatic polyamides in amide-salt systems are depending on the specific donor-acceptor interaction force. Mainly the cation dissolves in the dipolar non-acidic solvent (such as NMP, DMA, HMPT, dimethylsulphoxide (DMSO) etc), due to the exposed oxygen atom. The anion is freely bonded to the amide protons of the polymer. The cation should not be bonded too strongly to the solvent molecules as no interaction with the polymer is obtained anymore. This suggests a delicate balance of interaction strengths to gain optimal dissolution effects.

The intrinsic viscosity depends on the specific salt-polymer system and content, a maximum was found at a molar ratio salt:amide of 2:1. A shift in the ^1H -NMR spectrum was also described in a publication of Vert et al. [42]. This shift was found to depend on the nature and concentration of the salt. A rapid exchange between free form and complex was observed, indicative of a dynamic equilibrium. Similar results are presented in chapter 3 based on NMR experiments.

Nekrasov et al. [43] determined several parameters like sedimentation and intrinsic viscosity of poly-m-phenyleneisophthalamide in dimethylformamide (DMF) and DMF-LiCl. They derived relations for M_w and here from calculated chain- and Kuhnlength as well as a χ parameter.

Panar [44] suggested the interaction of Cl^- with the amide proton through hydrogen bonding, resulting in a negatively charged chain. The chain is subsequently stabilized by Li^+ cations. The cations in turn interact with the solvent molecules.

Kim et al. [45] found a similar interaction pattern by studying the interaction of CaCl_3^- and Ca_2Cl_4 with cyclic aromatic amides. They found the $\text{CaCl}_3^- \cdot \text{DMA}_3$ complex to bind inside a cyclic hexamer ring of amides (six m-phenylenediamine molecules) in which the chloride atoms interact with the hydrogen atoms of the amide units through hydrogen bonding. In between two such cyclic moieties a Ca^{2+} stabilizes the negatively charged rings. They

concluded that in general salts increase the solubility of polyamides by breaking the H-bonds of the amide groups and thus preventing the formation of β -sheet like structures of p-aramid.

Figure 2.11 depicts the proposed structure of Panar. This picture agrees with the suggestion of complex formation between benzanilide and DMA-LiCl as proposed by Federov [28].

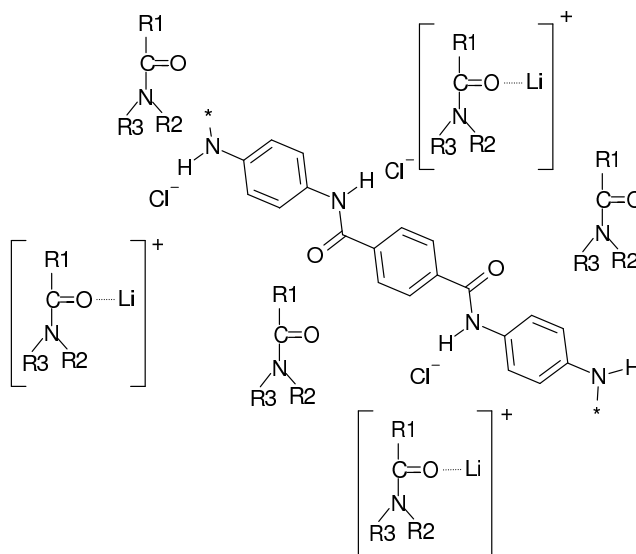


Figure 2.11: The proposed interaction scheme by Panar in which the polymer chain is negatively charged and stabilized by the cations interacting with the solvent.

Iovleva et al. [46] wrote a review article discussing the effect of addition of LiCl to solutions of different solvents and/or polymer. The following is a summary of that article.

In studying solutions of poly-p-benzamide (PBA) in DMA containing LiCl, Panar [47] advanced a hypothesis in which LiCl in dissociated form is mainly responsible for increasing the solubility of the polymer. Cl^- ions attach to the amide nitrogen of PBA resulting in a poly-electrolyte. Li^+ ions simultaneously complex with the carbonyl oxygen of DMA. These complexes interact with the polymer and hence prevent precipitation. Evidence was found in the electrophoresis of the solution upon adding Cl^- ions and in spectroscopic data for which the model compound benzanilide was used.

Mitchenko et al. [48] proposed a slightly different mechanism in which ion pairs are responsible for complex formation. They investigated solutions of poly-m-phenylene isophthalamide (PMPIA) in DMA, DMF, NMP, HMPT, to which LiCl is added. Based on the chemical shift of the CH_3 groups in

NMR measurements, they conclude that the reaction of LiCl with the solvent decreases according to the order mentioned previously. This indicates decreasing solvent power. Moreover, the donor number which characterizes solvation, increases in the same order which indicates increased solvent power.

Their explanation for the apparent paradox is the presence of ion pairs rather than ions. Due to energetically advantageous contacts between ion pairs and the amide groups of the polymer, polymer-polymer contacts are prevented, keeping the polymer in solution.

A similar mechanism was proposed, also by Mitchenko et al. [49], for solutions of LiCl in polyamidohydrazide (PAH). It was shown that the interaction of salt with a polymer molecule is determined by strength ratios of the solvent dipole and the ion pair and the dipole of the dissolved molecule, which is related to the polymer and solvent properties.

To that purpose, they dissolved a low molecular model compound N-(p-benzoamidebenzoyl)-N'-benzoylhydrazine (HABA), figure 2.12, which consists of a benzanilide unit and an aromatic hydrazine, in various solvents (DMF, NMP, DMA, DMSO, HMPT) and measured chemical shifts in proton NMR upon adding LiCl. These shifts could only be explained under the assumption of formation of ion pairs from which the dipole depends on the specific solvent.

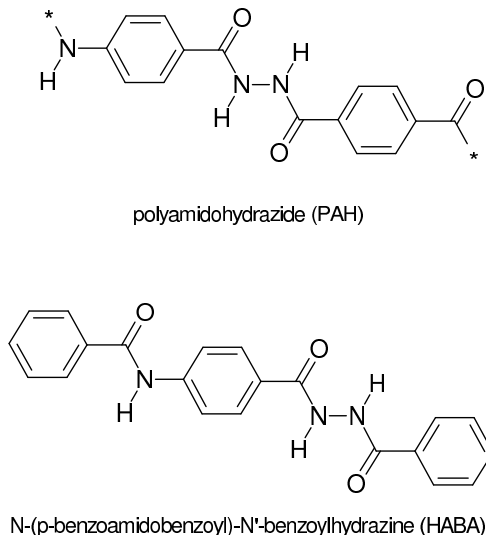


Figure 2.12: Chemical structure of polyamidohydrazide and N-(p-benzoamidobenzoyl)-N'-benzoylhydrazine.

Preston et al. [50] showed that the charged resonance structure of HABA was stabilized with a given dipole moment depending on the type of solvent. Molecular interactions in the solution will therefore be determined by the type

of dipole-dipole effect of both solvent molecules and the dipole of the resonance form of HABA and the dipole of the ion pair of the salt.

Evidence for ion pair formation was given by comparison of the expected chemical shifts in the case of a fully ionized salt and in the case ion pair formation is assumed. Chemical shifts for fully ionized salts can be calculated based on the Buckingham equation in which the distance of the ion to a NH proton was estimated to range between 2 and 3 Å. This results in an expected shift of -3.88 ppm and -1.26 ppm respectively. Based on the bjerrum theory the ions are able to approach each other close enough to be well in the range of stable ion pair formation. The overall uncharged ion pairs experience a dipole. If the dipole charge is assumed to be that of the free ions, the calculated chemical shifts are -1.44 ppm (2 Å) and -0.38 ppm. (3 Å) respectively. These are in much closer agreement with the experimentally observed values, ranging from -0.03 to -0.70 ppm. The observed effects take place when LiCl is added and are explained by the following mechanism. Before LiCl is added, solvent molecules form a "fur coat" around the dissolved compound. When LiCl is added, ion pairs disrupt this solvation shell. To which extent this disruption occurs depends in a complex manner on the structural and physical-chemical parameters. For instance in the case of DMA or NMP used as a solvent the dipole of the LiCl pair is large enough to disrupt the solvated shell and directly interact with -NH protons of amide and hydrazine groups, reflected in changes in spectra. In the case of DMSO the ion pair is not able to disrupt the solvated shell and no chemical shift is observed. HMPT is an intermediate case. LiCl is able to disrupt the solvated shell around the amide group, but not around the hydrazide group. This is illustrated in figure 2.13.

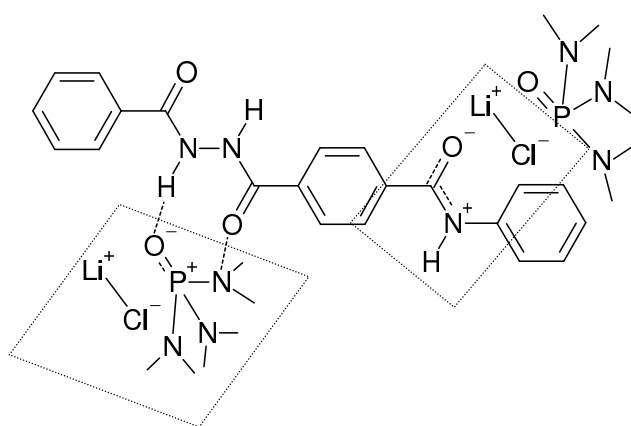


Figure 2.13: Sketch of the direct contact of the LiCl ion pair with the amide group and the indirect contact through HMPT with the hydrazide group.

This sketch demonstrates the complex interactions that may take place in amide salt systems containing aromatic polymers. Indications for the formation of a mantle structure of NMP around benzanilide were found for NMP-CaCl₂-benzanilide solutions, based on NMR results and are presented in chapter 3. The effect of the salt depends on interrelated parameters like the dipole strength and equilibrium constants of ion pair-dissociated salt. These are determined by solvent characteristics. The interaction of salt with the polymer is determined by the ratio of the dipole strength of the solvent and ion pair and the dipole of the dissolved molecule, which in turn is determined by macromolecular structure and interactions in solution.

Evidence for the above mentioned mechanisms is also found by studies of Prozorova [51]. Polymerizations of polyamidobenzimidazole (PABI) in DMA and DMA-LiCl resulted in significant higher molecular weight by polymerization in the presence of LiCl. Also the intrinsic viscosity of polymer dissolved in DMA-LiCl was found not to decrease dramatically when heated up to 100°C as is the case when no LiCl is present. Both effects were attributed to strong interactions of LiCl with the polymer chains.

Another interesting phenomenon was found by Lobanova et al. [52]. The viscosities of 14% and 17% solutions of PAN (molecular weight 25000 g/mol) in DMF were found to decrease by a factor of two when LiCl was added. The decrease in viscosity became even larger by a factor of 4 when the molecular weight of the polymer increased to 90000 g/mol. The conclusion was that intramolecular bonds are broken by LiCl, causing an increase of the mobility of the system.

2.2.3 Conclusions

Due to the above discussed interactions, amide-salt systems can act as good polymerization media for polyamides and aromatic polyamides. Different mechanisms describing these interactions have been proposed by various authors. It may be the anion, the cation or ion-pair that are responsible for the interactions. The specific type of solvent and salt and also the ratio salt to amide influence interaction strengths. There is not a decisive argument determining the precise interaction scheme. It is a delicate balance of all the participating components that determines the strength of the interactions and the degree of solubility and hence the suitability as a polymerization medium.

Commercially PpPTA is polymerized in the NMP-CaCl₂ medium in which the CaCl₂ content is set equal to the PpPTA content on weight basis. As the molar weights of CaCl₂ (110 g/mol) and an amide unit in PpPTA (119 g/mol) are roughly the same this corresponds to ratio 1:1 on a molar basis.

Experimentally this is found to be an optimum ratio. This deviates from the ratio 2:1 found by Dibrova et al. [41] and again indicates the specific nature of the interactions between solvent, salt and polymer determining optimum conditions.

In the case of NMP-CaCl₂ the physical and chemical phenomena as an dissolving medium for PpPTA will be discussed in more detail in the remainder of this thesis. As this solution is found to show birefringent behaviour, the main theories describing structure formation in liquid crystalline systems are discussed first.

2.3 Theories on Liquid Crystalline behaviour

Semi-flexible polymers as PpPTA are known to show orientational order in solutions as shown in the introduction, figures 1.5 and 1.6, resulting in anisotropic phases at certain concentration and temperature combinations. The theories describing the isotropic-anisotropic transitions can be split in two categories, energy based and entropy based. Maier-Saupe theory is a mean field theory and introduces an anisotropic potential. On the other hand Onsager introduced a theory based on excluded volume to find an expression for the transition. The essentials of both theories are discussed below. First however, the term order parameter is clarified as both theories make use of this parameter. More extended derivations for the theories now presented can be found in textbooks e.g. [53] and [54].

2.3.1 Order parameter

To express the amount of orientational order in a solution an order parameter can be constructed in the following way. On a unit sphere every molecule is pictured as a rod (representative of the persistence length) represented by the three Euler angles α , β and γ with a common director \mathbf{n} . In figure 2.14 this is visualized.

All the molecules inside this sphere are distributed according to an orientational distribution function $f(\alpha, \beta, \gamma)$. As a nematic phase of cylindrically symmetric molecules is described, rotation about the molecular symmetry axis does not modify the orientational distribution function, which implies no γ dependence. The orientational distribution is also invariant under rotation about the director, the axis of symmetry, implying no α dependence. The number density on the unit sphere now becomes:

$$2\pi N(\beta)d\beta = 2\pi f(\beta) \sin \beta d\beta \quad (2.1)$$

and the probability to find the molecule at some point on the unit sphere

$$\int_1^{-1} N(\beta) d\beta = \int_1^{-1} f(\beta) \sin \beta d\beta = 1 . \quad (2.2)$$

In the isotropic case the orientational distribution function is a constant giving:

$$f(\beta) \int_{-1}^1 d \cos \beta = 1 \Rightarrow f(\beta) = \frac{1}{2} . \quad (2.3)$$

Use is made of the fact that in a steady state the number of molecules in the unit sphere is constant. This is expressed by the Laplace equation:

$$\nabla^2 f(\alpha, \beta, \gamma) = 0 . \quad (2.4)$$

In the book of Luckhurst and Gray [53] in chapter three a nice derivation of the order parameter is given. In essence it comes down to that any well behaved function of the three Euler angles $f(\alpha, \beta, \gamma)$ can be expanded in a Wigner series [55]. The solution of equation 2.4 on the surface of the unit sphere in spherical coordinates results in a solution of the orientational distribution function, as the orientational distribution function is a density function on the unit sphere.

$$f(\alpha, \beta, \gamma) = \sum f_{l,m,n} D_l^{m,n}(\alpha, \beta, \gamma) , \quad (2.5)$$

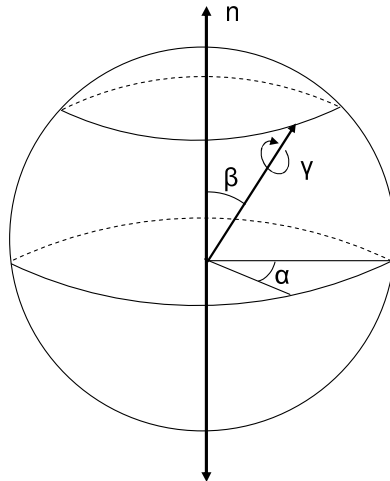


Figure 2.14: Order sphere representing the orientation of a polymer molecule as a vector represented by the three Euler angles with respect to the director n .

here $D_l^{m,n}(\alpha, \beta, \gamma)$ are the Wigner rotation matrices, defined by l, m and n , which in our case are integer values. As said before a nematic phase of cylindrically symmetric molecules is described, so the rotation about the molecular symmetry axis does not modify the orientational distribution function. This implies $n=0$ in equation 2.5 and the orientational distribution is invariant under rotation about the director, the axis of symmetry, implying $m=0$. As the nematic phase has a symmetry plane perpendicular to the director only terms with even l can appear in equation 2.5. So for a cylindrically symmetric phase composed of cylindrically symmetric particles, the orientation distribution function only depends on the angle β and equation 2.5 reduces to:

$$f(\beta) = \sum f_{2l} D_{2l}^{0,0}(\beta) = \sum f_{2l} P_{2l}(\beta) , \quad (2.6)$$

in which $P_{2l}(\beta)$ are the Legendre polynomials. The expansion coefficients are now obtained by multiplying both sides with the complex conjugate $D_l^{*0,0}(\beta)$ and integrating over β :

$$f_{2l} = \frac{1}{2}(4l+1) \langle P_{2l} \rangle . \quad (2.7)$$

Inserting this into equation 2.6 gives the distribution function:

$$f(\beta) = \sum_{l=0}^{\infty} \frac{1}{2}(4l+1) \langle P_{2l} \rangle P_{2l}(\beta) \quad (2.8)$$

and the order parameters are just averages of the even Legendre polynomials. In practice often only the $\langle P_2 \rangle$ is used as order parameter, by realizing that $\langle P_0 \rangle = 1$. The final expression for the orientational order parameter then is the average second order Legendre polynomial:

$$\langle P_2 \rangle = \langle \frac{1}{2}(3 \cos^2 \beta - 1) \rangle . \quad (2.9)$$

The value of the order parameter can take any value between zero, in the case of isotropy, and 1 in the case of perfect alignment along the director. This is shown as follows. The order parameter is the average second order Legendre polynomial and can by definition be written as:

$$\langle P_2 \rangle \equiv \frac{\int_{-1}^1 f(\beta) P_2 d \cos \beta}{\int_{-1}^1 f(\beta) d \cos \beta} . \quad (2.10)$$

In the case of isotropy the orientational distribution function $f(\beta) = \frac{1}{2}$ as shown in equation 2.3. The order parameter then becomes:

$$\langle P_2 \rangle = \frac{\int_{-1}^1 f(\beta) P_2 d \cos \beta}{\int_{-1}^1 f(\beta) d \cos \beta} = \frac{1}{2} (\cos^3 \beta - \cos \beta) \Big|_{-1}^1 = 0 . \quad (2.11)$$

In the case of complete alignment along the director, $\beta=0$ and according to equation 2.9 $\langle P_2 \rangle = 1$. In figure 2.15 the distribution function is depicted. In the case of isotropy it is a constant with value $\frac{1}{2}$ and in the case on anisotropy it is peaked around $\beta = 0$ and $\beta = \pi$.

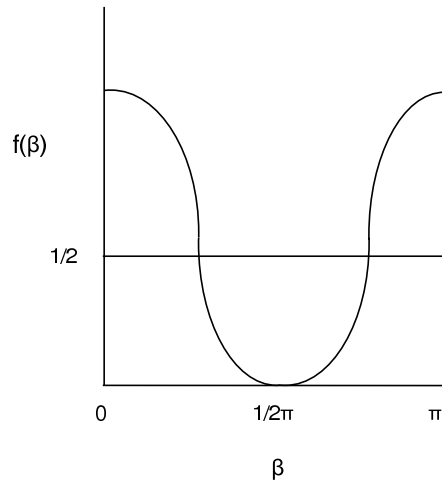


Figure 2.15: *Two characteristic distribution functions. In the anisotropic case it is peaked around $\beta=0$ and $\beta=\pi$, in the case of isotropy the distribution function takes the constant value $\frac{1}{2}$.*

Picken showed [11], that the persistence length, which is normally reported at about 20°C, has a $1/T$ temperature proportionality when the polymer length exceeds the persistence length. As a consequence the temperature at which the isotropic-nematic transition occurs depends on the concentration of the polymer solution. Moreover, as the molecules feel each others presence the transition is also temperature dependent. For PpPTA in sulphuric acid the phase diagram has been cleared up by Picken [56] and Rommel [57]. In figure 2.16 this phase diagram is presented.

A model to describe the temperature dependence of the isotropic-nematic transition is given by Wilhelm Maier and Alfred Saupe. This model is discussed next, followed by the Onsager model which in contrast to the Maier-Saupe model is a-thermal.

2.3.2 Maier-Saupe model

Wilhelm Maier and Alfred Saupe have developed a model to describe the isotropic-nematic transition by introducing a continuous, long range nematic potential [58], [59], [60]. As a result of attractive dispersion forces this potential is responsible for the existence of a nematic phase. They assumed the molecules to be rigid and symmetric around the molecular axis. The potential exists of a scalar and a anisotropic part. Only the anisotropic part is of interest as this will determine the transition conditions. It is written as:

$$U_a(r_{12}, \beta_{12}) = -u(r_{12})P_2(\cos \beta_{12}) , \quad (2.12)$$

P_2 is the second order Legendre polynomial and u_{12} defined positive, so the molecules tend to align with the molecular axis parallel. The potential depends on the intermolecular distance between molecules and their relative orientation β_{12} and is a pair potential. By taking the averages over the pair potential with respect to distance and the orientations a mean field approximation is introduced. The potential may now be written in an ensemble form:

$$U(\beta) = -\varepsilon \langle P_2 \rangle P_2(\cos \beta) , \quad (2.13)$$

where ε is a positive constant that can be thought of as the strength of the orienting potential. It depends on the radial distribution and is in fact the

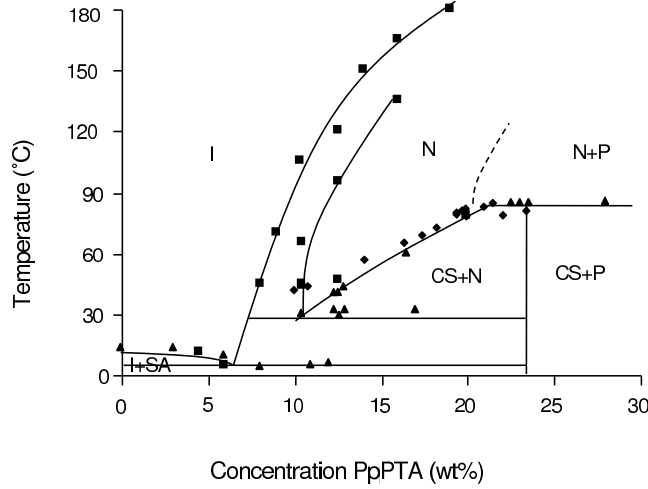


Figure 2.16: Phase diagram of PpPTA in sulphuric acid. Squares based on crossed polarized measurements, triangles based on DSC measurements according to Rommel [57] and checkers additional recent measurements based on DSC.

average of the radial distribution. $\langle P_2 \rangle$ is the order parameter as defined before. The distribution function now becomes:

$$f(\beta) = Z^{-1} e^{\frac{\varepsilon}{kT} \langle P_2 \rangle P_2(\cos \beta)} , \quad (2.14)$$

Z is the partition function:

$$Z = \int d \cos \beta e^{\frac{\varepsilon}{kT} \langle P_2 \rangle P_2(\cos \beta)} . \quad (2.15)$$

The order parameter then follows from inserting the expression of the distribution function 2.14 in equation 2.10.

$$\langle P_2 \rangle = Z^{-1} \int_{-1}^1 d \cos \beta P_2(\cos \beta) e^{\frac{\varepsilon}{kT} \langle P_2 \rangle P_2(\cos \beta)} . \quad (2.16)$$

From equation 2.16 the relationship between $\langle P_2 \rangle$ and kT/ε is obtained and shown in figure 2.17. Above $kT/\varepsilon = 0.222$, $\langle P_2 \rangle = 0$ is the only solution and the isotropic phase is the stable one. Below $kT/\varepsilon = 0.222$ there is another solution for $\langle P_2 \rangle$ corresponding to the ordered nematic phase. By evaluating the nematic potential, equation 2.13 which should be minimal, the ordered phase turns out to be the stable one. This means the critical point is reached at a value of 0.222 for kT/ε and the corresponding order parameter is 0.43. At the transition the order parameter changes discontinuously from 0.43 to zero. The temperature at which the critical point is reached depends on the specific value of ε and is called T_{NI} .

This relationship predicts a single T_{NI} regardless of volume (concentration). As the radial distribution function would surely depend on volume, Maier-Saupe introduced a volume dependence for the potential strength parameter ε :

$$\varepsilon = \varepsilon_0 V^{-\gamma} . \quad (2.17)$$

The distance dependence of u_{12} was taken from the Lennard-Jones potential to scale with $1/r_{12}^6$ or $1/V^2$ and γ was set to 2. Other authors made extensions of the theory in which different relationships of the pair potential with the intermolecular distance was used and used γ as an adjustable parameter; Humphries et al. [61] used 4 as a value for γ to describe the temperature dependence of the order parameter for rod like molecules. In the phase diagram of PpPTA in sulphuric acid, figure 2.16 the nematic-isotropic transition

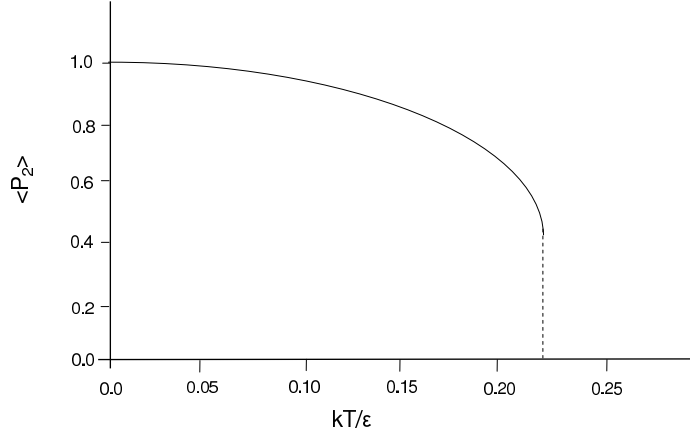


Figure 2.17: Relationship between temperature and order parameter based on a Maier-Saupe potential. The critical point is reached at $kT/\varepsilon = 0.222$. Below this point the nematic phase is stable, above this point the isotropic phase. The corresponding order parameter at the transition is 0.43.

depends on the PpPTA concentration. To describe the nematic transition for PpPTA dissolved in sulphuric acid, the following relationship for ε was proposed by Picken [56]:

$$\varepsilon = \varepsilon^* c^\gamma L(T)^\delta, \quad (2.18)$$

γ and δ were set to 2 based on similar reasoning as Maier and Saupe that attractive dispersive interactions scale as $1/r^6$ or $1/V^2$ or c^2 and that the potential is an average over all two particle interactions giving a L^2 dependence. It was shown to work very well in predicting T_{NI} values.

In the reasoning so far excluded volume contributions to the free energy have been neglected. A model developed by Lars Onsager is based on the contribution of excluded volume and predicts in contrast to the Maier-Saupe model an a-thermal isotropic-nematic transition.

2.3.3 Onsager model

A second model, developed by Lars Onsager [62], is based on the excluded volume resulting from the presence of polymer molecules. This results in an entropy based isotropic-anisotropic transition. The derivation runs as follows.

For hard spheres (gas molecules) an expression for the corresponding free energy follows from statistical mechanics, e.g. Landau [63].

$$F = F_0 + kT(\ln(c) + \frac{1}{2}cV_e) + O(c^2). \quad (2.19)$$

Now by replacing spheres by hard rods, not only the concentration needs to be specified but the orientation as well. The amount of rods per unit volume pointing in the direction, given by unit vector \vec{a} around angle $d\phi$ is $c_a f_a d\phi$, in which f_a is the distribution function. Integration over the whole volume must give the total concentration.

$$\int_V c_a f_a d\phi = c . \quad (2.20)$$

The excluded volume V_e between two hard rods, with dimensions L and D , ($L \gg D$) and orientation \vec{a} and \vec{a}' is given by

$$V_e = 2L^2 D |\sin \gamma| . \quad (2.21)$$

Schematically this is sketched in figure 2.18

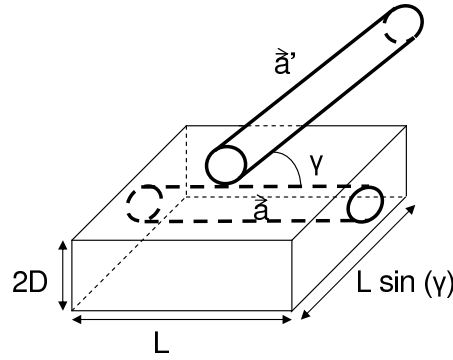


Figure 2.18: Schematic picture of two hard rods pointing in the directions \vec{a} and \vec{a}' under an angle γ . The box represents the excluded volume of the rod pointing in direction \vec{a} . This gives rise to a potential kTV_e .

Inserting this into equation 2.19 and neglecting non linear terms leads to:

$$F = F_0 + kT \left(\int f_a \ln(4\pi f_a c) d\phi + \frac{1}{2} c \iint f_a f_{a'} 2L^2 D |\sin \gamma| d\phi d\phi' \right) . \quad (2.22)$$

The first term on the left hand is an additive constant, the second term is associated with the entropy drop upon alignment and the third term is an interaction term related to the excluded volume of the hard rods. Based on equation 2.22, Onsager [62] derived an expression for the order parameter and introduced a trial function.

$$f_a = C \cdot \cosh(\alpha \cos \beta) . \quad (2.23)$$

C is chosen such that it satisfies constraint 2.20, α is a variational parameter and β the angle between \vec{a} and the nematic axis. The order parameter is written in analogy of equation 2.10

$$\langle P_2 \rangle = \frac{1}{2} \int f_a (3 \cos^2 \beta - 1) d \cos \beta . \quad (2.24)$$

Inserting equation 2.23 in 2.24 and the fact that in the region of interest α turns out to be large, this can be simplified to:

$$\langle P_2 \rangle \approx 1 - \frac{3}{\alpha} (\alpha \gg 1) . \quad (2.25)$$

Minimizing the free energy, equation 2.22 with respect to α , a function is obtained showing a first order transition from isotropic ($\alpha=0$) to nematic ($\alpha=18.6$). This gives for the order parameter at the critical concentration:

$$\langle P_2 \rangle_c \approx 0.84 . \quad (2.26)$$

For the isotropic-nematic transition, based on the volume fraction of the rods $\Phi = c \frac{1}{4} \pi D^2 L$, the volume fraction in the nematic phase at the transition point is given by:

$$\Phi_{c,nematic} = 4.5 \frac{D}{L} \quad (2.27)$$

at the same point the fraction in the isotropic phase is:

$$\Phi_{c,isotropic} = 3.3 \frac{D}{L} . \quad (2.28)$$

Note that the transition is not temperature dependent. In figure 2.19 a typical Onsager phase diagram is depicted.

2.4 Structure formation of PpPTA in NMP-CaCl₂

In the case of solutions of PpPTA in NMP-CaCl₂ an isotropic-nematic transition is found at 2.5 wt%. This corresponds to a volume fraction of 2.3 vol% by taking the solution density 1.07 gr/cm³. According to the Onsager theory the corresponding aspect ratio's (L/D) follow from equations 2.27 and 2.28 and are calculated to be 144 and 196 respectively. This would correspond to persistence lengths of 617 Å and 841 Å, by taking the diameter of the polymer molecule 4.3 Å.

The persistence length of PpPTA is 287 Å according to Ying et al. [7] who determined this value for PpPTA dissolved in sulphuric acid at room temperature. In the same article it was shown that the persistence length does not depend on the ionic strength of the solution and therefore the same value is expected in NMP-CaCl₂ solutions.

Thus the experimentally calculated persistence length exceeds the PpPTA persistence length by far, indicating the presence of much larger aggregate particles in the solution. The presence of such particles was studied by X-ray diffraction and is discussed in the next chapter.

The assumption of Onsager behaviour in NMP-CaCl₂ solutions is justified based on the following argument. Due to the formation of aggregates of the constituent polymer molecules the nematic potential becomes far less dominant. This as the potential depends on the intermolecular distance according to equation 2.12 and the distance between aggregates is very large compared to molecular distances. As a result the isotropic-nematic transition, which is now governed by the aggregates becomes entropy based and shows a-thermal behaviour.

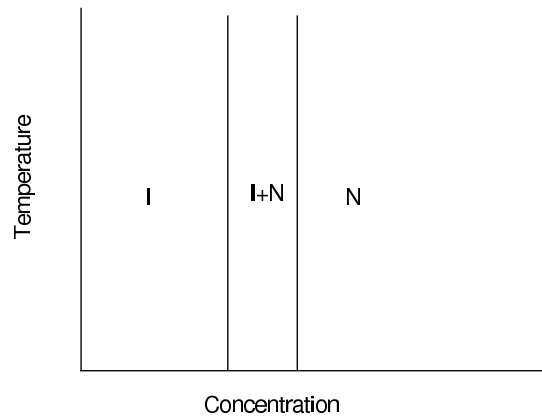


Figure 2.19: *Typical phase diagram for hard rods based on the Onsager model [62].*

This chapter ends with the remark that different authors have reported the formation of aggregate structures upon dissolving rigid rods, giving rise to an enormous increase in aspect ratio, corresponding to a shift of the isotropic-nematic transition to lower concentration, according to the equations 2.27 and 2.28 of Onsager's theory. In the work of Viale [17] aggregate formation of Sulpho-PpPTA in aqueous solution was reported. In similar systems Chu et al. [64] explained viscosity behaviour by an association model of molecules and based on shear experiments Mendes et al. [65] concluded the existence of needle like aggregates with small cross section that readily align upon shear. Cavalleri [66] found aggregate formation for block copolymers of poly(p-benzamide) and poly(m-phenylene isophthalamide) in DMA-LiCl.

In the next chapter where experimental results concerning PpPTA in NMP-CaCl₂ are presented it will become clear that in these metastable solutions aggregate formation occurs. The phase behaviour will be seen to agree with an Onsager model.

3. Structure, Stability and Kinetics of PpPTA in amide-salt Solutions

In this chapter the stability of solutions of PpPTA in NMP- CaCl_2 is investigated. It is found that these solutions form a nematic phase at a low PpPTA concentration. The solutions are meta-stable and evolve over time. Phase separation occurs along the formation of molecular aggregate structures that in a final stage crystallize.

3.1 Introduction

In the previous chapter an overview of the interaction mechanisms as can be found in literature was presented, followed by some introductory remarks on the models predicting transitions from the isotropic to the nematic phase. In this chapter experimental results are presented regarding this isotropic-nematic transition and meta-stable behaviour of PpPTA-NMP- CaCl_2 solutions. After having discussed the solution preparation process, metastable behaviour using microscopic and rheological measurements is presented. Next using calorimetric and again rheological techniques, a more detailed study on the NMP- CaCl_2 solvent is presented. The phase diagram of NMP- CaCl_2 is cleared up and effects of adding water or benzanilide (used as a model compound for PpPTA) are discussed. From ^1H -NMR experiments no stable complex formation between salt and NMP or benzanilide was detected but rather dynamical interactions were found to take place. Also there are indications for the formation of a mantle structure of NMP molecules around benzanilide at low salt concentrations. Electrical conductivities of NMP- CaCl_2 solutions, both with and without PpPTA, show electroweak behaviour and the presence of salt aggregates. The peculiar viscosity drop upon neutralization after polymerization as shown in figure 1.10 in chapter 1 is explained. Finally structure formation in PpPTA-NMP- CaCl_2 is shown using X-ray diffraction techniques.

These results nicely show structural changes in time responsible for the meta-stability observed. A "phase diagram" of PpPTA in NMP-CaCl₂ is given. As the phases indicated in this diagram are not stable, it is not a true phase diagram. The chapter therefore ends with the intriguing question why NMP-CaCl₂, in contrast to sulphuric acid, does not act as a true solvent and whether it is possible to construct a novel solvent based on a non-acidic medium. That will be the topic of the next chapter in which the thermodynamics of these solvents are treated.

3.2 Solvent and solution preparation

Solvents of NMP-CaCl₂ or NMP-CaCl₂-benzanilide used in the experiments were prepared using NMP extra dry, water content < 50 ppm, purity 99.5% from Acros Organics, CaCl₂ Anhydrous granular 99.5% from J.T. Baker and benzanilide, 98% from Acros Organics, CAS: 93-98-1, EINECS: 202-292-7.

CaCl₂ was dried for about 16 hours in an oven under vacuum at 250°C. NMP was further dried for over a week using a molecular sieve, type 3A at ambient temperature to a water content, < 20 ppm. The molecular sieve itself was first dried under vacuum at 250°C for about 16 hours.

Solutions containing also PpPTA were prepared by polymerization in a batch reactor with a volume of 160 l. Molecular weight was controlled by adjustment of the monomer ratio (PPD/TDC). After polymerization the mixtures contained 5 wt% PpPTA, from which batches containing less than 5 wt% PpPTA were prepared by dilution with NMP. Typical molecular weights (M_w) after synthesis range from 10000 to 30000 g/mol. The solvent used in these reactions was regenerated NMP-CaCl₂ from previous polymerizations.

By subsequently adding CaCl₂ to NMP at 25°C the maximum solubility was found to be approximately 5.5 wt% CaCl₂, above which solid precipitation occurred.

3.3 Meta-stability of the PpPTA-NMP-CaCl₂ solution

By observing the PpPTA in NMP-CaCl₂ solutions over time a transformation from a homogeneous solution to a phase separated one is seen. A sort of gelling out process of a highly viscous phase occurs. The rate at which this process takes place can vary from hours till many months depending on the solution characteristics and storage temperature. It has only been observed though, for solutions containing over 1 wt% PpPTA.

This meta-stable behaviour was confirmed in calorimetric and shear experiments. Especially the changing structure in time is remarkable.

Water has a negative influence on the so called stability of these solutions. In large quantities it is used as a coagulant after polymerization to precipitate and wash the polymer, but in smaller quantities water reduces the stability of such solutions. From a practical point of view this is undesirable and it is necessary to work under dry conditions during processing of these solutions. The observed features when adding water will be addressed further on.

3.3.1 Phase separation / Aggregate formation

In time it is visually observed that an NMP-CaCl₂-PpPTA solution solidifies. At lower PpPTA concentrations (< 2.5 wt%) a clear separate liquid phase, containing NMP is formed. At higher PpPTA concentrations the whole solution seems to solidify. The rate at which this process evolves can differ strongly depending on the specific conditions of the solution. A large number of solutions that were polymerized in the 160 l reactor have been judged visually over time at 21°C to gain insight in meta-stable behaviour. The criterion was the observation of solidifying of the solution. Solutions containing PpPTA concentrations between 2 wt% and 6 wt% and a molecular weight (M_w) between 10000 and 30000 g/mol, were examined. The visually observed stability varies randomly from a few days up to months. No clear correlation between either molecular weight or concentration of PpPTA and the stability of the solution was found. In figure 3.1 the solution stability is plotted against the molecular weight and polymer concentration.

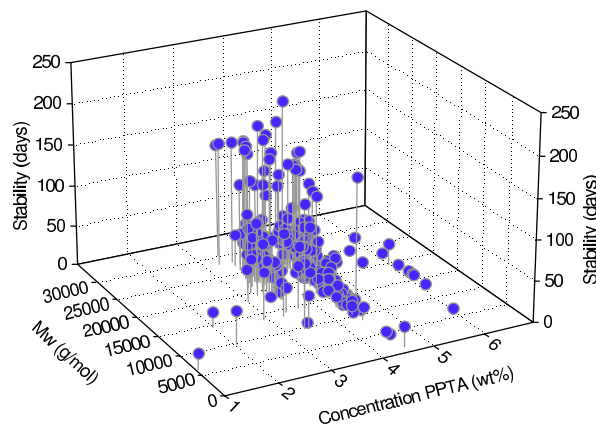


Figure 3.1: *Stability of solutions of PpPTA in NMP-CaCl₂ as a function of molecular weight and concentration of PpPTA, based on visual observation of phase separation and solidifying of the solutions.*

As the stability of solutions seem to vary largely under seemingly similar conditions four solutions were prepared and observed over time at different temperatures. Molecular weight (M_w) of the polymer was varied between 15000 g/mol and 23000 g/mol respectively. Conditions were chosen such that after polymerization the PpPTA concentration in all solutions was 5 wt%. Discharging from the reactor was done in parts and subsequently diluted with NMP to respectively 4-3-2.5-2-1.5 and 1 wt% PpPTA. Of each combination, molecular weight-polymer concentration, a sample was stored at -20°C , 4°C and 21°C . In time these samples were visually examined and the moment on visual transformation recorded. See figure 3.2.

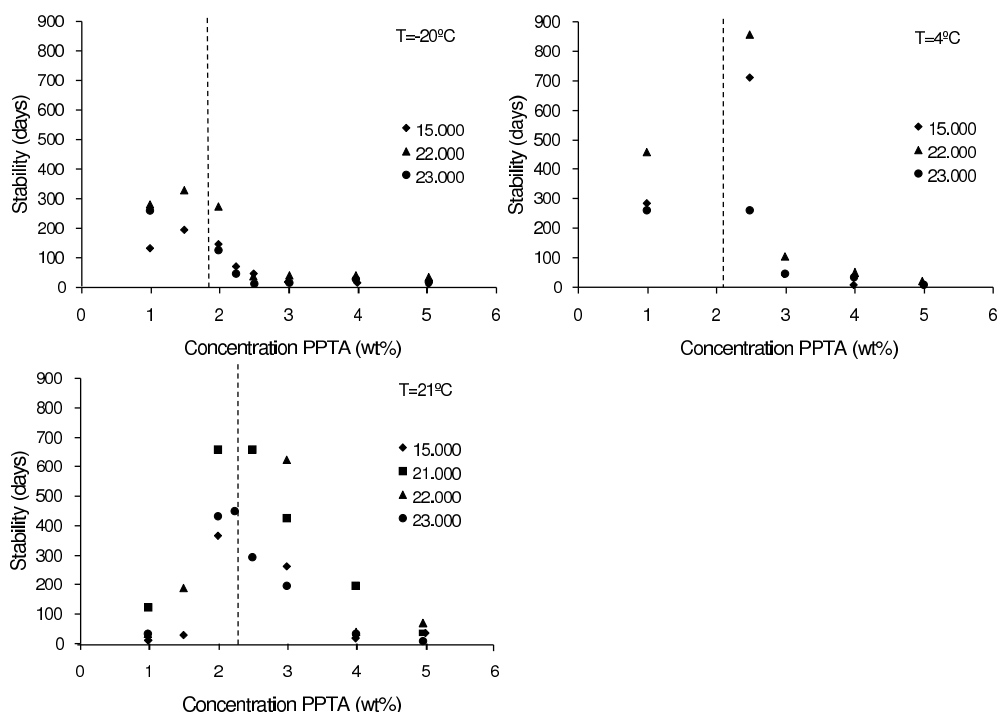


Figure 3.2: Stability of PpPTA-NMP-CaCl₂ solutions stored at different temperatures. M_w varied between 15000 and 23000 g/mol.

A maximum in the stability with respect to concentration is found, which seems to shift from 1.75 wt% to 2.25 wt% with increasing temperature. Also the actual maximum shifts from 350 days to over 900 days (at 900 days solutions between 1.5 and 2.25 wt% stored at 4°C and solutions between 2 and 2.5 wt% stored at 21°C were still found not to have solidified), where the most stable solutions occur at 4°C . The temperature dependence can be explained from kinetic and thermodynamic potentials with regard to the meta-stable behaviour. Higher temperatures result in faster molecular movement and thus

faster phase separation. This in contrast to lower temperatures in which case the thermodynamic potential towards phase separation increases and thus an optimum exists. Further similar analysis at elevated temperatures (35°C, 50°C and 80°C) revealed this optimum to lie between 4°C and 21°C. Finally no significant influence of molecular weight was found.

Besides visual observation also microscopic images between crossed polarizers were made to observe any structural changes. Six days after synthesis microscopic images were taken from some of the samples stored at 21°C, figure 3.3.

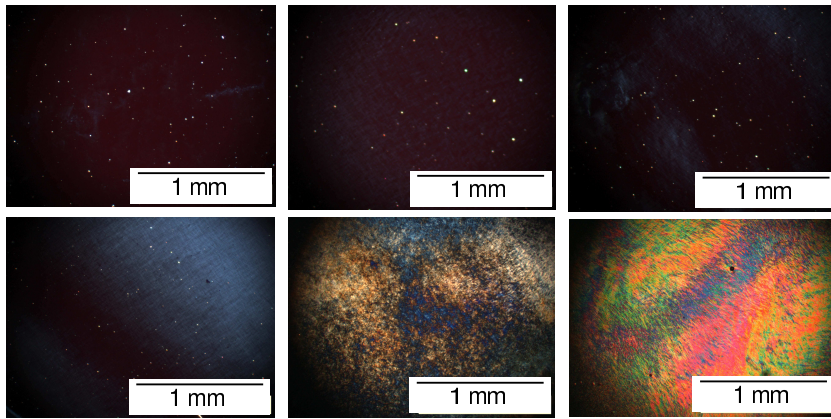


Figure 3.3: *Microscopic images of solutions taken 6 days after synthesis, between crossed polarizers. PpPTA: M_w 15000 g/mol and different concentrations in NMP-CaCl₂, from left to right and top to bottom 1.5-2-2.25-2.5-3-4 wt%, stored at 21°C.*

From 2.5 wt% PpPTA up, birefringence is observed, indicative for a nematic phase. The solutions stored at lower temperatures show identical pictures and are therefore not shown separately. The observed birefringence is at a surprisingly low concentration as for identical polymer solutions in sulphuric acid the isotropic-nematic solution is not observed until 8 wt% [56]. Images were taken again 36 days after synthesis from all samples, figure 3.4.

Besides the birefringent effect at remarkable low concentration, aggregate formation is observed in due time. Temperature is seen to have an influence on the rate of aggregate formation/phase separation as the images show different stadias of phase separation at different temperatures. The 1 wt% solution stored at 21°C also shows some signs of birefringence. This may be due to kinetic effects being more profound at higher temperature, hence accelerating crystallization of the polymer chains. The 2.5 wt% solution at -20°C already shows aggregate formation. All images of higher concentrations show aggregate formation and phase separation.

Images taken from a different solution, figure 3.5 show these aggregates

more clearly. Particles that have an eight-like shape were observed that seem to have grown from a center point in two opposite directions. One sample has been subjected to shear and as a result the aggregates have aligned.

Besides visual observation, meta-stability is also observed in flow behaviour. When a sample of a master solution is submitted to shear flow in a rotational rheometer, shear thinning occurs. When in time successive samples of this master solution are measured, the viscosity is seen to gradually drop over the whole range of shear rates followed by a sudden rather steep increase ending well above the initial value. Measurements were performed on a Haake Rheo Stress 600 rheometer with 2° cone-plate geometry. In figure 3.6 a typical time dependence of the shear viscosity is depicted. To accentuate the sudden increase in viscosity in figure 3.7 the upturn is made better visible by explicitly

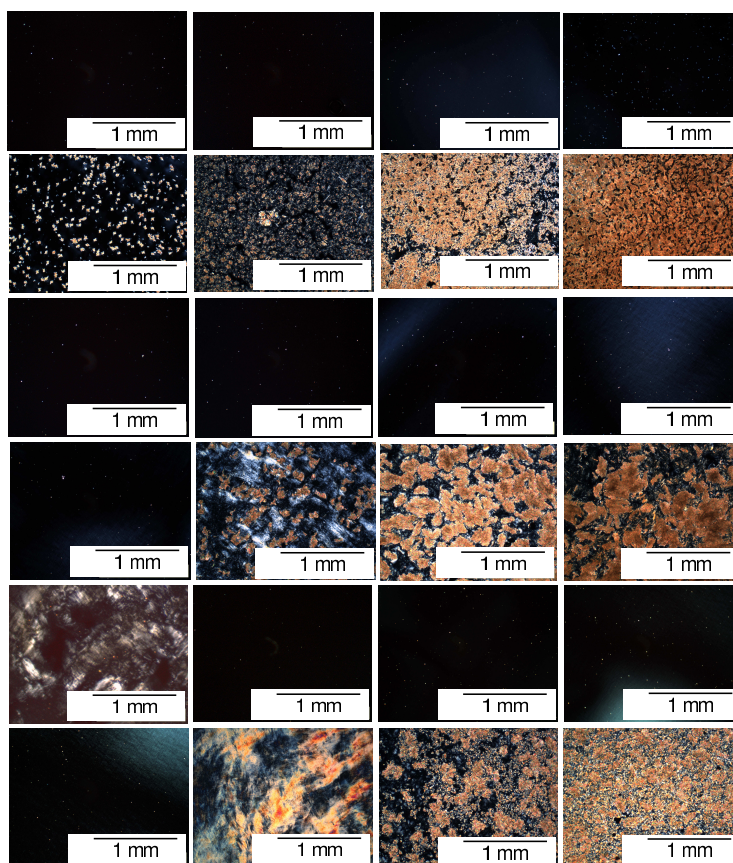


Figure 3.4: Microscopic images of solutions taken 36 after synthesis, between crossed polarizers. PpPTA: M_w 15000 g/mol and different concentrations in NMP- CaCl_2 stored at -20°C (row 1 and 2), 4°C (row 3 and 4) and 21°C (row 5 and 6). From left to right and top to bottom 1-1.5-2-2.25-2.5-3-4-5 wt% PpPTA.

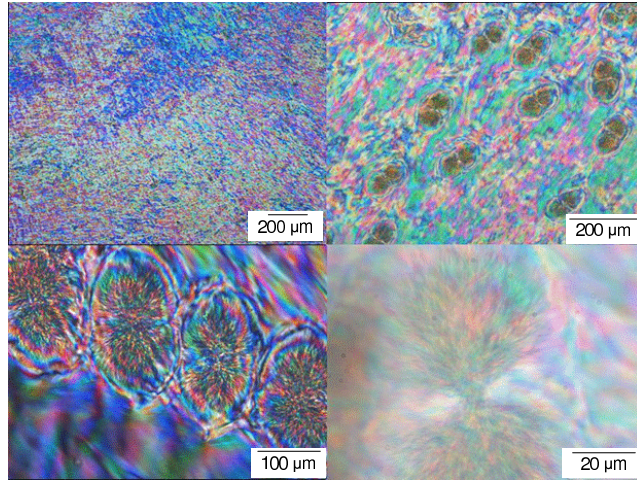


Figure 3.5: *Optical microscopic pictures taken of a solution between crossed polarizers. PpPTA: 3.8 wt%, M_w 17000 g/mol. The top left is taken 37 days after synthesis and shows no particles. Particle formation is not observed until 45 days after synthesis, other pictures.*

showing the viscosity behaviour in time at one specific shear rate (1 s^{-1}).

Samples from the same master solution were simultaneously subjected to calorimeter scan experiments ($0.2^\circ\text{C}/\text{min}$). In these scans a transition is observed at about 75°C . This transition is probably indicative of the phase separation as it was found to be irreversible and the solutions appear visually phase separated after heating. When samples of the master solution were scanned over time the endothermic heat effect became progressively smaller and finally disappeared, see figure 3.8. As it concerns an endothermic heat effect the corresponding entropy change is positive and is due to the increased freedom of the NMP molecules upon phase separation.

The disappearance of the heat effect coincides with visual phase separation of the master solution. Even more striking is the coincidence with the upturn of the viscosity in the shear flow experiments. At day 47 the transition has completely disappeared in the calorimetric scans and this is also the time that the shear viscosity starts to increase. The two phenomena thus seem related.

The birefringence appearing in the microscopic recordings of PpPTA concentrations of 2.5 wt% and higher indicates an isotropic-nematic transition and is discussed in more detail now.

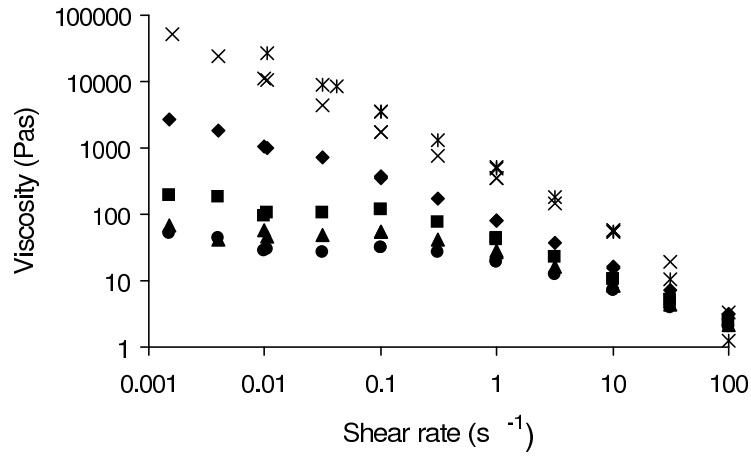


Figure 3.6: Rotational shear experiments, 2° cone-plate geometry, over time (numbers indicate days after the preparation of the master solution) of a NMP- CaCl_2 -PpPTA solution. PpPTA: 3.8 wt%, M_w 17000 g/mol. The viscosity is first seen to drop followed by a rather sudden increase.

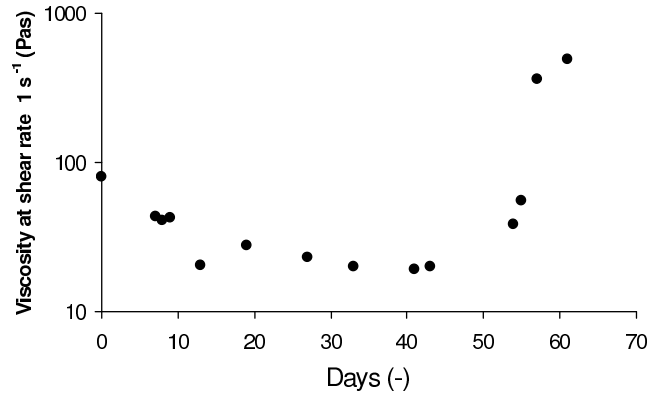


Figure 3.7: Rotational shear experiments, 2° cone-plate geometry, over time at shear rate 1 s^{-1} of a NMP- CaCl_2 -PpPTA solution. PpPTA: 3.8 wt%, M_w 17000 g/mol. The viscosity is first seen to drop followed by a rather sudden increase.

3.3.2 Isotropic-Nematic transition

A characteristic for the isotropic-nematic transition is a steep peak in the viscosity upon this transition. Normally increasing polymer concentration gives rise to an increase of the viscosity. At the transition however, the molecules start to align, leading to the forming of the nematic phase as discussed in chapter 2. This causes the shear viscosity in the direction of flow to drop. After further rise of the polymer concentration the viscosity will increase again. In figure 3.9 viscosity values, based on yield stress measurements in a rotation (2° cone-plate geometry) rheometer, are shown for three different molecular

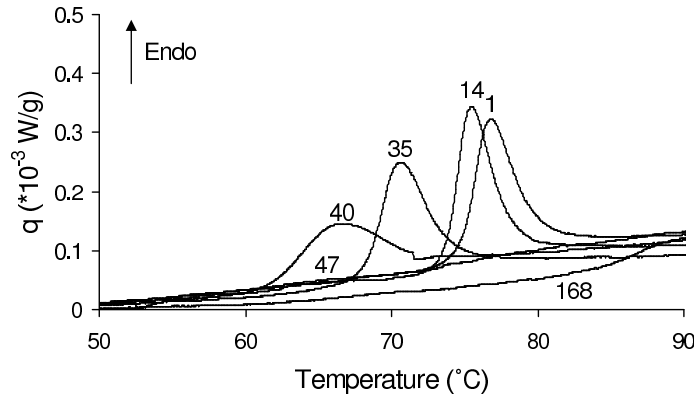


Figure 3.8: DSC scans (rate $0.2^\circ\text{C}/\text{min}$) over time of a NMP- CaCl_2 -PpPTA solution, PpPTA: 3.8 wt%, M_w 17000 g/mol. In time the endothermic heat effect disappears, indicated by the numbers in days.

weight polymers. The yield stress is determined by measuring the stress during a ramp of the shear rate. The point at which the sample starts shear thinning the stress (and related the viscosity) decreases by further increase of the shear rate. By extrapolating to zero shear the zero shear viscosity is obtained.

The peak in this viscosity, characteristic for an isotropic-nematic transition is found at about 2.5 wt% for all three samples.

The absolute maximum values of the shear viscosity increase by roughly two orders of magnitude when the molecular weight increases from 12000 to 18000 to 28000 g/mol. The results for the 28000 g/mol solution may be doubted as this material is highly viscous and may cause inhomogeneous filling of the rheometer during measurement. For this sample the double refractive index difference was measured as well, table 3.1. A significant value is already seen at 1.5 wt% and a jump is observed between 2.25 and 3 wt%, corresponding to the peak in the viscosity and the appearance of birefringence. Images 3.3 and 3.4 show birefringence from 2.5 wt% up.

From the double refractive difference the order parameter ($\langle P_2 \rangle$) can be estimated. Hereto the Debye equation is used to calculate the refractive indices in a mixture, based on pure substances [67].

$$\frac{\varepsilon_r - 1}{\varepsilon_r + 2} = \frac{\mathcal{N}}{3\varepsilon_0} \left(\alpha + \frac{\mu^2}{3kT} \right), \quad (3.1)$$

with \mathcal{N} the number density of molecules (the number per unit volume), α is the polarizability and μ the dipole moment of a specific substance. From the Maxwell equations the refractive index (this is the ratio of the speed of light

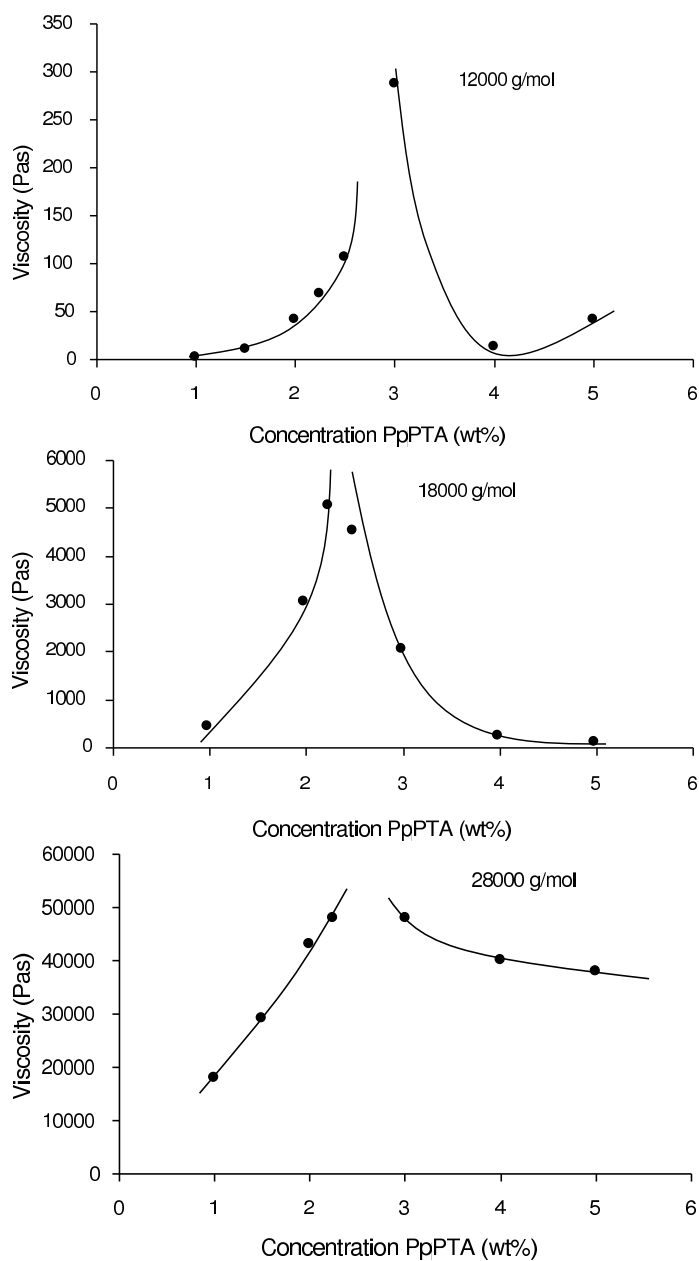


Figure 3.9: Zero shear viscosity of PpPTA in NMP- CaCl_2 based on yield stress measurements in a rotation rheometer for (top) M_w 12000 g/mol (middle) M_w 18000 g/mol and (bottom) M_w 28000 g/mol

in a vacuum to its speed in a medium: $n_r = c/v$) in a non-magnetic medium is related to the relative permittivity by $n_r^2 = \epsilon_r$. For a two component mixture the average refractive index follows from a mixing rule based on the relative weight of the components in the mixture. Hereof several are in use and Mehra [68] has compared different mixing rules for various binary systems. The conclusion was that all relations performed well within experimental error. Equation 3.2, the Lorentz-Lorentz mixing rule, is most frequently used.

$$\frac{n_{12}^2 - 1}{n_{12}^2 + 2} = \phi_1 \frac{n_1^2 - 1}{n_1^2 + 2} + (1 - \phi_1) \frac{n_2^2 - 1}{n_2^2 + 2} . \quad (3.2)$$

Here ϕ represents the volume fraction of the specific component in the mixture. The refractive indices of NMP and CaCl₂ given in table 3.2 result for a 4 wt% CaCl₂-NMP mixture in an average refractive index of $n_{NMP-CaCl_2}=1.48$.

The three principal refractive indices of PpPTA fiber, given in the same table, were determined by Yabuki et al. [69] according to the orthotropic model structure. These indices correspond to perfect alignment of the polymer molecules in a fiber. In the calculation of the corresponding refractive indices of PpPTA in a mixture with NMP-CaCl₂, again to according to equation 3.2, the refractive indices perpendicular to the molecular axis were taken average. The refractive index of 1.48 was used for the NMP-CaCl₂ solution

Table 3.1: *Double refractive index difference for a number of concentrations of PpPTA: M_w 28000 g/mol in NMP-CaCl₂, at 25° C.*

PpPTA (wt%)	Δn
1.00	0.0001
1.50	0.0009
2.00	0.0014
2.25	0.0012
3.00	0.0042
4.00	0.0060

Table 3.2: *Refractive indexes of some substances, at 25° C.*

Compound	average refractive index
NMP	1.47
CaCl ₂	1.60
CaCl ₂ .6H ₂ O	1.52
PpPTA _{⊥1}	1.73
PpPTA _{⊥2}	1.51
PpPTA _{//}	2.05

in which PpPTA was dissolved. This was done for all the weight fractions PpPTA mentioned in table 3.1. The outcome are values for the respective average perpendicular and parallel refractive indices of PpPTA in a mixture with NMP-CaCl₂. The difference of these values is the so called double refractive index difference and is plotted in figure 3.10 against the concentration PpPTA. Also the measured double refractive index differences as mentioned in table 3.1 are plotted together with the ratio of the measured- to the calculated values of the double refractive index. This ratio is a measure for the order parameter $\langle P_2 \rangle$.

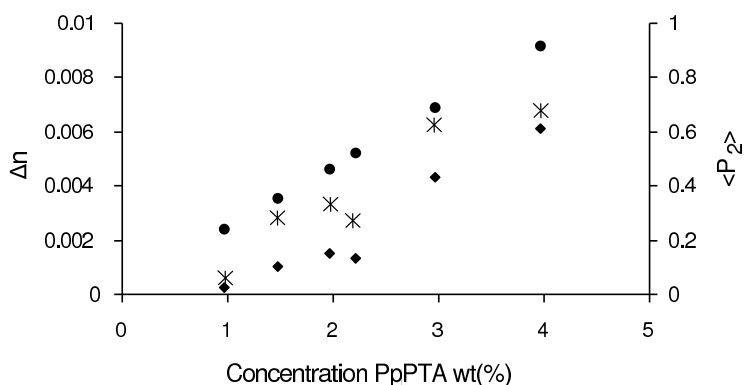


Figure 3.10: *Calculated double refractive index differences for perfect aligned PpPTA molecules at different concentrations in a NMP-CaCl₂ (4 wt%) solution (bullets) and measured values (checkers). The ratio of the two is expressed as the order parameter (asterisk).*

The order parameter is seen to increase from zero to 0.66 with a jump between 2 and 3 wt%. This indicates the isotropic-nematic transition around 2.5 wt%. In comparison with the Maier-Saupe and Onsager models the order parameter at the transition would be expected to be 0.43 and 0.84 respectively, as discussed in the previous chapter. The calculated order parameter at the transition lies in between these two values.

As stated before, the transition would be expected to occur at much higher concentration (8 wt%), corresponding to the transition of a solution of PpPTA in sulphuric acid. The low critical concentration can be explained by aggregate formation and an entropy driven transition as was explained at the end of the previous chapter.

Later on when the structure of these solutions is discussed this issue will be addressed again. First the phase behaviour of the solvent NMP-CaCl₂ is discussed to verify any structure formation herein before turning to the polymer solutions.

3.4 The NMP-CaCl₂ solvent system

In the past at the time of the search for a suitable polymerization medium for PpPTA, many salt-solvent combinations were tested at the Akzo Nobel laboratories. This was done on the basis of the solubility-swelling behaviour. These research efforts resulted in a patent of Vollbracht et al. [70] in which the CaCl₂-NMP medium was appointed the optimal system. It was found that the presence of CaCl₂ is essential to gain high molecular weight (in the order of 30000 g/mol) PpPTA during polymerization. If it is omitted immediate precipitation of low molecular weight polymer occurs. Water is used as a coagulant during processing and causes PpPTA to precipitate. It is therefore necessary that the polymerization medium is free of water. To some extent it is always present however, as will be shown up to limited amounts no negative effects were found.

In the NMP-CaCl₂ system under specific conditions solid complexes are present. The study at the time of process development mainly focused on these complexes as they appear in the CaCl₂ concentrations applied in the polymer production process (11 wt%). At lower CaCl₂ concentration, up until 6 wt%, these solid complexes are not observed. For spinning purposes this is attractive to develop a process to spin fibres or fibrils directly from this polymerization medium. To have an overview of the various phases existing in the NMP-CaCl₂ mixture, its phase diagram was cleared up. The exact conditions under which complex formation occurs are now known. When discussing the thermodynamics of these solutions in the next chapter, it will become clear why identification of complex formation is of great importance to predict whether a mixture is suitable as a dissolution medium and this knowledge will be used in order to predict the suitability of other non-acidic solvent systems.

3.4.1 Phase diagram of NMP-CaCl₂

Research activities within Akzo Nobel at the 1970's on NMP-CaCl₂ mixtures revealed different solid complex forms of NMP with CaCl₂. Maximum solubility of CaCl₂ in NMP was determined by equilibration of supersaturated mixtures at various temperatures. Afterwards the CaCl₂ content in the liquid and solid phase was determined. The techniques used to analyse the composition of the solid complexes vary from X-ray diffraction, thermogravimetric analysis (TGA) in which the NMP is evaporated to titration methods on chloride (complexometric titration (using EDTA), Mohr titration and potentiometric titration). In the liquid phase the chloride content was determined

through titration.

Three complex forms between NMP and CaCl_2 have been identified in solid form, $\text{CaCl}_2 \cdot 1\text{NMP}$, $\text{CaCl}_2 \cdot 2\text{NMP}$ and $\text{CaCl}_2 \cdot 6\text{NMP}$. Based on the data the transition regions from one solid complex to another were identified. The region in which no solid complexes are present could not be determined clearly from this data and successive experiments were needed. Calorimetric scan experiments of concentrations up to 10 wt% CaCl_2 in NMP were done to determine the transition from clear solutions to ones containing solid complexes and reverse. This enabled the construction of the phase diagram depicted in figure 3.11.

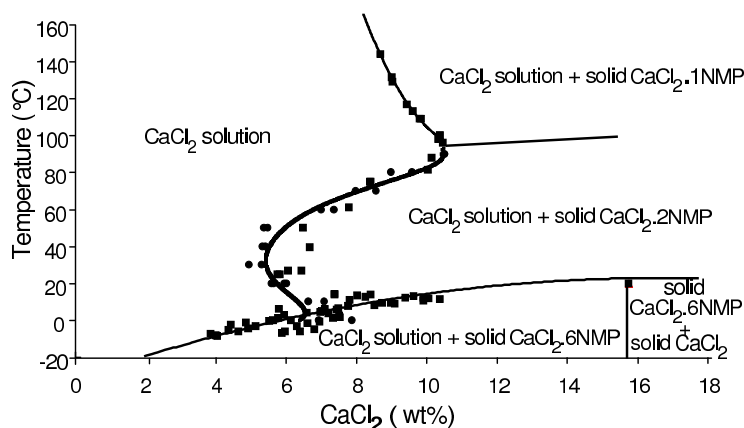


Figure 3.11: Phase diagram of CaCl_2 in NMP. Squares indicate phase transitions based on static temperature, supersaturated equilibrium experiments. Circles indicate phase transitions based on temperature scans from calorimetric analysis.

In large parts of the diagram solid complexes are present. At moderate temperatures only up to 5.5 wt% a solid free phase exists. This part of the diagram is of particular interest for performing dissolution experiments with PpPTA as it limits the possible interactions with the pure components NMP and CaCl_2 without interference of derivative products. (Possible solutions for spinning purposes need to be in this region as it is required that no solid particles are present for they have a negative effect on the mechanical properties of fibers.)

To investigate whether truly no particle formation is taking place in the solid free region it was checked for the existence of stable complex formation in a dissolved state. This was done on the basis of NMR experiments and these are discussed next.

As an NMR diagram of an NMP- CaCl_2 -PpPTA mixture would be very complex due to the presence of the different molecular weight molecules with

different end groups (carbonyl and amine) combined with the inherent meta-stable behaviour of such mixtures (possible PpPTA-PpPTA complexation) benzanilide, see figure 2.2, was used as a model compound for PpPTA in the experiments. This is a clearly defined molecule and does not form complexes with itself, and thus any dissolved complexes would be the result of interactions with NMP and/or CaCl₂. In this investigation also NMR measurements of LiCl, LiBr and HCl in combination with NMP and benzanilide were performed to gain insight in a more general way of the interactions of salt with NMP and benzanilide.

3.4.2 NMR on NMP-salt solutions

NMR experiments were performed to investigate the influence of different salts on complex formation with NMP, also the diffusion coefficients of NMP, were measured using 2D DOSY NMR, a technique explained further on. Samples were prepared in the solid free region of the phase diagram of NMP-CaCl₂ as well as samples of LiCl, LiBr and HCl in NMP containing no solids.

As water may very well interact with salt it is necessary to work under as dry as possible conditions. Therefore the NMP-salt solvent samples were prepared in a glove box to exclude water as much as possible. The solutions containing HCl were prepared by bubbling HCl gas through the NMP. Hereto in a separate vessel CaCl₂ was added to sulphuric acid, the formed HCl gas was subsequently bubbled through the NMP solution. The whole was covered under a nitrogen blanket.

The samples were measured as such in 5 mm NMR tubes containing a closed melting capillary filled with DMSO-d₆ for NMR lock and shimming, that were sealed by heating the tip. The NMR tubes were capped and then sealed. Spectra were recorded on a Bruker Avance DRX600 spectrometer with a proton resonance frequency of 600 MHz and a carbon resonance frequency of 150 MHz. 1D DOSY spectra are recorded to optimize acquisition parameters of 2D DOSY experiments. All spectra were recorded at 27°C.

In table 3.3 an overview of the sample contents is given.

The concentrations HCl are low compared to the salt containing samples due to experimental limitations. By bubbling HCl gas through NMP, the inlet tube of HCl got constipated after some time. According to Cox et al. [71] NMP is protonated in an acidic environment of sulphuric acid and protonation is complete in a 60% sulphuric acid environment. Gaseous NMP in the HCl inlet may readily be protonated, figure 3.15, as the inlet contains pure HCl and as such forms a solid structure.

The final concentration of HCl in NMP was measured by titration with

a 1 mol/l NaOH titrant (Metrohm 716 DMS Titrino, electrode: Metrohm Combined pH glass electrode 6.0233.100).

Diffusion

DOSY (Diffusional Ordered Spectroscopy) is a technique to measure the translational motion of a molecule and subsequently a diffusion coefficient can be calculated from it. The principal of this technique is to apply an external controlled magnetic field gradient. This gradient spatially encodes the position of each nuclear spin. This spatial distribution can be decoded after waiting a short time by applying a second gradient. If the waiting time is very short between the encoding and decoding gradients the spins will not have had a chance to change position and in turn the magnetization will refocus without a net phase change. The spins that have moved during the waiting time between the encoding and decoding steps will acquire a net phase change. The summation of the accumulated phases over the entire sample will lead to partial cancellation of the observable magnetization and hence an attenuation of the NMR signal. This signal attenuation is dependent on the strength of the applied gradients, the time between the gradients (diffusion time) and the diffusion coefficient of the molecules under study.

DOSY experiments were conducted on the same samples listed in table 3.3. The resulting diffusion coefficients of NMP are plotted in figure 3.12.

Almost linear relationships between the different salt concentrations and the diffusion coefficient of NMP are observed. In NMP samples to which HCl was added only a slight effect on the diffusion coefficient of NMP is seen. CaCl_2 is most effective in complex formation with NMP, compared to HCl and both lithium salts, and results in the stronger decrease in diffusion coefficient of

Table 3.3: *Samples of salts and HCl dissolved in NMP used in NMR recordings.*

Sample number	CaCl_2 (wt%)	LiCl (wt%)	LiBr (wt%)	HCl (wt%)
1	-	-	-	-
2	2	-	-	-
3	4	-	-	-
4	6	-	-	-
5	-	2	-	-
6	-	4	-	-
7	-	-	2	-
8	-	-	4	-
9	-	-	-	0.5

NMP. Combining the viscosity data with the diffusion coefficients the average hydrodynamic radius r_s of each of the complexes formed can be estimated using the Stokes-Einstein equation (implicitly assuming spherical geometries of the complexes):

$$D = \frac{kT}{6\pi\eta r_s} , \quad (3.3)$$

where k is the Boltzmann constant, T the absolute temperature, η the dynamic viscosity and r_s the hydrodynamic radius of a sphere. In order to calculate the dynamic viscosity the kinematic viscosities (ν) and densities (ρ) for various NMP-CaCl₂ solutions were measured. The density of the samples was determined by hollow oscillator measurement, using an Anton Paar DSA 5000 Density & Sound Analyzer.

A U-shaped tube is filled with the sample, using a pump. The tube is held at a constant temperature of 25°C and vibration is applied. The resonant frequency of the vibration depends on the mass of the tube and hence - since at constant temperature the internal volume of the tube is constant - on the density of the substance within the tube. The frequency is measured and converted to the density.

The kinematic viscosity was measured using the Ubbelohde method. Hereto the flow time of the sample is measured at 25°C in an Ubbelohde viscometer. The kinematic viscosity is then calculated by multiplying the flow time (t) by the known Ubbelohde constant. The dynamic viscosities were calculated from

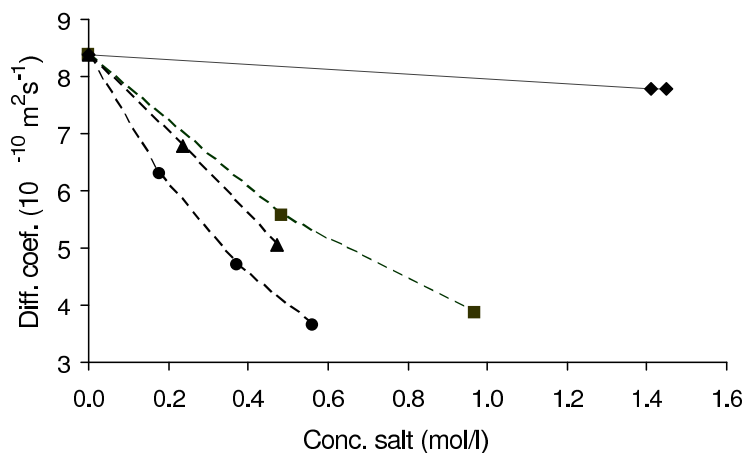


Figure 3.12: Diffusion coefficients of NMP, based on DOSY measurements and calculated using the Stokes-Einstein relation, for solutions of CaCl₂, LiCl, LiBr and HCl at various concentrations in NMP.

these measurements and follows from the relationship:

$$\eta = \rho \cdot \nu . \quad (3.4)$$

In table 3.4 for each solution the average diffusion coefficient, average hydrodynamic radius of NMP together with the density and dynamic viscosity are listed.

Table 3.4: *Diffusion coefficients of NMP (determined by DOSY), density, kinematic viscosity, dynamic viscosity and average hydrodynamic radius of NMP-salt solutions.*

Salt (wt%)	D_{NMP} ($10^{-10}m^2/s$)	ρ (kg/m^3)	ν ($10^{-6}m^2/s$)	η ($10^{-3}Pas$)	$r_{s,NMP}$ ($10^{-9}m$)
Pure NMP	8.38	1032.6	1.61	1.662	0.158
CaCl ₂ (2)	6.30	1050.4	2.15	2.258	0.154
CaCl ₂ (4)	4.70	1065.4	2.84	3.026	0.154
CaCl ₂ (6)	3.66	1083.3	3.92	4.247	0.142
LiCl (2)	5.56	1044.6	2.40	2.507	0.154
LiCl (4)	3.85	1058.6	3.80	4.023	0.164
LiBr (2)	6.78	1069.3	2.04	2.181	0.145
LiBr (4)	5.06	1066.2	2.77	2.953	0.170
HCl (0.48)	7.78	1031.1	1.69	1.745	0.187
HCl (0.52)	7.78	1031.1	1.66	1.714	0.161

The calculated hydrodynamic radius of pure NMP is somewhat smaller than would be expected from a calculation based on the density alone (0.27 nm). It must be realized though, that the Stokes-Einstein equation assumes spherical particles. More important are relative changes in the hydrodynamic radius, indicating interactions. It is clear that an increase in the viscosity results in a decrease in diffusion coefficient.

For both lithium salts the hydrodynamic radius of the complexes that are formed, only show a slight increase with increasing concentrations of salt. For CaCl₂ a slight decrease of the hydrodynamic radius is observed with increasing the salt concentration. These observations suggest that the influence of the salt on the hydrodynamic radius is very moderate and underline the dynamic nature of the complexes, with exchange rates much faster than the NMR detection rate. This agrees with results published by Vert et al. [42], mentioned in chapter 2.

¹³C-NMR

Carbon NMR shows that addition of salts to NMP causes polarization of the carbonyl group of the solvent. Through this polarization de-shielding of

all carbon sites within NMP is induced resulting in a downfield shift, with the carbonyl site most affected. In the case of a downfield shift electrons are withdrawn from a chemical site causing less shielding from the applied magnetic field. Upfield shifts are caused by increased shielding through a denser electron cloud.

A similar effect by ^{13}C NMR was found by El-Kafrawy [72] in solutions of cellulose in LiCl-NMP . The formation of these polarized NMP molecules is shown in schemes 3.13, 3.14 and 3.15.

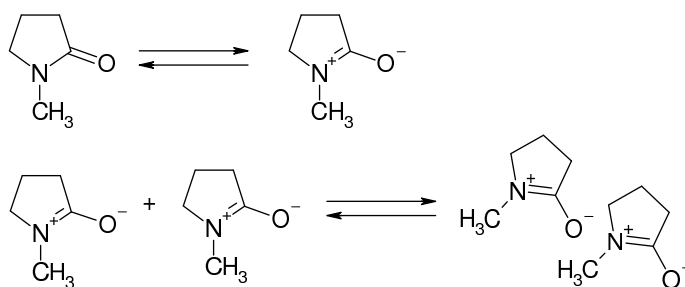


Figure 3.13: Formation of a Zwitter-ion due to keto-enol tautomerism, followed by NMP-NMP complexation

In the case of salt addition a complex between NMP and the salt is possibly formed as given for CaCl_2 as an example.

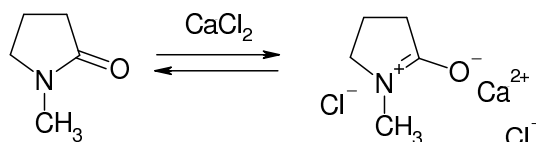


Figure 3.14: Complexation of NMP with CaCl_2 .

In contrast to salt, addition of HCl will probably protonate the NMP resulting in a protonated complex. The consequence of complexation with salt or protonation with HCl is that the formation of NMP-NMP complexes will be less favourable.

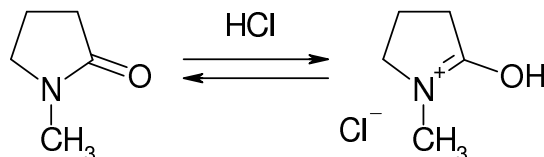


Figure 3.15: Protonation of NMP upon interaction with HCl .

In graph 3.16 the chemical shift for each carbon peak (Hz/(mol/l)) relative to the blank value of NMP is shown (average values of the chemical shifts for the different amounts of salt used in the various experiments are shown). The chemical shifts are numbered according to the carbon numbering in the NMP scheme. The experiments obviously show that the carbonyl carbon is the most affected site within NMP.

From this data it is clear that addition of CaCl_2 causes much more polarization of NMP compared to both lithium salts. LiBr shows more polarization of NMP compared to LiCl. This is in agreement with the findings of El-Kafrawy [72]. The greater de-shielding effect of the bromide over the chloride anion can be explained by the fact that bromide is a stronger nucleophile than chloride. Therefore, bromide can enhance the polarization of the carbonyl group by nucleophilic attack.

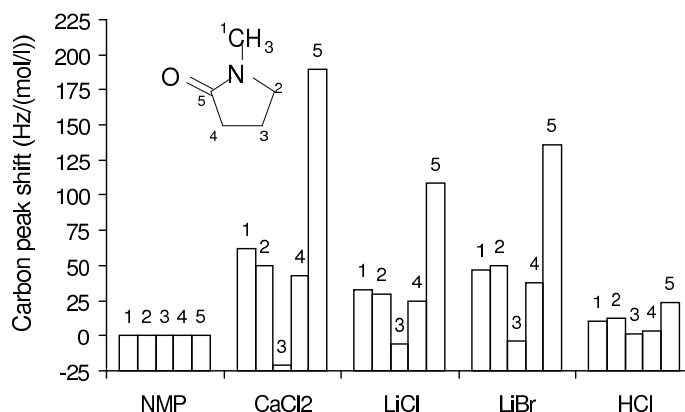


Figure 3.16: Chemical shifts of ^{13}C upon dissolving different salts or HCl in NMP relative to pure NMP. The numbers correspond to the carbon numbering in the NMP molecule shown.

The shifts found for HCl added to NMP are far less significant than those for the salts. This could be caused by the fact that HCl probably forms a different complex with NMP resulting in the protonation of the carbonyl group of NMP according to scheme 3.15. On the other hand this would result in a much more pronounced effect on the chemical shifts observed or even resulting in the appearance of a NMP sub spectrum representing the more stable complex formed.

It should be noted that the absence of this sub spectrum can also be explained by the low amount of HCl added, resulting in complex formation below the detection limit of the ^{13}C spectra recorded. In the spectra of salt-NMP solutions no sub spectra are observed either. This indicates that the average lifetime of complexes between salt and NMP is below $1 \cdot 10^{-8}\text{s}$, corresponding

to a resonance frequency of 150 MHz.

The downfield shift of the carbonyl carbon correlates well with the results found for the diffusion coefficients and viscosity. Again from these results it can be concluded that CaCl₂ followed by LiBr and LiCl is the most effective dynamic complex former with NMP. Moreover, a downfield shift suggests interaction with the cation due to decreased electron density at the carbon nucleus.

¹H-NMR

Apart from the carbon spectra measured also proton spectra were recorded. In contrast to the downfield shift observed for carbon, the proton chemical shifts of NMP with added salt show an upfield shift compared to NMP without added salt. This seems to suggest that withdrawal of the electrons from the carbon nucleus induces a denser electron cloud (current) around the proton nucleus resulting in increased shielding (results not shown). On the contrary, for the NMP with HCl added, the proton spectrum shows a downfield shifted sub spectrum that could represent a stable NMP-HCl complex, see figure 3.17. From the integral values that could be obtained it was estimated that 15% of the HCl added has formed a complex with NMP. Also, more of the impurity N-Methyl-succinimide (NMS) is observed within the NMP sample with HCl added. Introduction of HCl in NMP catalyses the formation of NMS.

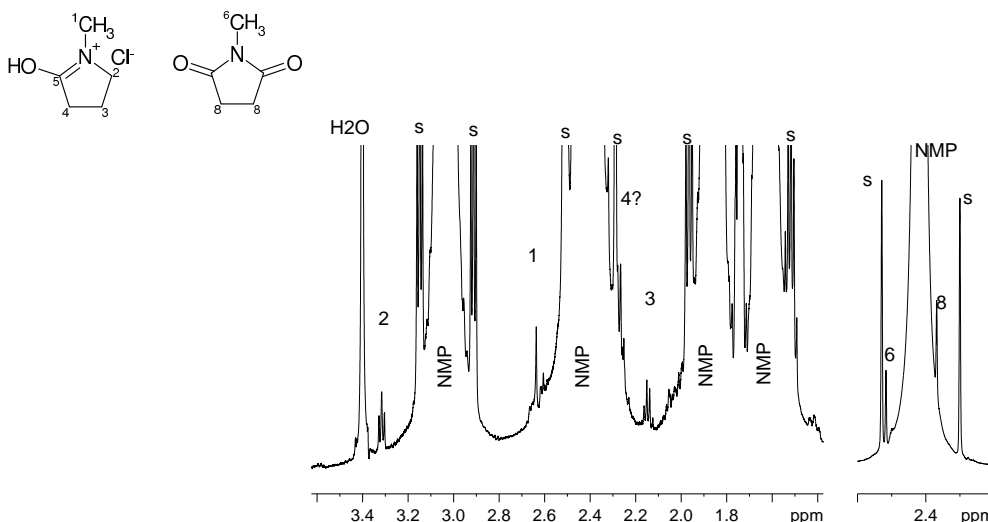


Figure 3.17: ¹H NMR spectrum of HCl in NMP. Next to the NMP signal a minor sub spectrum is seen originating from the protonated NMP. S indicates the ¹³C shuttle. On the right an inset around 2.4 ppm shows signals from N-methylsuccinimide, a known oxidation product of NMP. Signals are numbered according to the numbers in the molecules.

Again the missing of sub spectra for the salt containing samples suggests that dynamic complexes rather than stable complexes with the added salts and NMP are formed.

3.4.3 NMR with addition of benzanilide

To investigate the influence of LiBr and LiCl on the solution properties of PpPTA, 4 wt% benzanilide was dissolved as a model compound in NMP in the presence of different levels of LiCl and LiBr and CaCl₂. By means of ¹H and ¹³C NMR the effects on both NMP and benzanilide can be studied. Also now the diffusion coefficients of the individual components were measured by DOSY NMR. Combining these data with viscosity data on the same solutions the hydrodynamic radius of the dissolved components were calculated which provided a good indication of the nature of potential complexes formed. In table 3.5 the samples containing benzanilide, used in the experiments, are listed.

Table 3.5: *Samples of salts dissolved in NMP-benzanilide (4 wt%) solutions, used in NMR recordings.*

CaCl ₂ (wt%)	LiCl (wt%)	LiBr (wt%)
-	-	-
2	-	-
4	-	-
-	2	-
-	4	-
-	-	2
-	-	4

Benzanilide was used as a model compound for PpPTA to measure the effect of the addition of different salts in variable concentrations on the solution properties. Both ¹H and ¹³C NMR spectra were recorded of 4 wt% benzanilide in NMP with 2 wt% wt and 4 wt% of LiCl, LiBr or CaCl₂ added. In analogue to the observations made for a NMP-cellulose solution made by El-Kafrawy et al. [72] it is expected that addition of salts to the solvent system results in polarization of both the solvent and solute. This polarization affects the electron density of the different carbon and proton sites within the solvent and solute resulting in either up or down field chemical shifts with increasing salt concentration.

Chemical shifts of benzanilide

To study the effect of different salts on the benzanilide-NMP solvent the ^1H chemical shift of the amide proton, and both the meta- and ortho-protons of the anilide ring were plotted against the salt concentration in mol/l, figure 3.18. Above approximately 0.2 mol/l, the molarity of benzanilide, the chemical shifts of benzanilide change far less by further salt increase.

Panar and Beste [44] have done similar experiments with benzanilide in tetramethylurea and dimethylacetamide and they also observed no changes in the amide chemical shift above equimolar quantities of salt and benzanilide. This indicates that either the cation or anion associates with benzanilide resulting in polarization of the amide linkage. Based on electrophoresis data on similar solvent systems they concluded that the chloride associates with the amide unit of benzanilide. The appearance of a downfield shift at the amide proton would indicate association with a cation. In the case of benzanilide the interaction structures are however far more complicated than in the previous case of addition of salt to NMP, as will become clear further on.

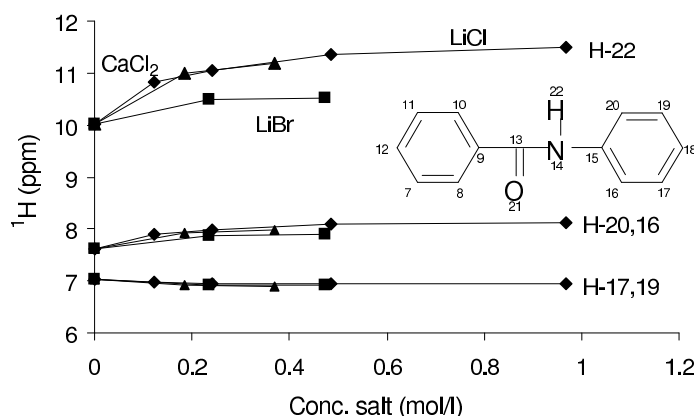


Figure 3.18: ^1H chemical shift of benzanilide (0.2 mol/l) in NMP against the salt concentration in mol/l.

In figure 3.19 all the chemical shifts for the protons of benzanilide are shown. Protons close to the amide and of the amide itself show downfield shifts, protons far from the amide an upfield shift. This indicates less electron density at the amide group. The most effective interaction is with CaCl_2 .

Similar effects of salts on the ^{13}C chemical shifts were found. Addition of salts results in a downfield shift for the carbons in close vicinity to the amide group except for the quaternary carbon belonging to the benzoyl ring and the carbonyl group. All other carbons show an upfield shift. Also these results clearly show that the amide linkage is polarized by the presence of salt. Again

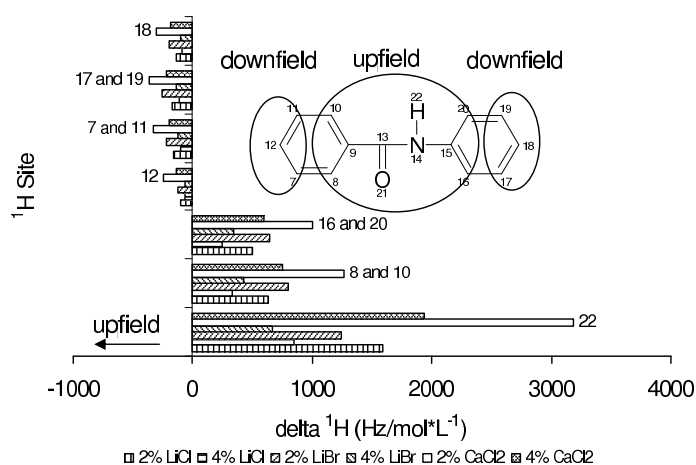


Figure 3.19: ^1H chemical shift ($\text{Hz}/(\text{mol}/\text{l})$) of benzanilide ($0.2 \text{ mol}/\text{l}$) in NMP against the salt concentration in mol/l of different salts. The shifts are numbered according to the numbers of the benzanilide molecule.

the chemical shifts do not seem to change above an equimolar benzanilide:salt ratio.

Chemical shifts of NMP

To see whether introduction of benzanilide to the solvent affects the solvent properties, the difference between NMP-salt or NMP-salt-benzanilide and blank NMP ^{13}C chemical shifts was calculated in $\text{Hz}/(\text{mol}/\text{l})$. The values obtained for the chemical shifts of the carbonyl carbon when salt is introduced are represented in figure 3.20. The data suggests that introduction of benzanilide in a NMP-salt solvent does not result in less polarization of the NMP molecule. Consistently, the 2 wt% solutions of LiBr, LiCl and CaCl_2 in NMP containing benzanilide do show increased polarization of the carbonyl group of NMP compared to NMP-salt solutions without benzanilide.

Panar [44] showed that there is a strong preference of the chloride anion to associate with benzanilide and in the previous section it was shown that NMP preferentially interacts with the cation. This indicates that up to equimolar quantities of salt:benzanilide the carbonyl of NMP associates with the cation leaving a charged NMP molecule. At higher salt concentrations this charged NMP molecule is neutralized by the anions not associated with benzanilide.

These results suggest the promotion of ion pair formation above a 1:1 ratio of benzanilide to salt. Similar results were discussed in chapter 2, see figures 2.8, 2.9 and 2.10 and references [37] ... [40].

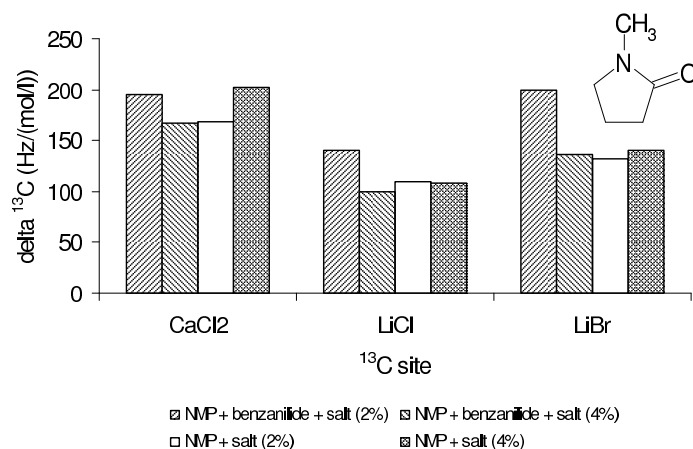


Figure 3.20: ^{13}C chemical shifts of the carbonyl group of NMP for different salts and concentrations with and without benzanilide.

Diffusion

The data up till now indicates that complex formation between salts and NMP or benzanilide can take place. However, benzanilide-salt-NMP complexes can form also. In combination with viscosity measurements, DOSY NMR was used to detect the presence of such complexes. DOSY separates different components within a solution according to their average diffusion coefficient. The Stokes-Einstein equation was used again to estimate the hydrodynamic radius of the complexes formed. In figure 3.21 the diffusion coefficients obtained for NMP were plotted against the salt concentration in mol/l. At low concentrations the diffusion coefficients of NMP without benzanilide are much higher indicating that apart from the salts themselves also benzanilide influences the diffusion coefficient of NMP. It may be caused by the effect that benzanilide has on the viscosity of the system. On the other hand the results obtained for the ^{13}C chemical shifts, figure 3.20, also show that the carbonyl of NMP is much more polarized at the lower salt concentrations. Since, the degree of polarization strongly influences the diffusion coefficient it is more likely that this, rather than the viscosity of the mixture explains the difference in diffusion coefficients.

At higher salt concentrations the diffusion coefficients of NMP, with or without benzanilide added, come more alike, most profoundly seen for LiBr in the top graph of figure 3.21. In the bottom graph of the same figure the diffusion coefficients found for benzanilide are plotted against the salt concentration in mol/l. It clearly illustrates that upon increasing the salt concentration the diffusion coefficient decreases. From this it can be concluded that apart from

NMP-salt complexes also benzanilide salt complexes are formed. The drop of the diffusion coefficient between 0 and 2 wt% added salt is much stronger than between 2 and 4 wt% of added salt. Again this seems to correlate well with the more effective polarization of both NMP and benzanilide at lower concentrations. More importantly, as the diffusion coefficients of NMP with or without benzanilide come closer, this also indicates that above a certain concentration no additional effect on the diffusion coefficient can be expected.

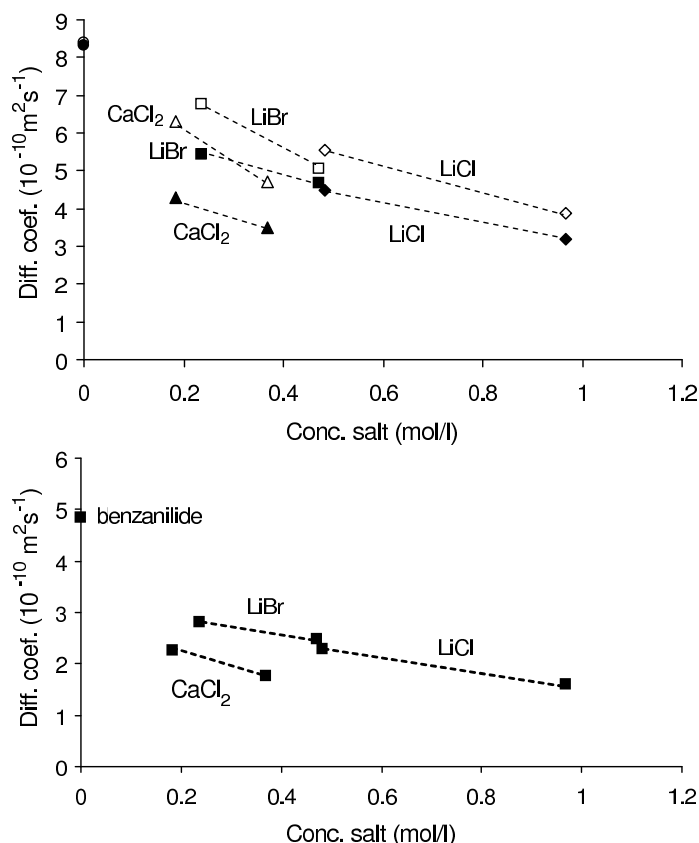


Figure 3.21: Diffusion coefficients, based on DOSY measurements and calculated using the Stokes-Einstein relation. Top figure: diffusion coefficients of NMP measured in solutions of various salt concentration to which either no benzanilide (open symbols) or 4 wt% benzanilide (filled symbols) is added. Bottom figure: diffusion coefficient of benzanilide measured in solutions of various salt concentrations.

The data obtained from the Stokes-Einstein equation are listed in table 3.6. The value for the hydrodynamic radius calculated for benzanilide 0.25 nm is smaller than calculated from the density of benzanilide, 0.4 nm, an effect also found for NMP. The measured viscosity of the NMP-benzanilide mixture, $1.84 \cdot 10^{-3}$ Pas, is what would be expected from the Einstein relation for mixtures, $1.83 \cdot 10^{-3}$ Pas. This relation relates the increase in viscosity to

the volume fraction of the dissolved compound and is expressed as a relative number.

$$\varepsilon_{rel} = 1 + 2.5\phi, \quad (3.5)$$

in which ϕ is the volume fraction of the dissolved compound. Given the fraction benzanilide of 4 wt% and a density of 1.03 g/cm³, equation 3.5 yields 1.1 as the relative number and thus $1.83 \cdot 10^{-3}$ Pas as the expected viscosity (using $1.66 \cdot 10^{-3}$ as the viscosity for pure NMP, as given in table 3.4). This calculation was done for all solutions and the calculated prediction is also given in table 3.6 between brackets in the column listing the dynamic viscosities based on measurements with benzanilide added. Most values are slightly larger than expected based on the addition of benzanilide only indicating somewhat larger particles.

The values obtained for the hydrodynamic radius of NMP in the case LiBr and larger amounts of LiCl are added, are similar compared to the data obtained for NMP without benzanilide, table 3.4. When CaCl₂ or a smaller amount of LiCl is added, the hydrodynamic radius of NMP and benzanilide increase, suggesting that benzanilide is probably surrounded by several NMP molecules forming a kind of mantle structure. Such a structure has been suggested by Panar [44] as was shown in the previous chapter.

Table 3.6: *Diffusion coefficients of NMP and benzanilide (determined by DOSY), density, kinematic viscosity, dynamic viscosity and average hydrodynamic radius of solutions of NMP-salt-benzanilide (4 wt%) solutions. The dynamic viscosities given between brackets are values calculated from the Einstein relation for mixtures according to equation 3.5.*

Salt wt%	D_{NMP} $10^{-10}m^2/s$	D_{benz} $10^{-10}m^2/s$	ρ kg/m^3	ν $10^{-6}m^2/s$	η $10^{-3}Pas$	$r_{s,NMP}$ $10^{-9}m$	$r_{s,benz}$ $10^{-9}m$
benz-NMP	8.32	4.85	1030.1	1.79	1.84 (1.83)	0.14	0.25
CaCl ₂ (2)	4.29	2.26	1054.7	2.42	2.55 (2.49)	0.20	0.38
CaCl ₂ (4)	3.48	1.76	1071.2	3.30	3.53 (3.33)	0.18	0.35
LiCl (2)	4.48	2.29	1053.3	2.30	2.42 (2.75)	0.20	0.40
LiCl (4)	3.19	1.60	1065.1	4.42	4.71 (4.43)	0.15	0.29
LiBr (2)	5.43	2.82	1058.7	2.70	2.86 (2.40)	0.14	0.27
LiBr (4)	4.68	2.48	1069.3	2.94	3.14 (3.25)	0.15	0.28

Interaction of benzanilide and NMP with different salts

Combining the data obtained from the different NMR experiments and viscosity measurements it turns out that the properties of the solutions are dependent on the type and concentration of salt added. Using the combined data and known mechanisms of similar solvent systems containing cellulose

[72], [73], [74] poly(1,4-benzamide) [44], poly amic acid [75] and model amides [76] [77] [23] [78] some possible complexes are hypothesized. CaCl_2 shows the strongest effect on both NMP and benzanilide followed by LiCl . At 2 wt% of added CaCl_2 and LiCl the average radius increases by approximately 50% indicating that benzanilide is surrounded by NMP molecules or that the addition of salt results in slower exchange rates of the complexes resulting in a higher average hydrodynamic radius figure 3.22 (a similar structure is expected in the case of CaCl_2 , although from molecular modeling results, to be presented in chapter 5, calcium is expected to interact less strong with the polymer due its size). At 4 wt% of added salt probably enough salt is present to shift the equilibrium more towards a 1:1 salt-NMP complex, see figure 3.14 (a similar structure is expected in the case of LiCl) making less salt available for complex formation with benzanilide. This mechanism will lower the average hydrodynamic radius of benzanilide as observed for LiCl and to some extent for CaCl_2 , see table 3.6. The effect is not seen in the case of LiBr . Apparently bromide does not interact strongly with benzanilide as also in a 2 wt% mixture the hydrodynamic radius of benzanilide is similar to that of benzanilide in pure NMP.

The results found by Federov et al. [28] as discussed in the previous chapter are worth mentioning here. They reported an optimum in molecular weight during polymerization with respect to the salt concentration, which was attributed to ion pair formation at higher salt concentrations. Ion pairs lead to decreasing charge on the polymer chains, see figures 2.8 ... 2.10.

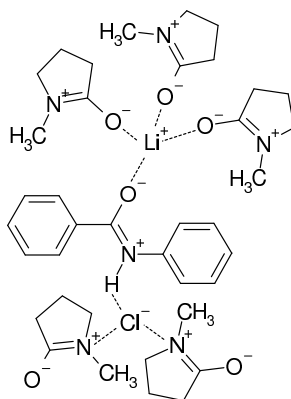


Figure 3.22: *Formation of a NMP-benzanilide-salt complex. At low salt concentrations competition for the salt occurs between NMP and benzanilide. Exceeding the molar amount of benzanilide salt will complex with NMP and hence lower the average hydrodynamic radius.*

With regard to complex formation in the solid free part of the phase di-

agram of NMP-CaCl₂ the electrical conductivity was studied to gain insight into the presence of ionic particles.

3.4.4 Electrical conductivity measurements in NMP-CaCl₂(-PpPTA)

The electrical conductivities ¹ of NMP-CaCl₂ mixtures both with and without PpPTA were measured to gain insight into the manner in which NMP-CaCl₂ mixtures behave as an electrolyte.

Conductivity measurements were carried out on a InoLab Cond Level 1 from WTW. Various series of samples were measured. The first series contained 0.1 to 5 wt% CaCl₂ in NMP the others also contained PpPTA or benzanilide in the range from 0.1 to 6 wt%, where the amide-unit concentration was always equal to the CaCl₂ concentration on a weight basis.

In this way the conductivity was measured as a function of the CaCl₂ concentration. Additionally, three solutions of NMP containing 4 wt% benzanilide and different concentrations CaCl₂ were also measured to investigate possible effects on the conductivity when a difference in concentration between amide-units and CaCl₂ is present.

Additions of PpPTA or benzanilide were found not to influence the conductivity significantly, indicating bi-phase behaviour in which the conductivity is predominantly determined by the NMP-CaCl₂ phase. Also the viscosity of the mixture increases enormously upon adding PpPTA, though no significant influence on the conductivity is observed. In all cases it was found that the molar conductivity decreases rapidly as the concentration CaCl₂ is increased. This indicates weak electrolyte behaviour. In the case of not neutralizing the polymer mixture after polymerization the conductivity remains a factor two to three higher than in the case of neutralization. Normally CaO is added to neutralize the HCl in order to obtain less viscous and better processable mixtures, to be discussed shortly.

In order to determine the amount of CaCl₂ present in ionic form, the following equilibrium relation is defined:



Y^+ represents an arbitrary cation and X^- an arbitrary anion. As the equation, in this form, is arbitrary in molar quantities n can be set to unity. Through this definition of the equilibrium the possibility remains for CaCl₂

¹From here on, in the remainder of this chapter, the term conductivity is used to express electrical conductivity unless explicitly stated otherwise.

molecules to form complexes. From definition 3.6 an equilibrium constant can be defined:

$$K = \frac{(\nu_+ \alpha)^{\nu_+} (\nu_- \alpha)^{\nu_-}}{1 - \alpha} C_0^{(\nu_+ + \nu_- - 1)} . \quad (3.7)$$

Here α represents the fraction of CaCl_2 in ionic state and is equal to the ratio of the CaCl_2 concentration in the equilibrium state over the initial CaCl_2 concentration, C_0 . Herein it is assumed that activities can be represented by concentrations. This ratio is assumed to be equal to the molar conductivity in the equilibrium state over the molar conductivity at infinite dilution (also known as the limiting conductivity).

$$\alpha = \frac{1 - [\text{CaCl}_2]_{t \rightarrow \infty}}{[\text{CaCl}_2]_{t=0}} = \frac{\Lambda_m}{\Lambda_m^0} . \quad (3.8)$$

The limiting molar conductivity was obtained by fitting the experimentally determined values of the molar conductivities for the CaCl_2 solvent, as shown in figure 3.23, using a kinetic fit function and was found to be $0.0044 \text{ Sm}^2/\text{mol}$. In the measurement of the molar conductivity also viscosity and ionic atmosphere effects are present. Both effects result in decreased mobility and therefore decreased conductivity. Correction for the viscous effect in the CaCl_2 phase was done by dividing by the dynamic viscosity (η). These were taken from table 3.4 as the NMP- CaCl_2 phase determines the conductivity.

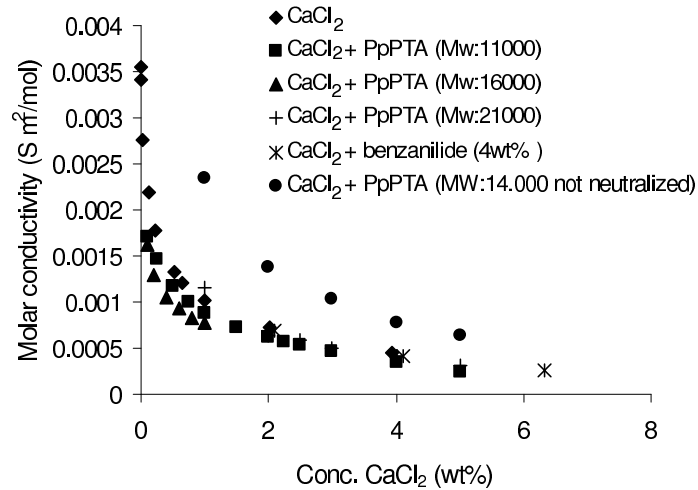


Figure 3.23: Conductivity (Sm^2/mol) as a function of the concentration CaCl_2 (wt%) of NMP- CaCl_2 mixtures and of NMP- CaCl_2 -PpPTA/benzanilide mixtures.

The ionic atmosphere gives rise to a relaxation effect, caused by the application of an electric field and an electrophoretic effect which results in an increased viscous drag caused by counter ions.

To correct for ionic atmospheric effects, use was made of a Kohlrausch-like expression following from the Debye-Hückel-Onsager theory:

$$\Lambda_m = \Lambda_m^0 - \mathcal{K}\sqrt{C} . \quad (3.9)$$

In equation 3.9 \mathcal{K} is a factor that depends on the specific electrolyte, and can be written in the form:

$$\mathcal{K} = A + B\Lambda_m^0 , \quad (3.10)$$

in which:

$$A = \frac{z^2 e F^2}{3\pi\eta} \sqrt{\frac{2}{\epsilon RT}}$$

$$B = q \frac{z^3 e F^2}{24\pi\epsilon RT} \sqrt{\frac{2}{\pi\epsilon RT}} .$$

q in the expression for B is a quantity that depends on the nature of the electrolyte. In the case of 1:1 electrolytes it takes the value 0.5. This value was used in the calculations. (It will become clear further on that it is justified to do so). Using the measured conductivities indicated in figure 3.23 the fraction of CaCl₂ in ionic state can now be calculated and ranges from 20% (concentration CaCl₂ 1 wt%) down to only 6% (concentration CaCl₂ 6 wt%). This means that in practical solutions the fraction CaCl₂ present in ionic form is in the order of 6%.

To understand in what form the ions are present in solution, the equilibrium constant K , as defined in equation 3.7, was determined graphically. Hereto the fraction $\frac{1-\alpha}{\nu_+ \alpha^{\nu_+} + \nu_- \alpha^{\nu_-}}$ was plotted against $C_0^{(\nu_+ + \nu_- - 1)}$. The slope represents the equilibrium-constant K and thus a straight line should be obtained. This was done by varying the ν_+ and ν_- . The optimum was found with $\nu_+ = \nu_- = 2/3$. See figure 3.24.

Given $\nu_+ = \nu_- = 2/3$ equation 3.6 can now be written as:



The presence of component $2Ca_{1.5}Cl_2^+$ can be regarded as the net result of two different complex forms:



This implies the presence of cations as aggregates of Ca^{2+} and Cl^- as well as non-clustered Cl^- . This may very well be, as NMP forms a rather a-polar environment in which separate ions do not reside well.

Based on these findings a possible interaction scheme between NMP and $CaCl_2$ is shown in figure 3.25. This updates scheme 3.14.

The conductivity of NMP- $CaCl_2$ solutions were found to be unaffected by addition of PpPTA. Apparently the ions present in the solution are relatively free to move and PpPTA does not hinder ionic movement. When no salt is added only very low molecular weight polymer is obtained during polymerization, due to rapid precipitation of the polymer. Ions retard the precipitation process by hindering chains to move close.

The phenomenon of viscosity drop as mentioned in the introduction, see figure 1.10 can now be explained. In the case of not neutralizing the polymer

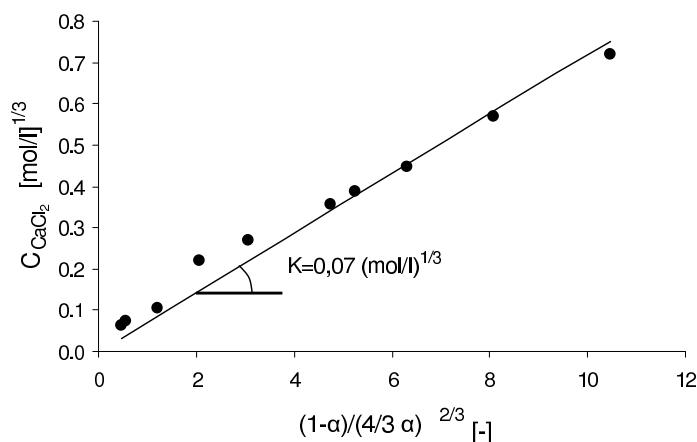


Figure 3.24: Representation of the concentration $CaCl_2$ against the fraction split in ionic form, such that the equilibrium constant follows from the slope.

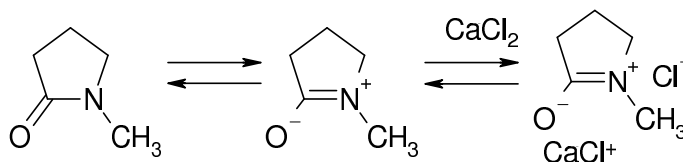


Figure 3.25: Proposed interaction scheme between NMP and $CaCl_2$ based on the findings of a $CaCl_2$ independent hydrodynamic radius and no stable complex formation.

mixture with CaO, HCl remains present in the mixture. As the HCl is formed during the polymerization at the forming amide-unit it is plausible that it remains at this amide-unit forming a complex as presented in figure 3.15.

The chains themselves are highly negatively charged preventing chains to come into close contact. Due to these repulsion forces between polymer chains, a high viscous mixture results. When the HCl is neutralized by CaO according to the reaction equation 3.14 the small hydrogen ions are replaced by large calcium ions.

To check whether chains will actually hinder each other in the case of HCl present, due to their charge, the average distance between chains can be compared to the bjerrum length. The bjerrum length (l_B) is a measure for the distance at which kinetic - and coulomb forces balance is defined as:

$$l_B = \frac{e^2}{4\pi\epsilon_0\epsilon_r kT} , \quad (3.13)$$

e is the elementary charge, $1.6 \cdot 10^{-19} \text{C}$, ϵ_0 the electric constant, $8.85 \cdot 10^{-12} \text{F/m}$, ϵ_r the relative dielectric constant and k the Boltzmann constant, $1.38 \cdot 10^{-23} \text{J/K}$. With the relative dielectric constant of NMP 32, [79] the bjerrum length is calculated to be 17 Å. This means that within a distance of 17 Å coulomb interactions exceed thermal motion of ions and movement of charged chains will be hindered due to repelling forces. In a 4 wt% PpPTA solution and with the molecular weight of the amide unit in PpPTA 119 g/mol, the ratio of the number of amide units to the number of NMP molecules is 29. This means the average distance between amide units is 3 NMP molecules. With the length of a NMP molecule approximately 6 Å (the density of NMP is 1.033 g/cm^3), the distance between amide units is about the same as the bjerrum length and thus chains will hinder each others movement.

Upon neutralization with CaO, HCl is replaced by CaCl₂ according to reaction equation 3.14. As the fraction CaCl₂ in ionic form is very limited, as shown before, the polymer chains become less charged causing the bjerrum length to decrease. This results in more translational freedom for the chains and a decrease in viscosity.



The specific interaction strength between polymer, solvent and salt depends strongly on the specific molecules involved as discussed in chapter 2, Federov [28], [36] discussed the influence of the cation and anion on the solvent power and hence molecular weight of the resulting polymer. Interaction of the

anion with the solvent should be weak and as a consequence it will interact with the liable hydrogen of the amide in the polymer. The cation on the other hand can bind to either the solvent carbonyl or the polymer carbonyl. Interaction is favourable with the solvent thus creating a cation-solvent complex interacting with the negatively charged polymer amide-anion complex. This is in agreement with the conclusion drawn before from NMR results on NMP-salt-benzanilide mixtures, in which an increase of the salt concentration above the amide-unit concentration results in complexation of salt in ion pairs with NMP, see figure 3.22. In the case of increasing the salt content more ion pair formation thus occurs, resulting in neutral polymer molecules in which the amides are bonded to an ion-pair and hence decrease solubility due to a decrease of repelling forces. Charge in this respect is essential to manufacture polymer chains and keep them in solution. Other articles discussing similar behaviour are from Gopal [38], Diorio [39] and Paul and Sreenathan [37].

In the case of hydrogenchloride present in the polymerization mixture a strong interaction of protons with NMP is reasonable and a charged structure as described here will be present. In contrast to salt-cations like calcium or calcium-complexes, protons can far more effectively distribute their charge upon interaction with NMP as depicted in figure 3.15 in which the proton is covalently bonded to NMP. The net result is a further shift from HCl as molecule to ions and thus creating more negatively charged polymer chains and hence contributing to a higher viscosity. Indications of the presence of the adduct were already found in NMR measurements, figure 3.17. Also the decrease in conductivity upon neutralization is in favour of it.

In the case of neutralization all protons are substituted by calcium(-complex). Due to the observed decrease in conductivity upon neutralization and the weak electrolyte behaviour, ion pair formation is very probable, reaction equation 3.12, causing the polymer chains to become less charged and thus decrease the viscosity of the mixture.

In chapter 5 where the NMP-CaCl₂-PpPTA mixtures are discussed using molecular modeling techniques, it will be shown that the CaCl₂ tends to form aggregate structures. This agrees with the proposed complexes in reaction equations 3.11 and 3.12.

Influence of water in NMP-CaCl₂ solutions

The presence of CaCl₂ is needed during polymerization of PpPTA in NMP, to prevent immediate precipitation. The dissolution of CaCl₂ in NMP was found to be very slow, requiring a few days. During this process small particles form at first that disappear in due time. As the difference in refractive index

between NMP and CaCl₂ is very small, see table 3.2, it is difficult to observe the particles and they may seem to be fully dissolved.

In this section, laser diffraction and optical microscopy experiments are presented in order to determine the size of particles present in NMP, as well as the influence of water (0-3wt%).

Laser diffraction experiments were carried out using a Malvern Zetasizer Nano ZS, fitted with a 633nm ('red') laser. This instrument can measure particle sizes (ranging from 0.6nm to 6 μm) and zeta potentials. Particle sizes are determined by measuring the dynamic light scattering (DLS). The particles scatter light, and the scattering pattern changes in time due to the brownian motion of the particles, which in turn depends on their size. Thus the (lack of) similarity between patterns recorded at different points in time can be used to deduce the particle size. The correlation function, expresses the similarity between scattering patterns as a function of the time interval between their recording and is therefore one of the key basic results from DLS experiments.

Three samples were tested, each containing 4 wt% CaCl₂ in NMP. To the first sample no water was added (containing 0.16 wt% water). To the other two samples 1.7 wt% and 3.2 wt% water was added respectively. The samples were prepared several days in advance. Square glass cuvettes with a round aperture, closed with a teflon cap, were used. The particle size distributions (PSD) are shown in figure 3.26 and table 3.7.

Table 3.7: *Observed mean particles sizes for CaCl₂ (4.0wt%) in NMP samples differing by the amount of water added. Between brackets the peak width is given.*

Sample	peak 1 mean (nm)	peak 2 mean (nm)
0.16 wt%	1180 (160)	-
0.16 wt%	1200 (87)	-
1.7 wt%	933 (189)	5190 (483)
1.7 wt%	858 (77)	3290 (454)
3.2 wt%	737 (46)	-

In all experiments, particle sizes in the order of 1 μm are observed. In all cases, a warning concerning sedimenting particles is issued by the software, and the estimated average particle size (not shown here) is larger than the size given by the first peak in the PSD diagram. This indicates that next to the 1 μm particles, much larger particles are also present, which cause the sedimentation and lead to the higher average size. In the 1.7 wt% water sample, a second peak could indeed be fitted. Since the interpretation of the data is based on the assumption that all particle movements result from

brownian motion, sedimentation is a disturbing factor in the derivation of the PSD. The results, in particular related to the larger particles, should therefore be treated with some suspicion.

Given the observed particles sizes in the order of $1\mu m$, and the uncertainty due to the larger particles disturbing the measurements, optical microscopy was used to further study the samples.

Droplets of each of the three samples were observed in phase contrast mode. Representative images are shown in figure 3.27, where the particles are observed as white spots in the images.

The microscopic images show particles of about $1\mu m$, and an increase in

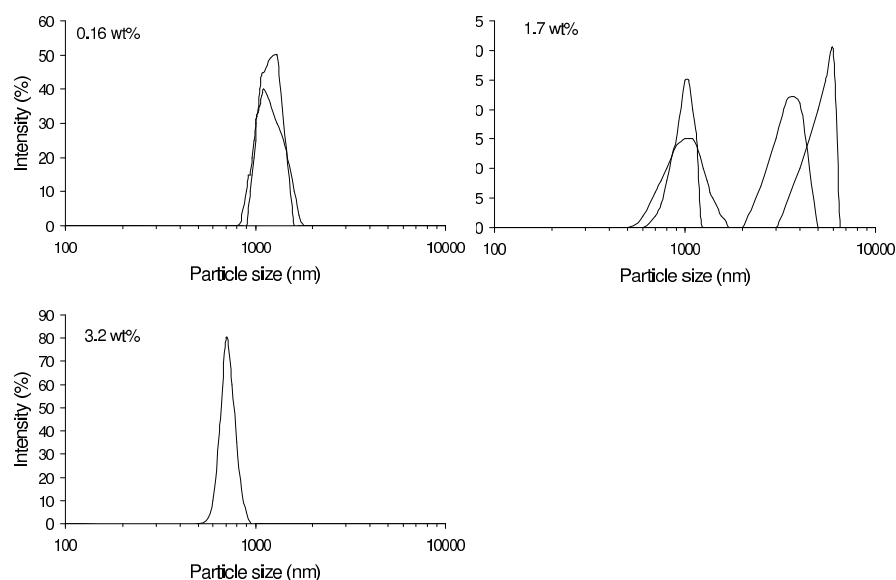


Figure 3.26: PSD for CaCl_2 (4.0 wt%) in NMP samples. Top left: no water added (0.16 wt%), two measurements on the same sample. Top right: 1.7 wt% water, two measurements on the same sample. Bottom: 3.2 wt% water.

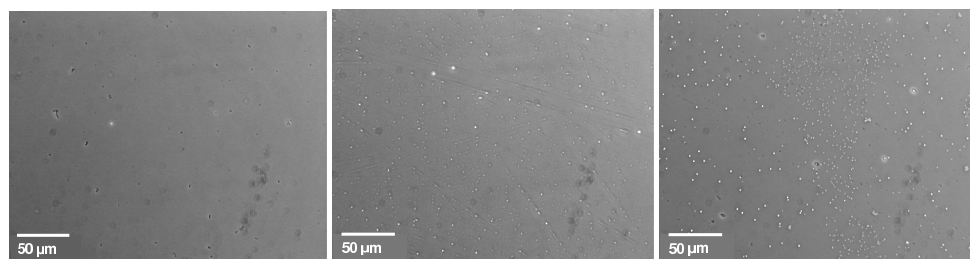


Figure 3.27: Microscopic images of NMP- CaCl_2 samples. Left: no water added, middle: 1.7 wt% water added, Right: 3.0 wt% water added. Particles are observed as white spots in the images.

their number when more water is added to the solution. This confirms the observations by DLS about the particle size.

The size of the particles suggests that their presence should be directly observable, since they are large enough to scatter light, and thus should lead to an opaque or hazy liquid. The fact that the liquid is clear may be explained by the fact that the refractive indexes of the particles is likely to be very close to the value for NMP, see table 3.2. The difference in refractive index between NMP and CaCl₂ crystals is rather small, and is even smaller for hydrated crystals. Thus scattering will be limited.

The small difference in refractive index can easily suggest complete dissolution of the calcium chloride, when still micron-sized particles are present. The main conclusion from the presence of water is the increase of particles in the micro-meter range. It is likely that water agglomerates with CaCl₂ thus forming these particles. As a consequence less "free" CaCl₂ is available and this has a negative effect on the stability of PpPTA solutions in NMP-CaCl₂. Since the microscopic image of the sample to which no water was added, representative for samples used in experiments throughout this thesis, showed very little particles, the influence of water will be neglected further on.

Now the structure formation in solutions to which PpPTA is added is discussed. The phenomena concerning the meta-stable behaviour as discussed before will be related to this structure formation process.

3.5 Phase behaviour of - and structure formation in solutions of NMP-CaCl₂-PpPTA

Upon polymerization of PpPTA in NMP-CaCl₂, after neutralization with CaO, depending on molecular weight and concentration a solution is obtained which can range from fluid-like up to a crumbly gel, [12], [13], [14]. In order to obtain a solution suitable for processing it is required for the solution to be fluid-like. Experimentally it was found that the scope of adding polymer is limited up to about 5 wt% and a molecular weight (M_w) around 25000 g/mol. As discussed before, the neutralization step is essential as it decreases the viscosity by at least one order of magnitude. If neutralization is omitted the resulting solution is much too viscous and processing is limited to very low molecular weights.

Due to the meta-stable behaviour of the solutions, in due time all solutions phase separate and/or gel out. The separated phase was analysed to be NMP. In this section the phase behaviour of NMP-CaCl₂-PpPTA as well as structure formation is discussed explaining the meta-stable behaviour. This is done

on basis of calorimetric and X-ray diffraction measurements. In the next chapter the phase separation process is discussed in more detail on the basis of thermodynamics.

3.5.1 Phase behaviour of NMP-CaCl₂-PpPTA

To check whether the Onsager approach, applied to estimate the isotropic-nematic transition at the end of chapter 2, is valid for PpPTA-NMP-CaCl₂ solutions, calorimetric scans were performed. In the Onsager theory no heat effect indicating a isotropic-nematic transition should be detected. Calorimeter scan experiments were done close to the nematic transition of solutions with a molecular weight of 16000 g/mol. In figure 3.28 the heat flows (mW/g) are given as a function of temperature. The base line values should not be taken absolute as these have been manipulated for clarity purposes and have no effect on the magnitude of the actual transitions. Indicated in the figure are three different transitions marked (I), (II) and (III) that are all endothermic. Type (I) appears only in the scans of 2 and 2.25 wt% PpPTA at approximately 60°C. The inset shows these transitions, enclosed by the dashed rectangular, enlarged. The thermal effects are 0.06 kJ/mol and 0.27 kJ/mol respectively. These values are in the order of heat effects of isotropic-nematic transitions reported in the book of Chandrasekhar [80]. In a similar experiment a 2 wt% PpPTA solution was cooled and a transition of the same magnitude but opposite sign was observed at 60°C. The effect is thus reversible upon successive heating and cooling the samples.

As an enthalpy effect is found a pure Onsager approach to describe the transition is not valid. As these transitions are absent in the scans of 1 and 2.5 wt% the isotropic-nematic transition occurs however over a very small concentration range. Therefore the use of the Onsager approach to predict the isotropic-nematic transition seems reasonable.

Type (II) is seen in every scan, shifting to higher temperatures for higher concentrations. This is the phase separation transition. As mentioned before this transition is always observed in due time and is very rapid at the peak temperature. Type (III) has been found to depend on the amount of water present in the sample and together with the peak temperature of 120°C it indicates a reaction between NMP and water.

Reference scans of pure NMP and NMP-CaCl₂ were made to check on transitions in these systems. Transition types (I) and (II) were not present, and are thus resulting from interactions with PpPTA. Type (III) transitions were present confirming interactions/reactions between NMP and water. Based on the above, a schematic phase diagram of PpPTA in NMP-CaCl₂ can be

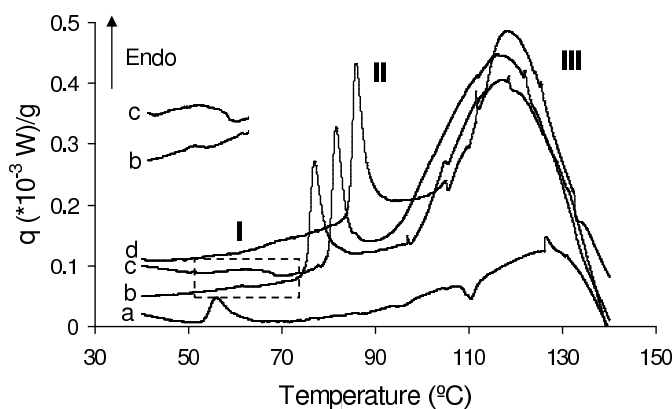


Figure 3.28: DSC scans at $0.2\text{ }^{\circ}\text{C/min.}$ of (a) 1 wt%, (b) 2 wt%, (c) 2.25 wt% and (d) 2.5 wt% PpPTA in NMP-CaCl₂, M_w 16000 g/mol. Three types of transitions are seen (I) a nematic transition in the 2 wt% and 2.25 wt% solutions at $\sim 60^{\circ}\text{C}$. (II) phase separation, observed in all scans. (III) This effect is related to the amount of water present. At $\sim 120^{\circ}\text{C}$ NMP reacts with water.

drawn, see figure 3.29. It is stressed though that this diagram, as it is time dependent, can not be interpreted as a true phase diagram. The area above the curved solid line represents solutions in which phase separation already has occurred on the experimental timescale. Below these temperatures the solutions are meta-stable for at least some time. This line follows to some extent the viscosity behaviour which reaches its maximum at 2.5 wt%. The solutions of M_w 28000 g/mol though, phase separate at much more elevated temperatures then the other solutions, they lie well above the experimental phase separation line. As the viscosity of these solutions is much higher than those of the lower molecular weight solutions this can be explained by reduced dynamics.

The slightly tilted vertical dashed line represents the isotropic-nematic transition. It is based on the calorimetric scans mentioned before and is indicative for almost a-thermal behaviour.

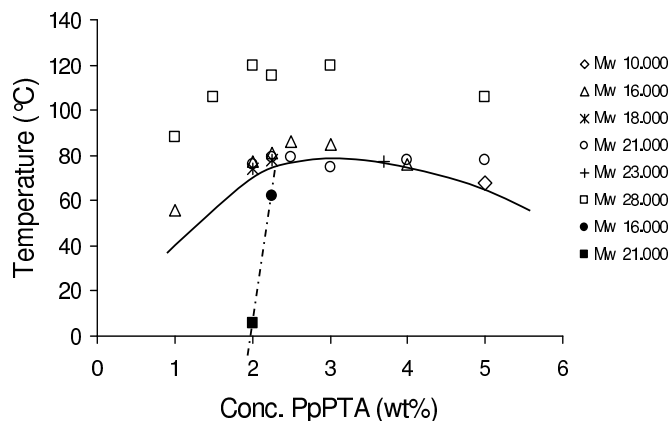


Figure 3.29: *Initial phase behaviour of PpPTA dissolved in NMP-CaCl₂ based on calorimetric data. Above the curved line immediate phase separation occurs (open symbols). This curve does not represent a true thermodynamical transition but rather a line above which dynamics match the experimental time scale. Almost a-thermal behaviour is observed for the isotropic-nematic transition indicated by the slightly tilted vertical line around 2 wt% PpPTA. (filled symbols)*

3.5.2 X-Ray diffraction

Based on the occurrence of a nematic transition at low concentrations and its a-thermal character there seem to be particles present exceeding the molecular dimensions. X-ray analysis was done in order to verify this.

Measurements were carried out on a P4 diffractometer with graphite monochromatic Cu-K α radiation, 0.5 mm collimator and a Histar detector (from Bruker). The measurements were carried out either in Intermediate Small Angle X-ray Scattering (ISAXS) mode (sample-detector distance 22.60 cm) or Wide Angle X-ray Scattering (WAXS) mode (sample-detector distance 7.65 cm). Measuring conditions: capillary in vertical position, 0.2 mm collimator, ISAXS sample-detector distance calibrated with a zinc stearate reference sample, WAXS sample-detector distance calibrated with a Corundum reference sample, spatial distortion and flood field corrections applied and air scattering subtracted unless mentioned otherwise.

Two samples were submitted to X-ray analysis. A 5 wt%, M_w 21000 g/mol and a 4 wt%, M_w 16000 g/mol PpPTA solution. Several recordings were made over time to investigate particle development, figure 3.30.

Clearly, both the 4 wt% and 5 wt% samples crystallize, as can be seen from the development of Bragg reflections in the wide angle region. The 5

wt% sample crystallizes on a time scale of a few days, whereas the 4 wt% sample crystallizes on a time scale of a few weeks. The measured spacings of the reflections are 12.1 (indicated in the figure) 8.5 and 7.2 Å. The 12.1 Å spacing in the diffraction patterns of the 4 and 5 wt% solutions is probably due to the PpPTA chain repeat unit. A similar spacing is observed in crystal solvates of PpPTA and H₂SO₄. The other spacings (8.5 and 7.2 Å) are relatively large compared to the spacings associated with the lattice of the known PpPTA crystal modification. Several authors investigated solvated structures of PpPTA in H₂SO₄ and spacing values are given by Arpin [81] and Iovleva [82]. The unit cell dimensions of crystalline PpPTA have been reported by several authors: $a=7.87$ Å $b=5.18$ Å and $c=12.9$ Å by Northolt [83], $a=7.80$ Å, $b=5.19$ Å and $c=12.9$ Å by Tadokoro [84] and $a=7.78$ Å, $b=5.28$ Å and $c=12.9$ Å by Penn and Larsen [85]. This implies that the crystalline unit cell of the ordered material in the 4 and 5% samples is larger than that in PpPTA crystal structure. The relatively large magnitude of the spacings points to the presence of a PpPTA-solvate or a PpPTA salt.

Structural ordering is also evident from the development of diffuse small angle scattering, observed in due time in both the 4 and 5 wt% samples. The more slowly crystallising 4 wt% sample shows an intense diamond-shaped small angle scattering pattern prior to the development of the WAXS reflec-

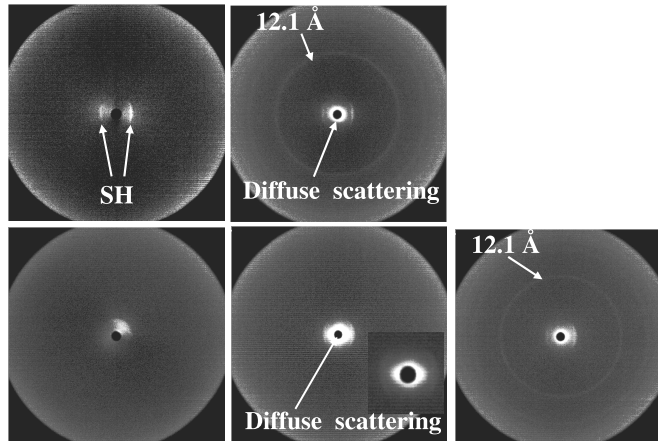


Figure 3.30: 2D diffraction patterns of 5 wt% solution of PpPTA in NMP-CaCl₂ ($M_w = 16000$ g/mol) recorded 1 day after synthesis (top left) and 3 days after synthesis (top right). The reflections marked with SH are due to the sample holder (capillary) and 2D diffraction patterns of a 4 wt% solution of PpPTA in NMP-CaCl₂ ($M_w = 21000$ g/mol) measured 14 days after synthesis (bottom left), 20 days after synthesis (bottom middle) and 35 days after synthesis (bottom right). The inset in the middle picture shows the centre part enlarged.

tions. It is very well possible that this stage also occurred in the 5 wt% sample. In that case it was just not measured due the faster aggregate formation of that sample. In the measurement of the 4 wt% sample, where the WAXS reflections are observed the diamond-shaped pattern has weakened to the extent that only some residual ISAXS intensity is observed. This suggests that the particles formed have become so large that their ISAXS intensity is outside the scope of the instrument. The diamond-shaped pattern is interpreted as oriented diffuse small-angle scattering, indicating that elongated particles are formed. These particles may be oriented. These elongated particles are (initially) not crystalline, since the WAXS reflections are observed at a later stage.

Apart from orientation of the ISAXS pattern also some orientation of the WAXS pattern was observed, figure 3.31. The orientation direction of the ISAXS pattern coincides with that of the WAXS pattern. This suggests that the ISAXS and WAXS scattering are related. The particles formed, as observed via their ISAXS scattering, undergo further ordering leading to crystallization, which is measured as WAXS reflections.

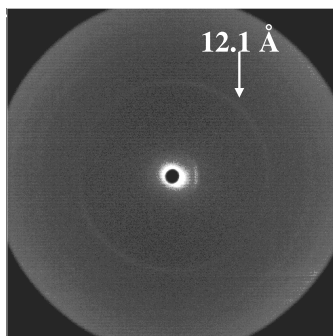


Figure 3.31: 2D diffraction pattern of a 4 wt% PpPTA in NMP- CaCl_2 solution ($M_w = 21000$ g/mol) measured 35 days after synthesis, showing orientation in both ISAXS and WAXS patterns.

As mentioned before, optical microscopy under crossed polarizers shows the development of aggregates over time, see figure 3.5. The particles observed in the ISAXS measurements may well be the initial stages of crystallization. The crystallization then eventually leading to WAXS reflections.

3.5.3 Structural picture

This leads to the following picture of structure development in NMP- CaCl_2 -PpPTA solutions. During polymerization when the PpPTA chains are formed, some amides of different chains interact through hydrogen bonding, though

crystallization is prevented at this stage through complexation with CaCl₂ and NMP. In this manner a very dilute network is formed. After polymerization this network is characterized by dimensions characteristic for a nematic transition at 2.5 wt%. In time higher concentrations of amide-amide bonds are formed at random positions. These form the loci of particle formation. These loci have orientation due to the rigidity of the PpPTA chains. The growing of the spherulitic particles therefore proceeds in two opposite directions leading to orientation within the particles, which are randomly distributed themselves. At this stage these particles are zones of more highly concentrated solution. Outside these zones the concentration is subsequently decreased leading to a phase with diminished viscosity. Since phase separation steadily progresses, a more and more dense phase is formed. At a certain moment the growing zones of denser particles start to overlap and form a continuous phase resulting in a major increase of the viscosity. As this phase will continue to phase separate in time true crystallization will occur. Sketch 3.32 is an impression of this process. It shows the presence of chain-chain links through hydrogen bonds, randomly distributed in the beginning. In time clusters of chain-chain links will develop, resulting in particle formation and eventually crystallization.

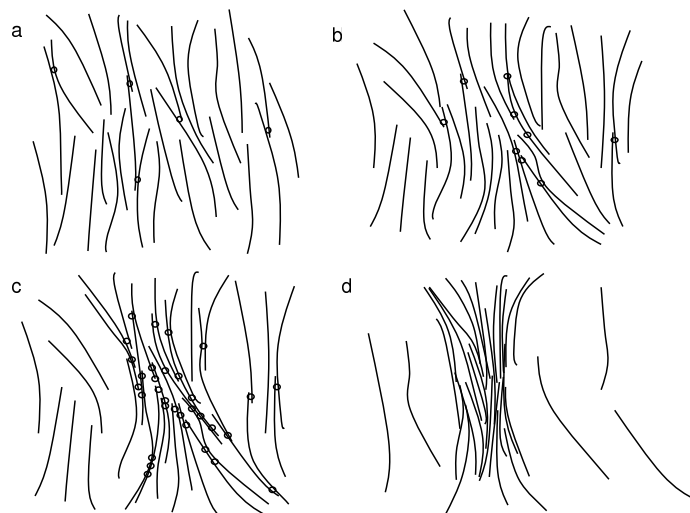


Figure 3.32: *Impression of the phase separation and particle formation process as pictured to happen in NMP-CaCl₂-PpPTA solutions. The time scale at which this process proceeds depends very much on the specific conditions of the solution. The circles in sketches a,b and c are to indicate positions at which different chains have formed amide-amide bonds through hydrogen bridges. In sketch d these are left out to avoid disorder. The surroundings of the particle formation becomes less and less dense causing the viscosity to drop.*

3.6 Conclusions

Solutions of PpPTA polymerized in NMP- CaCl_2 were found to be meta-stable when containing over 1 wt% PpPTA. This meta-stability results in phase separation/aggregate formation and the rate of this process depends strongly on its contents and the specific storage conditions. Above 5 wt% PpPTA, at ambient temperatures the solutions are very unstable and show very short "life time", not suitable for any kind of processing. From visual observation both an increase as well as a decrease in temperature, compared to ambient temperature, lead to even shorter life times. At lower temperatures the tendency towards crystallization increases due to a higher thermodynamic force. At higher temperatures the molecular movement increases facilitating orientation of the PpPTA chains.

From calorimetric measurements of these solutions a transition was seen at about 75°C . The transition was found to disappear in time. This vanishing of the transition coincides with an increase in shear viscosity. The shear viscosity first drops in time after which it increases rather steeply. Due to the coincidence of the two phenomena they seem to be related. From X-ray diffraction measurements, a diffuse scattering was observed to appear in time in which orientation could be distinguished. This suggests the formation of particles that are not crystalline. Due to limitations of the recording machine, the magnitude of the particles could not be determined. Only later Bragg reflections appear, indicating crystallization.

The solutions show birefringence already above 2.5 wt%, indicating the formation of a nematic phase. This is at a surprisingly low concentration, as based on the polymer dimensions the nematic transition would not be expected until 8 wt% polymer as observed in solutions of PpPTA in sulphuric acid. This also indicates particle formation already in an early stage, probably as soon as during polymerization.

Using calorimetry and supersaturation measurements a phase diagram of the NMP- CaCl_2 solvent was established. In large parts of the phase diagram solids of $\text{CaCl}_2 \cdot x\text{NMP}$ complexes were found to exist. At lower concentration (< 5.5 wt%) a solid free region exists. From NMR analysis of samples in the solid free region it became clear that dynamic complex formation is taking place between NMP and CaCl_2 . The same is seen when other salts like LiCl, LiBr or HCl are dissolved in NMP. Polarization of the carbonyl group revealed strong interaction with cations. When benzanilide is introduced the polarization of this carbonyl group is more profound in the case of low salt concentrations. At the same time the calculated hydrodynamic radius of NMP, based on DOSY NMR measurements, increases. When the salt concentration

exceeds the concentration of benzanilide a decrease of this radius is found. This suggests formation of a mantle structure of NMP molecules around benzanilide which is facilitated by the introduction of salt, the anions having a preference for benzanilide and the cations for NMP. As soon as an excess of salt is reached, anions and cations will be stabilized in ion pair formation with NMP.

From electrical conductivity experiments on the solvent system as well as on the solutions containing PpPTA, it was found that only a small amount of CaCl_2 is present in ionic form and furthermore that the cations are present in an aggregate manner as Ca_2Cl_3^+ and CaCl^+ and the anion is present in a non-clustered way as Cl^- . PpPTA was found not to influence the electrical conductivity.

The meta-stability and structure development in NMP- CaCl_2 -PpPTA solutions raised the question whether the NMP- CaCl_2 solvent system can ever act as a true solvent for PpPTA. In order to answer this question a model was developed based on volume fraction statistics to describe the thermodynamic behaviour of liquid mixtures in general and then applied to the NMP- CaCl_2 -PpPTA mixtures. In the next chapter this model is introduced and the consequences for the solvent system are discussed.

4. Thermodynamics of Polyaramid Solutions

In this chapter a thermodynamic model, based on volume fraction statistics is introduced to predict the solubility of PpPTA in amide-salt solvents. It makes use of an interchange term, a parameter that describes the heat effect upon changing simultaneously A-A and B-B interactions into A-B interactions. As it is the free enthalpy of fusion of PpPTA that needs to be compensated for upon dissolution, several manners to arrive at an estimate of its value are presented. A TDP-index is introduced as a parameter to express the solubility power of a solution. In the case it exceeds unity in theory a true thermodynamically stable solution is obtained. It is shown that indeed there are PpPTA-amide-salt combinations that have a TDP-index larger than one.

4.1 Introduction

In the previous chapter experimental evidence was presented showing meta-stable behaviour of mixtures resulting when PpPTA is polymerized in NMP-CaCl₂. This raised the question whether this solvent or more generally non-acidic media can act as true solvents for PpPTA in the way strong acids, like sulphuric acid, can. To develop a potential one step process for the manufacturing of PpPTA fibers a non-acidic environment is required as in an acidic environment polymerization is not possible. In order to give an answer to this question the chemical potentials of the components in the mixture need to be determined.

For a mixture to be thermodynamically stable the chemical potentials of all components should be negative upon mixing. The two contributions to the chemical potential are the partial molar enthalpy and partial molar entropy. The partial molar enthalpies were determined using experimental data on enthalpies of mixing/dissolution, gained by measuring the heats of mixing/dissolution of the components making up a mixture, using a calorimeter.

A Flory-Huggins expression was used to calculate the partial molar entropy.

A model was developed to calculate thermodynamic excess enthalpies. An excess value of a thermodynamic property represents the difference of that property between an ideal- and real mixture. It is based on molecular interactions between components. The model makes use of:

1. Volume fraction statistics to represent the amount of interactions between molecules.
2. An interchange term to indicate the magnitude of interactions between molecules.

An interchange term is an expression for the amount of heat involved upon changing simultaneously the surrounding of a component A from A to B and of component B from B to A. It thus assumes the components in the mixture in the liquid state and upon dissolving a solid component, as in the case of PpPTA, the free enthalpy of fusion of that component needs to be added separately to calculate the chemical potential.

In a mixture the amount of heat is related to the volume fractions of the components as their volume fractions are taken representative for the amount of interactions. A characteristic of the interchange term is that it is constant over the complete composition range of the mixture and independent of the number and identity of the components.

A definition of the interchange term can be found in the appendix, where the complete model is derived. In the model calculations homogeneous mixing and the absence of preferential orientation is assumed. Although the model is able to include these features by the introduction of correction factors, this will complicate the mathematical description and calculations tremendously. The model is therefore valid only in a weak-ionic environment since no static electric interactions are taken into account. For mixtures of PpPTA-NMP- CaCl_2 these assumptions are validated by the fact that no (stable) complexes are formed between these components below 5.5 wt% CaCl_2 and the amount of ions present in these mixtures is very limited, as was discussed in the previous chapter.

A further extension of the model can be made by introducing group contributions. The molecules are then divided in predetermined molecular groups and the interchange terms between these molecular groups and other components in a mixture can subsequently be determined. At the end of the appendix it is shown that for binary mixtures it is possible to calculate the partial excess molar free enthalpy, that is the excess chemical potential, ana-

lytically. In the case of three or more components however, it is necessary to compute them numerically.

From dissolution experiments of PpPTA in sulphuric acid the interchange term between PpPTA and sulphuric acid was determined as well. As this environment is far more ionic than NMP-CaCl₂, as will become clear from electrical conductivity experiments to be discussed in chapter 6, its exact value must be taken with great care. It is still a useful parameter though and is used to estimate the free enthalpy of fusion of PpPTA. This is the amount of energy that needs to be matched by interactions between solvent and PpPTA in order for PpPTA to dissolve. As PpPTA does not melt upon heating, it degrades before it melts, the free enthalpy of fusion can only be estimated indirectly and this was done in several ways. It is the most important parameter in determining solubility of PpPTA.

For comparison reasons the heats of dissolution of the isomers PmPTA, PBA and DABT of PpPTA, in sulphuric acid, NMP and NMP-CaCl₂ were also determined. For the para-aramids similar values were found as for PpPTA and they were also found only to dissolve in sulphuric acid. The meta-aramid PmPTA also dissolved readily in pure NMP. This agrees with the observation that the dominant factor upon dissolving seems the free enthalpy of fusion, leading to the para-aramids to be soluble only in sulphuric acid and PmPTA also soluble in NMP-CaCl₂ systems.

The interchange terms between NMP, CaCl₂ and PpPTA were determined. Benzanilide was used in the experiments as a model compound to mimic PpPTA as the polymer itself does not dissolve upon immersion in NMP-CaCl₂. The interchange term between benzanilide and CaCl₂ was found to be far larger than the interchange term between PpPTA and sulphuric acid. This means that CaCl₂ (or other salts) are essential in keeping PpPTA dissolved in amide-salt mixtures. The calculated partial excess molar free enthalpy values however, lead to the conclusion that no stable solution can be found above 1 wt% PpPTA in a NMP-CaCl₂ mixture, in agreement with experiment.

The real usefulness of interchange terms lays in the earlier mentioned group contributions. In a second series of experiments, the interchange terms between benzanilide and other amide-salt combinations were measured. The combinations were chosen such that it was possible to determine group contributions. As interchange terms represent an enthalpy change per volume, excess heats upon mixing molecules consisting of specific groups can be calculated ones these group contributions are known. This based on volume fraction statistics of the contributing groups, as their volume fractions are representative for the amount of interactions occurring. From the results favourable amide-salt combinations can be constructed and used to construct an opti-

mum solvent for PpPTA. A drawback of the model results must be noted. As in the model calculations it is assumed that the absence of preferential orientation is valid, the formation of complexes between components is not included. These complexes are very well conceivable due to ionic interactions, especially in amide-salt solvents that are more ionic than NMP- CaCl_2 . The results are therefore indicative and useful for directing research activities in attempting to develop an optimum non-acidic solvent.

As the interchange terms between salts and PpPTA were found to be so large, dissolution experiments of PpPTA in sulphuric acid to which an amount of salt was added were conducted. The addition of CaF_2 to sulphuric acid was found to increase the maximum solubility of PpPTA compared to pure sulphuric acid.

4.2 The NMP- CaCl_2 (-benzanilide) system

4.2.1 Calorimetric experiments

In order to determine the heat of dissolution of CaCl_2 in NMP isothermal measurements were conducted with the use of a Setaram calorimeter C80II. Hereto two stainless steel reversal mixing vessels are used (Setaram, mixing vessel by return SE 31/1419, Caluire, France). Each vessel consists of two concentric compartments which can be filled with different substances. The measurement cell contains the NMP and CaCl_2 separated by a stainless steel wall. The reference cell contains an equal amount of NMP. The measurement starts by equilibration for a period of at least two hours and then rotating the calorimeter 180° for as long as is needed for complete dissolution. In this way the NMP and the CaCl_2 can come into contact. The measurement is continued until the signal has returned to its base line level. The heat flow is registered by the calorimeter and represented as a dissolution peak. The corresponding surface under this peak represents the total amount of energy released or consumed during the dissolution process.

The maximum solubility of CaCl_2 in NMP is determined by adding CaCl_2 to NMP until a solid precipitated at 25°C , the solution was left to equilibrate for at least a month. From the saturated solution the CaCl_2 concentration was determined using TGA measurement in which the solvent was evaporated (up until 500°C) while recording the mass loss.

To determine the heat of dissolution of CaCl_2 in NMP-benzanilide, dissolving experiments of CaCl_2 (0 wt% - 5 wt%) in 10 wt%benzanilide-NMP were performed. Measurements were carried out similar as discribed for CaCl_2 in NMP. From the difference between these values and those for CaCl_2 in pure

NMP, the interchange term between CaCl₂ and benzanilide was obtained.

To exclude possible reaction with the stainless steel also experiments with pure NMP or NMP containing 4 wt% CaCl₂ against an empty reference were performed. The error in the measured values is in the order 0.3% and is neglected in further discussions.

4.2.2 Chemical potentials

The main question is whether the NMP-CaCl₂ system can act as a true solvent for PpPTA. In order to answer this question the free enthalpy change upon mixing must be determined and should be negative in the case of a true solution. From thermodynamics the free enthalpy is defined as:

$$\Delta G = \Delta H - T\Delta S . \quad (4.1)$$

Upon mixing different components, a measure for the interactions between the different components is given by the excess properties. These excess properties express the difference between the actual change upon mixing and the change in the ideal situation. The ideal situation is the case in which interactions between the components are neglected and can be envisioned as follows. Consider two ideal liquid components contained in two separate volumes, one containing component A and the other component B. The volumes are brought into contact such that components can exchange. In that case A-A and B-B interactions will be broken and A-B interactions formed. In the ideal case there are no interactions between particles so that the enthalpy change will be zero and there will only be a contribution of the entropy of mixing to the free enthalpy change. In the ideal case the change in volume upon mixing the components can be neglected and the entropy of mixing is proportional to the respective mole fractions of the components in the mixture. In the non-ideal case the molar volumes of the components must be taken into account and the entropy of mixing becomes proportional the the volume fractions of the components in the mixture. Expressed in molar quantities (symbolized by a bar above the quantity) the excess quantities become:

$$\Delta \bar{S}_m^E = \Delta \bar{S}_m - \Delta \bar{S}_m^{id} \quad (4.2a)$$

$$\Delta \bar{H}_m^E = \Delta \bar{H}_m - \Delta \bar{H}_m^{id} \quad (4.2b)$$

in which the subscript *m* refers to mixture and superscripts *E* and *id* to excess and ideal respectively. From 4.1 and 4.2 an expression for the excess molar

free enthalpy in terms of the excess properties is given by:

$$\Delta \bar{G}_m^E = \Delta \bar{H}_m^E - T(\Delta \bar{S}_m^E + \Delta \bar{S}_m^{id}) , \quad (4.3)$$

with $\Delta H^{id} \equiv 0$. The chemical potential (equal to the partial excess molar free enthalpy) for component k now is:

$$\mu_k = \Delta \bar{H}_k^E - T(\Delta \bar{S}_k^E + \Delta \bar{S}_k^{id}) . \quad (4.4)$$

A model, based on volume fraction statistics, was used to find an expression for the heat of dissolution. A parameter $\sigma_y(k, i; l, j)$ is defined as the interchange term and represents the interaction for thermodynamic property Y upon mixing between molecules k and l , consisting of molecular groups i and j respectively. The derivation is given in the appendix. When group contributions are left out and the molecules are regarded as whole, appendix equation A.34 for the excess molar enthalpy simplifies to:

$$\Delta \bar{H}_m^E = \bar{V}_m \sum_{k=1}^C \sum_{l=1}^C \phi_k \phi_l \sigma_h(k; l) . \quad (4.5)$$

Herein, \bar{V}_m is the molar volume of the mixture, ϕ_k and ϕ_l are the volume fractions of components k and l respectively and $\sigma_h(k; l)$ is the interchange term referring to the enthalpy change upon changing the surrounding of component k from k to l and simultaneously of component l from l to k . The apparent excess molar heat of dissolution of component k is then:

$$\Delta \bar{H}_{k,\phi}^E = \frac{\bar{V}_m}{x_k} \sum_{k=1}^C \sum_{l=1}^C \phi_k \phi_l \sigma_h(k; l) . \quad (4.6)$$

An expression for the partial excess molar enthalpy, from appendix equation A.10, now reads:

$$\Delta \bar{H}_k^E = \Delta \bar{H}_{k,\phi}^E + x_k(1 - x_k) \left(\frac{\partial \Delta \bar{H}_{k,\phi}^E}{\partial x_k} \right) \quad (4.7)$$

and is found by substituting 4.6 in 4.7:

$$\Delta \bar{H}_k^E = \frac{\bar{V}_m}{x_k} \sum_{k=1}^C \sum_{l=1}^C \phi_k \phi_l \sigma_h(k; l) + x_k(1-x_k) \left[\frac{\partial \frac{\bar{V}_m}{x_k} \sum_{k=1}^C \sum_{l=1}^C \phi_k \phi_l \sigma_h(k; l)}{\partial x_k} \right]. \quad (4.8)$$

For binary mixtures the apparent excess molar enthalpy for component 1, by realizing the volume fraction for component 1: $\phi_1 = \frac{x_1 V_1^*}{V_m}$, can be written, according to appendix equation A.41, in the form:

$$\Delta \bar{H}_{1,\phi}^E = 2\bar{V}_1^* \sigma_{h(1;2)} \phi_2. \quad (4.9)$$

The superscript * refers to the pure component and is due to taking the excess volume zero, as volume changes upon mixing are usually small. Similarly an expression for the partial excess molar enthalpy for a binary mixture is found from appendix equation A.42:

$$\Delta \bar{H}_1^E = 2\bar{V}_1^* \sigma_{h(1;2)} \phi_2^2 = \Delta \bar{H}_{1,\phi}^E \phi_2. \quad (4.10)$$

In the above equations homogeneous mixing and the absence of preferential orientation of the molecules is assumed. The following observations as discussed in the previous chapter validate these assumptions for mixtures of PpPTA-NMP-CaCl₂. A nematic transition occurs at 2.5 wt%, although this effects the orientation of the polymer chains relative towards themselves it has no direct consequence for the NMP-CaCl₂ environment. From the phase diagram of NMP-CaCl₂, figure 3.11 it can be seen that below 5.5 wt% CaCl₂ and above zero degrees celcius no solid complexes are present and NMR analyses showed the presence of dynamical interactions in the liquid phase, see chapter 3. From electrical conductivity experiments also discussed in chapter 3 it was found that about 6% of the CaCl₂ is present in ionic form at a 6 wt% CaCl₂ concentration. The cations are present in an aggregate nature Ca₂Cl₃⁺ and CaCl⁺, the anions are present in a non-clustered way, Cl⁻, meaning only monovalent ions exist in the mixture.

In order to calculate the partial excess molar enthalpy as expressed in equation 4.10, which is needed in the expression for the chemical potential, equation 4.4, an interchange term must be determined based on measured values of the apparent excess molar enthalpy, equation 4.9. The interchange terms between NMP, CaCl₂ and PpPTA in a mixture were determined in the

following way. The enthalpy of dissolution of CaCl_2 in NMP was measured. These enthalpies equal the apparent excess molar enthalpy for the dissolved component. The corresponding interchange term between CaCl_2 and NMP was estimated from these values.

As PpPTA does not dissolve directly in a NMP- CaCl_2 environment a model compound, benzanilide, was used to study the heat of dissolution upon mixing with NMP- CaCl_2 solvent. The amide unit of benzanilide then mimics the amide unit of PpPTA. Subsequently heats of dissolution, of CaCl_2 in a solution of 10 wt% benzanilide in NMP, were measured. The interchange term between CaCl_2 and benzanilide follows from the difference of these measured values with the ones of dissolving CaCl_2 in pure NMP.

The interchange term between NMP and benzanilide was not measured directly but determined from group contributions from previous measurements performed by Zegers and van Baardwijk [86]. They determined the interchange terms between various groups making up organic molecules. The group interchange terms are listed in table 4.9.

For practical purposes the apparent excess enthalpy can be expressed in J/g. Hereto the density (ρ_1) of component 1 in solution needs to be determined. Equations 4.9 and 4.10 then become respectively:

$$\Delta \tilde{H}_{1,\phi}^E = \frac{2}{\rho_1} \sigma_{h(1;2)} \phi_2 \quad (4.11)$$

and

$$\Delta \tilde{H}_1^E = \frac{2}{\rho_1} \sigma_{h(1;2)} \phi_2^2 = \Delta \tilde{H}_{1,\phi}^E \phi_2, \quad (4.12)$$

where the \sim symbol above a property refers to a quantity per gram.

The measured apparent excess enthalpies per gram (corresponding to the heats of dissolution) of CaCl_2 in pure NMP and CaCl_2 in NMP containing 10 wt% benzanilide are shown in figure 4.1¹. To determine the interchange terms between NMP and CaCl_2 and between (NMP-benzanilide(10 wt%)) and CaCl_2 the heats of dissolution at infinite dilution are required, equation 4.12 then becomes independent of ϕ_2 as it approaches unity. The heats of dissolution at infinite dilution were obtained by extrapolating to infinite dilution. The fitted lines are also shown in figure 4.1.

The interchange terms are calculated from the measured apparent excess enthalpies (dissolution heats) per gram according to equation 4.11, in which

¹In figures in which heat effects are shown, negative values refer to exothermic heat effects and positive values to endothermic heat effects, unless explicitly stated otherwise.

CaCl₂ is component 1 and the solvent is component 2. Hereto, the intercept of the apparent excess enthalpy per gram at infinite dilution according to the model equation (dashed lines) is made to correspond with the extrapolated value to infinite dilution of the measured data. The corresponding interchange terms were found to be -1613 J/cm³ ² between NMP and CaCl₂ and -1847 J/cm³ ³ between (NMP-benzanilide(10 wt%)) and CaCl₂ respectively. The interchange terms are expressed in J/cm³ as this is the unit required in equation 4.11

In figure 4.2 the model calculations of the dissolution heats are shown for the whole range of volume fractions of CaCl₂. As expected these model calculations show a linear dependence of the heat of dissolution with the volume fraction CaCl₂ with a zero heat of dissolution when the fraction CaCl₂ reaches 1 (no heat effect will occur when CaCl₂ is dissolved in pure CaCl₂). In the real solutions preferential solvation may very well be present. That is a preference for one component to interact with another component. This preference can be concentration dependent and explain the deviations between measured and calculated heats of dissolution as clearly seen in figure 4.1. The interest is however in the values of the heats of dissolution at infinite dilution. By adjusting the interchange term a match between the extrapolated values from the measured data at infinite dilution and the corresponding value of the model can be obtained.

The interchange term between benzanilide and CaCl₂ is found to be -4093 J/cm³ (calculated from best fit (-1847 J/cm³) and then corrected for weight fraction in the sample solution). This value was taken representative for the interchange term between PpPTA and CaCl₂. It is a remarkable high value and largely responsible for the dissolving power of the NMP-CaCl₂ solvent. The interchange term between benzanilide and NMP was calculated using

²This interchange term refers to the interchange of liquid NMP and solid CaCl₂. Normally interchange terms are defined between components in the liquid state and therefore a correction for the enthalpy of fusion of CaCl₂ should be made. As experimental solutions are however all under the melt temperature of CaCl₂ ($T_{melt,CaCl_2} = 782^\circ\text{C}$), in order to dissolve CaCl₂ this enthalpy of fusion needs always be compensated for and in the calculation of the eventual chemical potential a reverse correction needs to be done. It is therefore more convenient to define the interchange term between liquid NMP and solid CaCl₂ as in the experimental values the enthalpy of fusion is included. A similar reasoning is valid for dissolution experiments of other salts in NMP to be discussed further on.

³The interchange term between CaCl₂ and benzanilide is calculated from the difference of the interchange term between CaCl₂ and a solution of 10 wt% benzanilide in NMP and the one between CaCl₂ and pure NMP. As both are based on CaCl₂ in solid form, the resulting interchange term between CaCl₂ and benzanilide refers to both components in the liquid state. As this interchange term is taken representative for the interaction between CaCl₂ and PpPTA in the calculation of the chemical potential for PpPTA, it will have to be corrected for the enthalpy of fusion of PpPTA.

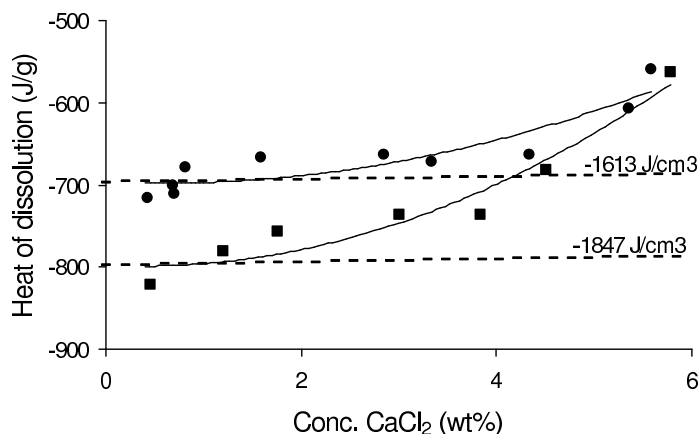


Figure 4.1: Heats of dissolution of CaCl_2 in NMP (bullets) and CaCl_2 in NMP-10 wt% benzanilide (squares) together with fit lines to infinite dilution. Calculated model values for the heats of dissolution (dashed lines) as well as the corresponding interchange terms are also given. All at 25°C .

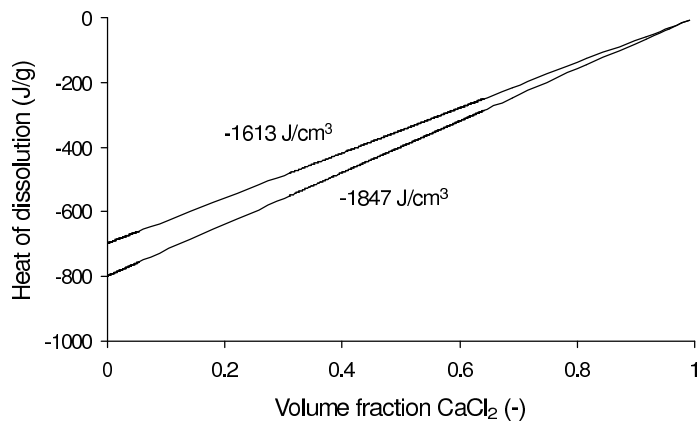


Figure 4.2: Calculated heats of dissolution of CaCl_2 in NMP and NMP-benzanilide(10 wt%) according to model equation 4.12 for the whole range of volume fractions of CaCl_2 at 25°C . The interchange term between NMP and CaCl_2 is -1613 J/cm^3 and between (NMP-benzanilide(10 wt%)) and CaCl_2 -1847 J/cm^3 .

equation 4.13 and data obtained from group contributions to the interchange term:

$$\bar{H}_1^{E,\infty} = 2\bar{V}_1^* \sum_{i=1}^{g_1} \sum_{j=1}^{g_2} \alpha_{1,i}^* \alpha_{2,j}^* \sigma_h(1, i; 2, j) . \quad (4.13)$$

Herein, $\bar{H}_1^{E,\infty}$ is the measured heat of dissolution of component 1 in component 2 at infinite dilution, the α^* symbols represent the respective group volume fractions, according to table 4.6 and $\sigma_h(1, i; 2, j)$ the corresponding group-group interchange terms according to table 4.9. Equation 4.13 is analogous to appendix equation A.38, which derivation is given in appendix and noting that for the enthalpy the interchange terms between identical components is zero.

By introducing benzanilide in NMP, interactions between groups of benzanilide and NMP are formed and NMP-NMP as well as benzanilide-benzanilide interactions are broken. The corresponding heat effects are calculated according to the ratio of their respective group volume fractions in the molecules. The volume fraction follows from the ratio of the group volume over the molecular volume. This method is discussed in section 4.4 where it will become clear how this value is obtained. For now its numerical value is given for the sake of completeness and to show the huge heat effects upon introducing salts with respect to only amide-amide interactions. In table 4.1 the interchange terms are grouped together.

Table 4.1: *Interchange terms, gained from dissolution experiments, between NMP and CaCl₂ and between benzanilide and CaCl₂. The interchange term between NMP and benzanilide is calculated from group contributions. Standard deviations are given between brackets.*

components	Interchange term (J/cm ³)
NMP-CaCl ₂	-1613 (13)
benzanilide-CaCl ₂	-4093 (246)
NMP-benzanilide	-1 (0.7)

To answer whether NMP-CaCl₂ can act as a solvent for PpPTA besides the excess enthalpy also the excess entropy, defined by equation 4.2 has to be determined. The Flory-Huggins relation was used to find an expression for the molar entropy of a mixture and is, for ideal solutions, defined as:

$$\Delta \bar{S}_m^{id} \equiv -R \sum_k x_k \ln x_k . \quad (4.14)$$

In the non-ideal case the molar fraction is replaced by the volume fraction:

$$\Delta \bar{S}_m = -R \sum_k x_k \ln \phi_k . \quad (4.15)$$

The partial excess molar entropy for component k follows directly from 4.15, as in this case it is a linear summation over all the partial contributions.

$$\Delta \bar{S}_k = -R \ln \phi_k . \quad (4.16)$$

In the ideal case it is:

$$\Delta \bar{S}_k^{id} = -R \ln x_k . \quad (4.17)$$

The partial excess molar entropy for component k then becomes:

$$\Delta \bar{S}_k^E = -R \ln \frac{\phi_k}{x_k} . \quad (4.18)$$

After substitution of expressions 4.8, 4.17 and 4.18 in 4.4 an expression for the chemical potential is obtained.

$$\begin{aligned} \mu_k = & \frac{\bar{V}_m}{x_k} \sum_{k=1}^C \sum_{l=1}^C \phi_k \phi_l \sigma_h(k; l) + x_k (1 - x_k) \left[\frac{\partial \frac{\bar{V}_m}{x_k} \sum_{k=1}^C \sum_{l=1}^C \phi_k \phi_l \sigma_h(k; l)}{\partial x_k} \right] \\ & + RT \ln \phi_k . \end{aligned} \quad (4.19)$$

Equation 4.19 was solved numerically for a mixture of the three components NMP, CaCl_2 and PpPTA as the partial derivative can not be determined analytically. At ambient temperature the chemical potentials of NMP, CaCl_2 and PpPTA as a function of the CaCl_2 concentration for different PpPTA concentrations are given in figure 4.3. Values are expressed in J/g, obtained by dividing equation 4.19 by the respective molecular weights.

The chemical potential of CaCl_2 is always negative. As the model assumes all components in the liquid state, at 25°C the free enthalpy of fusion for CaCl_2 needs to be compensated for in order for CaCl_2 to dissolve. In the determination of the interchange term between NMP and CaCl_2 the heat of dissolution of solid CaCl_2 in NMP was measured. The heat effect of melting is thus already included for the enthalpy term. This leaves the entropy of fusion of CaCl_2 to be added. This is easily computed from $\Delta S_{\text{melt}, \text{CaCl}_2} = 0.218 \text{ J/gK}$

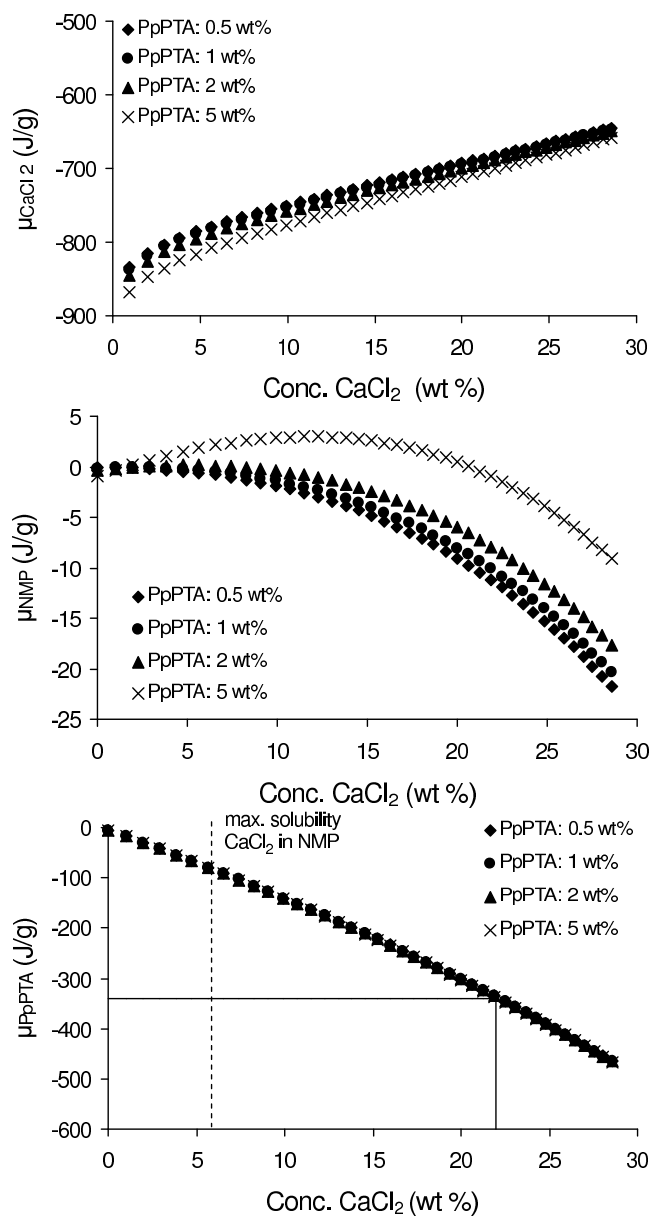


Figure 4.3: Chemical potentials of CaCl_2 (top), NMP (middle) and PpPTA, based on interchange terms with benzanilide (bottom) as a function of the CaCl_2 concentration for PpPTA concentrations ranging from 0.5 wt% up to 5 wt%. The black line in the bottom picture indicates the free enthalpy of fusion of PpPTA. All at 25° C.

resulting in an effect on the free enthalpy of fusion of $-T\Delta S_{melt, CaCl_2} = -65 \text{ J/g}$ at 25°C . This term contributes favourably to the chemical potential and CaCl_2 tends to remain dissolved ⁴.

Above 1 wt% PpPTA though, the chemical potential of NMP becomes positive and as a result NMP tends to separate from the solution. Experimentally this is also observed. To verify the stability below 1 wt% PpPTA, four solutions were prepared according to table 4.2, in which the PpPTA concentration was below 1 wt%. The CaCl_2 concentrations were kept at 1 wt% and 4 wt%. At the latter CaCl_2 concentration the chemical potential of PpPTA is the lowest. If the CaCl_2 concentration is decreased to 0.2 wt% or 0.6 wt%, solutions are stable for only a few days, but for the high CaCl_2 concentrations the stability is in fact increased dramatically and solutions were found to be stable for years. This may well be due to the fact that upon phase separation the solidifying of PPTA in the latter case is slowed down to a greater extent due to abundant CaCl_2 -PpPTA interactions that must be broken for PpPTA to crystallize.

Table 4.2: *Solutions of PpPTA in NMP- CaCl_2 under conditions in which the chemical potential of NMP is predicted to be negative.*

Sample	PpPTA (wt%)	CaCl_2 (wt%)
1	0.2	1
2	0.6	1
3	0.2	4
4	0.6	4

As discussed before mixtures of NMP- CaCl_2 containing a PpPTA concentration over 1 wt% are not thermodynamically stable and phase separate in due time. The chemical potential of PpPTA is calculated to be negative and independent of the PpPTA concentration up to 5 wt%, as is seen in figure 4.3, which would indicate thermodynamical stability. The model assumes however that all components are in the liquid state. The zero state therefore refers to PpPTA in liquid form. Upon dissolving solid PpPTA, the free enthalpy of fusion needs to be compensated for, in order to remain in solution. An estimate of the free enthalpy of fusion of PpPTA is made, discussed in the next section, indicated by the horizontal line in figure 4.3. In theory therefore it might be possible for PpPTA to dissolve in a NMP- CaCl_2 solution in which

⁴As the entropy of fusion contributes favourably to the chemical potential and does not influence the line of reasoning it is neglected in further discussions. The same argument holds for other salts to be discussed further on and the corresponding entropies of fusion will be neglected also.

the CaCl₂ concentration is over 22 wt%. In practice this is not possible. The explanation is found from the phase diagram of NMP and CaCl₂, as discussed in chapter 3. At higher concentrations solid complexes of CaCl₂ and NMP are formed thereby lowering the amount of CaCl₂ available for interaction with PpPTA. The maximum amount of CaCl₂ that can be dissolved in NMP at 25°C is 5.5 wt%.

The final conclusion is therefore that the NMP-CaCl₂ system can not act as a true solvent for PpPTA. It is a thermodynamically unstable mixture.

During polymerization the interactions of CaCl₂ with PpPTA are essential for keeping PpPTA long enough in a dissolved state in order to reach high degrees of polymerization and keep it suitable for processing. As discussed in chapter 3 the maximum amount of polymer that can be dissolved in NMP-CaCl₂ is approximately 5 wt% in order to remain processable. Instead of CaCl₂ other salts and amides may result in larger interchange terms and/or higher solubilities. It is therefore very compelling to investigate the possibilities. But before turning to investigate the effect of other salts and amides on the dissolution behaviour of PpPTA, the methods by which an estimate of the free enthalpy of fusion of PpPTA were made are discussed first.

4.2.3 Free enthalpy of fusion of PpPTA

The determination of the free enthalpy of fusion is indirect, as PpPTA does not melt. In this section several methods to arrive at a value are discussed. The first method is based on determination of the interchange term between PpPTA and sulphuric acid by dissolving experiments of PpPTA in sulphuric acid (100%), sulphuric acid is a good solvent for PpPTA. This was done at 25°C at first as this is the temperature at which the dissolution experiments in NMP-CaCl₂ were performed. The range of solutions is limited to very low PpPTA concentrations though, as already above 2 wt% the solutions become too viscous for measuring purposes. Therefore dissolution heats were also measured at 88°C. In figure 4.4 the measured data with a fit line to infinite dilution are displayed. A discontinuity in the experimental values for the heat of dissolution of PpPTA in sulphuric acid at 88°C is found at ~10 wt% (bullits to squares) and is due to the nematic transition. The minimum found in the isotropic region is small and may be due to solvent effects at low PpPTA concentrations.

In model calculations, according to equation 4.12 in which PpPTA is component 1 and sulphuric acid component 2, it is assumed that the absence of preferential interactions is valid and orientation is random (which is not true for the nematic phase). The densities of the pure components are used in this

calculation, as the density of the solution ($\rho_{solution} = 1.75 \text{ g/cm}^3$) agrees with the weight average of the respective pure components ($\rho_{sulphuricacid} = 1.84 \text{ g/cm}^3$ and $\rho_{PpPTA} = 1.45 \text{ g/cm}^3$ at 88°C). The resulting interchange terms are -357 J/cm^3 at 25°C and -327 J/cm^3 at 88°C , following from the intercept at infinite dilution as indicated in figure 4.4. An interesting observation is the fact that the interchange term between sulphuric acid and PpPTA is far smaller than between CaCl_2 and PpPTA (-4093 J/cm^3). The number of interactions between sulphuric acid and PpPTA are far more numerous than between CaCl_2 and PpPTA due to the limited solubility of CaCl_2 in NMP. The result is that sulphuric acid can act as a solvent for PpPTA.

The fact that the model curves deviate from the measured values for the heat of dissolution is indicating structural deviations from random mixing due to preferred interactions. At 25°C the slope exceeds the model curve which might be due to complex formation between PpPTA and sulphuric acid even at very low concentrations giving rise to larger particles and extra interaction terms between these complexes which are not taken into account in model calculations. At 88°C the slope is much smaller than model predictions. At this temperature it is likely that no complexes are present lowering the slope. That it is lowered even beyond model predictions may be due to structure breaking effects in sulphuric acid when polymer is introduced. A transition to the nematic phase again changes the curvature due to alignment of the polymer molecules.

The partial excess free enthalpy in J/g can now be calculated from equation 4.19 by dividing by the molecular weight for PpPTA (taken 20000 g/mol) to give the proper dimensions. For a binary mixture of sulphuric acid and PpPTA it simplifies to:

$$\tilde{\mu}_{PPTA} = 2 \frac{\bar{V}_{PPTA}}{M_{w,PpPTA}} \sigma_{h(PPTA;H_2SO_4)} \phi_{H_2SO_4}^2 + \frac{RT}{M_{w,PpPTA}} \ln \phi_{PPTA} . \quad (4.20)$$

From the phase diagram of PpPTA in sulphuric acid, figure 2.16 in chapter 2, it is seen that the maximum solubility at 88°C is 20 wt%. At this point the chemical potential of dissolution for PpPTA equals the chemical potential of fusion of PpPTA. This can be expressed in excess free enthalpies by the following equation:

$$\Delta G_{total}^E = \Delta G_{PpPTA}^{E,diss} + \Delta G_{PpPTA}^{fus} = 0 . \quad (4.21)$$

and thus:

$$\Delta G_{PpPTA}^{E,diss} = \Delta H_{PpPTA}^{E,diss} - T\Delta S_{PpPTA}^{E,diss} = -\Delta G_{PpPTA}^{fus} . \quad (4.22)$$

The minus sign in front of the free enthalpy of fusion of PpPTA is due to the fact that it is endotherm and the free enthalpy of dissolution is exotherm. The calculated value from equation 4.20 at 20 wt% PpPTA then exactly equals the free enthalpy of fusion (as the model calculation was based on assuming liquid components). Using the -327 J/cm³ as the interchange term, the corresponding partial excess free enthalpy per gram at maximum solubility of PpPTA in sulphuric acid was calculated to be -260 J/g at 88°C. Thus, the free enthalpy of fusion that needs to be compensated for, is 260 J/g. A similar calculation can be done at 25°C, using -357 J/cm³ as the interchange term. Again from the phase diagram the maximum solubility is now 23 wt% (the point at which solid polymer starts forming). As the resulting solution at higher concentrations PpPTA is now solid it is not possible to determine a quasi density in the liquid state at 25°C. It can only be assumed to be the same as at 88°C. A calculation results in the same value of 260 J/g for the free enthalpy of fusion. In the above calculation use was made of the model value for the apparent heat of dissolution according to equation 4.11. For a solution of 20 wt% PpPTA in sulphuric acid the apparent heat of dissolution can actually be measured though at 88°C and is -448 J/g as can be seen in figure 4.4. Using this value for the apparent heat of dissolution the corresponding partial excess molar enthalpy is calculated to be -340 J/g according to equation 4.12. As the contribution of the mixing entropy as given in equation 4.20 is rather small (-0.25 J/g), it follows that the free enthalpy of fusion is 340 J/g. Unfortunately at 25°C the heat of dissolution at high PpPTA concentration can not be measured due to too high viscosity of the resulting mixture (solid).

In contrast to the method based on interchange terms a second method to arrive at an indication for the free enthalpy of fusion of PpPTA is based on the hypothetical melt temperature of PpPTA. It is obtained from the TG-DSC diagram from thermo-oxidative degradation of PpPTA. In figure 4.5 the heat flow during thermo-oxidative degradation (exothermic heat effect) as well as the mass loss as a function of temperature are shown. The heat flow shows two overlapping peaks. These peaks coincide with the mass loss and correspond to a combustion peak. The dip occurring at higher temperature is thought to be caused by the melting of PpPTA (endotherm effect). This dip occurs at 808 K and is taken as the melt temperature of PpPTA. A measure for the entropy change upon melting PpPTA can be found by assuming equal entropy change upon melting a somewhat similar polymer, crystalline

polyamide 6 (PA6). Tonelli and Kotek [87] determined the enthalpy of fusion ($\Delta H_{fus,PA6} = 267.8 \text{ J/g}$) and the melting temperature ($T_{m,PA6} = 493 \text{ K}$) for 100% crystalline polyamide 6. This results in the melt entropy for polyamide 6 $\Delta S_{fus,PA6} = \frac{\Delta H_{fus,PA6}}{T_{m,PA6}} = 0.54 \text{ J/gK}$. At the melt temperature the free enthalpy of fusion is zero. The free enthalpy of fusion of PpPTA then follows from $\Delta H_{fus,PpPTA} = T_{melt} \cdot \Delta S_{fus,PA6} = 808 \text{ K} \cdot 0.54 \text{ J/gK} = 436 \text{ J/g}$. By taking the temperature dependence of the free enthalpy of fusion linear, at 25°C it becomes 275 J/g , in close proximity to 260 J/g found from the dissolution experiments.

A third way of arriving at the free enthalpy of fusion of PpPTA is by means of a theoretical melt temperature of PpPTA. A value for this theoretical melt temperature is based on a molar melt transition function, equation 4.23, which is the sum over all group contributions.

$$Y_m = \sum_{i=1}^n Y_{m,i} = T_m M . \quad (4.23)$$

For the repeat unit of PpPTA, $Y_m = 208 \text{ K kg/mol}$ and $M_w = 238.3 \text{ g/mol}$, van Krevelen [88], T_m is then calculated to be 873 K . A measure for the entropy change upon theoretical melting of PpPTA is again found by assuming equal entropy change upon melting polyamide 6 (PA6). The free enthalpy of fusion of PpPTA is now $\Delta H_{fus,PpPTA} = 873 \cdot 0.54 \text{ J/g} = 475 \text{ J/g}$ and the hypothetical free enthalpy change upon melting PpPTA at 25°C , $\Delta G_{melt,PpPTA,298\text{K}} = (475 - 298 \cdot 0.54) \text{ J/g} = 314 \text{ J/g}$. This value is in between the experimentally

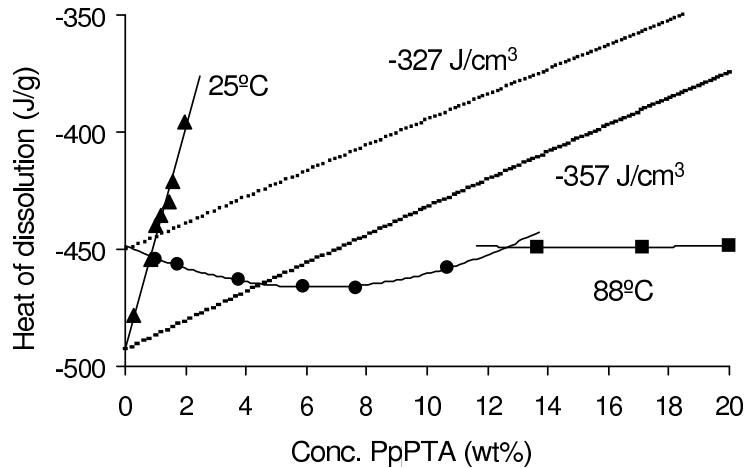


Figure 4.4: *Experimental heats of dissolution of PpPTA in sulphuric acid at 25°C and 88°C together with calculated values based on their respective interchange terms, gained from extrapolation to infinite dilution.*

determined 260, 275 and 340 J/g. In table 4.3 the various determined free enthalpies of fusion for PpPTA are listed.

Table 4.3: *Determined free enthalpies of fusion of PpPTA according to the various methods.*

$\tilde{\mu}_{fus,PPTA}$ (J/g) at 25°C	$\tilde{\mu}_{fus,PPTA}$ (J/g) at 88°C	Method
260	260	Int. term + calculated heat of dissolution
275	241	Thermo-oxidative degradation of PpPTA
314	281	Transition function v.Krevelen
-	340	Int. term + measured heat of dissolution

340 J/g, the largest value based on experimental data, is used as the amount of free enthalpy that must be compensated for, in the dissolving process of PpPTA in NMP-CaCl₂ (indicated by the horizontal line in figure 4.3 for the chemical potential of PpPTA). Although it is based on measurements performed at 88°C this value is used at 25°C as well. As it is not possible to measure this value at 25°C due to too high viscosity and also extrapolation from 88°C to 25°C is inaccurate due to formation of crystal solvate structures at 25°C, see phase diagram 2.16.

Now that an estimate of the free enthalpy of fusion of PpPTA is made and the knowledge that CaCl₂-NMP is not able to keep PpPTA dissolved, as discussed in the previous section, the effect of other salts and amides on the dissolution behaviour is investigated. First the effect of alternative salts on the

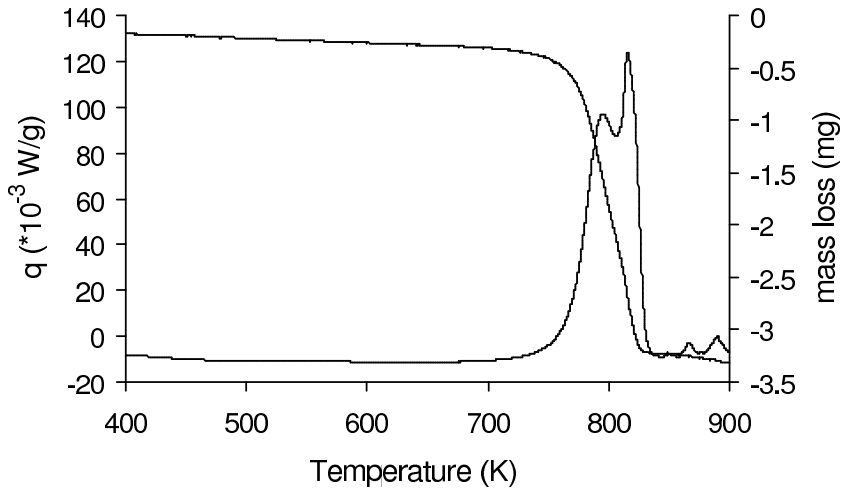


Figure 4.5: *TG-DSC diagram of the thermo-oxidative degradation of PpPTA. The dip in the peak at 808 K is thought to be due to the melting of PpPTA during the degradation process.*

dissolution behaviour is discussed and subsequent the effect of the composition of the amide solvent.

4.3 NMP-salt(-benzanilide) combinations

Besides the specific interaction between salt and polymer also the amount of interactions is important in determining the dissolving power of a system. This means that the maximum solubility is important too. This brings a delicate balance to light. On the one hand a large interaction between salt and polymer is required to compensate for its crystallization enthalpy, on the other hand too strong interactions may result in solid complex formation as seen in the phase diagram of NMP- CaCl_2 , see phase diagram 3.11.

As described in the previous section the magnitude of the interaction between CaCl_2 with PpPTA is expressed in an interchange term, see table 4.1. In this section the interchange terms between pure NMP and NMP with benzanilide (as a model for PpPTA) and other salts are discussed. As calcium is a rather large ion, lithium was chosen as a smaller alternative. Bromide and fluoride were chosen as alternative anions for chloride, fluoride being smaller and bromide being larger. This leads to the following salts investigated: LiCl , LiBr , LiF , CaF_2 and CaBr_2 .

LiF and CaF_2 do not dissolve in NMP, (probably the interaction of fluorine-salts with NMP is so large that all form solid complexes that do not dissolve, this was not investigated further). The interchange terms were determined in a similar way as for CaCl_2 . Hereto dissolution experiments of a salt in NMP and NMP containing 10 wt% benzanilide were done in a calorimeter and the heat effects measured. Doing this for a number of salt concentrations a heat of dissolution at infinite dilution can be obtained by extrapolation to infinite dilution. In figure 4.6 the measured data as well as the fit and calculated model data are presented.

Based on the interchange terms the chemical potentials of PpPTA in the different NMP-salt media can be calculated according to equation 4.19. In figure 4.7 the chemical potential of PpPTA (in J/g by dividing equation 4.19 by the molecular weight of PpPTA) is presented as a function of the respective salt concentrations. As the free enthalpy of fusion of PpPTA was estimated to be 340 J/g the minimal required amount of salt is found when the chemical potential drops below the line -340 J/g. For LiCl this is 13 wt%, LiBr 37 wt%, CaCl_2 22 wt% and CaBr_2 39 wt%.

As mentioned the maximum solubility of the salt is an important parameter because it limits the possible amount of interactions between PpPTA and salt. For the mentioned salts the maximum solubilities in NMP were

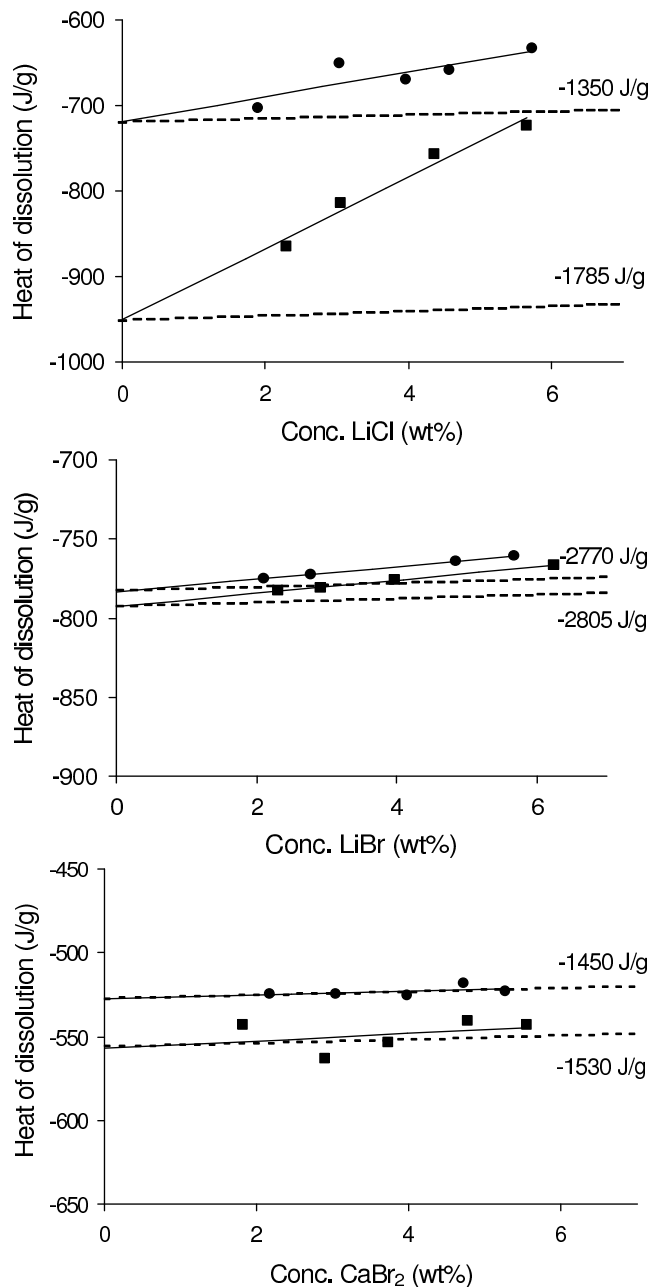


Figure 4.6: Measured heats of dissolution for LiCl , LiBr , and CaBr_2 in NMP(bullets) and NMP-benzanilide(squares) solutions, together with calculated model values (dashed lines). The corresponding interchange terms are given along.

determined by adding salt to NMP until a solid precipitated. The salt-NMP solutions were left to equilibrate for at least a month. From the saturated solution the salt concentration was determined using TGA measurement in which the solvent was evaporated (up until 500°C). In table 4.4 the interchange terms the maximum solubilities and an index term indicating the Theoretical Dissolution Potential (TDP) are given. The index term is defined as the ratio of the maximum solubility of a salt in a medium over the minimal required amount of dissolved salt as resulting from calculations based on the determined interchange parameter.

$$TDP = \frac{\text{maximum solubility salt}}{\text{minimal required salt concentration}} \quad (4.24)$$

For instance in the case of CaCl_2 in NMP the minimal required concentration to obtain a solution would be 22 wt% as was found from figure 4.3. The maximum solubility of CaCl_2 is only 5.5 wt%, table 4.4. Therefore the TDP in this case is $5.5/22=0.25$. The higher this index the more dissolving power may be attributed to the solvent. In the case the index exceeds unity a real solution would be achieved (provided no complex formation occurs between the components).

A number of points appear from this table:

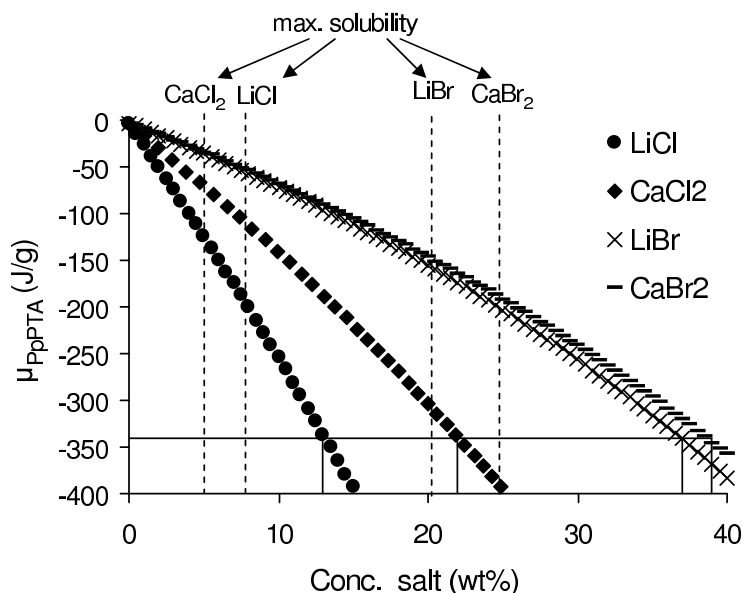


Figure 4.7: Chemical potential of PpPTA, based on interchange terms with benzanilide, as a function of salt concentration. For LiCl, CaCl_2 , LiBr, and CaBr_2 in NMP.

Table 4.4: *interchange terms from dissolution experiments and maximum solubilities from TGA, for NMP-salt and benzanilide-salt at 25° C. Standard deviations are given between brackets.*

Components	Interchange term (J/cm ³)	Max. solubility (gr/gr)	TDP
NMP-CaBr ₂	-1450 (5)	24.7	0.63
benzanilide-CaBr ₂	-2320 (150)	-	-
NMP-LiBr	-2770 (1)	20.1	0.54
benzanilide-LiBr	-3141 (22)	-	-
NMP-LiCl	-1350 (23)	7.8	0.60
benzanilide-LiCl	-6331 (268)	-	-
NMP-CaCl ₂	-1613 (13)	5.5*	0.25
benzanilide-CaCl ₂	-4093 (246)	-	-

*maximum solubility of CaCl₂ is taken from the phase diagram, figure 3.11.

- NMP-CaBr₂ shows the highest dissolution potential, none of these combinations can ever result a thermodynamical stable solution with PpPTA however.
- All salts show a stronger interaction with benzanilide than with NMP.
- LiBr interacts the strongest with NMP.
- LiCl interacts the strongest with benzanilide.
- The difference in interactions with NMP and benzanilide is the smallest for LiBr.

The conclusion is thus that none of the above systems is able to dissolve PpPTA. A further complicating factor is the chemical potential of NMP (not shown explicitly here) in the case of the chloride salts. They take positive values over a larger range of salt concentrations which will eventually cause phase separation. In the case of LiCl the interactions are rather large with benzanilide but not with NMP. This difference can well be responsible for preferred interactions and promote complex formation, which is undesirable. Therefore the interactions between salt-solvent and salt-benzanilide should not differ too much. These interactions are determined by the chemical composition of the specific amide. In the next section the effect of the chemical composition of different amide solvents is investigated.

4.4 Group contributions

To investigate the interactions of a salt with amides, contributions of specific molecular groups were determined. A high interaction between salt and amide is favourable for discriminating between group contributions. Therefore LiCl was chosen to perform the experiments as it shows the largest interaction with benzanilide (PpPTA), see table 4.4. In a second stage also interactions with other salts were measured.

For the calculation of group contributions to the interchange terms, besides the group molar volume fractions also the interchange terms between amides and salt are required. A number of amides were selected in such a way that they differ systematically with respect to their specific molecular groups. In figure 4.8 the molecular formulas of these amides are given.

Seven different molecular groups were distinguished from which all the amides are thought to be built from. As the NH-group is capable of formation of hydrogen bonds, a distinction was made between amide- and urea units that did or did not contain NH-groups. Also a distinction was made whether a phenyl-group is present in a molecule containing a NH-group. The group molecular formulas are given in figure 4.9.

Some of these amides are solid at room temperature and the experiments were therefore conducted by first making a 10 wt% solution of the amide in NMP. This is a similar procedure as was done before in the experiments in which benzanilide was dissolved in NMP. The apparent molar volumes of the amides follow from measuring the densities of the amides in NMP. For mixtures of organic solvents generally the apparent molar volumes are almost equal to the molar volumes of the pure substances and are used as such in the calculation of the contribution of molecular groups to the interchange terms.

In table 4.5 the selected amides are given together with their aggregation condition at room temperature, molar mass and molar volume. Next to that the number of molecular groups, as presented in figure 4.9, they consist of are listed.

From multiple linear regression the apparent molar volumes of the molecular groups can now be determined and are listed in table 4.6 (NMP is not taken along in the fit process as it contains a ring structure which deviates from the other molecular structures).

Based on the data as listed in table 4.6 the corresponding group molar volume fractions in each amide can now be calculated and are also listed in table 4.5 under the respective groups.

In a range of experiments LiCl was added to a 10 wt% amide-NMP solution and the resulting heat effect was measured. As the interchange term between

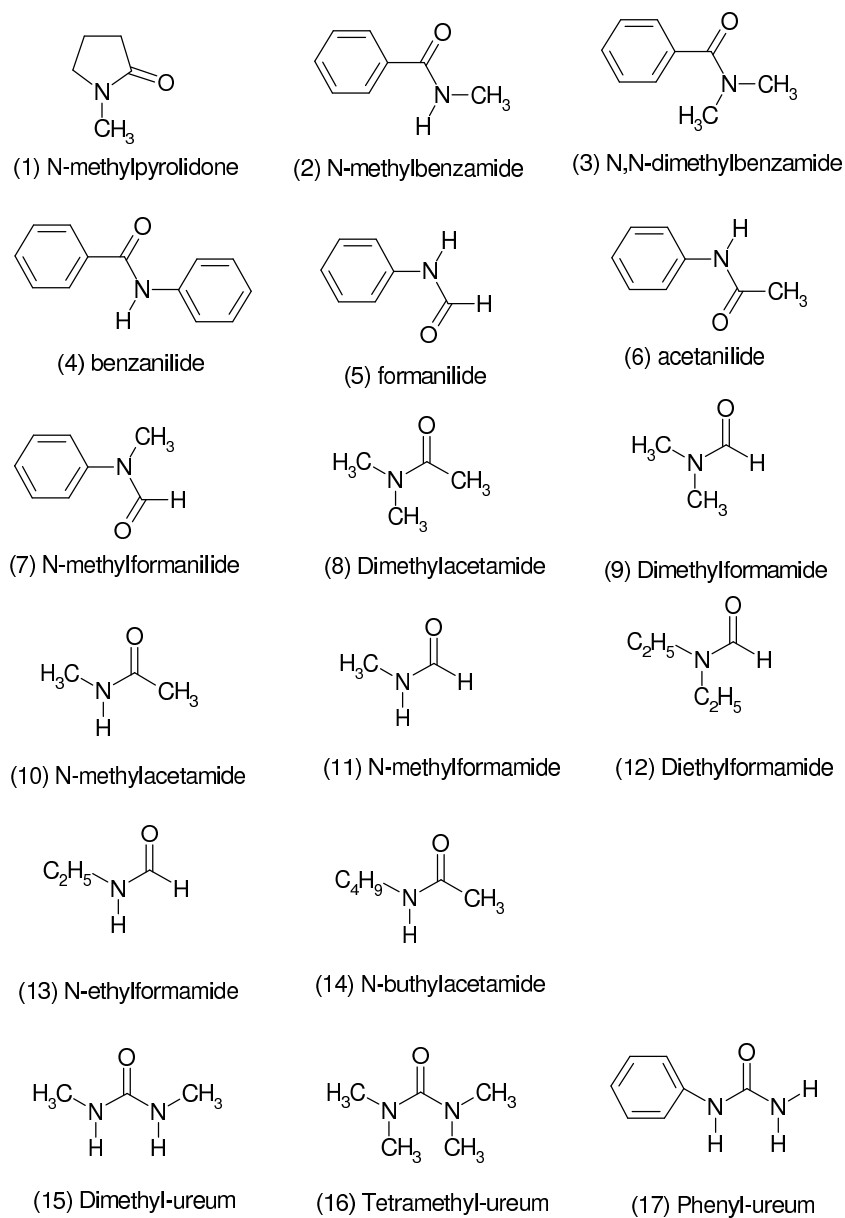


Figure 4.8: *The selected amides used for determining molecular group contributions to the interchange terms.*

Table 4.5: *Amide, aggregation condition at room temperature, molecular weight, molar volume and the volume fractions of their molecular groups. The molecular groups refer to figure 4.9.*

Amide	agg. (25°C)	M (g/mol)	V_m (cm ³ /mol)	N-amide	N,N-amide	Phenyl (NH)	Phenyl (no NH)	Alkyl (-CH ₂)	urea (NH)	urea (no NH)
(1) NMP	l	99.13	96.24	0	0.435	0	0	0.565	0	0
(2) N-methylbenzamide	s	135.17	121.67	0.348	0	0.512	0	0.140	0	0
(3) N,N-dimethylbenzamide	s	149.17	140.22	0	0.307	0	0.450	0.244	0	0
(4) Benzanilide	s	197.24	167.3	0.254	0	0.746	0	0	0	0
(5) Formanilide	s	121.14	105.01	0.405	0	0.595	0	0	0	0
(6) Acetanilide	s	135.17	121.51	0.348	0	0.512	0	0.140	0	0
(7) N-methylformanilide	l	135.17	122.73	0	0.349	0	0.512	0.139	0	0
(8) Dimethylacetamide	l	87.12	92.7	0	0.456	0	0	0.544	0	0
(9) Dimethylformamide	l	73.06	77.49	0	0.557	0	0	0.443	0	0
(10) N-methylacetamide	s	73.09	76.2	0.544	0	0	0	0.446	0	0
(11) N-methylformamide	s	59.06	59.2	0.713	0	0	0	0.287	0	0
(12) Diethylformamide	l	101.15	112.05	0	0.386	0	0	0.614	0	0
(13) N-ethylformamide	l	73.1	77.14	0.554	0	0	0	0.446	0	0
(14) N-butylacetamide	l	115.18	127.23	0.332	0	0	0	0.668	0	0
(15) Dimethyl-urea	s	88.11	82.08	0	0	0	0	0.419	0.581	0
(16) Tetramethyl-urea	l	116.16	120.46	0	0	0	0	0.566	0	0.434
(17) Phenyl-urea	s	136.15	108.8	0	0	0.569	0	0	0.431	0

NMP and LiCl is known to be -1350 J/cm^3 , see table 4.4, the interchange terms between LiCl and various amides can be calculated from the difference of the measured value and the one between NMP and LiCl. In table 4.7 the interchange terms between LiCl and various amides are listed.

The molecules having the largest interaction with LiCl are the ones containing a N-amide group. This group thus shows large interaction with LiCl. As the volume fraction of each molecular group in the amides is also known, it is possible to estimate group contribution from multiple linear regression. Values are listed in table 4.8 (again NMP was due to its deviating structure, left out of the fit process).

The most profound interactions are found for the NH containing group (N-amide and urea containing NH-groups), but also the phenyl group interacts strongly with the salt in this case. From what was concluded previously

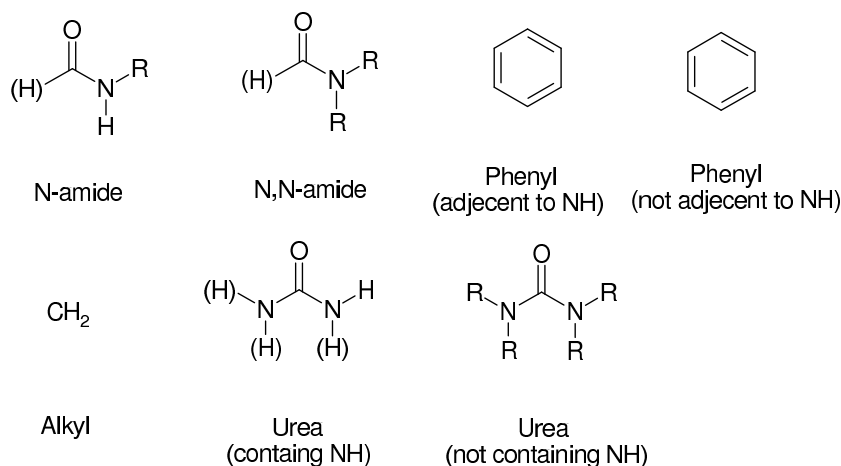


Figure 4.9: *The molecular groups from which the selected amides are build.*

Table 4.6: *Molar volumes of the groups given in figure 4.9. Standard deviations are given between brackets.*

Molecular Group	Molar volume (cm ³ /mol)
N-amide	41.40 (0.62)
N,N-amide	41.92 (0.77)
Phenyl (NH)	62.23 (0.48)
Phenyl (no NH)	62.98 (0.76)
Alkyl (-CH ₂)	17.05 (0.21)
Urea (NH)	47.25 (0.67)
Urea (no NH)	52.25 (1.13)

Table 4.7: *Interchange terms between LiCl and various amides. Standard deviations are given between brackets.*

Amide	Interchange term (J/cm ³)
(1) NMP	-1350 (23)
(2) N-methylbenzamide	-7006 (122)
(3) N,N-dimethylbenzamide	-1350 (151)
(4) Benzanilide	-6331 (268)
(5) Formanilide	-7965 (162)
(6) Acetanilide	-8884 (156)
(7) N-methylformanilide	-1665 (86)
(8) Dimethylacetamide	-2182 (135)
(9) Dimethylformamide	-2356 (67)
(10) N-methylacetamide	-7557 (156)
(11) N-methylformamide	-6948 (80)
(12) Diethylformamide	-1972 (122)
(13) N-ethylformamide	-6466 (108)
(14) N-butylacetamide	-6545 (174)
(15) Dimethyl-urea	-9184 (120)
(16) Tetramethyl-urea	-1350 (88)
(17) Phenyl-urea	-10676 (142)

Table 4.8: *Interchange terms between the molecular groups given in figure 4.9 and LiCl. Standard deviations are given between brackets.*

Molecular group	Interchange term (J/cm ³)
N-amide	-8847 (1397)
N,N-amide	760 (1992)
Phenyl (NH)	-7256 (954)
Phenyl (no NH)	-1943 (1590)
Alkyl (-CH ₂)	-4409 (1527)
Urea (NH)	-13559 (1620)
Urea (no NH)	2653 (2883)

NH: an NH-group is present in the molecule.

no NH: no NH-group present in the molecule.

from the NMR results in chapter 3, it is probably the anion interacting with the amide. The anion may thus form a hydrogen bond with the NH-group. The cation is stabilized by the carbonyl of the amides present. In the case of a phenyl group present in a molecule containing an NH-group a bridging complex between amide- and phenyl-group is probable, given the large contributions of both groups to the interaction. Schematically such a complex is drawn in figure 4.10 in which case benzanilide is used as an example molecule (X^- is used to symbolize the anion and M^+ as the cation). This resembles the structures proposed by Kawakami [27] mentioned in the beginning of chapter 2 when the interactions of salts with amides were discussed. Only in that case cations were forming, in what was called a bidentate-complex, see figure 2.5 in contrast to a complex with both ions here. In the case of an N,N-amide no NH-groups are present and the interactions of LiCl with both the N,N-amide-group and the phenyl-group are much weaker. (The calculated interchange term between the N,N-amide and LiCl is even positive, given the error range though this could actually also be slightly negative.)

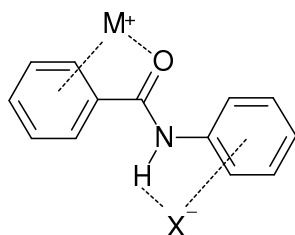


Figure 4.10: *Complex between benzanilide and salt. In which the salt is bridging between the amide and phenyl groups.*

4.4.1 Interchange terms between NMP, LiCl and PpPTA based on group contributions

In table 4.9 the interchange terms between different groups making up some of the amide molecules are listed. They were obtained from work of Zegers and van Baardwijk [86] in which similar work was done in determining interchange terms between various amides in the absence of salts. The table does not contain the urea group and the distinction between adjacent and non-adjacent NH-Phenyl groups as these were not measured.

By using the data from tables 4.6 and 4.9 it is possible to calculate the interchange term between NMP and PpPTA (as well as between NMP and benzanilide for which the value was already given in table 4.1), as now the molar volume of PpPTA in quasi liquid phase can be estimated from its group con-

tributions. PpPTA consists out of an N-amide group and a phenyl group. The interchange term NMP-PpPTA is calculated to be 0 J/cm^3 , using appendix equation A.38 (the contributions from specific groups to the total interchange term is proportional to their volume fractions). This is in close agreement with the value calculated for NMP-benzanilide, -1 J/cm^3 , mentioned in table 4.1.

From group contributions also an interchange term between LiCl and PpPTA can be calculated in the same way as was done for NMP and PpPTA. The repeat unit of PpPTA consists of 1 N-amide-group and 1 phenyl-group. The corresponding interchange term with LiCl therefore is -7900 J/cm^3 (product of the group contributions, table 4.8 proportional to their group volume fractions, table 4.6).

A similar calculation, as was done for benzanilide in NMP- CaCl_2 to obtain the chemical potentials, can now be done for PpPTA in NMP-LiCl. This according to equation 4.19, using the interchange terms as estimated from group contributions. Results for the chemical potentials for PpPTA and NMP as a function of the LiCl concentration are presented in figure 4.11.

PpPTA having a larger interchange term with LiCl than benzanilide causes NMP-LiCl already at 10.5 wt% LiCl to become a real solvent (TDP-index 0.7) instead of the calculated 13 wt% in the case of benzanilide (TDP-index 0.6), see figure 4.7. The solution is by no means stable at interesting PpPTA concentrations though, as is seen from the chemical potential of NMP in a 5 wt% PpPTA mixture. Moreover, complex formation is observed in these mixtures.

In a publication by Panar [44] it is claimed that PBA, see figure 1.3 for its structure, should be soluble in DMA-LiCl solutions and a phase diagram of the ternary system is presented at room temperature. As PBA, an isomer of PpPTA has similar interchange terms as PpPTA, based on our findings it should thus not be soluble. Experimentally it was not possible to dissolve

Table 4.9: *Interchange terms between molecular groups of NMP and benzanilide, according to Zegers [86]. Standard deviations are given between brackets.*

Interacting groups	Interchange term (J/cm^3)	
Alkyl - Phenyl	-22.14	(7.91)
Alkyl - N,N-amide	-144.93	(36.59)
Alkyl - N-amide	-107.02	(33.48)
Phenyl - N,N-amide	-61.74	(20.73)
Phenyl - N-amide	-62.82	(20.14)
N,N-amide - N-amide	-0.25	(17.51)

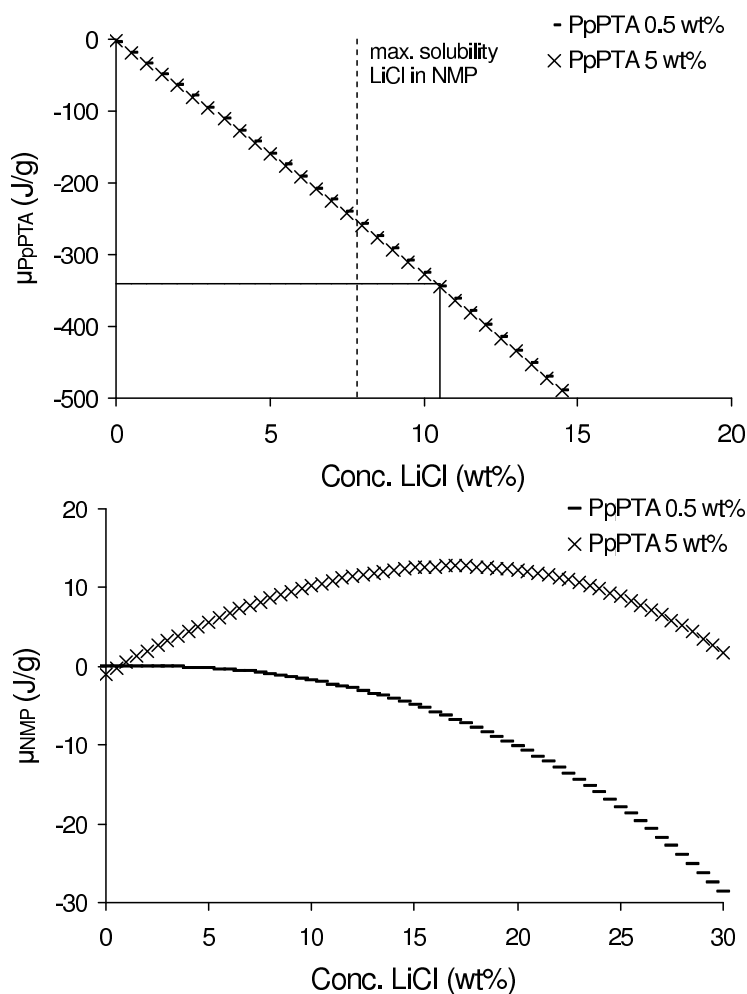


Figure 4.11: Chemical potentials of PpPTA and NMP as function of the LiCl concentration with interchange terms LiCl-NMP -1350 J/g from table 4.7, PpPTA-LiCl -7900 J/g and PpPTA-NMP 0 J/g (based on group contributions) for concentrations of 0.5 wt% and 5 wt% PpPTA. The black line in the top picture indicates the free enthalpy of fusion of PpPTA. All at 25°C.

PBA nor PpPTA in LiCl-NMP or LiCl-DMA solvents in which the maximum amount of LiCl was dissolved for the respective solvents at room temperature. In fact the maximum solubility of LiCl in DMA was measured to be only 4.6 wt% and this results in a TDP index of only 0.46. Also it can be pointed out that the system of 13 wt% PBA in TMU-LiCl (6.5 wt%), mentioned in the introduction chapter 1, is not able to form a true solution, but also forms a meta-stable mixture that will phase separate. The results correspond exactly with the results of PpPTA in NMP-LiCl as the interchange term between TMU and LiCl equals the one between NMP and LiCl (-1350 J/cm^3 , table 4.7) ⁵

4.5 Group contributions of other salts

Having determined the group contributions of interchange terms between molecular groups and LiCl, a limited selection of the most prominent amides can be made to measure the interchange terms between these amides and other salts. Subsequently the group contributions of these interchange terms can then be determined. The sub selection of amides is given in table 4.10 together with the corresponding interchange terms.

Table 4.10: *Interchange terms between a sub selection of amides and LiCl, LiBr, and CaCl₂. Standard deviations are given between brackets. LiCl is listed again for comparison purpose.*

Amide	LiCl (J/cm ³)	LiBr (J/cm ³)	CaCl ₂ (J/cm ³)
NMP	-1350 (23)	-2770 (1)	-1650 (13)
benzanilide	-6331 (268)	-3141 (15)	-4099 (247)
Dimethylformamide	-2356 (67)	-2909 (56)	- -
N-ethylformamide	-6466 (108)	-3434 (31)	-2884 (65)
N-methylbenzamide	-7006 (122)	- -	-3144 (73)
N,N-dimethylbenzamide	-1350 (151)	-2243 (63)	- -
Phenyl-urea	-10676 (142)	-4691 (70)	-4651 (82)
Dimethylacetamide	-2182 (135)	-2305 (205)	- -
N-methylformamide	-6948 (80)	-3841 (42)	-3411 (75)

In comparing values between LiCl and LiBr the major differences are found in the amides containing NH-groups. The interactions between these amides

⁵This conclusion assumes the free enthalpy of fusion of PBA to be equal to PpPTA. Using the transition function of van Krevelen, equation 4.23 with $Y_{m,PBA} = 98 \text{ kgK/mol}$ and $M_w = 119 \text{ g/mol}$, [88] a melting temperature of 824 K is estimated for PBA. Assuming the same argumentation to estimate the entropy contribution as in the case of PpPTA it follows that a similar enthalpy of fusion results and thus a comparable free enthalpy of fusion.

and LiCl are roughly a factor two larger. For CaCl_2 the N-amides were also measured and found to be comparable with LiBr. Also for LiBr group contributions were determined. As the number of amides is much smaller than for LiCl only five groups were distinguished for group contributions. No discrimination between NH-groups in the molecules was made. In table 4.11 the calculated values for the group contributions are listed. The procedure to arrive at these values is analogous to that described before in the case of LiCl.

Also for LiCl the interchange terms are based on the same five groups as for LiBr to be able to compare them, therefore they differ from the values as listed in table 4.8.

Table 4.11: *Interchange terms between the five selected molecular groups and LiCl, -LiBr. Standard deviations are given between brackets.*

Molecular group	LiCl (J/cm ³)	LiBr (J/cm ³)
N-amide	-8752 (1500)	-5010 (778)
N,N-amide	1205 (2129)	-3860 (1353)
Phenyl	-7315 (978)	-2289 (420)
Alkyl (-CH ₂)	-4664 (1562)	-1473 (1194)
Urea	-13492 (1692)	-7902 (902)

In comparing these values with the ones for LiCl they are roughly a factor of two smaller, however the interaction between N,N-amide and LiBr is much larger. This is peculiar since generally the interaction of LiBr is smaller than for LiCl. An explanation might be found in the nature in which LiBr and LiCl are present in the solution. From electrical conductivity measurements, table 4.12 of both LiCl and LiBr in various amide solutions it was found that the molar conductivity in the case of LiBr is larger than for LiCl. This indicates LiBr, to a larger degree to be present in ionic form. In the case of an amide containing an NH group the amide is accessible for salts and both LiCl and LiBr can interact with it. In the case of an amide containing an NR group the accessibility is much smaller and only smaller ions can now interact with the amide. That is Li ions can interact, but the larger counter ions only to a much less degree. As Li ions are more abundantly available in a LiBr solution, the interaction is more profound for LiBr then for LiCl.

4.6 Alternative amide-salt(-benzanilide) systems

Now that the interchange terms between various molecular groups and some salts have been determined as well as their maximum solubilities, it is time to look for combinations that have a TDP-index exceeding unity and may

Table 4.12: *Molar conductivity (σ) of solutions of 4 wt% salt dissolved in some amides and water. The latter is added for comparison.*

Amide/water	σ LiBr (Scm^2/mol)	σ LiCl (Scm^2/mol)	σ CaCl ₂ (Scm^2/mol)
NMP	11.83	2.56	4.23
N-ethylformamide	9.79	4.92	12.90
Dimethylacetamide	20.00	6.21	7.22
Dimethylformamide	21.42	7.39	9.29
Water	70.39	57.62	131.57

thus act as true solvents for PpPTA. As it is the combination of a large interaction between PpPTA and salt and a large maximum solubility of that salt in the amide solvent, which is favourable for dissolving purposes, the maximum solubilities of LiCl and LiBr were determined for the liquid amides at room temperature, see table 4.5. This was done through evaporation in a TGA (until 500°C), results are listed in table 4.13.

Table 4.13: *Maximum solubility of LiCl and LiBr in some amides at 25° C, together with the corresponding interchange term between that salt and PpPTA (based on benzanilide).*

Amide	LiCl (wt%)	Int. term LiCl (J/cm^3)	LiBr (wt%)	Int. term LiBr (J/cm^3)
NMP	7.8	-1350	19.5	-2770
N-methylformanilide	nihil	-1665	7.9	(-3377)
Dimethylacetamide	4.6	-2182	17.5	-2305
Dimethylformamide	5.1	-2356	7.6	-2909
N-methylformamide	13.3	-6948	25.2	-3841
Diethylformamide	13.0	-1972	8.1	(-2598)
N-ethylformamide	11.6	-6466	25.1	-3434
N-buthylacetamide	2.0	-6545	13.2	(-5155)
Tetramethylurea	10.1	-1350	16.8	(-3362)

For LiBr the values between brackets are estimated values based on group contributions.

N-methylformamide and N-ethylformamide are two amides showing the best combination of maximum solubility and a high interchange term, for both LiCl and LiBr. For these combinations the chemical potentials of PpPTA and the amide as a function of the LiCl and LiBr concentration were calculated. LiBr solutions resulted in TDP-indices below unity (0.73 and 0.65 for N-methylformamide and N-ethylformamide, respectively). The TDP-indices of the LiCl solutions however do exceed unity, 1.23 and 1.06 for N-methylformamide and N-ethylformamide, respectively and should in theory result in stable solutions. In figure 4.12 the chemical potentials for PpPTA and NMF, NEF are

presented for a 5 wt% and a 20 wt% PpPTA solution.

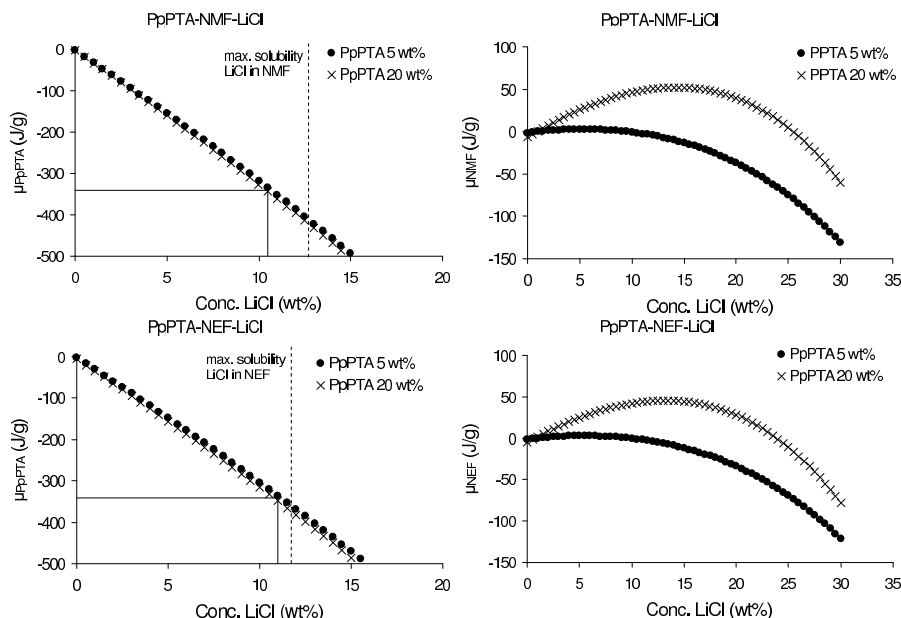


Figure 4.12: Chemical potentials of PpPTA and N-methylformamide (top two) as well as of PpPTA and N-ethylformamide (bottom two) for 5 wt% and 20 wt% PpPTA mixtures as a function of the LiCl concentration. For the calculations use was made from the interchange terms between N-methylformamide-LiCl -6948 J/cm^3 and N-ethylformamide-LiCl -6466 J/cm^3 (as given in table 4.7), LiCl-PpPTA -7900 J/cm^3 , N-methylformamide-PpPTA -6 J/cm^3 and N-ethylformamide-PpPTA -4.5 J/cm^3 (calculated from group contributions). The black lines in the left pictures indicate the free enthalpy of fusion of PpPTA. All at 25°C .

Above 5 wt% PpPTA the chemical potentials of both N-methylformamide and N-ethylformamide become positive over the entire concentration range in which LiCl is soluble and the mixtures are thus not stable.

Before discussing the experimental equivalent of the just mentioned theoretical solutions another phenomenon needs to be addressed first. This concerns a heat effect upon immersion of PpPTA in amide-salt media.

4.7 Effect of immersion of PpPTA in amide salt solvents

4.7.1 Immersion of PpPTA in amide and NMP-salt solvents

Hereto PpPTA was immersed in pure amides at 25°C and the heat effect recorded. The rate by which PpPTA is wetted depends strongly on the size of the amide solvent molecules, the smaller the faster the wetting progresses, see figure 4.13. The magnitude of the exothermic heat effect varies somewhat

over the amides but is roughly in the order of $80 \text{ J/g}_{\text{PpPTA}}$.

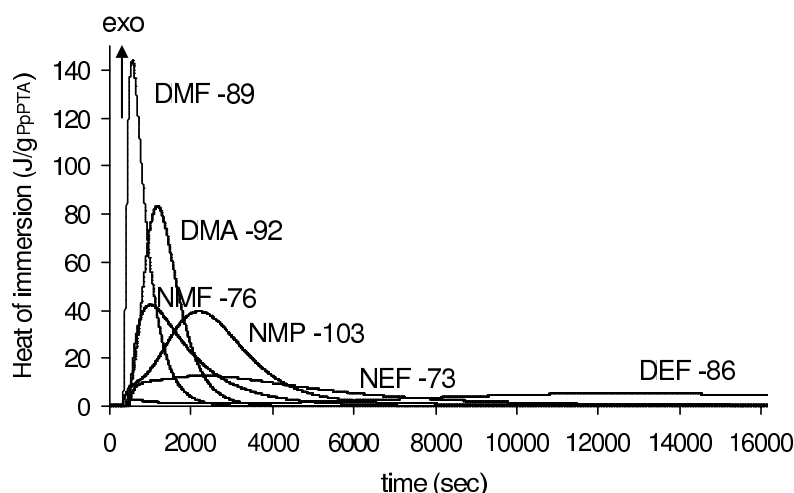


Figure 4.13: *Heat of immersion of PpPTA in several amides at 25°C. The corresponding amide molecule and the total heat effect in $\text{J/g}_{\text{PpPTA}}$ is given with each signal.*

Next, for a number of NMP-salt combinations the heat of immersion of PpPTA was recorded isothermally at 25°C (NMP pure and low salt concentrations) or in scan experiments in a micro calorimeter between 25°C and 120°C at a rate of 0.1°C/min for mixtures containing higher salt concentrations. Results are presented in figure 4.15.

Salt solutions were prepared in advance. In the case immersion of PpPTA was fast the heat effects were recorded isothermally at 25°C. In the case the mixtures contained an amount of salt such that a state of supersaturation at 25°C was obtained, the NMP-salt solutions were heated first to completely dissolve the salt and subsequently cooled back to 25°C. These supersaturated mixtures were found to be stable long enough to conduct a successive scan experiment. In the fully dissolved NMP(-salt) solution PpPTA was immersed and the recording started. Some remarkable features were observed. When PpPTA is immersed in pure NMP a substantial heat effect appears. This seems peculiar as PpPTA is known not to dissolve in NMP. Depending on the salt added and its concentration this heat effect is either in- or decreased. Never a dissolution of PpPTA was obtained after the experiment. There always was a clear separation between the PpPTA powder and solvent.

In most cases the temperature at which the heat effect occurs is a function of the salt concentration and increases accordingly. Also in most cases the heat effect passes through a minimum upon salt addition (maximum exothermic

heat effect).

In figure 4.15 the first experiment presented is performed in pure NMP and all the others contained an amount of a specific salt. Conditions for each salt for the first and last experiment of each curve are given in the legend, e.g. for LiBr the first experiment containing salt resulted in a heat effect at 25°C and the amide-units(PpPTA)/LiBr molar ratio was 0.99, the last experiment showed a heat effect at 86°C and a molar ratio of 0.2. The other experiments had conditions between these two extremes. The amount of PpPTA in all experiments was roughly kept constant and the salt concentration was varied. As no dissolution is observed the effect may very well be a recrystallization phenomenon.

Next to the standard crystal modification (PpPTA I) PpPTA is known to be able to crystallize in a second crystal modification (PpPTA II) [89]. The latter is energetically less favourable as PpPTA modification II transforms irreversibly into modification I upon annealing. In figure 4.14 structures of both modifications are presented, the view is along the chain axis.

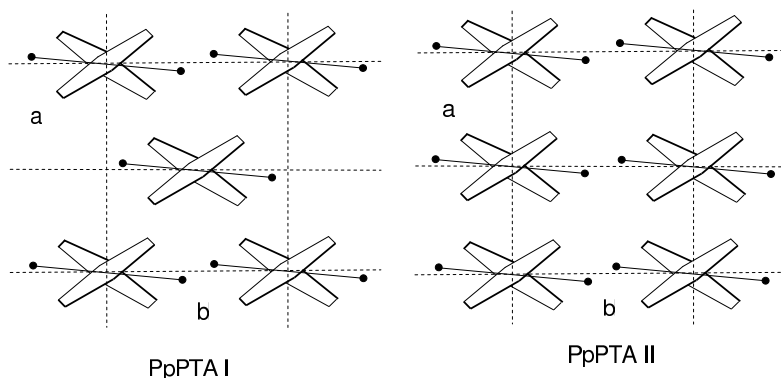


Figure 4.14: *Crystal modifications PpPTA I ($a=7.87 \text{ \AA}$, $b= 5.18 \text{ \AA}$) and PpPTA II ($a=8.0 \text{ \AA}$, $b= 5.1 \text{ \AA}$).*

The initial PpPTA used in the experiments was found to consist of $\sim 70\%$ of the PpPTA II structure, based on XRD measurement. When exposed to pure NMP the less dense crystalline parts (PpPTA II) may interact with NMP and swell to some extent. As was seen before the heat of interaction between NMP and PpPTA is negligible and the process is therefore entropy driven. In this somewhat swollen state the PpPTA molecules may rearrange in a more favourable position and recrystallize resulting in the observed heat effect. When salt is added, favourable interactions between PpPTA and salt are formed as well, causing the dissolution power to increase. This may result in a larger part of the PpPTA to recrystallize and therefore the salts that

induce this heat effect can be denoted as structure makers i.e. LiCl, LiBr and CaCl₂. Ofcourse it may also very well be due to complexation between salt and PpPTA. In the case of LiI or CaI₂ the observed heat effect diminishes as a function of the salt concentration, these salts can be denoted as structure breakers.

On the other hand the heat effects of LiCl, LiBr and CaCl₂ show a minimum. Not until a certain amount of salt is added enough dissolution power is generated to dissolve PpPTA. It is therefore conceivable that at first a zero heat effect should be registered before dissolution of PpPTA will occur. This means enough dissolution power and no structure inducing effects. In diagram 4.16 this is energetically sketched. PpPTA, if immersed in sulphuric acid, dissolves readily up to 20 wt%. Above this concentration the net free enthalpy change becomes positive and no more PpPTA can dissolve. In the case of immersion in a NMP-salt medium, due to a smaller change in free enthalpy upon dissolution, PpPTA does not dissolve in most of these media. As can be seen the recrystallization effect disfavours dissolution and forms an extra energy barrier that needs to be overcome. Only media that have enough dissolution power to drop under the dashed line are potential dissolution media (indicated by the arrow).

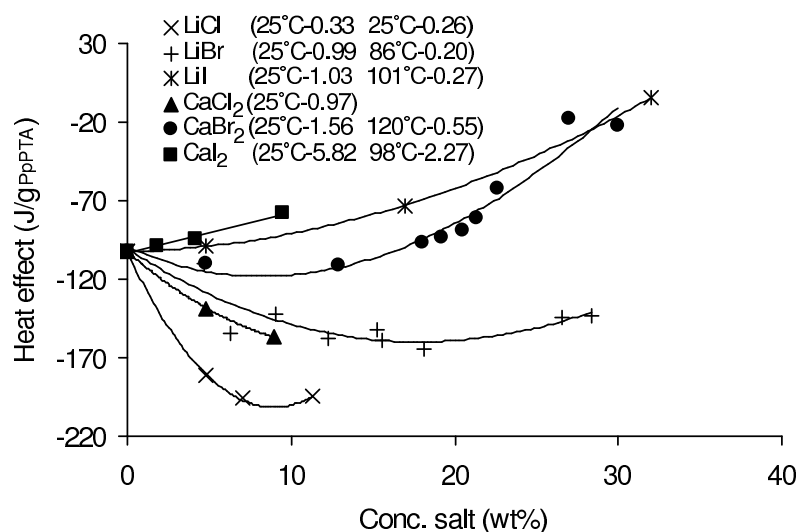


Figure 4.15: *Heats of immersion of PpPTA in NMP(-salt) solutions. In all cases no solution was obtained.*

As was discussed earlier the TDP-indices for dissolving PpPTA in NMF-LiCl and NEF-LiCl were calculated to exceed unity. This means that in principle the dissolution power is large enough to compensate for the free enthalpy of fusion of PpPTA. For this type of solvent however the activation

energy for dissolution apparently is high and recrystallization increases this barrier even more. It is this barrier that hinders dissolution.

4.7.2 Immersion of PpPTA in NMF-LiCl and NEF-LiCl

Similar immersion experiments of PpPTA were performed for NMF-LiCl as well as NEF-LiCl solutions. Solutions of various LiCl concentration were heated while recording the heat effect in a DSC. Results are displayed in figures 4.17 and 4.18.

Both solvents show a heat effect upon immersion of PpPTA in them. The

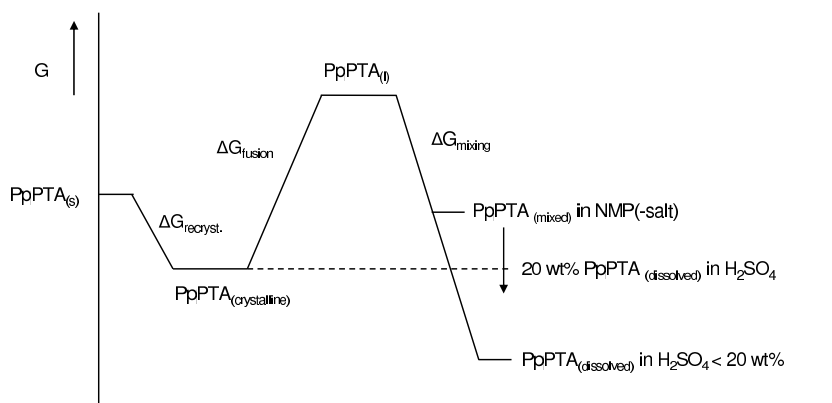


Figure 4.16: Sketch of the energy diagram of the dissolving of PpPTA.

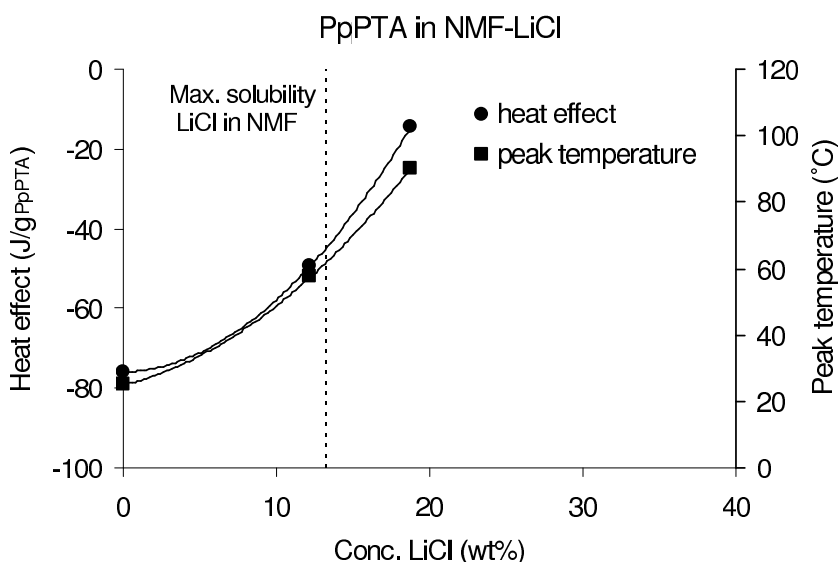


Figure 4.17: Heats of immersion of PpPTA in NMF-LiCl. Peak temperatures are the temperatures at which the heat effects occur.

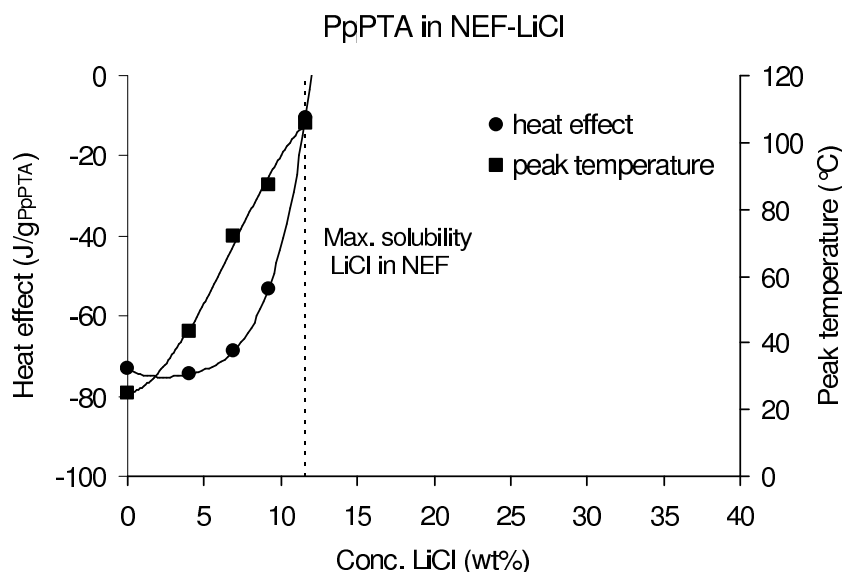


Figure 4.18: *Heats of immersion of PpPTA in NEF-LiCl. Peak temperatures are the temperatures at which the heat effects occur.*

dashed lines indicate maximum solubility of LiCl at 25°C, see table 4.13. The effect is smaller though and decreases more rapidly upon increasing the LiCl concentration in comparison with solutions of LiCl in NMP, see figure 4.15. For the NEF-LiCl solvent the effect almost vanishes at maximum solubility of LiCl. In this case the solution power should in principle be sufficient to dissolve PpPTA. Due to the high activation energy for dissolution in these media both solvents however do not result in thermodynamic stable solutions.

The PpPTA used in the experiments so far is manufactured according to the process as shown in figure 1.9 in the introduction. As mentioned before this PpPTA is highly crystalline and consists of $\sim 70\%$ PpPTA modification II, figure 4.14. Although this is not the most energetically favourable modification, which is modification I, it does have a high dissolution barrier. As was already mentioned in the introduction though, a new processing route for the manufacturing of PpPTA pulp was developed [12], [13] and [14]. In this new process PpPTA pulp is spun directly from the polymerization solvent (NMP-CaCl₂) and it turns out that this PpPTA is very low crystalline, based on X-ray measurements.

Upon immersion of this low crystalline PpPTA in NEF-LiCl a completely different heat effect is recorded in the DSC, figure 4.19 in comparison with figure 4.18. Instead of a decrease of the heat effect upon increasing the LiCl concentration it now slightly increases even without the need to increase the temperature. This is probably caused by (partial) dissolution of low crystalline

PpPTA due to a lower dissolution barrier. After the experiment a gel like substance is obtained, in contrast to the immersion of high crystalline PpPTA in which case after the experiment a PpPTA powder is still present in NEF-LiCl. (The dissolution process is probably still not complete as the total heat effect is lower than the required 340 J/g to compensate for the free enthalpy of fusion of PpPTA, as was estimated in section 4.2.3. It can very well be however that the low crystalline fraction of the sample has indeed dissolved.)

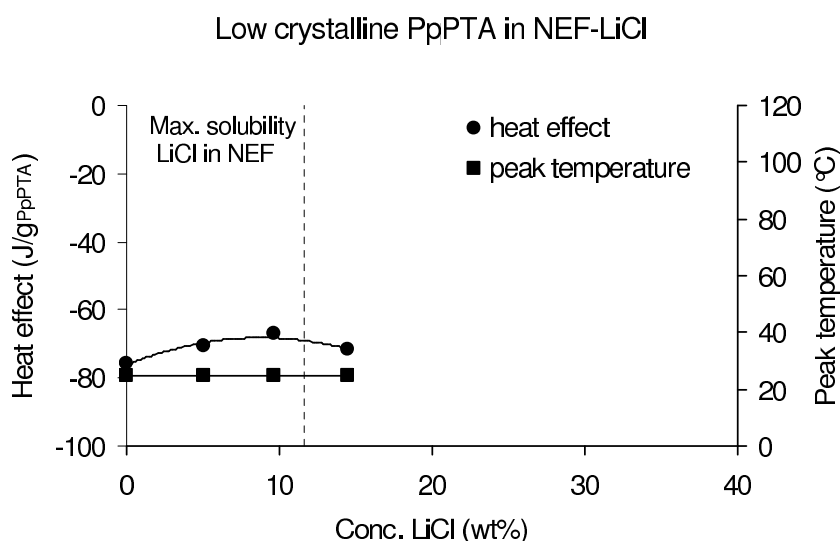


Figure 4.19: *Heats of immersion of low crystalline PpPTA in NEF-LiCl. Upon increasing the LiCl concentration the heat effects remains without elevating the temperature and is probably caused by (partial) dissolution of low crystalline PpPTA. Peak temperatures are the temperatures at which the heat effects occur and remains 25°C.*

4.7.3 Immersion of isomers of PpPTA in sulphuric acid and NMP-salt solvents

The dissolution of PpPTA in sulphuric acid was also compared with the dissolution of its isomers PBA, DABT and PmPTA in sulphuric acid and NMP-CaCl₂, see figure 1.3 for their chemical structures. The first two are para-aramids, like PpPTA, the other is a meta-aramid and is expected to be far less crystalline. All isomers were immersed in both sulphuric acid and NMP(-salt) at 25°C as well as 88°C. The para-aramids only dissolved in sulphuric acid, whereas PmPTA dissolved both in sulphuric acid as well as NMP(-salt) media. The heats of dissolution are presented in figures 4.20 and 4.21.

At 88°C the para-aramids show similar behaviour. Although their heats of dissolution at infinite dissolution show little variation the slopes are rather

small. The slope is related to the solute-solute interactions and their interchange terms are thus very similar. This is to be expected as the para-aramids, being isomers, on a molecular level will interact similar with sulphuric acid. In contrast, at 25°C the slopes are rather large for PpPTA and DABT. This may be due, as said before, to complex formation between PpPTA, (DABT) and sulphuric acid at low concentrations giving rise to larger particles and extra interaction terms between these complexes which are not taken into account in model calculations. At 88°C it is likely that no complexes are present and the slope is lower.

PBA does not show this behaviour at 25°C. Its molar weight was rather small (~ 1700 g/mol) compared to the other two (≈ 20000 g/mol), which might explain the difference.

PmPTA on the other hand showed similar behaviour at both 25°C and 88°C, indicating no complex formation between PmPTA and sulphuric acid. The value for the heat of dissolution at 88°C is somewhat larger than for the para-aramids (values at 25°C can not be compared as complex formation occurs). This may very well be due to a lower free enthalpy of fusion that need to be compensated for in the dissolving process due to lower crystallinity compared to the para-aramids, see figure 4.22 for a sketch of the energy profile for dissolving PmPTA. Furthermore, PmPTA dissolves readily upon immersion in NMP(-salt) systems. Although to dissolve PmPTA in NMP- CaCl_2 at 25°C it needs to be heated before dissolution occurs in contrast to dissolution in pure NMP in which case no heating is required.

Peculiar seems the heat of dissolution of PmPTA in NMP in the order of

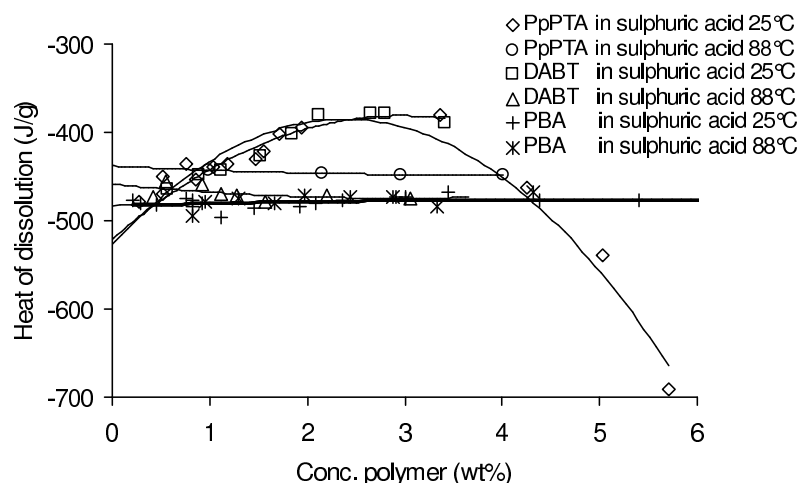


Figure 4.20: *Heats of dissolution of para-aramids: PpPTA, PBA and DABT in sulphuric acid. In all cases solutions were obtained.*

-200 J/g. As found before the interchange term between PpPTA and NMP is negligible (the interchange term between PpPTA and NMP was calculated to be 0 J/g, based on group contributions) and for PmPTA, an isomer it is, on first sight approximated that, on a molecular level, the interactions between the amide groups and NMP are similar for both isomers. For it certainly can not explain this rather large heat effect upon dissolution. PmPTA is a meta-aramid and has a much less rigid structure than the para-aramids. It exhibits flexible behaviour leading to far less efficient chain-chain interactions in the pure substance. Only a limited amount of the amide groups will fully interact with one another in hydrogen bonding, on one hand leading to a lower free enthalpy of fusion but also, upon dissolving in an amide solvent, in more effective amide-amide interactions. Due to the limited size of NMP, it is capable of penetrating between the flexible chains and effectively form hydrogen bonds with the amide groups of PmPTA. Therefore dissolution of PmPTA in NMP probably results in formation of more amide-amide bonds giving rise to an exothermic heat effect. Apart from the better penetration of NMP between the flexible chains of PmPTA, the activation energy to dissolve in amide-salt based solvents is less high for PmPTA. Both the exothermic heat effect and the lower barrier to dissolution explain the dissolution of PmPTA in NMP.

The observation that heating is needed to dissolve PmPTA in NMP- CaCl_2 can be explained by the fact that CaCl_2 increases the barrier to dissolution for PmPTA as it does for PpPTA, see figure 4.15.

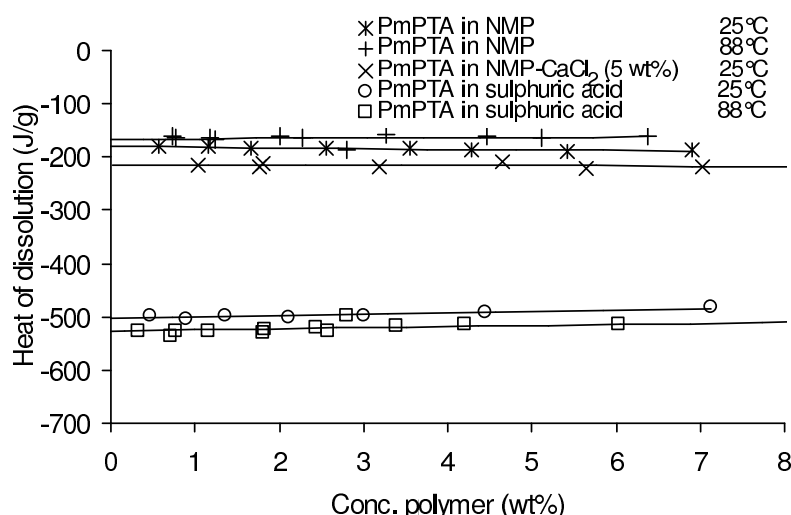


Figure 4.21: *Heats of dissolution of PmPTA in sulphuric acid as well as NMP(-salt). In all cases solutions were obtained.*

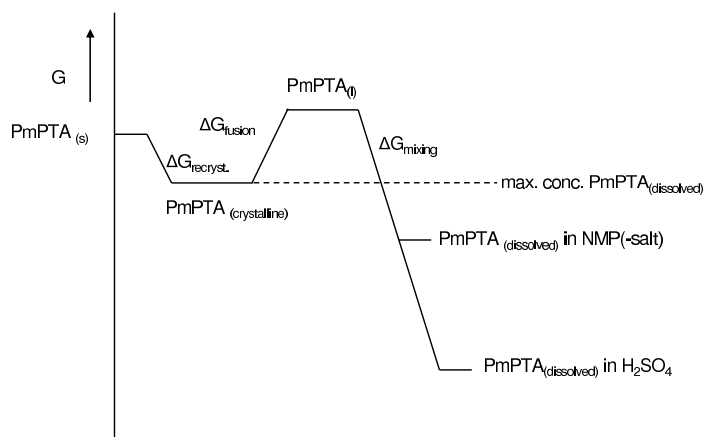


Figure 4.22: Sketch of the energy diagram of the dissolving of PmPTA.

4.8 The PpPTA-H₂SO₄-CaF₂ system

Salt was seen to be crucial in the dissolution power of amides. It is therefore interesting to investigate the influence of salt addition on the maximum solubility of PpPTA in sulphuric acid. Hereto CaF₂, CaCl₂ and CaBr₂ were added to sulphuric acid (100%). Both CaCl₂ and CaBr₂ solutions resulted in gas formation (HCl and HBr release). The CaF₂ however did not, but formed a clear solvent at 25°C. In order to determine the interchange term between PpPTA and CaF₂, PpPTA was dissolved in a solution of 1 wt% CaF₂ in sulphuric acid at 25°C and the corresponding heat effect was recorded in a calorimeter, figure 4.23. An interchange term between PpPTA and (H₂SO₄-CaF₂(1 wt%)) of -386 J/cm³ was calculated. The interchange term between PpPTA and sulphuric acid at this temperature is -357 J/cm³. From the difference, corrected for the weight fraction, the interchange term between PpPTA and CaF₂ is calculated to be -5280 J/cm³.

As CaF₂ has a profound interaction with PpPTA the maximum solubility of PpPTA in sulphuric acid to which CaF₂ is added, should exceed the maximum without CaF₂ (23 wt% at 25°C is the maximum solubility of PpPTA in pure sulphuric acid). In figure 4.24 the influence of the amount of CaF₂ on the chemical potential and subsequently on the maximum solubility of PpPTA is shown at 25°C.

The calculated chemical potentials of CaF₂ and sulphuric acid are negative for all compositions, meaning CaF₂ dissolves readily in sulphuric acid up to 2 wt%. The chemical potential of PpPTA increases when the PpPTA concentration is increased. In figure 4.24 therefore the difference of the chemical potential and the free enthalpy of fusion of PpPTA is given. Below zero

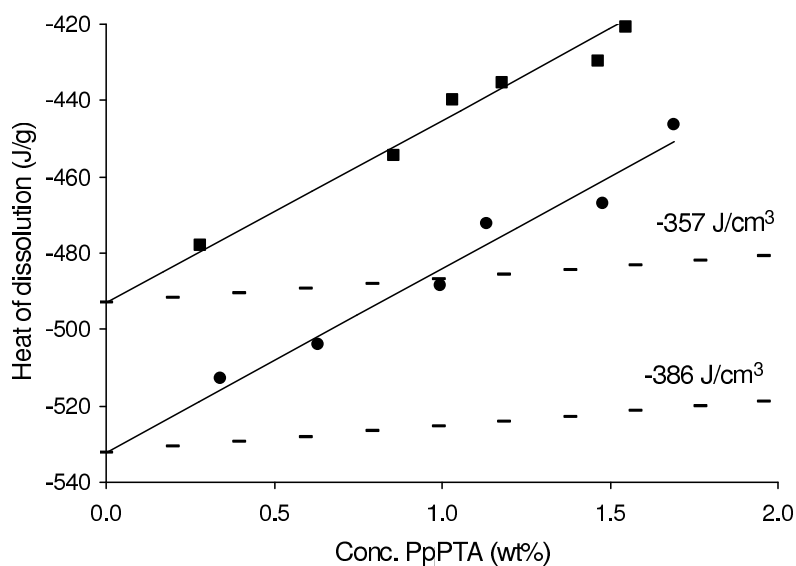


Figure 4.23: Measured heats of dissolution for PpPTA in pure sulphuric acid (squares) and in a solvent of 1 wt% CaF₂ in sulphuric acid (bullets) at 25°C together with calculated model data. Interchange terms are respectively -357 J/cm³ and -386 J/cm³.

PpPTA will remain in solution, above zero PpPTA will phase separate. Due to the large interaction of PpPTA with CaF₂ the maximum solubility increases substantially. At 25°C from 23 to 28 wt%. A similar effect, not explicitly displayed here, is expected at 88°C which would increase the maximum solubility from 20 to 25 wt% by addition of 1 wt% CaF₂. For spinning purposes this seems very beneficial.

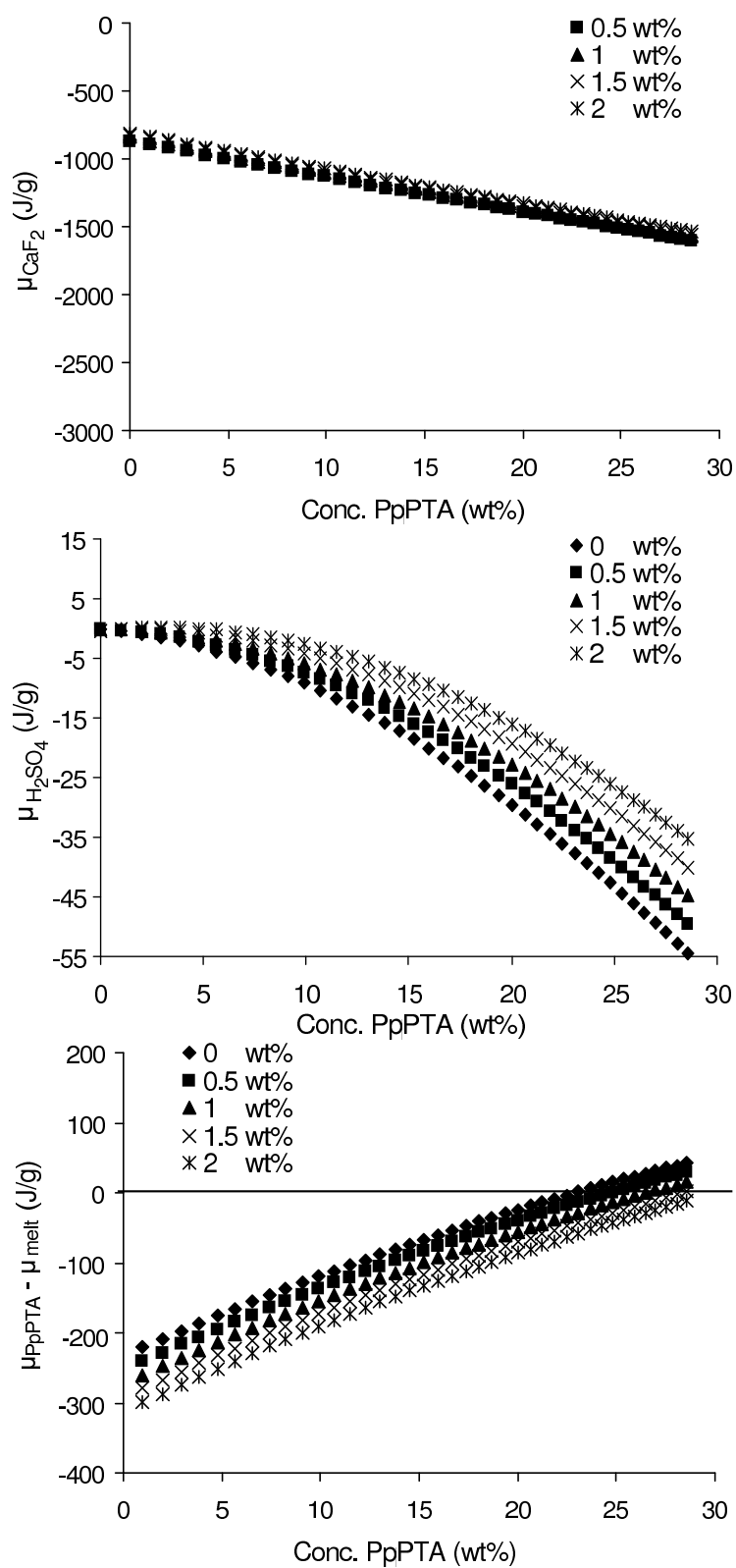


Figure 4.24: Influence of CaF_2 (0 to 2 wt%) on the chemical potential and thereby solubility of PpPTA at 25°C.

4.9 Conclusions

In this chapter the thermodynamics of mixtures of PpPTA in acidic and non-acidic media was discussed. Hereto a model was introduced to calculate the partial excess free enthalpy change upon mixing components. A parameter, the interchange term, was introduced based on volume fraction statistics referring to the change in enthalpy upon interchanging an A-A interaction with an A-B interaction and simultaneously a B-B interaction with an A-B interaction. The interchange terms were calculated based on measurements of interaction heats between the components of a mixture. For measurements on PpPTA-NMP-CaCl₂, benzanilide was used as a model compound for PpPTA as the polymer itself does not dissolve in NMP-CaCl₂. The interactions of benzanilide were taken representative for PpPTA. NMP and benzanilide interact strongly with CaCl₂, especially benzanilide has a high interchange term (-4093 J/cm³). NMP and benzanilide among themselves have a very low interchange term, meaning almost no heat effect is involved in mixing them. To compensate for the free enthalpy of fusion of PpPTA it is necessary to introduce enough CaCl₂-PpPTA interactions. Numerically the minimum required amount of salt needed, was calculated to be 22 wt%. Due to solid complex formation between CaCl₂ and NMP, the maximum amount of CaCl₂ that can be dissolved in NMP is limited to 5.5 wt% at 25°C, as was shown in the phase diagram 3.11 of NMP-CaCl₂ in the chapter 3. Therefore based on the specific interactions between PpPTA and NMP-CaCl₂ this mixture is thermodynamically not stable and NMP-CaCl₂ can never act as a true solvent for PpPTA.

In contrast sulphuric acid can act as a true solvent. In this case the interactions between PpPTA and sulphuric acid are strong and numerous enough to compensate for the free enthalpy of fusion of PpPTA, which was estimated, using several methods, to be about 340 J/g.⁶

The para-aramid isomers of PpPTA, PBA and DABT produce similar dissolution heats in sulphuric acid as PpPTA does, resulting in similar interchange terms and excess free enthalpies of fusion. The meta-aramid PmPTA is much less crystalline and has a lower heat of dissolution and also dissolves in NMP(-salt) media. This indicates a far lower free enthalpy of fusion, as expected due to non-rigid behaviour of meta-aramid. Although the interchange term between PmPTA and NMP was expected to be negligible, still a substan-

⁶Although the interchange term between PpPTA and sulphuric acid (-357 J/cm³) is far less than between PpPTA and CaCl₂ (-4093 J/cm³) at 25°C, the number of interactions between PpPTA and sulphuric acid are far greater than between PpPTA and CaCl₂ due to limited solubility of CaCl₂ in NMP.

tial exothermic heat effect was found upon dissolving PmPTA in pure NMP. This was explained by an increased amount of amide-amide interaction upon dissolving PmPTA in NMP due to better accessibility of polymer-amides by NMP molecules compared to pure PmPTA in which the amides are confined to the chain and are therefore unable to interact optimally.

From interchange terms between PpPTA and other NMP-salt systems, LiCl interacts strongest with PpPTA (interchange term -7900 J/cm^3). Its maximum solubility at 25°C is limited to 7.8 wt% and this is also too low to compensate for the free enthalpy of fusion of PpPTA (minimal 10.5 wt% needed).

By varying the solvent amide molecules, group contributions to interchange terms were determined. That is, from different amides the interchange terms with LiCl and benzanilide were determined and from it the contributions of various groups to these interchange terms calculated. Especially amides containing an NH-group contribute largely to the interchange term and to some extent also the phenyl-group adjacent to an NH containing amide-group. This indicates mainly the binding of anions to the chain. As the anions (chloride) are rather large compared to the cations (lithium) it can be expected that large groups substituted to the amide, NR-groups, result in lower interaction. When instead of LiCl, LiBr is used the group contributions are lower, as expected because the interchange term between LiBr and PpPTA is also lower (-3387 J/cm^3). In this case however the amides containing an NR-group also show significant interaction with LiBr. Since, bromide is larger than chloride it possesses far less ionic strength. As a result the electrical conductivity of LiBr in NMP is roughly five times larger than in the case of LiCl in NMP. This means more ions present in the LiBr solvent. It can be expected that here the lithium ions, to a much larger degree, contribute to the interaction with the amide of the polymer.

Two factors can be distinguished to determine the dissolution power of an amide-salt combination. One is the interaction heat between salt and polymer as expressed by the interchange term. The second is the maximum solubility of the salt in the amide solvent, which determines the maximum amount of favourable interactions between salt and polymer. This was expressed in the TDP-index (ratio of the maximum possible amount of dissolved salt over the calculated minimal required amount of dissolved salt) and needs to be optimized to enhance dissolution power. If this index exceeds unity the medium is theoretically able to dissolve PpPTA. It is theoretical as the index does not take into account complex formation between salt and PpPTA, which might alter, due to changed interactions, the dissolution power considerably.

As temperature influences the maximum solubility of salts considerably

PpPTA was immersed in NMP-salt combinations and subsequently heated. In pure NMP and solutions with low salt concentration a recrystallization effect appeared. The initial PpPTA used in the experiments consisted of an energetically less favourable crystalline structure, i.e. PpPTA II for $\sim 70\%$. Upon immersion in NMP(-salt) it swells to some extent and then recrystallizes in the more favourable PpPTA I structure. This recrystallization effect decreases in the series $\text{LiCl} > \text{CaCl}_2 > \text{LiBr} > \text{CaBr}_2 > \text{LiI} > \text{CaI}_2$. The smallest and thus most strong ions result in the largest effect in recrystallization in which the anions dominate the cations. The larger ions are ultimately better soluble and thus able to interact more favourably with PpPTA. None of the amide-salt combinations resulted in the actual dissolution of PpPTA though.

In general the larger ions, thus the ions with the lesser ionic strength, give the best results, due to their increased solubility and their tendency to decrease the recrystallization effect. Probably these salts have less tendency to form complexes with either solvent-amide or polymer. The solubility of CaI_2 , which would be expected to be largest in the series, is however much smaller (1.9 wt% at 25°C).

Amide-salt combinations found to exhibit a TDP-index exceeding unity are NMF-LiCl (1.23) and NEF-LiCl (1.06). When PpPTA of high crystallinity was immersed in NEF-LiCl solely a recrystallization effect was observed. When PpPTA of low crystallinity was immersed however, signs of true dissolution were observed in DSC experiments. In the latter case the dissolution barrier is much lower and can to an extent be overcome.

Finally it was found that salts may also influence the solubility of PpPTA in sulphuric acid favourably, based on the same mechanism as in the case of amide-salt systems, a high interchange term between salt and PpPTA. Adding only up to 2 wt% CaF_2 to sulphuric acid increased the solubility of PpPTA from 23 to 28 wt% at 88°C .

5. Modeling of the NMP-Polyaramid System

After having discussed experimental evidence on the meta stable behaviour of PpPTA in NMP-CaCl₂ in chapter 3 and the thermodynamics of these solutions in chapter 4, in this chapter the interactions between the components are investigated using molecular modeling techniques. The anion is found to be mostly in the vicinity of the PpPTA amide-unit and the cations reside in the solution mainly in an aggregate manner.

5.1 Introduction

In the previous chapter evidence was presented that showed NMP-CaCl₂ unable to act as a true solvent for PpPTA. This was based on a thermodynamic model and the assumption that benzanilide interactions could mimic the PpPTA interactions. A strong interaction was found between benzanilide and CaCl₂, causing the salt to be mainly responsible for lowering the chemical potential of PpPTA in the mixture and so determining the dissolution power. The mechanisms by and the way in which interactions between different components take place however, remains unclear. From electrical conductivity experiments it was found that cations are present in the form of clusters: CaCl⁺ and Ca₂Cl₃⁺. In order to verify these findings computational modeling is a useful tool in studying the dynamical behaviour of mixtures.

In this and the following chapters the dynamical processes going on, on a molecular level are discussed based on molecular modeling techniques. One goal is to verify the conclusions from the previous chapters. Secondly new insights may provide leads to a more fundamental understanding of the determining phenomena in dissolving PpPTA. This can be beneficial in trying to find other dissolving systems then currently known.

5.2 Methods

The calculations presented in this and the following chapters are based on three different computational techniques:

- 1. Calculations on particle-particle interactions in the liquid phase via the conductor-like screening model (COSMO).
- 2. Molecular Dynamics (MD), which describes the dynamic behaviour of the system at the atomic level.
- 3. Quantum Mechanics (QM), which is used to calculate more accurately the relative energies of different configurations of the system.

5.2.1 COSMO

The COSMO method calculates interactions in the liquid phase, where particles are in close contact, but are still mobile. First, a quantum chemical calculation is done on each component. In this calculation, the component is placed inside a conducting surface, simulating the presence of a high-dielectric medium, allowing for back-polarization (the particle polarizes the conductor, which in turn leads to additional polarization of the particle and so on). The charge distribution of the component causes a complementary charge distribution on the conductor surrounding it. This conducting surface is then divided into small segments, and the charge density of each segment is calculated. These data are stored as a histogram, showing how frequent a particular screening charge density occurs, called sigma profile, see figure 5.1. The sigma profile shows the electrostatic properties of the component, and is the basis for calculating the electrostatic interactions.

Electrostatic interactions arise primarily at the contact surface between two components. This interaction can be approximated by pairwise matching the surface segments present in the system, see figure 5.1 for a system containing CaCl_2 dissolved in NMP. This match is optimal if each segment is in contact with a segment of opposite charge; non-optimal matches may result from the shape of the sigma profiles as well as temperature effects. The temperature is represented as different geometries of matches in the system.

The polarity of a component can be assessed from its sigma profile. Another characteristic function can be derived from this profile, the sigma potential. It shows the energy of a surface segment placed in an environment described by the given sigma profile, as a function of its charge density. It thus shows how well a component (with a particular sigma profile) will interact with another component. As an example, the sigma potential of NMP, shown

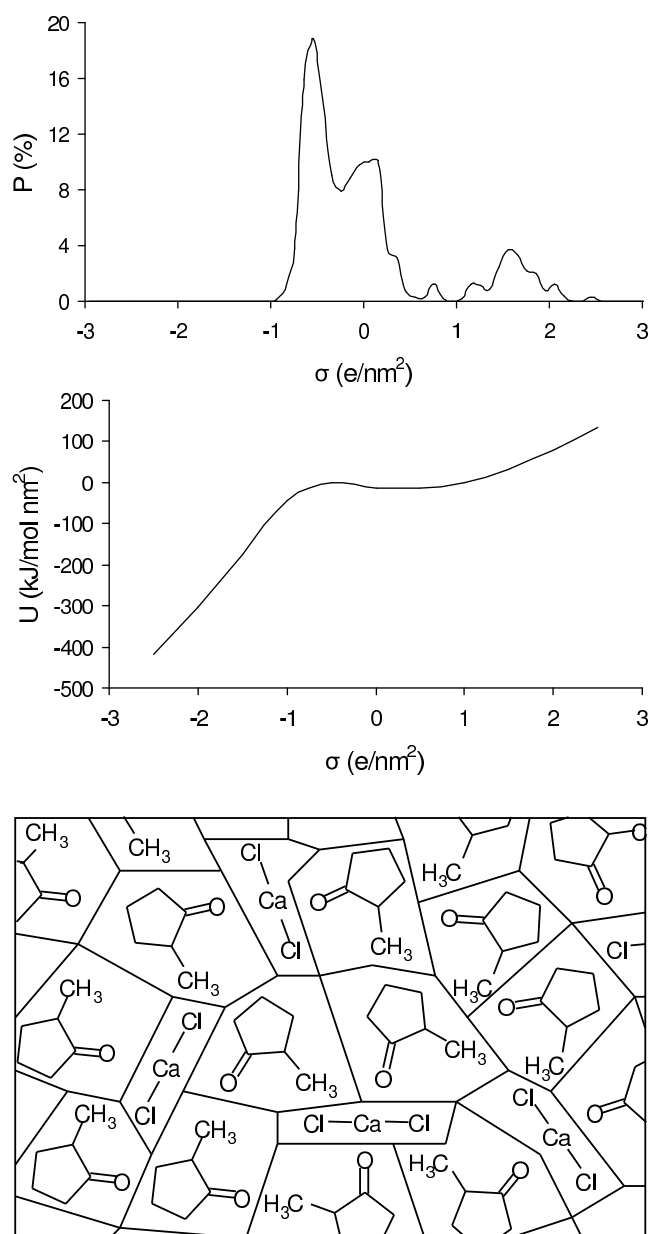


Figure 5.1: *Sigma profile (top) and sigma Potential (middle) of NMP and matching of surface segments of CaCl_2 in NMP (bottom).*

in figure 5.1, may be taken. It is low for negatively charged surfaces, showing affinity for negative screening charges, and high for positively charged screening surfaces. The calcium ion, which has only negatively charged screening surface, will therefore have a negative (favourable) interaction energy with NMP; the opposite holds for the chloride ion. This can also be understood by looking at the components directly: the exposed, negatively charged carbonyl oxygen of NMP (causing a positive screening charge) will have a favourable interaction with the positively charged calcium ion (which has a negative screening charge).

The total interactions between the surface elements consists, next to the electrostatic component described above, of van der Waals interactions, and in specific cases hydrogen bond interactions. The computer program used in this research has its own empirical parameters to account for these two additional types of interactions. Due to the mobility of the components in the liquid, different interactions occur as a function of temperature. The interaction energy is calculated by considering a statistical distribution of matches between surface elements.

The Cosmo method has been implemented in a number of computer programs. The program used for this research is called COSMOTerm¹. The quantum chemical calculations were done using the Turbomole² package.

5.2.2 Molecular dynamics

Molecular dynamics (MD) is a method to simulate the motion of particles at the atomic/molecular level by applying Newton's law of motion ($\vec{F} = m \cdot \text{veca}$) on the atoms from which the system is built up. By calculating the energy of each atom as a function of its position, for each atom the force, acceleration, velocity and position can be calculated as a function of time, given its initial position and motion due to thermal energy. This is done at discrete time intervals, typically 10^{-15} s . Depending on the system, statistically reliable data require simulations of the order of 10^{-9} s , equaling 10^6 time steps. This implies the individual energy calculations should be fast, and therefore a relatively simple, empirical type of energy function is commonly used, called a molecular mechanics force field. It basically consists of (extensive) lists of equilibrium atomic distances, angles and torsion angles, associated force constants, and so on. Electrostatic interactions are taken into account by assigning electric charges to the individual atoms. During a simulation, the hybridization of the

¹COSMOTerm is available from COSMOLogic GmbH & Co. Burscheider Str. 515, D-51381 Leverkusen Germany; <http://www.cosmologic.de/>.

²Turbomole is developed at the group of Prof. Ahlrichs at the University of Karlsruhe, Germany and supplied via COSMOLogic GmbH.

atoms and their connectivity do not vary, and atomic charges are also fixed, and for example do not change as a function of molecular conformation or intermolecular interactions. In general, the method gives acceptable results for molecular conformations near equilibrium.

MD can be used to study the dynamics of a process, e.g. dissolution at a crystal surface, but also to obtain a representative set of structures from which structural data at a particular pressure and temperature can be obtained. For example, torsion angles, inter atomic distances, pair correlation functions and diffraction data may be obtained as an average or as a function of time. The software used for the MD calculations described here is Materials Studio³. All simulations were done using the COMPASS⁴ force field, which (contrary to some other force fields available) reproduces the crystal structures of CaCl₂ and NMP very accurately, and can therefore be considered suitable for the simulations. Long-range interactions in periodic systems were calculated using the Ewald summation technique.

5.2.3 Quantum mechanics

Quantum Mechanics (QM) describes a chemical system as a set of atomic nuclei and electrons. The energy of a configuration is calculated by assuming the electrons are optimally distributed given the positions of the nuclei. As a consequence, the method imposes no restrictions on hybridization and charge distribution, as opposed to methods using a molecular mechanics force field. QM offers an alternative to these methods which is in general more accurate, but several orders of magnitude slower.

As the time required for QM calculations strongly depends on the system size, keeping the system under investigation as small as possible is important. This can for example be done by doing the calculations on a molecule smaller than, yet representative of, the molecule under actual investigation, and by representing the surrounding medium/solvent by a continuum to which a certain dielectric value is assigned. The QM software used here (Turbomole⁵), uses the Cosmo approach [90], [91] to take into account the surrounding dielectric.

³Material Studio is available from Accelrys, <http://www.accelrys.com/>.

⁴COMPASS (Condensed-phase Optimized Molecular Potentials for Atomistic Simulation Studies) is an ab initio forcefield that has been parameterized and validated using condensed-phase properties in addition to various ab initio and empirical data for molecules in isolation.

⁵Turbomole is developed at the group of Prof. Ahlrichs at the University of Karlsruhe, Germany and supplied via COSMOLogig GmbH.

5.3 PpPTA in NMP-CaCl₂

The objective of this section is to obtain insight on a molecular level into the structure of NMP-CaCl₂ solutions and their interactions with PpPTA chains, in order to explain the effect of CaCl₂ on the solubility of PpPTA in NMP from a dynamical point of view.

As shown in the previous chapter, adding CaCl₂ increases the solubility by decreasing the chemical potential, but the mechanism behind this was not well-established. Better knowledge of the mechanism will be beneficial in the development of improved solvents, and optimizing the properties of the solution, such as stability. In this study, molecular modeling is used to obtain more insight in the interactions between CaCl₂, NMP and PpPTA. First the solubility of CaCl₂ in NMP was studied.

For the COSMO calculations, first the sigma profiles of the molecules/ions of interest had to be obtained. The Turbomole software was used, employing a TZVP basis with polarizing d-set, and a BP DFT functional. The geometry of each molecule was optimized in a quantum chemical calculation, leading to a (either local or global) energy minimum, for which the sigma profile was calculated. Molecular structures of the simulated components are shown in figure 5.2, sigma surfaces, profiles and potentials are shown in figure 5.3.

Next to NMP and the chloride and calcium ions, four model structures were used. Model components 1 ... 3 are increasingly large molecules representing a PpPTA polymer chain. Since PpPTA in its crystalline form has a somewhat twisted geometry, see figure 4.14 of the PpPTA crystal modifications in the previous chapter, model component 2 has been modeled twice differing in their conformation, once in an almost flat geometry, and once in a slightly twisted geometry. Their sigma profiles and potentials are very similar, so no significant difference between these two models is to be expected in the COSMO calculations. PpPTA itself was represented by a model component in which exactly one repeat unit is involved.

Model component PpPTA is taken from model component 3, but leaving out the surface segments at both ends of the molecule. Only those central surface segments that correspond to one single repeat unit of PpPTA are used for the sigma data. Those data should give the best representation of true PpPTA in the calculations.

The Ca²⁺ ion causes some conceptual problems because its size, which determines at what distance the conducting surface is to be placed and thereby the charge density on the surface, is rather debatable. Based on the advice of the software vendor, a radius of 3.1 Å was chosen. Because of the spherical symmetry, a larger radius will result in a larger peak in the sigma profile (more

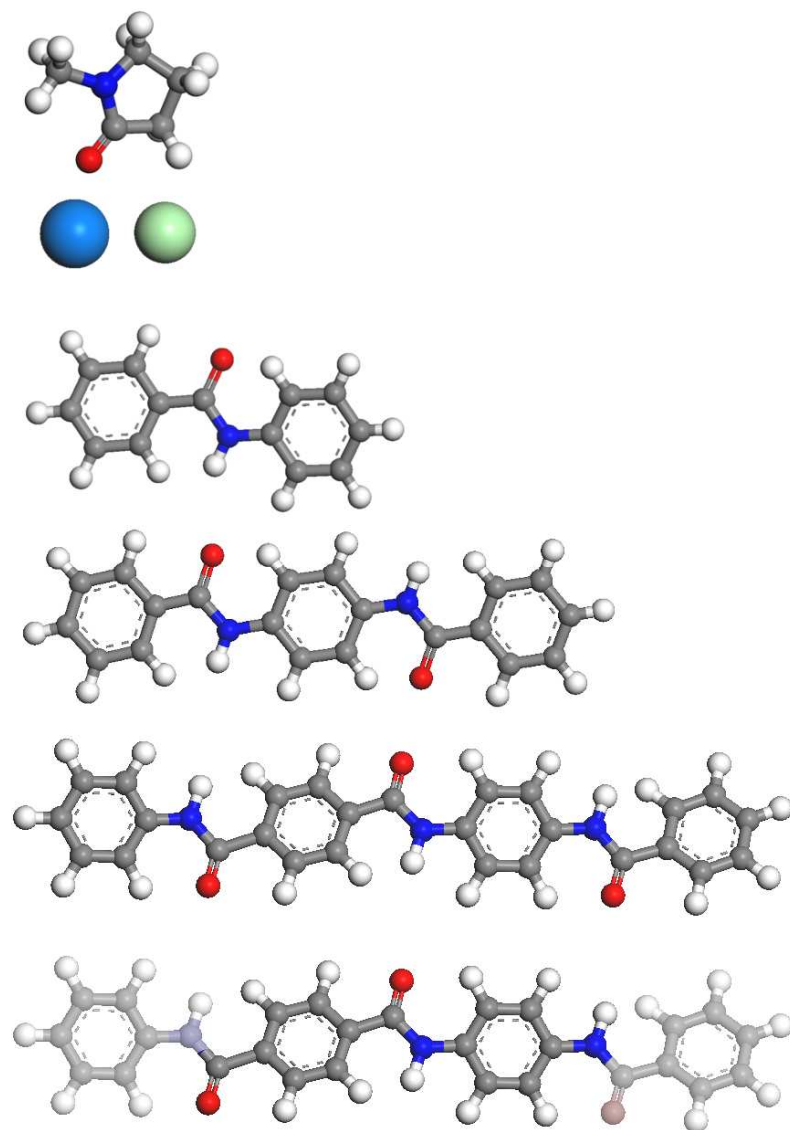


Figure 5.2: Structures of simulated molecules from top to bottom NMP, calcium ion (blue) and chloride ion (green), model component 1 (benzanilide), model component 2 (*N,N'*-(*p*-phenylene)dibenzamide, PPDB), model component 3 and model component PpPTA.

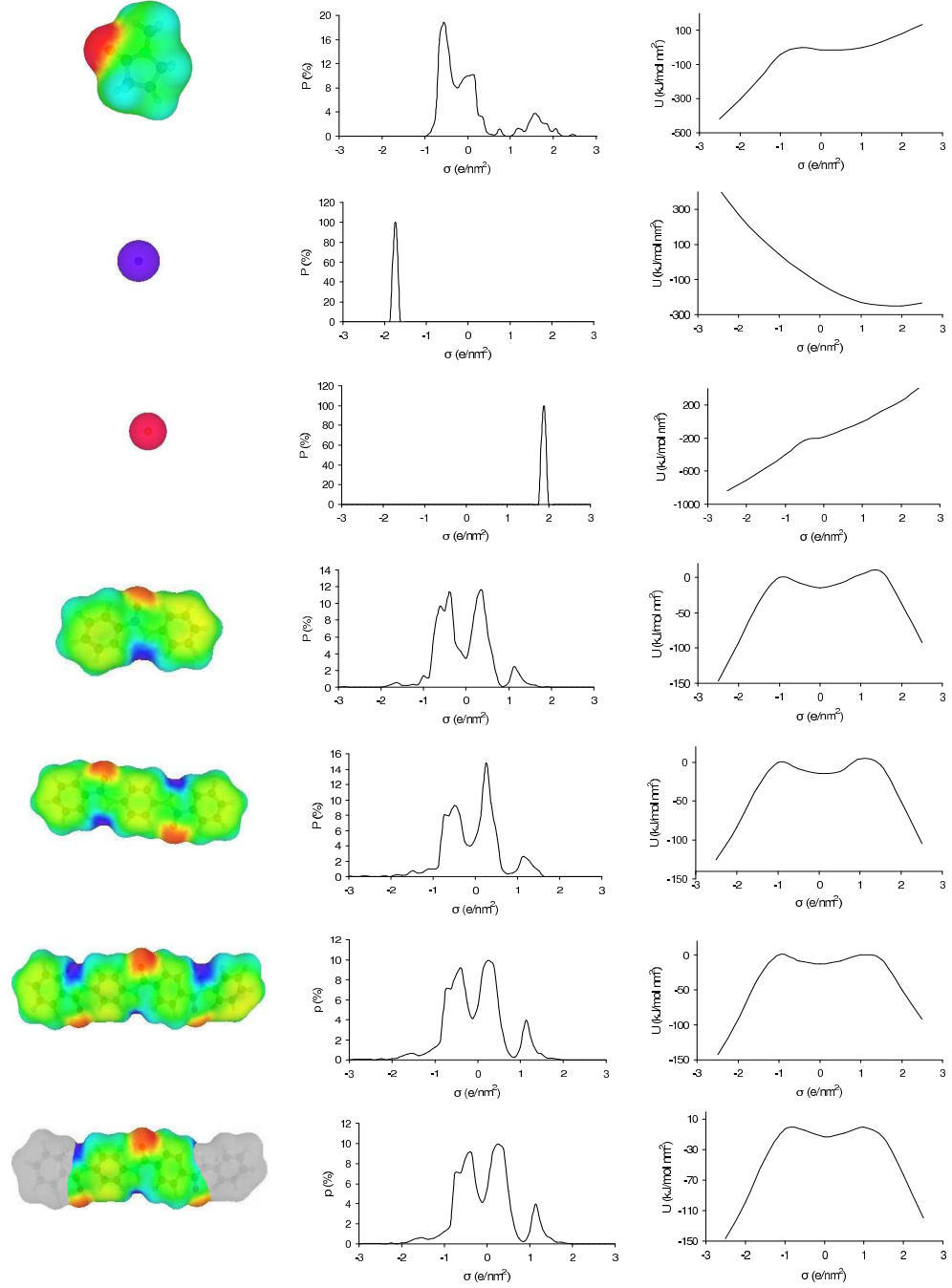


Figure 5.3: Charge distribution, sigma profile and sigma potential of simulated molecules. From top to bottom NMP, calcium (purple) and chloride (red), model component 1 (benzanilide), model component 2 (N,N'-(p-phenylene)dibenzamide, PPDB), model component 3 and model component PpPTA.

segments are needed to cover the large surface) at a higher (less negative) charge density value. Modeling the Cl⁻ ion causes similar concerns, but more effort has already been put into obtaining optimal values.

5.3.1 Solubility of CaCl₂ in NMP

In order to calculate the maximum solubility an expression for the chemical potential difference for CaCl₂ in the dissolved state and the pure salt state is required. Hereto the chemical potential can be expressed in terms of the fugacity. The fugacity relates the chemical potential of a solution to the chemical potential of the corresponding vapour pressure, and is defined for component i as:

$$d\bar{G}_i \equiv RT d \ln \hat{f}_i , \quad (5.1)$$

\hat{f}_i is the fugacity of component i in solution. As it is not a partial molar property of the solution but rather related to the vapour it is identified by a circumflex rather than an overbar. With the notion that $\bar{G}_i = \mu_i$ integration of equation 5.1 at constant temperature results in:

$$\mu_i = RT \ln \hat{f}_i + \Theta_i(T) , \quad (5.2)$$

with $\Theta_i(T)$ some integration constant depending on temperature only, which will vanish in the course of integration at constant temperature. For i in the pure state equation 5.2 becomes:

$$\mu_i^* = RT \ln f_i + \Theta_i(T) . \quad (5.3)$$

If the integration of 5.1 at constant T and P is performed for the change of component i from a state of pure i , where $\bar{G}_i = G_i$ and $\hat{f}_i = f_i$, to a state in solution at arbitrary mole fraction x_i the result is:

$$\mu_i - \mu_i^* = RT \ln \frac{\hat{f}_i}{f_i} = RT \ln a_i , \quad (5.4)$$

a_i is the activity of component i . Non-ideal behaviour is expressed by the activity-coefficient γ_i , $a_i = \gamma_i x_i$. In ideal solutions $\gamma_i = 1$. By substitution equation 5.4 becomes:

$$\mu_i - \mu_i^* = RT \ln x_i + RT \ln \gamma_i . \quad (5.5)$$

According to the Debye-Hückel Theory, the mean ionic activity coefficient γ_{\pm} for a salt M_pX_q dissolved to give a solution of ions $M^{+|z^+|}$ and $X^{-|z^-|}$ in the ratio $p : q$ is given by:

$$\gamma_{\pm} = (\gamma_+^p \gamma_-^q)^{\frac{1}{p+q}} . \quad (5.6)$$

The solubility of a salt M_pX_q can now be calculated from:

$$\mu_{salt,sol} - \mu_{salt}^* = RT(p+q)(\ln x_{salt} + \ln \gamma_{\pm}) , \quad (5.7)$$

in which $\mu_{salt,sol}$ expresses the sum of the chemical potentials of the ions in solution, μ_{salt}^* the sum of the chemical potentials of the ions Ca^{2+} and $2Cl^-$ in the pure state and x_{salt} the fraction salt in the dissolved state.

COSMOTerm treats the solid phase as a sub cooled liquid phase, so the free enthalpy of fusion needs to be added separately. The chemical potentials of the ions in the sub cooled liquid and in the dissolved state are calculated from interaction energies based on the sigma potential profiles. The enthalpy contribution to the chemical potential follows from the magnitude of the interactions and is determined at infinite dilution. The entropy contribution results from the number of matching surface configurations belonging to a specific interaction energy. From these the activity can be calculated.

For $CaCl_2$ the melting temperature, $T_m = 1055K$ and the heat of fusion, $\Delta \bar{H}^{fus} = 25522 \text{ kJ/mol}$ [92]. The free enthalpy of fusion ($CaCl_{2(s)} \rightarrow Ca_{(l)}^{2+} + 2Cl_{(l)}^-$) is now calculated from:

$$\Delta \bar{G}^{fus} \approx \Delta \bar{H}^{fus} (1 - T/T_m) . \quad (5.8)$$

Solubility of Ca^{2+} - Cl^- in NMP

For $CaCl_2$ the solubility, the mole fraction dissolved $x_{CaCl_2,sol}$ can be calculated by the following expression:

$$RT \ln a_{CaCl_2,sol} = \frac{\mu_{CaCl_2,melt} - \mu_{CaCl_2,sol}}{3} - \Delta \bar{G}_{CaCl_2}^{fus} . \quad (5.9)$$

The difference between the chemical potentials of the pure melt state and the dissolved state is reversed compared to the former expressions and is due to the way COSMOTerm calculates these chemical potentials. $\mu_{CaCl_2,melt}$ is the sum of the chemical potentials of Ca^{2+} and $2Cl^-$ in the sub cooled liquid and $\mu_{CaCl_2,sol}$ the sum of the chemical potentials of Ca^{2+} and $2Cl^-$ in

solution at infinite dilution. The division by three follows from the formation of three ions upon melting CaCl₂. By calculating the chemical potential at infinite dilution it is implicitly assumed that the mixture behaves ideal and the activity becomes equal to the mole fraction. This assumption is only true for small fractions of CaCl₂ dissolved and will prove to be valid from the results about to be presented. In table 5.1 the calculated results are shown.

Table 5.1: *Chemical potential of CaCl₂ in the sub cooled liquid state and the dissolved state of Ca²⁺ and Cl⁻ ions at infinite dilution in NMP, calculated by COSMOTerm. Free enthalpy of fusion according to equation 5.8 and calculated solubility according to equation 5.9 for a temperature range of 250-360 K.*

T (K)	$\mu_{\text{CaCl}_2, \text{melt}}$ (kJ/mol)	$\mu_{\text{CaCl}_2, \text{sol}}$ (kJ/mol)	ΔG^{fus} (kJ/mol)	$x_{\text{CaCl}_2, \text{sol}}$ (10 ⁻⁹)
250	6.613	75.403	19.474	1.41
260	8.168	79.302	19.233	2.36
270	9.571	83.131	18.991	3.82
280	10.954	86.888	18.749	6.03
290	12.317	90.573	18.507	9.29
300	13.658	94.182	18.265	14.01
310	14.978	97.716	18.023	20.70
320	16.275	101.173	17.781	30.07
330	17.551	104.553	17.539	42.99
340	18.804	107.854	17.297	60.58
350	20.034	111.077	17.055	84.24
360	21.243	114.222	16.813	115.74
370	22.429	117.289	16.571	157.26
380	23.594	120.278	16.330	211.49
390	24.737	123.190	16.088	281.76
400	25.860	126.026	15.846	372.08

The fraction dissolved, x_{CaCl_2} is much smaller than is experimentally observed. From the phase diagram presented in figure 3.11 dissolution is possible up to approximately 5.5 wt% at 300 K. As the molar weights of CaCl₂ ($M_w=110$ g/mol) and NMP ($M_w=96$ g/mol) are quite similar the mole fraction dissolved should also be approximately 5.5% at 300 K.

A number of factors may be responsible for this difference.

- the ionic radii of Cl⁻ and in particular Ca²⁺ are somewhat arbitrary. A smaller radius will lead to different interactions strengths, e.g. stronger hydrogen bonds. A larger Ca²⁺ radius may lead to a quantitatively better result.
- the calculated chemical potentials of Ca²⁺ and Cl⁻ are based on infinite

dilution, and not on the actual concentration. To obtain the value for a saturated solution, an iterative procedure would be necessary. As can be seen in table 5.1 the fraction dissolved CaCl_2 is rather small however.

- Other components than just Cl^- and Ca^{2+} are likely to be present in the solution, as can be observed from MD simulations (which will be discussed further on in this chapter).
- The ions are surrounded by a strongly bonded layer of solvent molecules, and it could be argued that instead of only the ion, also the first dissolved shell should be taken into account in the quantum mechanical description of the ion.
- small amounts of water are known to be present in the solution that could interact strongly with the dissolved CaCl_2 .

The components, the ionic radius of Ca^{2+} and the effect of water appear to be important factors influencing the result. These are investigated in more detail in the next sections.

Effect of ionic radius on the solubility of CaCl_2

As mentioned earlier, the ionic radius to be used in the Cosmo calculations is not well defined, and it is worthwhile to investigate whether a different radius leads to quantitatively better results. Moreover, it is to be expected that the effect of the ionic radius in the calculations has its counterpart in reality when going from one cation to another: the observed trend is expected to be the same. To study this effect, the Ca^{2+} radius used in the Cosmo calculations was changed from its original value of 3.1 Å to 2.8 Å and 3.5 Å, and the sigma profiles obtained were used to recalculate the CaCl_2 solubility. Results are shown in table 5.2.

It can be seen that the calculated solubility of CaCl_2 increases with increasing radius of Ca^{2+} . This is caused by the combined effect of a higher energy in the melt and a lower energy in the solution (not shown in the table); still, the solubility is too low when the larger radius of 3.5 Å is used.

Effect of components on the solubility of CaCl_2

The occurrence of other components than the individual ions in the solution may also have a significant effect on the solubility. The solubility in NMP of fully dissociated CaCl_2 is calculated to be very low, and MD simulations (presented later) indicate that Ca_xCl_y clusters with a net charge between -1 and

Table 5.2: *Effect of the radius of Ca²⁺ on the calculated solubility of CaCl₂ in NMP for a temperature range of 250-360 K.*

T (K)	r= 2.8 Å x (10 ⁻¹¹)	r= 3.1 Å x (10 ⁻⁹)	r= 3.5 Å x (10 ⁻⁶)
250	2.95	1.41	1.48
260	5.98	2.36	1.81
270	11.57	3.82	2.23
280	21.46	6.03	2.72
290	38.31	9.29	3.33
300	66.10	14.01	4.07
310	358.44	20.70	4.96
320	653.36	30.07	6.04
330	1151.18	42.99	7.35
340	1968.96	60.58	8.92
350	3272.91	84.24	10.81
360	5301.77	115.74	13.07
370	8386.40	157.26	15.78
380	12977.25	211.49	19.00
390	19676.54	281.76	22.84
400	29275.76	372.08	27.39

+1 are more common in the solution. Therefore solubility calculations were carried out for CaCl₂ dissociated into CaCl⁺-Cl⁻, and CaCl₂ "molecules".

Solubility of CaCl⁺-Cl⁻ in NMP

The sigma surface, profile and potential of CaCl⁺ is shown in figure 5.4. For calcium, a radius of 3.1 Å was used.

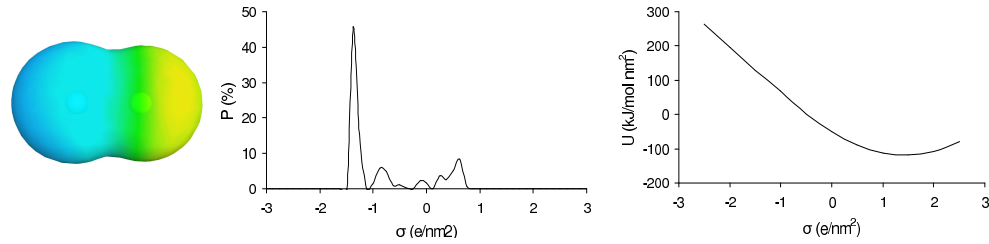


Figure 5.4: *Charge distribution, sigma profile and sigma potential of a CaCl⁺ cluster.*

The solubility is given by:

$$RT \ln a_{\text{CaCl}_2, \text{sol}} = \frac{\mu_{\text{CaCl}_2, \text{melt}} - \mu_{\text{CaCl}_2, \text{sol}}}{2} - \Delta \bar{G}_{\text{CaCl}_2}^{\text{fus}}, \quad (5.10)$$

in which $\mu_{\text{CaCl}_2, \text{melt}}$ is the sum of the chemical potentials of CaCl^+ and Cl^- in the sub cooled liquid and $\mu_{\text{CaCl}_2, \text{sol}}$ the sum of the chemical potentials of CaCl^+ and Cl^- in solution at infinite dilution. By calculating the chemical potential at infinite dilution it is again implicitly assumed that the mixture behaves ideal. $\Delta \bar{G}^{fus}$ now is the free energy change upon going from solid CaCl_2 to a melt of CaCl^+ and Cl^- . This free energy change is not known; it is estimated to be 1/2 of the value for complete melting into individual ions. Note the denominator has changed to 2, as the number of ions formed upon melting CaCl_2 is now 2 (CaCl^+ and Cl^-). The calculated solubility is shown in table 5.3.

Table 5.3: *Chemical potential of CaCl_2 in the sub cooled liquid state and the dissolved state of CaCl^+ and Cl^- ions at infinite dilution in NMP, calculated by COSMOTherm. Free enthalpy of fusion is taken to be half of the value for complete melting into individual ions and calculated solubility according to equation 5.10 for a temperature range of 250-360 K.*

T (K)	$\mu_{\text{CaCl}_2, \text{melt}}$ (kJ/mol)	$\mu_{\text{CaCl}_2, \text{sol}}$ (kJ/mol)	ΔG^{fus} (kJ/mol)	$x_{\text{CaCl}_2, \text{sol}}$ (10^{-5})
250	7.066	27.005	9.737	7.63
260	8.384	29.248	9.616	9.38
270	9.675	31.420	9.495	11.47
280	10.937	33.523	9.374	13.95
290	12.172	35.556	9.253	16.88
300	13.379	37.520	9.132	20.33
310	14.558	39.417	9.011	24.39
320	15.709	41.248	8.891	29.13
330	16.832	43.014	8.770	34.66
340	17.927	44.716	8.649	41.07
350	18.995	46.357	8.528	48.48
360	20.037	47.937	8.407	57.03
370	21.051	49.459	8.286	66.84
380	22.040	50.925	8.165	78.07
390	23.004	52.336	8.044	90.86
400	23.942	53.694	7.923	105.40

The fraction dissolved for the $\text{CaCl}^+ - \text{Cl}^-$ pair is calculated to be about four orders of magnitude higher compared to the fully dissociated salt, but still much lower than the observed solubility. Although this may be partly due to limitations in the calculation (e.g. ignoring a first dissolved shell; using an "improved" radius for Calcium), the main conclusion is that the solubility of this ion pair in NMP is indeed rather low.

Solubility of CaCl₂ clusters in NMP

Another alternative is to consider the solubility of neutral CaCl₂ clusters in NMP. The charge distribution, sigma profile and sigma potential of CaCl₂ are shown in figure 5.5. Again a 3.1 Å radius was used for calcium.

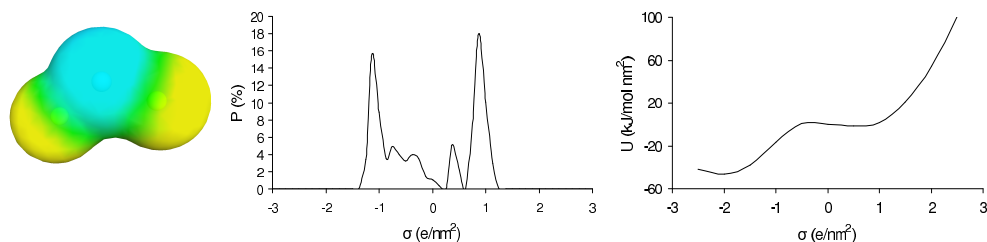


Figure 5.5: *Charge distribution, sigma profile and sigma potential of simulated CaCl₂ cluster.*

The solubility is now given by:

$$RT \ln a_{\text{CaCl}_2, \text{sol}} = \mu_{\text{CaCl}_2, \text{melt}} - \mu_{\text{CaCl}_2, \text{sol}} - \Delta \bar{G}_{\text{CaCl}_2}^{\text{fus}}, \quad (5.11)$$

in which $\mu_{\text{CaCl}_2, \text{melt}}$ is the chemical potentials of CaCl₂ in the sub cooled liquid and $\mu_{\text{CaCl}_2, \text{sol}}$ the chemical potential of CaCl₂ in solution at infinite dilution. By calculating the chemical potential it is again implicitly assumed that the mixture behaves ideal. $\Delta \bar{G}^{\text{fus}}$ now is the free energy change upon going from solid CaCl₂ to a melt of CaCl₂. This free energy change is not known; it is estimated to be 1/3 of the value for complete melting into individual ions. Note the denominator has changed to 1, as the molecules do not split up into ions upon melting. The calculated solubility is shown in table 5.4.

The calculated solubility of CaCl₂ molecules is six to seven orders of magnitude higher than the calculated value for the completely dissociated salt, and is in much better agreement with experimental observations, see phase diagram 3.11 in chapter 3.

Effect of water on CaCl₂ solubility

NMP-CaCl₂ solutions normally contain (traces of) water, influencing the solubility of CaCl₂. The effect on the solubility of the different components was studied by doing calculations while varying the composition of the solvent, from pure NMP to pure water. The results are shown in figure 5.6.

The calculations were done taking into account one single type of component at a time, assuming the other components are not present. As a result, the absolute numbers at higher concentrations are not reliable. The graph

Table 5.4: Chemical potential of CaCl_2 in the sub cooled liquid state and the dissolved state but in cluster form (non-ionic) at infinite dilution in NMP, calculated by COSMOTherm. Free enthalpy of fusion is taken to be a third of the value for complete melting into individual ions and calculated solubility according to equation 5.11 for a temperature range of 250-360 K.

T (K)	$\mu_{\text{CaCl}_2, \text{melt}}$ (kJ/mol)	$\mu_{\text{CaCl}_2, \text{sol}}$ (kJ/mol)	ΔG^{fus} (kJ/mol)	$x_{\text{CaCl}_2, \text{sol}}$ (10^{-2})
250	-14.805	-15.111	6.427	5.26
260	-13.980	-14.206	6.347	5.89
270	-13.178	-13.334	6.267	6.58
280	-12.400	-12.494	6.187	7.30
290	-11.643	-11.684	6.107	8.08
300	-10.911	-10.905	6.027	8.90
310	-10.203	-10.156	5.948	9.77
320	-9.518	-9.435	5.868	10.68
330	-8.857	-8.742	5.788	11.63
340	-8.219	-8.077	5.708	12.62
350	-7.604	-7.438	5.628	13.65
360	-7.011	-6.824	5.548	14.72
370	-6.440	-6.235	5.469	15.82
380	-5.890	-5.671	5.389	16.95
390	-5.362	-5.130	5.309	18.11
400	-4.854	-4.611	5.229	19.29

does show the overall trend however. A slow decrease in (CaCl_2) cluster solubility is predicted upon increasing the relative amount of water. The total solubility increases, due to the strong effect on the solubility of the compo-

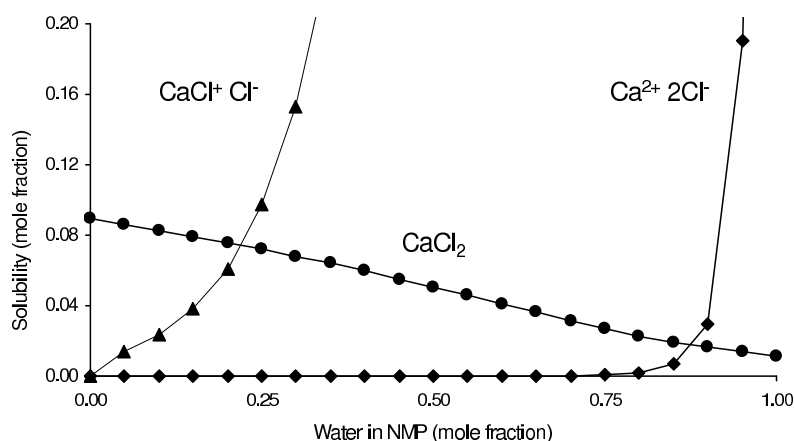


Figure 5.6: Effect of water on CaCl_2 solubility in NMP at 300K, calculated by COSMOtherm.

nent $\text{CaCl}^+-\text{Cl}^-$. Only if the mole fraction of water is more than approx. 0.8, dissociation into individual ions starts playing a role.

No steep increase in solubility is predicted if a small amount of water is added, for any of the components. This may either indicate an inadequacy in the calculation method, or the presence of other, more soluble components, such as larger clusters of ions.

5.3.2 Molecular dynamics simulations of NMP- CaCl_2

Molecular dynamics was used to obtain insight into the structure of the solution, specifically the interaction between the ions and the solvent molecules. MD simulations were carried out on solutions of 4 wt% and 10 wt% CaCl_2 in NMP, at different temperatures. The model systems consisted of 6 CaCl_2 , split into ions, in 160 NMP (4 wt% solution) and 60 NMP (10 wt% solution) respectively. To avoid surface artifacts, periodic boundary conditions were used: the contents are put inside a box, surrounded by identical boxes in all three dimensions. Thus, an infinitely large bulk system is simulated. The simulation boxes are shown in 5.7.

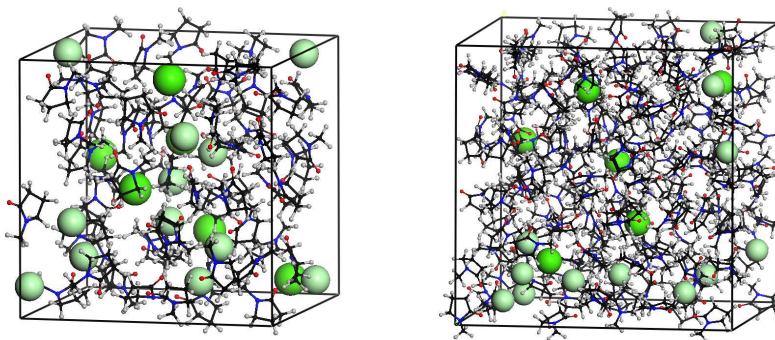



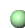



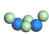

Figure 5.7: *Simulation boxes of 10 wt% (left) and 4 wt% (right) CaCl_2 in NMP.*

Simulations were carried out at constant temperature and pressure. Depending on temperature and pressure, the system may be solid or liquid, and the overall mobility may vary. Simulations done at 473K and 0.01GPa were used to see the most important structural features. The box volume is 31700 \AA^3 (4 wt% CaCl_2) and 12400 \AA^3 (10 wt% CaCl_2); the simulated time was 339ps (4 wt%) and 1285ps (10 wt%), taking 124 hours and 101 hours of CPU time respectively.

Ca_xCl_y clusters in NMP

Initially, the ions are distributed more or less randomly in the solution. During the simulations, clusters of ions developed, as shown in table 5.5. The occurrences of different components are based on the configuration at the end of the simulation.

Table 5.5: *Structure, calcium-chloride distance and number of different ion clusters in NMP solutions developed during MD simulations.*

component	structure	d (Ca-Cl) Å	number 4 wt%	number 10 wt%
Ca^{2+}		-	0	0
Cl^-		-	2	2
CaCl^+		2.46-2.60	3	1
CaCl_2		2.54-2.68	1	1
Ca_2Cl_3^+		2.58-3.00	0	1
Ca_2Cl_4		2.51-2.69	0	1
Ca_2Cl_5^-		2.56-2.80	1	0

There is a strong tendency for the ions to form clusters. In addition, only the formation of clusters is observed during the simulation, and no breaking up of clusters into fragments. Whether these clusters are inherently stable or would further agglomerate to form a crystal-like structure cannot be concluded from a simulation on this small (time) scale.

From the sigma profiles of Ca^{2+} and Cl^- and the sigma potential of NMP, it can be concluded that Ca^{2+} has a rather favourable interaction with NMP, whereas Cl^- has not. Still, all Ca^{2+} ions are part of a cluster, and two single Cl^- ions are observed. This can be explained by the following:

- poor statistics due to the small system size,
- the smaller number of Ca^{2+} ion compared to Cl^-
- the even more favourable interaction of Ca^{2+} with Cl^- compared to NMP
- the fact that no Ca^{2+} ions are left to form pairs with the remaining single Cl^- ions; instead these Cl^- ions have to join CaCl^+ , CaCl_2 , clusters, which may be energetically less favourable.

The presence of small clusters instead of single ions has a significant impact on the solubility, as seen before, because their thermodynamic potential in the solution is very different.

Solvent structure around Ca_xCl_y clusters

The NMP molecules play an important role in stabilizing the ions and clusters as illustrated in figure 5.8. The molecules surrounding the chloride ion all have their oxygen atom (red) pointing away from the ion, as a logical result from the electrostatic interaction between the chloride ion and the negatively charged oxygen. If a CaCl⁻ or CaCl₂ cluster is formed, the carbonyl oxygens of NMP molecules point toward the exposed part of the calcium ion, and again away from the chloride ion. There is a direct relation with the sigma surfaces (see figure 5.3), a good match exists between the shielding charges of oxygen and calcium, and a relatively good match between the shielding charges around the NMP ring and on the chloride ion.

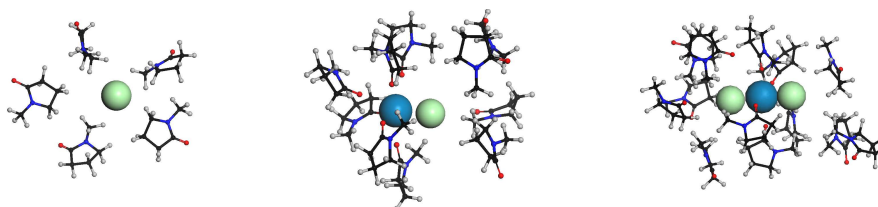


Figure 5.8: *Solvation of ion clusters by NMP. Cl⁻ shown in green, Ca²⁺ shown in blue.*

Structure of NMP-CaCl₂ with water present

Solutions of NMP-CaCl₂ contain small amounts of water. Solutions only become clear after adding some water, indicating that it is essential to the complete dissolution of CaCl₂. The structure of a NMP solution containing 10 wt% CaCl₂ and 0.7 wt% water was studied in a 1.5 ns MD simulation at 400 K and 0.1 Mpa. A cube-shaped periodic cell of c. 12000 Å³ (c.23 Å cubed) containing 60 NMP, 6 CaCl₂ and 4 H₂O was used. The initial geometry was taken from a previous MD run without water present, and the water was randomly distributed over the cell. Snapshots taken at 300 ps intervals are shown in figure 5.9.

Initially, the water molecules are in close contact with NMP only. After 110 ps, each water molecule is in contact with a CaCl₂ cluster. These contacts are hardly ever broken during the remainder of the simulation. The contacts start as Cl⁻ ··· H close contacts, which is plausible because the general shape of the clusters corresponds to calcium ions being surrounded by chloride ions. Eventually, in all cases spatial rearrangements lead to the formation of Ca²⁺ ··· O contacts. In both types of configurations, Ca²⁺ ··· NMP contacts are minimized; these are apparently unfavourable. Initially, 8 CaCl₂ clusters exist (cluster

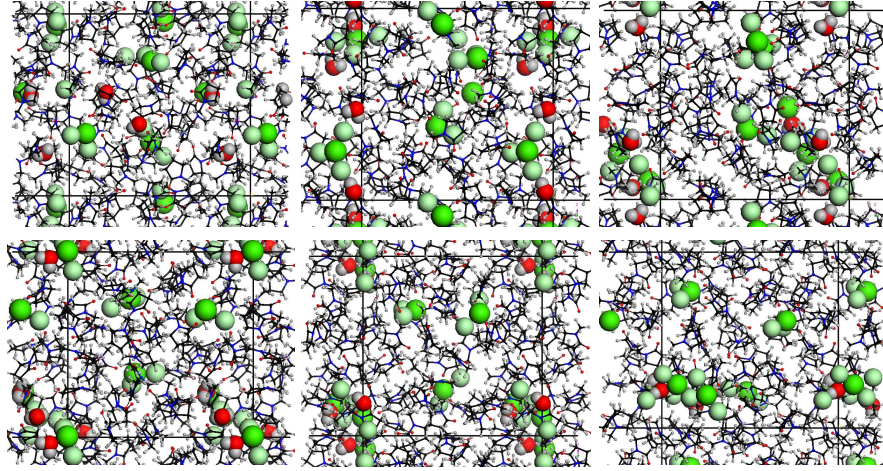


Figure 5.9: MD simulation of a NMP CaCl_2 (10 wt%) water (0.7 wt%) solution. Snapshots taken at 300 ps intervals (0-1500 ps).

here refers to any configuration of calcium and chloride, they may be interacting or completely separate). Their number reduces to 6 (300 ps), 4 (600 ps), 4 (900 ps), 4 (1200 ps), and 3 (1500 ps). At 1500 ps, one $(\text{CaCl}_2)_4\text{H}_2\text{O}$ cluster and two CaCl_2 clusters exist. The large cluster has a rather elongated shape, as can be seen in the last snapshot in figure 5.9. Although the system may not yet be fully in equilibrium, it seems reasonable to assume that this shape, which leads to a large surface area, is facilitated by the favourable interaction between water and both CaCl_2 and NMP.

5.3.3 Solubility of PpPTA in NMP- CaCl_2

The solubilities of the model components, as presented in figure 5.2, in NMP- CaCl_2 solutions were calculated via COSMOtherm. CaCl_2 was assumed to be present as neutral clusters in the solution. The solubility of the model component is given by an equation very similar to 5.11:

$$RT \ln a_{m,\text{sol}} = \mu_{m,\text{melt}} - \mu_{m,\text{sol}} - \Delta \bar{G}_m^{\text{fus}}, \quad (5.12)$$

where m refers to the specific model component, the subscript "melt" to the model component in the molten state and the subscript "sol" to the model component in NMP- CaCl_2 solution. Based on the mole fraction x , the solubility in wt% is calculated, given by:

$$\text{wt}\%_m = \frac{x_m \cdot M_{w,m}}{x_m \cdot M_{w,m} + (1 - x_m) \cdot M_{w,\text{NMP}}} \cdot (5.13)$$

The 10% difference in molecular weight between NMP and CaCl₂ is neglected here.

Estimates for $\Delta\bar{G}^{fus}$ and the melting temperature of model components 1 to 3 were obtained using the ProPred software, available from ICAS⁶. These are given in table 5.6. This program uses the method of Marrero en Gani [93] based on group contributions to estimate the enthalpy of fusion and the melting temperature. Values for the PpPTA model component cannot be obtained by this method. Estimates of the melting temperature were made in the previous chapter and range between 808 K, based on oxidative degradation and 873 K, based on a transition function by van Krevelen [88]. Here an additional estimation can be made based on extrapolation of the melting points of the low molecular model components. Hereto use is made of a relation derived by Flory [94]:

$$\frac{1}{T_m} = \frac{1}{T_\infty} + \frac{B}{M_n}, \quad (5.14)$$

By plotting $\frac{1}{M_n}$ against $\frac{1}{T_m}$ a linear relationship is obtained which gives the melting point at infinite molecular weight at the intercept. In figure 5.10 this plot is presented. The arrow indicates the intercept value corresponding to $\frac{1}{T_\infty}$.

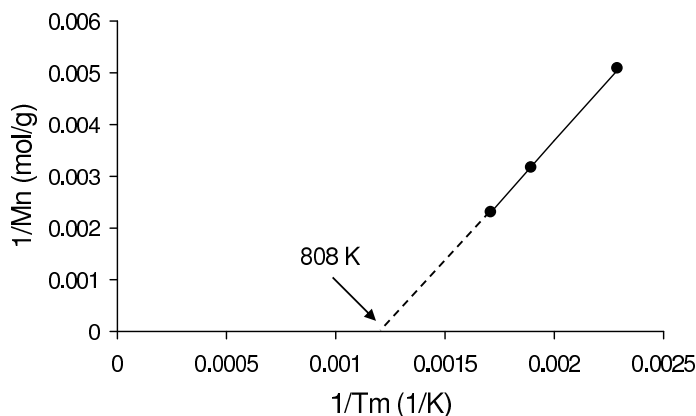


Figure 5.10: *Estimated melt temperature of PpPTA based on the melt temperatures of low molecular model components.*

The resulting estimate of the melt temperature for PPTA then follows to be 808 K. This is in close resemblance with the values found in chapter 4. As

⁶ICAS Version 8.0, by Rafiqul Gani and Partners, Computer Aided Process-Product Engineering Center (CAPEC), Dept. of Chem. Eng., Denmark Technical University, DK-2800 Lyngby, Denmark.

the software is not able to predict thermodynamic values for polymers, the data for PpPTA was obtained from chapter 4 in which the heat- and entropy of fusion were extensively discussed. The entropy of fusion was taken from 100% crystalline PA6, 0.54 J/gK.

Table 5.6: *Thermodynamic data for the model components, gained from ProPred software (between brackets are experimental values).*

model component	ΔH^{fus} (J/g)	ΔS^{fus} (J/gK)	T_{melt} (K)	M_w (g/mol)
1	150 (145)	0.34	436.2	197.23
2	163 (169)	0.31	528.3	316.35
3	169	0.29	584.6	435.47
PpPTA	436	0.54	808	238.26 repeat-unit

Based on the above data, the solubility of the model components in NMP at 300K was calculated as a function of the CaCl_2 concentration. The results are shown in table 5.7.

Table 5.7: *Calculated solubility of model components in NMP at 300K and different CaCl_2 cluster concentrations in wt%. CaCl_2 is present as neutral clusters.*

x_{CaCl_2}	m1	m2	m3	model PpPTA
0.00	35.544	2.962	0.170	5.10E-8
0.01	34.276	2.758	0.153	4.81E-8
0.02	33.053	2.569	0.138	4.54E-8
0.03	31.875	2.394	0.125	4.29E-8
0.04	30.739	2.232	0.112	4.05E-8
0.05	29.645	2.082	0.102	3.83E-8
0.06	28.591	1.943	0.092	3.62E-8
0.07	27.575	1.814	0.083	3.43E-8
0.08	26.596	1.694	0.075	3.24E-8
0.09	25.652	1.583	0.068	3.07E-8
0.10	24.743	1.479	0.062	2.91E-8

Going from model components 1 to 3 to model component PpPTA, the solubility decreases; this is mostly due to the increasing magnitude of ΔG^{fus} . The calculated effect of CaCl_2 is opposite to what might be expected from experiment: going from 0% to 6% CaCl_2 , the stability of solutions was found to increase. Stability however, is kinetically determined and solubility thermodynamically. In this calculation moreover, use was made of CaCl_2 molecules as this was found to agree most with experimentally found dissolution fractions CaCl_2 in NMP, table 5.4. From electrical conductivity experiments it is known that part of the CaCl_2 is present in ionic form and it is probably this ionic

form that influences the solubility of PpPTA by partly charging PpPTA. The main conclusion however is that the amount of PpPTA dissolved is negligible, corresponding to experiment.

5.3.4 Molecular dynamics simulations of PpPTA in NMP-CaCl₂

Single PpPTA chains in NMP-CaCl₂

The interaction between a single PpPTA chain and NMP-CaCl₂ solutions was studied via molecular dynamics simulations. Two simulation set ups were used, representing 4 wt% and 10 wt % CaCl₂ solutions. In each system, a PpPTA fragment of two repeat units (4 rings) was placed in a periodic box, parallel to one of the axes. Thus, an infinitely long chain is created, consisting of symmetry-related copies of the 4-ring fragment, as shown below in figure 5.11.

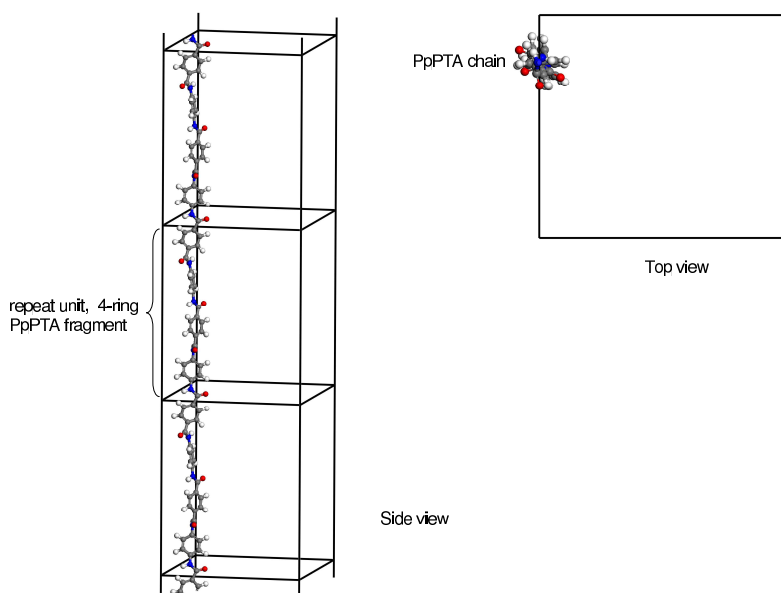


Figure 5.11: *Side view (left) and top view (right) of the PpPTA chain in the simulation box. NMP and CaCl₂ are not shown.*

For the 4 wt% solution, a rectangular box of 23.04 x 23.04 x 25.80 Å containing 75 NMP molecules and 3 (dissolved) CaCl₂ units was used; for the 10 wt% solution a rectangular 23.3736 x 20.6334 x 25.80 Å box, containing 60 NMP molecules and 6 CaCl₂ units. The size along the c-axis is dictated by the length of the PpPTA fragment used. The position of the chain (as well as the other components) can be chosen arbitrarily: its absolute (x,y,z) coordinates are irrelevant to the calculation. The only constraint is that it

should be parallel to one of the axes, to allow the individual fragments to become an infinite chain.

Simulations were carried out at constant temperature and volume (fixed cell dimensions), to avoid strong deformations of the simulation box that would occur at constant pressure (when cell dimensions, including angles, are free to vary). For the 10 wt% CaCl_2 system, 1850 ps were simulated (taking about 165 hours of CPU time); for the (larger) 4 wt% CaCl_2 system, 1666 ps (taking 210 hours CPU) were simulated. Snapshots of the systems during the simulation are shown in figure 5.12, showing the initial and final frame, and an intermediate frame showing the interactions between the PpPTA chain and the ions.

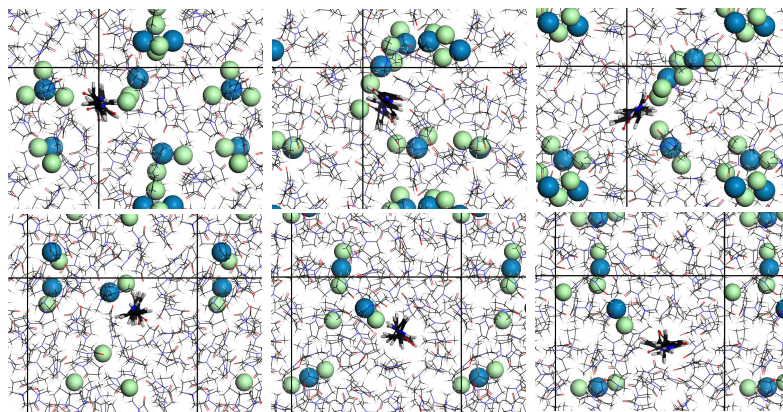


Figure 5.12: Snapshots from the MD simulations on PpPTA in 10 wt% CaCl_2 in NMP (top) and 4 wt% CaCl_2 in NMP (bottom). View along the polymer chain axis. The initial frame (left), final frame (right) and a frame at 1000 ps (top, middle) and 1293 ps (bottom, middle) are shown.

The snapshots show the overall mobility of the molecules and ions in the system, the presence of isolated ions and clusters, and the interaction of the chain with the ions; the latter is shown in more detail in figures 5.13 and 5.14. The polymer chain always interacts with the ion cluster via hydrogen bond formation between the amide proton and a chloride ion. The chloride ion may be a single ion, or part of a larger cluster. As a result of its charge distribution, it has a strong ordering effect on the NMP molecules surrounding it.

Visual inspection of the MD trajectories shows intermittent $(\text{PpPTA})\text{NH}\cdots\text{Cl}$ hydrogen bonds between the chain and the ions, in particular in the 4 wt% CaCl_2 system. These interactions are not predominant, and do not appear strongly preferred over $\text{PpPTA}\cdots\text{solvent}$ contacts $((\text{PpPTA})\text{NH}\cdots\text{OC}(\text{NMP}))$. In the 10 wt% CaCl_2 system, the occurrence of close $(\text{PpPTA})\text{NH}\cdots\text{Cl}$ contacts appears to be more frequent. A more quanti-

tative result was obtained by calculating, from the trajectories, the pair correlation functions (PCF's) for (PpPTA)NH \cdots OC(NMP) and (PpPTA)NH \cdots Cl. These functions show how frequent interatomic distances between selected atom pairs are found, relative to the occurrence if the atoms were distributed uniformly. A value of 1 corresponds to the expected value if no specific interaction is present (calculated from the concentrations). In figure 5.15 the PCF's are shown graphically as the frequency of occurrence of a particular distance $g(r)$ as a function of the atomic separation distance.

In all cases, no distances are observed below 1.5-2.0 Å, corresponding to the minimum distance possible, given the atomic radii. At large distances, the

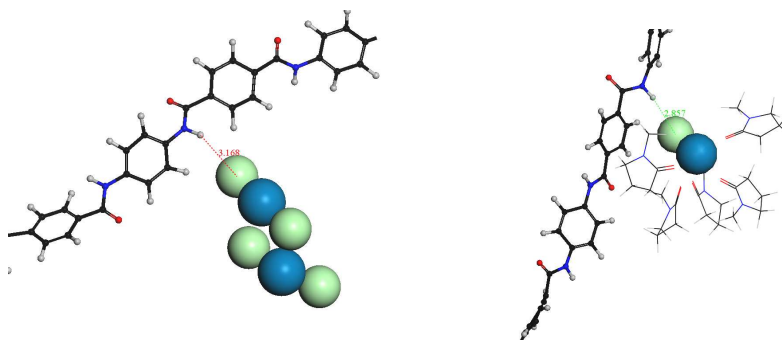


Figure 5.13: *Typical interaction between PpPTA chain and CaCl₂ clusters observed in the MD simulations.*

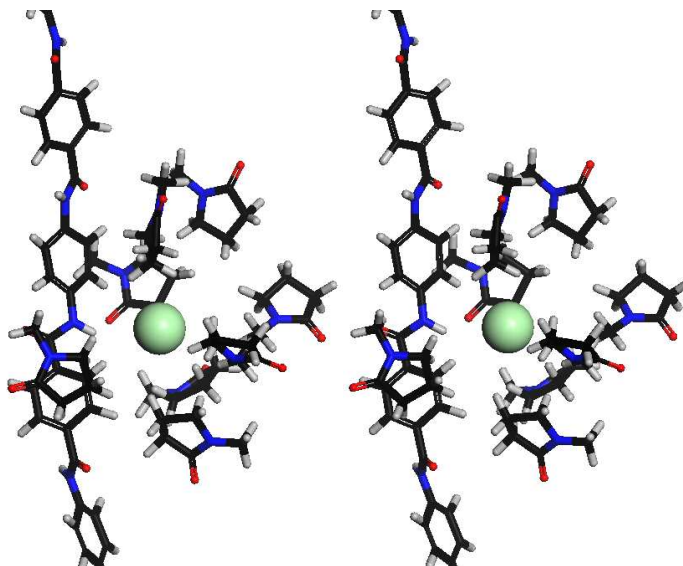


Figure 5.14: *Cross-eyed stereoscopic view of the interaction between a PpPTA chain and a single Cl⁻ ion.*

PCF tends to go to 1.0, corresponding to a uniform distribution. The peak observed at 2.0-2.5 Å indicates a relatively favourable interaction at short distances between the amide hydrogen and either the chloride or the NMP oxygen, which is as expected.

At high CaCl_2 concentration, the short distance $(\text{PpPTA})\text{NH}\cdots\text{Cl}$ peak is prominent. It shows a strong preference of chloride to be near the $(\text{PpPTA})\text{NH}$ over being in the solution. The corresponding $(\text{PpPTA})\text{NH}\cdots\text{OC}(\text{NMP})$ peak is present, albeit very low. This interaction is favourable, but only possible if no interaction with chloride is taking place.

At low CaCl_2 concentration the picture is quite different. Although similar peaks are observed, the short distance $(\text{PpPTA})\text{NH}\cdots\text{Cl}$ peak is much lower than at high concentration. The low concentration itself cannot explain this, as the numbers are relative to a uniform distribution of atoms, which takes into account the concentration. Apparently at low concentration, solvation by NMP has become relatively favourable. The peak at 2 Å in the $(\text{PpPTA})\text{NH}\cdots\text{OC}(\text{NMP})$ PCF shows the preferred interaction between these groups as expected.

At 8 Å an additional peak is present, also seen in the $(\text{PpPTA})\text{NH}\cdots\text{Cl}$ PCF at high concentration. It corresponds to the distance between an atom

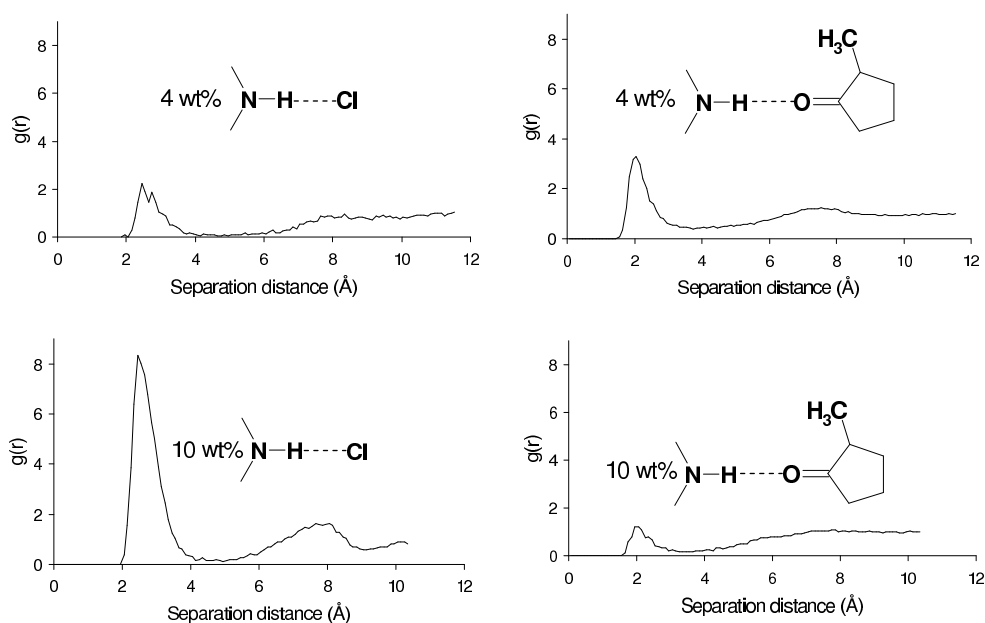


Figure 5.15: Pair correlation functions for $(\text{PpPTA})\text{NH}\cdots\text{Cl}$ (left) and $(\text{PpPTA})\text{NH}\cdots\text{OC}(\text{NMP})$ (right) at different CaCl_2 concentrations: 4 wt% (top) and 10 wt% (bottom).

interacting with a (PpPTA)NH, and the (PpPTA)NH group located at the opposite side of the ring, see figure 5.16.

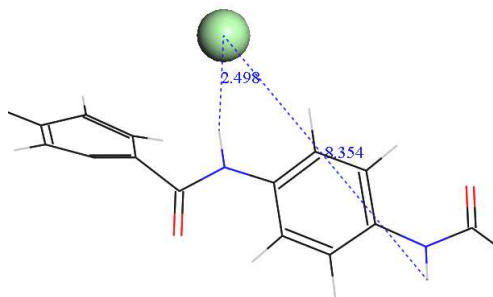


Figure 5.16: *Observed distances between chloride and both sides of the amide unit of PpPTA .*

In summary, these MD simulations show (in particular via the PCF's) a tendency for CaCl₂ clusters to form hydrogen bonds to the amide proton, if CaCl₂ is present at sufficiently high concentrations.

Multiple PpPTA chains in NMP-CaCl₂

In order to dissolve solid PpPTA, the hydrogen bonds linking the individual chains together must be broken. CaCl₂ may well play an important role in this process. In addition to the MD simulations on a single PpPTA chain in NMP-CaCl₂ (10 wt%), simulations were done on a single-layer PpPTA sheet and a dual-layer interrupted sheet, as shown in figure 5.17. Using these two configurations, interactions between CaCl₂ and the surface of the sheets, as well as the side faces of the sheets can be observed. For both configurations 2500 ps of molecular dynamics was carried out, at constant temperature (473K) and volume.

Although again hydrogen bond formation between the PpPTA chains and CaCl₂ clusters is observed, these interactions do not break up the PpPTA layers or peel them apart. In the single-layer dynamics run, the interactions between the chains and the clusters is through (PpPTA)NH...Cl hydrogen bonds. Pair correlation functions for the (PpPTA)NH...Cl, (PpPTA)NH...OC(NMP) and (PpPTA)NH...H(NMP) pairs, the latter is with any H of NMP, in the single layer simulation are shown in figure 5.18.

A striking effect in the PCF's for the single layer system of PpPTA is that at short distance, the value of the PCF's is very small. This is due to the geometry of the system, as the amide group is to a large extent buried in

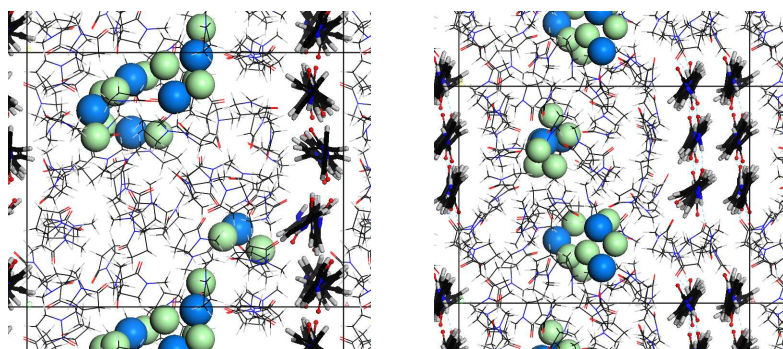


Figure 5.17: Snapshots of the MD simulations of a single PpPTA layer and an "interrupted" dual-layer PpPTA structure in NMP- CaCl_2 .

the polymer layer, its accessibility for atoms in the solution is very limited. The $\text{H}(\text{amide}) \cdots \text{H}(\text{NMP})$ PCF (which can serve as a reference for the case that no strong interactions are present) illustrates this point. It also drops rapidly below 5-6 Å. A better, but more complicated, view on the interactions at the amide group is obtained by dividing the PCF's as shown here by the PCF for the pair (any solution atom) $\cdots \text{H}(\text{amide})$. In that case, a strong preference for the NMP oxygen to be near the amide proton is again observed. In addition, it is found that the chloride is located, at average concentrations, either very near the amide group or at a distance of 10 Å and more, but hardly in the range 3 to 7 Å. This corresponds to the presence of a rather permanent single layer of NMP between the PpPTA strands and the chloride, as can be observed in figure 5.17. Compared to a single PpPTA chain, the geometry of the sheet structures limits the accessibility of in particular the polar parts of the chains, which can explain why the interaction with CaCl_2 is small for the sheet structures.

The limited length scale of the simulations (2.5 ns) could be a bottleneck in observing dissolution of PpPTA chains; the interaction with CaCl_2 is not very strong, but hydrogen bond formation is frequently observed. Another 2.5 ns MD simulation also did not show dissolution of PpPTA.

Multiple PpPTA chains in NMP- CaCl_2 with water present

NMP is well miscible with water, and a MD simulation of PpPTA chains in NMP with some water present (but no CaCl_2) shows that the water fully mixes with the NMP, occasionally forming hydrogen bonds with the oxygen and the amide proton of the amide group. The behaviour of water in a NMP- CaCl_2 solution was investigated using a model similar to the interrupted sheet, shown here fore. Four molecules of water were added (equivalent to 0.7 wt% water).

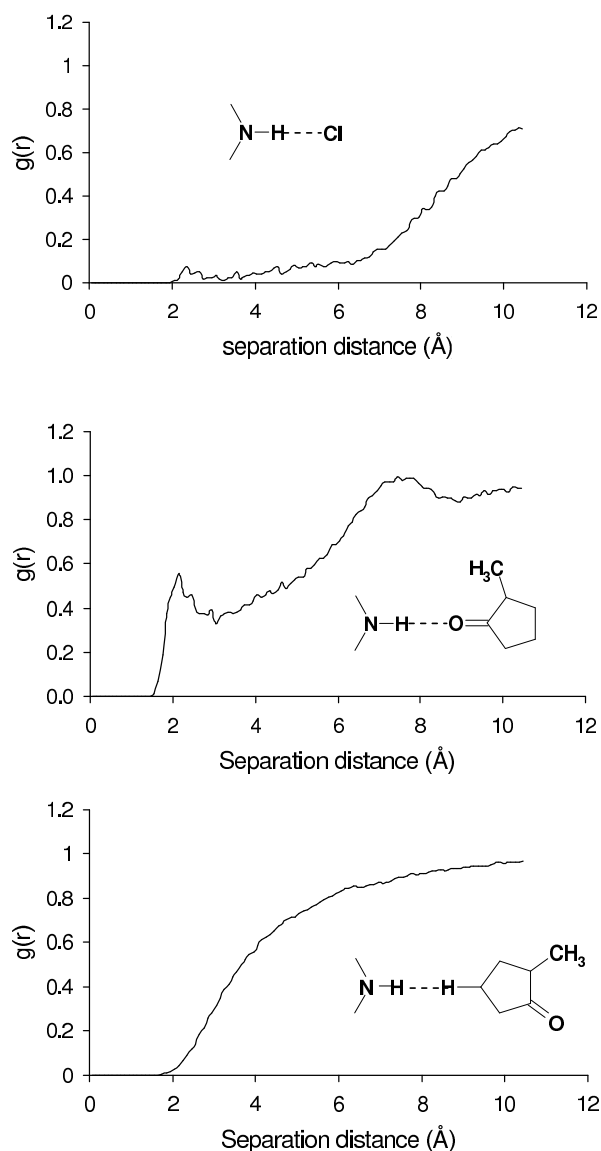


Figure 5.18: *Pair correlation functions for the single PpPTA layer system in a 10 wt% NMP- CaCl_2 solvent, $(\text{PpPTA})\text{NH}\cdots\text{Cl}$ (top), $(\text{PpPTA})\text{NH}\cdots\text{OC}(\text{NMP})$ (middle) and $(\text{PpPTA})\text{NH}\cdots\text{HN}(\text{NMP})$ (bottom).*

A 1500 ps MD simulation at constant temperature (400 K) and pressure (0.1 MPa) was carried out on a system containing 6 PpPTA chains, 60 NMP, 6 CaCl_2 , and 4 water molecules. Similar to what was observed for the system without the PpPTA chains, the water molecules quickly bind to the CaCl_2 clusters. During the simulation, no CaCl_2 -PpPTA contacts or water-PpPTA contacts are observed. The limited accessibility of the polar parts of the

PpPTA chains can again serve as an explanation.

The MD simulation on systems containing CaCl_2 and water thus show two phenomena:

- The presence of water facilitates the dissolution of CaCl_2 (into clusters) via its interaction with NMP and CaCl_2 at the interface.
- The presence of CaCl_2 leads to a strong decrease in the amount of water dissolved in the NMP solution, by binding it to the interface of the ion clusters. CaCl_2 acts as a drying agent in the simulations.
- Due to enhanced cluster formation between CaCl_2 and water, CaCl_2 is less available for interactions with PpPTA.

5.4 PpPTA in other solvents

Spinning of PpPTA requires PpPTA to be present in a stable solution. Solutions of NMP to which a few percent of CaCl_2 has been added were found to be thermodynamically unstable resulting in the instability phenomena described in chapter 3.

In the previous section, it was found that the most likely mechanism which keeps the polymers dissolved is the formation of hydrogen bonds between chloride ions, present in small CaCl_2 clusters, and N-H groups present in PpPTA. These hydrogen bonds prevent, or at least retard the formation of $(\text{PpPTA})\text{C}=\text{O} \cdots \text{H}-\text{N}(\text{PpPTA})$ hydrogen bonds between different polymer chains, and thus keep the individual chains in solution. In order to investigate the potential to improve the solubility of PPTA in NMP, the behaviour of NMP-LiCl and NMP-HCl solutions containing PpPTA chains has been studied using molecular modeling. The interactions between LiCl and PpPTA and between HCl and PpPTA were studied. Based on observed structure and statistics on inter atomic distances, LiCl appears to be a more promising candidate to improve PpPTA solubility in NMP than HCl. Molecular modeling of the proton, present in the HCl systems, is difficult and no definitive conclusions can be drawn from those simulations.

5.4.1 PpPTA in NMP-LiCl

Validity of the force field

A molecular dynamics simulation was carried out to observe the behaviour of LiCl dissolved in NMP, with PpPTA present. The first step, was to check the validity of the energy function used for simulations with LiCl. In this

case, energies were calculated using the Compass force field. As a basic check, the crystal structure of LiCl was taken from the database and its geometry optimized using Compass, as implemented in the Materials Studio software. Upon optimization, the crystal structure retained its symmetry (Fm3m), and cell parameters changed from 5.12954 Å to 5.13954 Å. The force field was therefore considered to be adequate.

Molecular Dynamics simulation: set up and results

Next, a suitable model for use in a MD simulation was constructed. To avoid surface artifacts, again periodic boundary conditions were used; calculations were done on a central simulation box, which was surrounded by an infinite number of identical boxes in all three dimensions. The simulation box contained one PpPTA chain of 4 monomer units length (4 rings), 16 Li⁺ and 16 Cl⁻ ions, embedded in 60 NMP molecules. The box was taken rectangular and had a fixed size of 23.3736 x 20.6334 x 25.800 Å³ throughout the simulation, which was therefore at constant volume. In a first simulation the system was equilibrated for 300 ps. The resulting end geometry contained cluster formations of the ions that were almost non-charged. This situation was used as the initial geometry for a second simulation. Snapshots of the initial and final geometries are shown in figure 5.19.

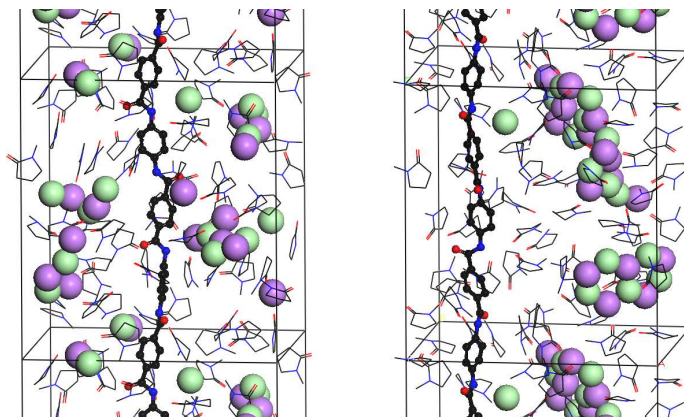


Figure 5.19: *Initial (left) and final geometry (right) of the simulation box, used in the MD simulation of PpPTA in NMP-LiCl. Simulation box contains one PpPTA chain, 16 LiCl, and 60 NMP molecules.*

A molecular dynamics simulation was carried out for 2500 ps, at 473 K and fixed volume (NVT conditions), taking 179 hours of CPU (7.5 days). Two observations can be done regarding the behaviour of the LiCl:

- **Clustering:** After 2500 ps, the LiCl appears in three clusters: one single

chloride ion, a cluster of 5 Li^+ and 5 Cl^- , and a cluster of 11 Li^+ and 10 Cl^- ; the latter two clusters are shown in 5.20. This behaviour is very similar to that of CaCl_2 in NMP, which also has a strong tendency to form clusters.

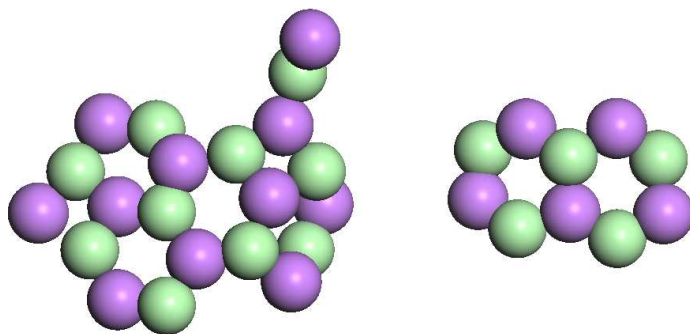


Figure 5.20: *LiCl* clusters present after 2500 ps of MD.

- Chain interaction:** The PpPTA chain has a remarkable tendency to form hydrogen bonds to the lithium and (in particular) chloride ions. As is seen from a series of snapshots, taken 300 ps apart during the last 1500 ps of the simulation 5.21, close contacts between the polymer chain and the ions are frequently observed. Figure 5.22 shows this in a more quantitative manner, by means of pair correlation functions. Short distances are encountered relatively often for both $(\text{PpPTA})\text{CO}\cdots\text{Li}$ and $(\text{PpPTA})\text{NH}\cdots\text{Cl}$, this intimate relation between amide and Li was also observed by Cox [22] as described in the chapter 2. In addition, the area under the short-distance peak for $(\text{PpPTA})\text{NH}\cdots\text{Cl}$ is relatively large, showing that this interaction occurs frequently. For comparison, in the same figure the corresponding PCF for the $(\text{PpPTA})\text{CO}\cdots\text{Ca}$ distance is shown, as observed in an earlier MD simulation of a single PpPTA chain dissolved in 60 NMP and 6 CaCl_2 . No preferred short-range interactions between Ca and $(\text{PpPTA})\text{CO}$ are observed at all. The preferred $(\text{PpPTA})\text{CO}\cdots\text{Ca}$ distance at $\sim 8 \text{ \AA}$ is a result of $(\text{PpPTA})\text{NH}\cdots\text{Cl}$ interactions. The chlorides appear in CaCl_2 clusters, and a close $(\text{PpPTA})\text{NH}\cdots\text{Cl}$ contact in such a cluster automatically leads to a $(\text{PpPTA})\text{CO}\cdots\text{Ca}$ distance of 6-10 Å .

In conclusion, similar to CaCl_2 , LiCl tends to form clusters in NMP. The chloride ion forms hydrogen bonds to the NH group of PpPTA, apparently more frequently than in the case of CaCl_2 . In contrast to CaCl_2 , in this case the positive ion also frequently has short-distance interactions with the poly-

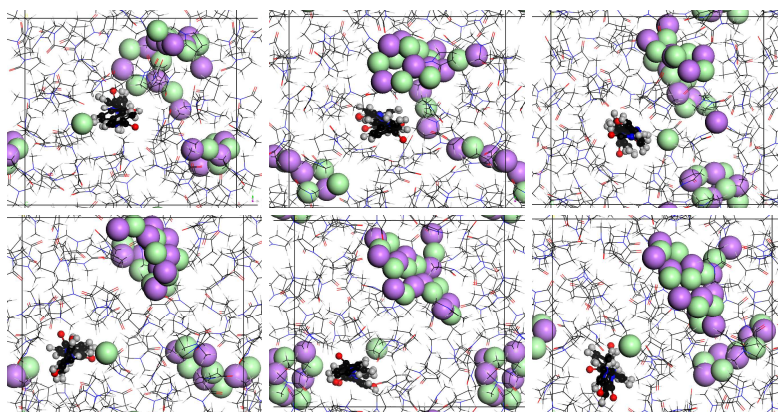


Figure 5.21: Snapshots from the NMP-LiCl MD simulation, taken at 1000 ps, 1300 ps, 1600 ps (top), 1900 ps, 2200 ps and 2500 ps (bottom). PpPTA chain, Li^+ (purple) and Cl^- (green) ions are shown bold.

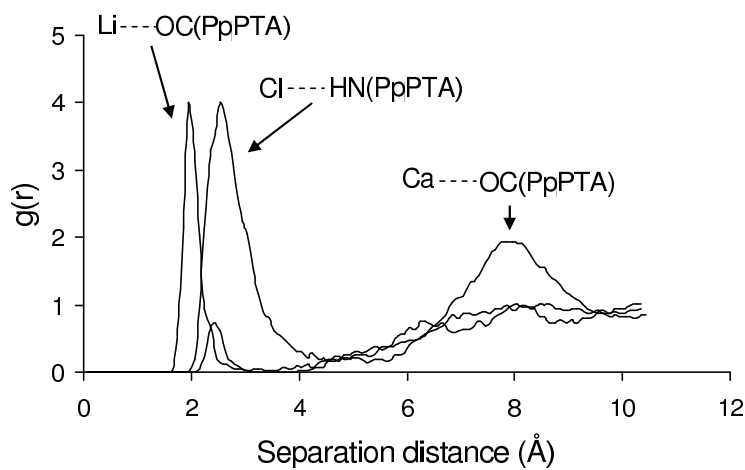


Figure 5.22: Pair correlation functions for $(\text{PpPTA})\text{NH}\cdots\text{Cl}$ and $(\text{PpPTA})\text{CO}\cdots\text{Li}$. The pair correlation for $(\text{PpPTA})\text{CO}\cdots\text{Ca}$ is given as a reference.

mer chain. This result corresponds to the larger interchange term found experimentally between LiCl and PpPTA (-6331 J/cm^3) compared to CaCl_2 and PpPTA (-4093 J/cm^3), based on interactions of these salts with benzanilide, see table 4.4.

5.4.2 PpPTA in NMP-HCl

Validity of the force field

The proton exists as a separate atom type in the Compass force field, but it is unclear what data have been used to arrive at the specific parameters (e.g. van der Waals parameters). Since the parameters of the Compass force field are not released to the user, the numbers used to describe a proton also cannot be compared to those describing other atom types. The only number that can be observed by the user is the partial atomic charge, which by default is taken to be zero for the proton. Fortunately, the atomic charge can be specified by hand as well. Nonetheless it seems questionable how well one can expect this force field to perform on systems containing protons. Since some form of transfer of electrons is likely to occur in such systems, molecular mechanics force fields could be considered inadequate in the first place in this case; still it was decided to at least try some calculations, treating the protons as small van der Waals spheres with charge $+1e$.

Molecular Dynamics simulation: set up and results

A model suitable for MD simulation was constructed as follows: 4 PpPTA chains and 12 $\text{H}^+\text{-Cl}^-$ units were placed in a box containing 60 NMP molecules. The dimensions of the rectangular box were $26.05 \times 20.88 \times 25.80 \text{ \AA}^3$. As in the LiCl simulation, periodic boundary conditions were used to avoid surface artifacts. Again a 300 ps simulation was performed to equilibrate the system. The ions, similar to the LiCl simulation, formed almost non-charged clusters and this geometry was used as the initial geometry of a simulation of 2500 ps at 473 K and fixed volume (NVT conditions), taking 288 hours of CPU time (12 days). The geometry of the initial model and snapshots taken every 500 ps are shown in figure 5.23.

As was observed in the simulations of CaCl_2 and LiCl in NMP, also in this case the ions have a strong tendency to cluster together. A striking difference with the LiCl simulation is the geometry of the HCl clusters, which take the shape of a chain rather than a sheet. This difference in cluster geometry can be explained from the relative size of the H^+ , Li^+ , and Cl^- ions. Taking the geometry shown in figure 5.20 as a starting point, a decrease in the size of the

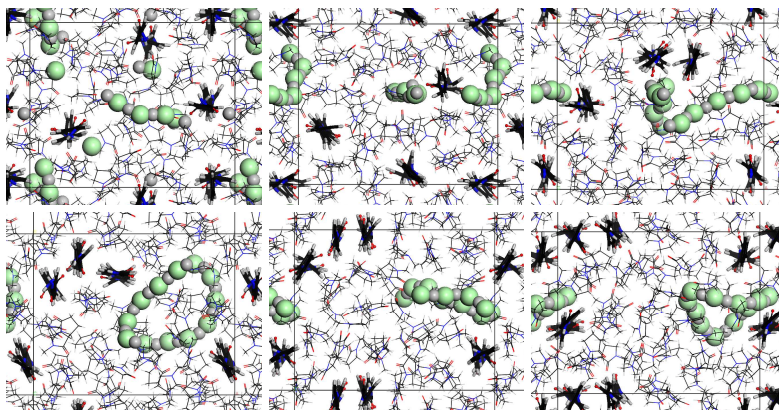


Figure 5.23: Snapshots from the NMP-HCl MD simulation, taken at 0 ps, 500 ps, 1000 ps (top), 1500 ps, 2000 ps and 2500 ps (bottom). PpPTA chain and HCl shown bold. Simulation box contains 4 PpPTA chains, 12 HCl (H gray and Cl green), and 60 NMP molecules.

positive ions will eventually lead to direct contact between the negative ions, which is energetically unfavourable. This contact can be avoided by assuming a linear structure, at the expense of loosing some of the favourable interactions as well. In this case, one end of the chain has encountered the other end in the same simulation box, forming a closed loop. It seems likely that it might just as well have encountered the other end in a neighboring box, which would have lead to an infinite chain instead of a loop.

A preferred interaction between the ions and the PpPTA chains is not observed, as can be seen in the PCF in figure 5.24. At short distance, the pair correlation functions for both $(\text{PpPTA})\text{NH}\cdots\text{Cl}^-$ and $(\text{PpPTA})\text{CO}\cdots\text{H}^+$ pairs do not exceed 1, so neither of the ion types is expected to take part in hydrogen bond formation to the chain. For reference the PCF for the interaction $(\text{PpPTA})\text{CO}\cdots\text{Ca}$ is shown also.

After approx. 500 ps of simulation, some alignment appears to take place between the PpPTA chain and a HCl chain, as shown in figure 5.25. This apparent interaction is short lived though, and not likely to be significant.

In conclusion, first of all it should be noted that the parameters used to describe the protons are questionable, and one should therefore be cautious interpreting the results. The general trend though appears to be that HCl has a strong tendency to form chain like clusters in NMP, which do not specifically interact with PpPTA.

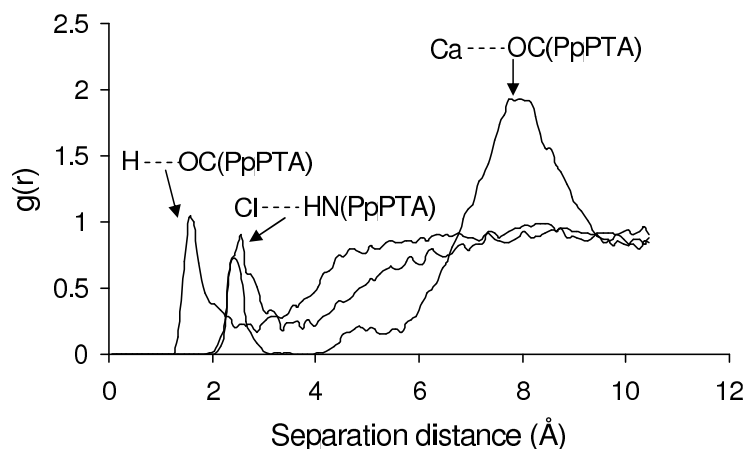


Figure 5.24: Pair correlation functions for $(PpPTA)NH \cdots Cl$ and $(PpPTA)CO \cdots H$ distances. The pair correlation for $(PpPTA)CO \cdots Ca$ is given as a reference.

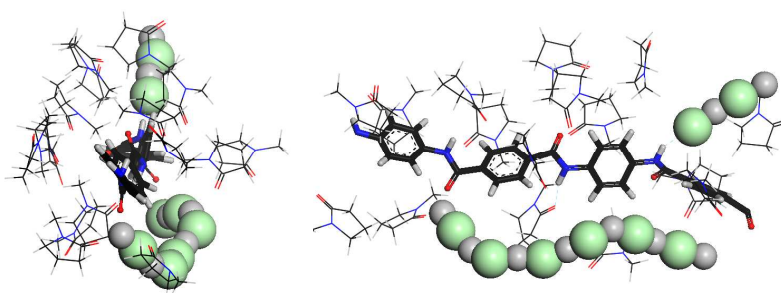


Figure 5.25: Alignment of polymer and HCl chains after 500 ps: view along chain axes (left) and perpendicular (right).

5.5 Conclusions

COSMOtherm calculations were carried out on the solubility of $CaCl_2$ in NMP and the solubility of PpPTA and model components in NMP and NMP- $CaCl_2$. The following observations were made:

$CaCl_2$ solubility

- The calculated solubility of $CaCl_2$ in NMP depends strongly on the dissolved component. Solubility at 300K is very low (approx. 10^{-6} wt%) if dissociated completely, dissociation into $CaCl^+$ and Cl^- leads to a higher (approx. 0.02 wt%) solubility, and the solubility for neutral $CaCl_2$ particles is again higher (approx. 9 wt%). The latter is in line with experimental observations.
- The ionic radius used for the Ca^{2+} ion affects the calculated solubility, a

larger radius leads to an increase in solubility for the ions. The solubility of the fully dissociated salt remains low however.

- Water enhances the solubility of the charged components, in particular of $\text{Ca}^{2+}\text{-Cl}^-$. Although the solubility of the neutral clusters decreases, the total solubility is found to increase when water is added.

In the absence of water, CaCl_2 dissolved in NMP will exist as clusters of ions, with zero or only a small net charge and showing increasing solubility for more neutral clusters. This followed from the MD simulations, showing a strong tendency for the ions to cluster, and of experimental observations, the solution formed is not (optically) clear.

A strong interaction exists between CaCl_2 and water present in NMP solutions. Although well soluble in NMP, water molecules bind almost irreversibly to CaCl_2 clusters during MD simulations. Water promotes the dissolution of CaCl_2 in NMP due to its interaction at the interface between the two, and CaCl_2 clusters in turn remove water from the bulk NMP solution by binding it at the surface. The net effect of water therefore is the effective removal of CaCl_2 .

PpPTA solubility

The solubility of PpPTA in NMP is calculated to be negligible, and even decreasing when CaCl_2 clusters are present. Similar results are found assuming the presence of $\text{Ca}^{2+}\text{-Cl}^-$ ions or traces of water.

MD simulations

- Upon dissolution in NMP, CaCl_2 tends to form clusters which have a net charge between -1 and +1. Consequently, few single chloride ions and almost no single calcium ions are expected to be present in NMP- CaCl_2 solutions.
- Water molecules present in a NMP-PpPTA solution in the absence of CaCl_2 mix well with the NMP, and occasionally interact with the PpPTA chains.
- Water molecules present in a NMP- CaCl_2 -PpPTA solution bind quickly and strongly to the CaCl_2 clusters, and appear to facilitate a larger surface area of the ion clusters, as a result of a more elongated shape of the clusters. The CaCl_2 effectively removes the water from the NMP solution due to the strong interaction between the two.

- at high (10 wt%) CaCl_2 concentrations, single (dissolved) PpPTA chains show a relatively strong interaction with chloride ions through hydrogen bond formation by the amide proton, where the chloride tends to replace the NMP oxygen atoms.
- at low (4 wt%) CaCl_2 concentration, the preference for CaCl_2 to interact with the amide proton is much weaker, as the ion clusters tend to stay "in solution".
- at high (10 wt%) CaCl_2 concentrations, PpPTA chains in a sheet-like formation show only few interactions with CaCl_2 clusters, likely due to the limited accessibility of the amide group.
- the presence of a small amount of water in NMP does not obviously influence the interaction between dissolved CaCl_2 and PpPTA.

No single decisive factor could be identified to explain the increased solubility of PpPTA in NMP upon adding CaCl_2 as found experimentally. The most prominent effect observed in MD simulations is the interaction of chloride ions with the amide proton. COSMOtherm calculations did not show a positive effect on the solubility when CaCl_2 was added, charged chains were not modeled though and such effects were not taken into account with the simulation methods used. Removal of water from the solution by CaCl_2 clusters may also contribute to an increased solubility of PpPTA as CaCl_2 is then available for interaction with PpPTA creating net charged chains.

Both LiCl and HCl form ionic clusters in NMP. LiCl appears to have a stronger, polar, interaction with PpPTA than CaCl_2 and might be more effective as a dissolution salt as CaCl_2 . This agrees with experimental data presented in the previous chapter in which it was found that LiCl interacts stronger with PpPTA than CaCl_2 . Also the pair correlation functions of LiCl and PpPTA show a short distance interaction between lithium and the carbonyl oxygen of PpPTA. The occurrence of this interaction agrees with the explanation given in the previous chapter that LiBr shows a significant interaction with amides containing NR-groups in contrast to LiCl due to the presence of substantially more Li-ions in NMP-LiBr solvents than in NMP-LiCl solvents, as derived from electrical conductivity measurements.

Due to the limited interaction between HCl and PpPTA, HCl does not appear to be a promising candidate to improve PpPTA solubility in NMP. The fact however that during polymerization HCl is formed at the amide site, might result in the presence of one HCl at the amide site of PpPTA and prevent clustering, as appeared in the simulation. This argument might be

considered plausible as the viscosity of PpPTA-NMP-CaCl₂ solutions drops after removal of HCl by neutralization with CaO as was discussed in chapter 3. This indicates interaction between PpPTA and HCl.

6. Modeling of the H_2SO_4 -Polyaramid System

In this chapter the interactions between PpPTA and sulphuric acid are investigated using molecular dynamics. It is found that the relative dielectric constant of the environment is the main parameter to influence protonation of the amide-units in PpPTA and thereby determines the solubility of PpPTA in sulphuric acid. Upon introducing water to the mixture the relative dielectric constant decreases rapidly and causes the PpPTA chains to crystallize. An explanation for the mechanism of crystallization of PpPTA upon adding water to the mixture is presented based on electrical conductivity measurements.

6.1 Introduction

Experimentally it is known that PpPTA readily dissolves in sulphuric acid of approximately 100%, although high shear rates are necessary to overcome the high viscous phase at the isotropic-nematic transition around 8 wt% PpPTA. Once the solution is formed it is thermodynamically stable. In this chapter the mechanism of dissolution is discussed using modeling techniques to support it. First the protonation of PpPTA in sulphuric acid is discussed and an explanation for the necessity of 100% sulphuric acid in order to act as a solvent is given. Then the possibility of protonation by HCl and the influence of water are discussed.

The structure of PpPTA when dissolved in sulphuric acid was studied using available experimental information and molecular modeling. The polymer is protonated at the carbonyl sites upon interaction with sulphuric acid. The resulting net positive charge on the polymer chains forces them to move apart and mix with sulphuric acid. Calculations also show that a necessary condition for protonation is a high relative dielectric constant of the solution. As the relative dielectric constant of concentrated sulphuric acid drops rapidly with

increasing water concentration, it is concluded that dissolution in sulphuric acid via protonation of the polymer is only possible if the acid concentration is close to 100%. Experimental evidence for the protonation of PpPTA was found in electrical conductivity experiments. When PpPTA is added to 100% sulphuric acid the polymer acts as an electrolyte and electrical conductivity increases linearly up to a maximum. From this point on the polymer hinders free movement of the ions hence decreasing electrical conductivity. If a controlled amount of water is added to sulphuric acid and subsequently PpPTA is dissolved herein, water seems to bind with the polymer until the molar amount of water exceeds the amount of amide units of the polymer. From this point on "free" water causes the electrical conductivity to rise. From these findings a mechanism for the coagulation of PpPTA in water is suggested.

6.2 Protonation of PpPTA

Protonation of the amide unit is likely to play a key role in the dissolution of PpPTA in sulphuric acid, as it will put a net charge on the polymer chains. Due to repulsive electrostatic forces, the charged molecules will not crystallize (unless a compensating charge is present). Two potential protonation sites are present in the amide group: the nitrogen and oxygen atoms. The oxygen atom is preferred for accepting a proton, as is shown below.

6.2.1 Resonance structures

Amides have two important resonance structures, see figure 6.1, which make the group rather polar. The occurrence of the charged form depends on the medium: in a polar environment, this form will occur more frequently than in a non-polar environment.

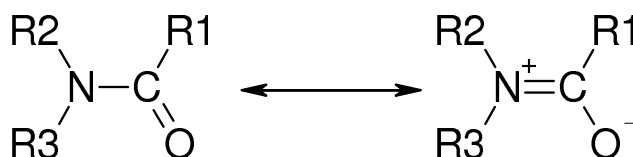


Figure 6.1: *resonance structures of the amide.*

In amides, the C-N distance in the amide unit is 1.32 Å, which is in between the normal single bond C-N distance (1.45 Å) and the double bond distance (1.20 Å), indicative of the important contribution of the charged structure. Similarly, in PpPTA the C-N distance is 1.37 Å. The charged resonance struc-

ture suggests that the oxygen atom rather than the nitrogen is most likely to accept a proton donated by sulphuric acid.

6.2.2 Quantum chemistry

Quantum chemical calculations were carried out on the model component para-phenylenediamine-terephthaloate (PPDT), shown in figure 6.2, and both its protonated forms. In the figure, relevant bond lengths are also shown

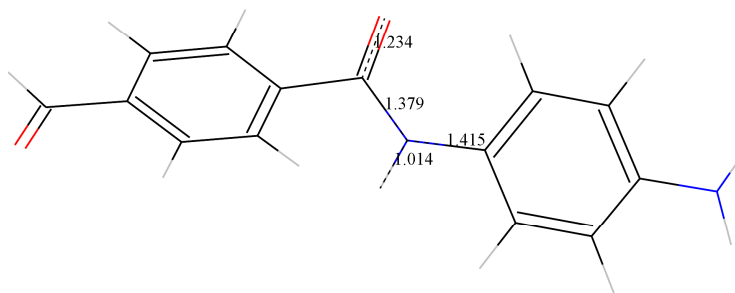


Figure 6.2: Model component (PPDT) used in QM calculations to verify the protonation site. Selected bond lengths (Å) are shown.

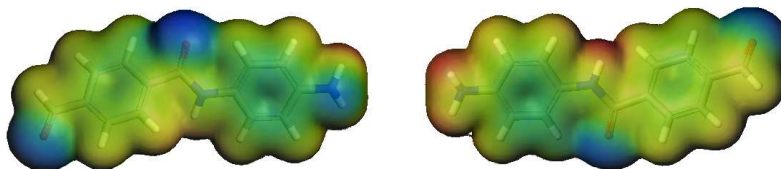


Figure 6.3: Electrostatic potential at the surface of PPDT. Pictures showing front and back of the molecule; blue corresponds to negative potential (=affinity for positive charge), red to positive potential.

The calculations were done using the DMol3 package [95], employing the GGA BP functional and a DNP basis set. Geometry optimizations were carried out on the model and on each of the protonated forms having a net charge of +1e. The electrostatic potential of the uncharged PPDT is shown in figure 6.3. The oxygen in the amide unit clearly has a well exposed, negatively charged surface, making interaction with a proton favourable. For the charged components, one geometry optimization started with the additional proton relatively close (about 2 Å) to the amide oxygen, the other had the proton close to the amide nitrogen. Two different structures resulted from these optimizations, referred to as hydroxyl and ammonium form, which are shown in figure 6.4.

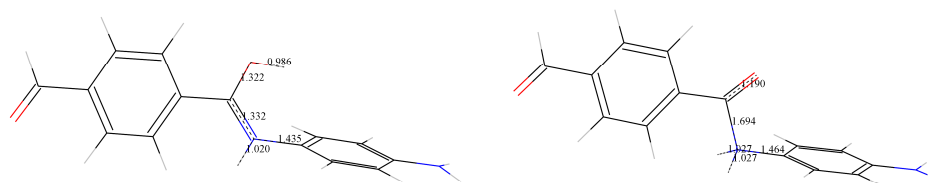


Figure 6.4: Structures of two forms of the protonated amide unit (hydroxyl, left, and ammonium, right), obtained from quantum chemistry. Bond lengths (in Å) are shown for selected bonds.

The hydroxyl form is 68.2 kJ/mol lower in energy than the ammonium form, and will therefore be strongly preferred. In the ammonium form, the C-N distance in the amide unit has become extremely long (1.69 Å as compared to 1.46 Å for the other N-C_{sp2} bond) suggesting the bond is effectively broken. In conclusion, the quantum chemical calculations also indicate that the hydroxyl form is the preferred protonated form.

6.2.3 Crystallographic data

A crystal structure of the 1:4 complex of N,N'-(p-phenylene)dibenzamide (PPDB) with sulphuric acid has been determined by Calabrese and Gardner in 1985, [96]. The structure, part of which is shown in figure 6.5, shows that in this solvate both carbonyl groups are protonated.

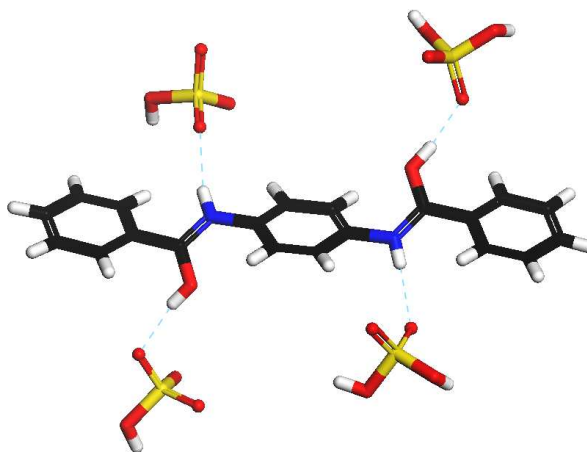


Figure 6.5: The crystal structure of $\text{PPDB} \cdot 4\text{H}_2\text{SO}_4$, local arrangement of solvate.

A striking feature moreover is the asymmetry of the structure: although (protonated) PPDB is in principle symmetric with respect to the central phenyl ring, the position of the solvate moieties breaks this symmetry: both sulphate ions are at one end of the PPDB molecule, and the sulphuric acid

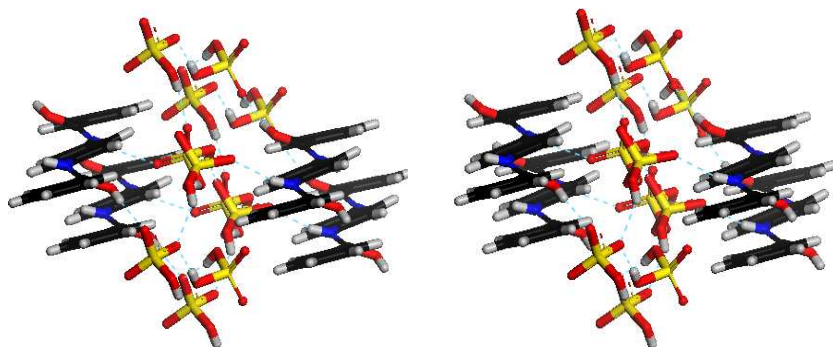


Figure 6.6: *Stacking of PPDB molecules and solvate structure in crystalline PPDB.4H₂SO₄. Stereoscopic crossed eyed view.*

molecules at the other end. A stereoscopic view of PPDB is given in figure 6.6.

In this structure, the C-O and C-N distances are 1.297 Å and 1.302 Å respectively, corresponding closely (within 0.03 Å) to the bond lengths in the hydroxyl form optimized by DMol.

6.3 Electrical conductivity measurements in sulphuric acid

As PpPTA readily dissolves in 100% sulphuric acid but coagulates when water is added the electrical conductivity ¹ of solutions of PpPTA in sulphuric acid were studied as well as the influence of water. The main purpose is to establish whether ions are responsible for the dissolution behaviour. In table 6.1 an overview of the solutions examined is given.

Table 6.1: *Overview of the PpPTA-sulphuric-acid-water solutions examined. The sulphuric-acid and water percentages add up to 100% and these mixtures act as the solvent to which additional PpPTA is added in the range given in the table.*

Conc. sulphuric acid (wt%)	Conc. water (wt%)	Conc. range PpPTA (wt%)
99.8	0.2	2-21
99	1	16-19
98	2	14-19
97.5	2.5	15-20
97	3	4-21

The conductivity measurements were carried out using a twin screw ex-

¹From here on, in the remainder of this chapter, the term conductivity is used to express electrical conductivity unless explicitly stated otherwise.

truder to prepare the solution, see figure 6.7. Solvent (sulphuric-acid water mixture prepared in advance, concentration measured with a Metrohm 716 DMS Titrino with a Metrohm Combined pH glass electrode 6.0233.100 electrode) and PpPTA (M_w 31000 g/mol) were dosed separately to the extruder. In the extruder the solution was prepared by mixing and shearing at a temperature of 85°C . The throughput of the extruder was 1.2 kg/hour resulting in a residence time of 10 minutes. The resulting solution was pushed through a toroidal conductivity measuring device (Yokogawa Inductive conductivity PFA-sensor model ISC40G and a Yokogawa Converter for Inductive conductivity model ISC450G). A schematic overview is depicted in figure 6.7.

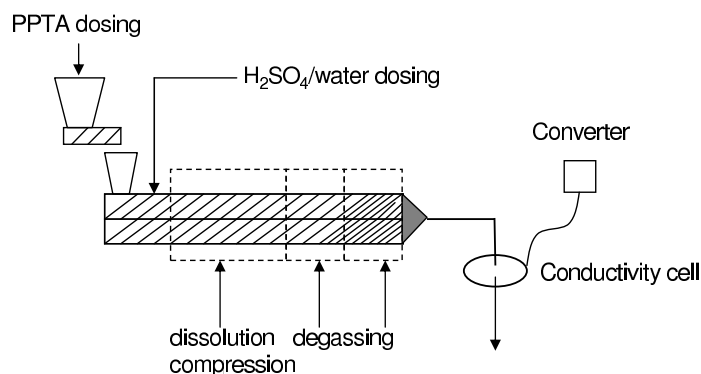


Figure 6.7: *Schematic overview of the experimental set-up for conductivity measurements.*

This measurement is based on inductive coupling of two ring transformers (Toroids) by the liquid. The transmitter supplies a reference voltage (V_1) at a high frequency (2kHz) to the drive coil. The heart of this coil is of high permeability magnetic material and so a strong magnetic field is generated in the toroid. The liquid passes through the hole in the toroid and can be considered as a one turn secondary winding. The magnetic field induces a voltage (V_2) in this liquid winding. There are 2 toroids mounted in the donut shaped sensor. The liquid also flows through the second toroid and therefore the liquid turn can be considered as a primary winding of the second ring transformer. The current in the liquid will create a magnetic field in the second toroid. The induced voltage (V_3) is the result of the magnetic field and can be measured as an output. The output voltage of this receive coil is therefore proportional to the specific conductivity of the process liquid. This principle is presented in figure 6.8.

The major advantage of toroidal conductivity is that the toroidal coils are not in contact with the solution. The drawback to the toroidal conductivity measurement is that it lacks the sensitivity of a contacting measurement. For

minimal obstruction of the flow and for an accurate measurement the measuring solution should flow freely around the donut. This results in allowing a minimum of 25 mm around the donut. As for practical reasons free flow around the cell was not possible, in consultation with Yokogawa an alternative setup was used.

In the opening of the measuring cell a Teflon tube is placed. On each side of this Teflon tubing a metal tube is connected. The two metal pipes are short-circuited with a metal wire because a closed system is necessary. The solution to be measured flows through the metal pipe then through the Teflon tube and again through the metal tube. A Pt-1000 temperature sensor is connected with the metal pipe and covered with isolation material. With this alternative assembly, immersion of the measurement cell into the solution is not necessary and the measurement principle is not affected. The cell constant had to be adapted to the length of the Teflon tube though. The assembly was tested with sulphuric-acid-water samples of 96 wt% and 99.75 wt% sulphuric acid. The resulting conductivities were found to be in good agreement with literature data [97], [98]. In figure 6.9 the construction is presented.

The conductivity of various concentrations PpPTA in sulphuric acid, containing practically 0 up to 3 wt% water was measured. The results are presented in figure 6.10. In the case of 99.8 wt% sulphuric acid an optimum in the conductivity is observed at approximately 14 wt% PpPTA. From low concentrations up, the conductivity increases due to increased ion concentration. When the concentration of PpPTA exceeds 14 wt% the conductivity decreases upon further PpPTA increase. This may be due to the reduction of the amount

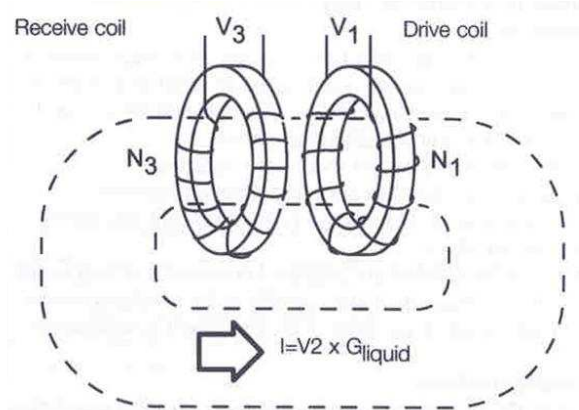


Figure 6.8: Principle of the inductive measuring device used in the measurement of the conductivity of PpPTA-sulphuric-acid-water solutions. G_{liquid} represents the conductivity.

of "free" sulphuric acid. At 14 wt% the ratio of the total amount of amide units to sulphuric acid moieties is 1:8, this decreases to 1:5 at 20 wt% PpPTA. The latter comes close to the ratio of 1:4 mentioned in the work of Calebrese et al. [96] in which the structure of $\text{N,N}'$ -p-Phenylenedibenzamide. $4\text{H}_2\text{SO}_4$ complex is discussed. In the article evidence is presented that in the complex form the amide-oxygen atoms are protonated and form hydrogen bonds with the sulphuric acid. This means that the free motion of sulphuric acid is hampered and hence the conductivity decreases. Thus, as the ratio approaches 1:4 conductivity decreases.

As this comes close to the 1:4 ratio, this may well be a reason for the maximum solubility of PpPTA in sulphuric acid to be 20 wt%. By increasing the PpPTA concentration above 20 wt% no more sulphuric acid is available to form hydrogen bonds. When water is added to the solution the conductivity behaviour between 14 wt% and 20 wt% does not change only at lower concentrations of PpPTA the conductivity shows an increase instead of a decrease. Apparently the amount of water added is only partly available for ion formation, depending on the PpPTA concentration. The dependence is almost linear. Water is probably bonded to the polymer chains and only the amount of water that exceeds the amount of amide units, takes part in ion formation. For a 97 wt% sulphuric acid and thus 3 wt% water, the molar amount of water is equal to the molar amount of amide units at a 20 wt% PpPTA solution

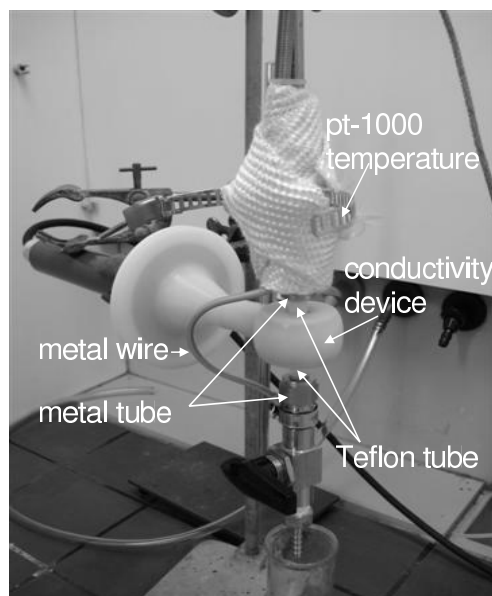


Figure 6.9: *Assembly of the adjusted construction to measure conductivity in-line by inductivity. The whole is mounted on the end of a twin screw extruder.*

and the conductivities of a 97 wt% and a 99.8 wt% sulphuric acid solvent are found to be equal at 20 wt% PpPTA. For a 98 wt% sulphuric acid equal molar quantities of water and amide units is reached at a 14 wt% PpPTA solution and now conductivities of 98 wt% and 99.8 wt% are found to equal at 14 wt% PpPTA and higher.

The protonation of amide units by sulphuric acid is thought to take place according:

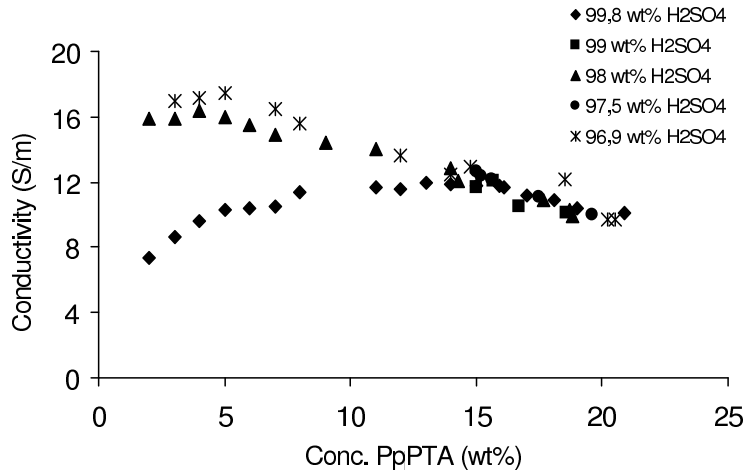


Figure 6.10: Conductivity of PpPTA dissolved in different sulphuric-acid-water mixtures at 85°C.

An expression for the equilibrium constant can be constructed as:

$$K = \frac{C_{amide,0}\alpha \cdot C_{acid,0}\alpha'}{(1-\alpha)C_{amide,0} \cdot (1-\alpha')C_{acid,0}} = \frac{\alpha\alpha'}{(1-\alpha)(1-\alpha')} , \quad (6.2)$$

here α denotes the fraction protonated aramid units and α' the fraction de-protonated sulphuric acid. From the mass balance of the fractions protonated amide units and de-protonated sulphuric acid a relation between α and α' is obtained:

$$\alpha' = \frac{C_{amide,0}}{C_{acid,0}}\alpha . \quad (6.3)$$

Inserting this in equation 6.2 results in the following expression for K :

$$\alpha = K' \sqrt{(1 - \alpha) \frac{C_{acid,0}}{C_{amide,0}} - \alpha + \alpha^2} , \quad (6.4)$$

$K' = K^{0.5}$. Values for α and α' are obtained from conductivity measurements. The molar conductivity is plotted against the concentration of PpPTA in figure 6.11. A kinetic equation is fitted through the data to obtain the limiting molar conductivity and α then follows from the ratio of the actual molar conductivity Λ_m and the limiting molar conductivity Λ_m^0 .

$$\alpha = \frac{\Lambda_m}{\Lambda_m^0} . \quad (6.5)$$

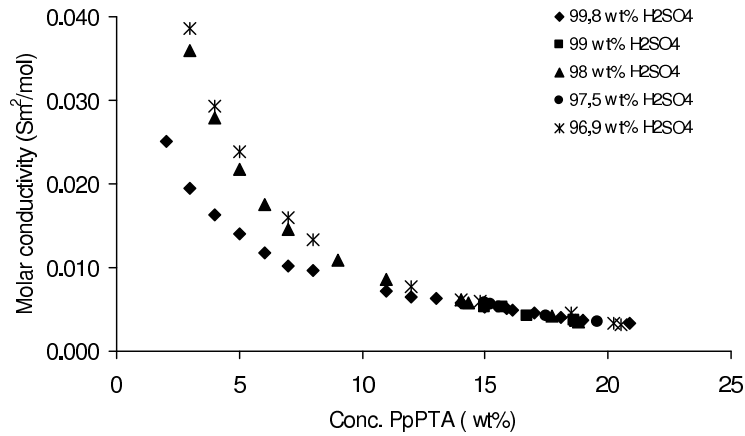


Figure 6.11: *Molar conductivity of PpPTA dissolved in different sulphuric-acid-water mixtures at 85° C.*

By plotting $[(1 - \alpha) \frac{C_{acid,0}}{C_{amide,0}} - \alpha + \alpha^2]^{1/2}$ against α a straight line should be obtained. The result is given in figure 6.12, note that the PpPTA concentration runs from high to low on the x-axis. Two linear regimes are present at low and high PpPTA concentrations of solutions not containing water. As an transition from isotropic to anisotropic occurs from low to high PpPTA concentration (~ 8 wt%) it is very probable that this structural change influences the equilibrium. The important observation is the linear relation. In the case water is present the relation is far from linear due to the formation of additional ions that are treated in the model as if they originated from amide unit protonation. An interesting point is the one at very low PpPTA concentration (2 wt%) in 99.8 wt% sulphuric acid. This deviates from the

linear relation. The small amount of water present in this solution shows its influence at very low PpPTA concentration.

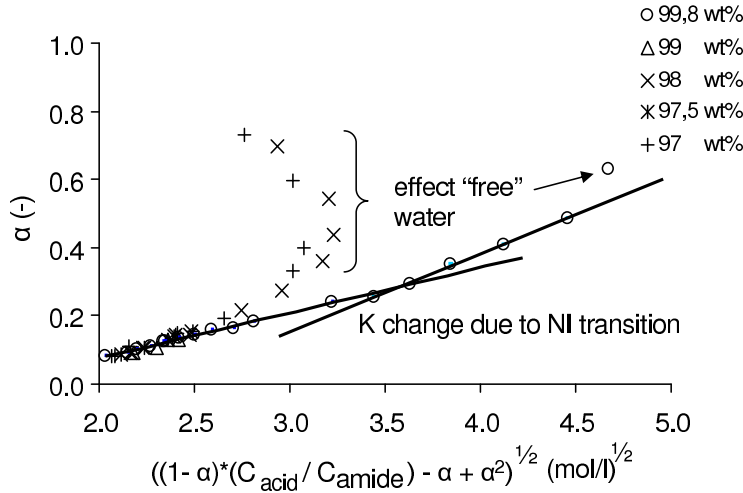


Figure 6.12: Linear regimes of the conductivity data agreeing with model predictions of protonation of PpPTA at 85°C.

Another important phenomenon is the decreasing of the relative dielectric constant (ϵ_r) when water is added to sulphuric acid. For 100% sulphuric acid the relative dielectric constant is 105 at 12°C and 95 at 25°C, this drops to 70 at 25°C when water is added and the concentration sulphuric acid drops to 99.5 wt% [99]. It is suspect that, due to the sharp fall of the relative dielectric constant when 0.5 wt% water is added, it will drop even more upon adding more water. At the same time the specific conductivity from sulphuric acid increases sharply from 0.85 to 10 S/m when it is diluted with water in the range from 100 to 96 wt%, according to Record [98].

In the case PpPTA is dissolved in a 100% sulphuric acid solution to a concentration of 20 wt% the relative dielectric constant is high and coulombic forces small. As the amide unit is susceptible for protonation and sulphuric acid is a strong acid, positively charged polymer chains repel each other strongly in a high dielectric environment with limited counterions present. Thus the polymer is in a dissolved state, according to Baird and Smith [100]. When water is added the amide units seem to bind it up to the point that no more free amide units are available, as discussed before. At 96 wt% the excess "free" water creates a lot of ions and decreases the relative dielectric constant. Due to these effects the counterions will shield the charged polymer chains, turning them neutral. These neutral chains do not repel each other and are able to approach each other and crystalize. The conditions under which shielding of counter ions actually occurs can be estimated by the bjer-

rum length. This is a measure for the distance at which kinetic- and coulomb forces are balanced. Recalling the definition of the bjerrum length, equation 3.13:

$$l_B = \frac{e^2}{4\pi\epsilon_0\epsilon_r kT} . \quad (6.6)$$

Having e^2 in the nominator balancing is realized when two elementary charges are balanced. That is, the average distance between charges on the polymer chain must equal the bjerrum length. This is expressed by the manning factor [101], [102]:

$$\xi = \frac{l_B}{b} . \quad (6.7)$$

b expresses the distance between charges on the polymer chain. When $\xi > 1$ ion condensation occurs (known as manning condensation). That is a fraction $1 - \frac{1}{\xi}$ of the counter ions are "condensed" on the polymer. In figure 6.13 the charges on a piece of a PpPTA chain are visualized and the distance between two successive charges is 7.5 Å.

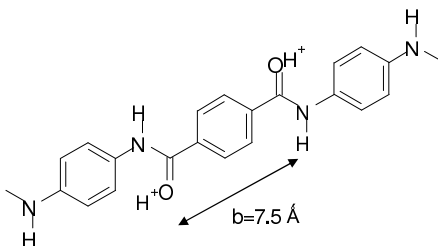


Figure 6.13: Protonation of the PpPTA polymer in a sulphuric acid environment.

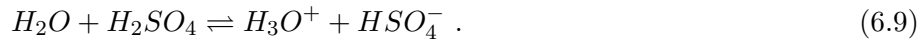
In the case of a 20 wt% PpPTA solution in 100% sulphuric acid the relative dielectric constant (ϵ_r) is roughly 100 and the bjerrum length then follows from equation 6.6 to be 5.6 Å. The manning factor is 0.75, this is smaller than unity and implies that counter ions are not condensed and are free to move about, resulting in charged, repelling polymer chains.

In the case of 0.5 wt% free water in sulphuric acid the relative dielectric constant has dropped to 70 and the bjerrum length increases to 8 Å and the manning factor to unity. This is the limiting case for binding counter ions. Further decrease of the relative dielectric constant, by adding more water, results in the manning factor to increase more and counter ions are bonded to the protonated polymer chains (manning condensation), resulting in more neutral chains that are now able to approach each other and crystalize.

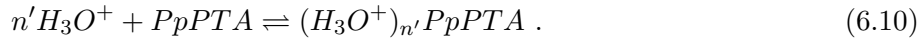
The above reasoning can be supported by a phenomenon called the nematic twist potential. Hereto, the following protonation equilibria are thought to exist. First PpPTA is partly protonated by sulphuric acid.



When subsequently water is added, this water is also protonated.



Now the hydronium ions will bind to the PpPTA and further charge the chain. This reasoning is justified by the observation that the (molar) conductivity, upon adding water, does not increase until the molar amount of water exceeds the molar amount of amide units in the PpPTA chains, see figures 6.10 and 6.11.



As a result of the binding of the hydronium ions, the chains will be charged more and therefore the nematic twist potential increases. This means more highly charged chains repel each other more severe resulting in a lower isotropic-nematic transition temperature, in figure 6.14 this process is made visible.

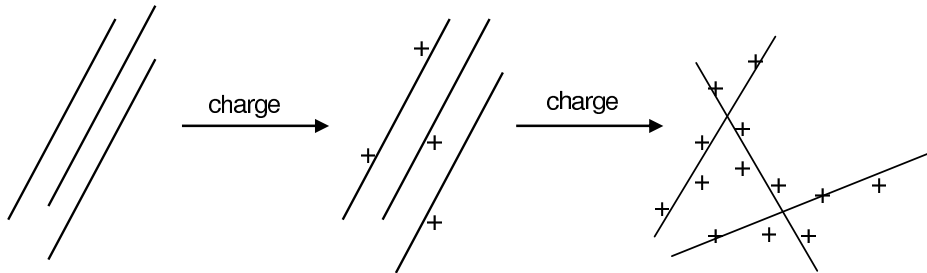


Figure 6.14: *Process of nematic to isotropic transition due to increased charging of the polymer chains, hence lowering the transition temperature.*

The effect of coulomb interactions on the nematic-isotropic temperature was investigated by Mishra et al. [103]. They showed that the observed transition temperature depends quadratically on the charge of the polymer chains. More highly charged chains showed a lower transition temperature. A similar effect was observed visually in a PpPTA film. A thin film of a 19.8

wt% PpPTA solution at 85°C was made varying from 0 to $100\ \mu\text{m}$. This film was subsequently exposed to air causing simultaneous cooling down and water absorption by the film. After coagulation in pure water microscopic images between crossed polarizers were made of the film at different positions differing in thicknesses. The images are shown in figure 6.15. The thinnest film shows opaque behaviour indicative for a nematic phase, by increasing thickness the opaqueness decreases indicating less anisotropy. During the exposure to air water is absorbed by the film. In the thinnest part this leads to immediate coagulation and a freezing in of the nematic structure. In the thicker parts the polymer molecules are longer free to move before coagulation freezes the structure. During this time the polymer molecules twist due to the increased amount of water as explained above, resulting in less anisotropic behaviour.

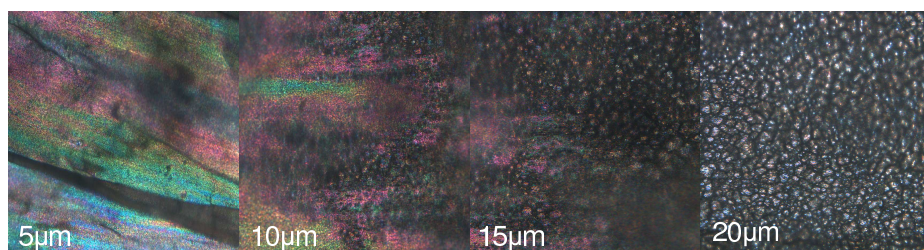


Figure 6.15: Microscopic images between crossed polarizers of films of different thickness of 19.8 wt% PpPTA in sulphuric acid. Films were manufactured at 85°C and subsequently cooled at air and coagulated in water.

Upon further addition of water the relative dielectric constant decreases and as a result the Bjerrum length increases, resulting in condensation of counter ions on the chains which in turn results in neutral chains and subsequent crystallization.

6.4 Energy effect of proton transfer

The energy change involved in proton transfer from sulphuric acid to the amide unit of PpPTA was calculated both for a dimer structure, PPDT, see figure 6.2 and a trimer structure, PPDB. $4\text{H}_2\text{SO}_4$, see figure 6.5. In the PPDT system, one sulphuric acid molecule is placed near the amide oxygen which is to be protonated; in the PPDB system the H_2SO_4 and HSO_4^- moieties are roughly positioned as observed in the corresponding crystal structure. For these calculations, the quantum chemical program Turbomole was used, employing a GGA BP functional and a TZVP basis set.

Numerical results from the quantum chemical calculations are given in table 6.2. Energy differences were calculated for the case that the model

components are in a vacuum, as well as in a continuum with a relative dielectric constant (ϵ_r) of 100 (corresponding to 100% H_2SO_4). In the case of vacuum, the protonated structures are not stable and convert to the unprotonated form upon energy minimization, indicating the absence of a significant energy barrier between the two states. Therefore, the energy of the protonated form of PPDT in vacuum was calculated by taking the geometry obtained using $\epsilon_r = 100$, and calculating the corresponding energy for $\epsilon_r = 1$ without further minimization, which should give a reasonable estimate of the true energy in vacuum. For PPDB, a geometry obtained midway the optimization process was taken, which had a low energy, but was still in the protonated form. Optimized geometries and energy differences are shown in figures 6.16 and 6.17.

Table 6.2: *Energy change (kJ/mol) associated with the protonation of PPDT and PPDB, using different relative dielectric constants.*

System	$\epsilon_r = 1$ (vacuum)	$\epsilon_r = 100$ (100% H_2SO_4)
PPDT	+46.0*	+1.2
PPDB	+58.0* (+29 per proton)	+7.9 (+4.0 per proton)

* protonated geometry is not stable.

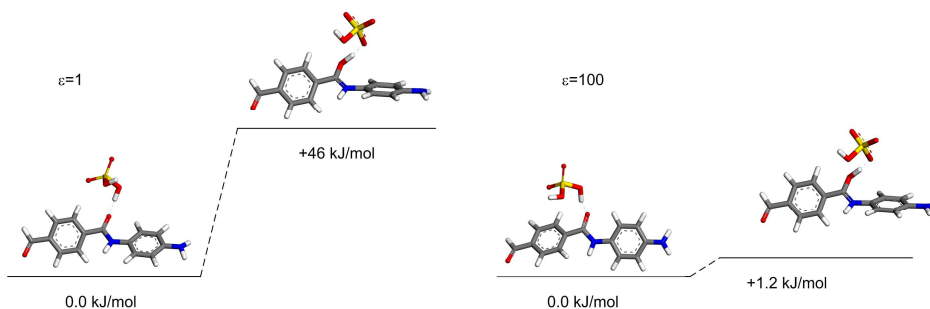


Figure 6.16: *Geometries and energies for PPDT. H_2SO_4 , depending on protonation and dielectric constant.*

A high relative dielectric constant appears to be essential to achieve proton transfer from sulphuric acid to the amide unit. If the relative dielectric constant is set to 100, the energy needed to transfer a single proton is small, 1.2 kJ/mol for PPDT and 4 kJ/mol for PPDB (two sites protonated). In vacuum, the required energy is 46 kJ/mol per proton for PPDT. H_2SO_4 , and 29 kJ/mol per proton for PPDB. $4\text{H}_2\text{SO}_4$. This difference is likely to be caused primarily by the presence of additional sulphuric acid molecules, which stabilize the local charges.

It can be concluded that a high relative dielectric constant is necessary to achieve protonation of the amide unit. The relative dielectric constant of

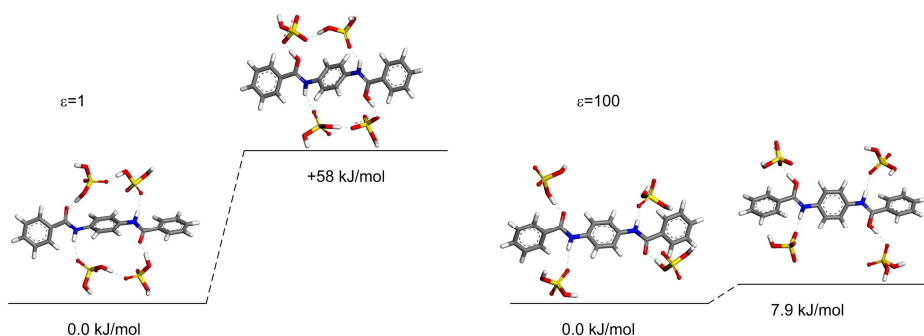


Figure 6.17: *Geometries and energies for PPDB.4H₂SO₄, depending on protonation and dielectric constant.*

concentrated sulphuric acid is known to be strongly dependent on the water concentration and the temperature, [99], [97]. For 100% sulphuric acid, $\epsilon_r=105$ at 12°C and $\epsilon_r=95$ at 25°C . At 25°C , ϵ_r drops to about 70 when water is added to increase the conductivity to 1.92 S/m; the concentration then is ~ 99.5 wt%. Decreasing the sulphuric acid concentration down to 97 wt% (25°C), ϵ_r drops even further. A concentration close to 100% is therefore needed to achieve substantial protonation of amide units. Based on the energy difference of 1.2 kJ/mol at $\epsilon_r = 100$ (100% sulphuric acid) and 25°C about 30% of the amide units are in the protonated state, for the energy difference of 4 kJ/mol this is about 17 wt%. This agrees with argumentation in the previous section that in pure sulphuric acid the PpPTA chains are partly charged and only upon adding water the amount of charged amide units increases through additional binding of hydronium ions.

6.5 Interactions in aromatic amide- H_2SO_4 - H_2O systems

As it is found experimentally that adding water to concentrated sulphuric acid-PpPTA solutions results in the precipitation of PpPTA. This does not occur however, when small amounts of water are added. As was shown earlier, the conductivity of a solution of PpPTA in anhydrous sulphuric acid does not increase until the amount of water exceeds (roughly) the number of amide units present in the solution. As mentioned before the dielectric constant of 100% sulphuric acid decreases rapidly if water is added. At the same time, the conductivity increases strongly [99], [97]. The conductivity of a solution of PpPTA in anhydrous sulphuric acid is higher than the conductivity of pure sulphuric acid (with no PpPTA dissolved). An explanation for the apparent formation of 1:1 amide unit-water complexes may be the electrostatic interaction between H_3O^+ and the (negatively charged) unprotonated oxygen atom

in the amide unit. The effect of small amounts of water added to 100% sulphuric acid has been studied using quantum chemical methods, to investigate whether such a strong interaction could be observed.

Extensive quantum chemical calculations on aromatic amide test molecules in contact with sulphuric acid and water, in an environment with $\epsilon_r=100$, showed no clear preference for the location of the water molecules but did show that, depending on the exact initial positions of the molecules, the amide unit in many cases ended up not being protonated. This leads to the following hypothesis: if water is added, the overall dielectric constant is likely less than 100, and many of the amide units will not be protonated. In that case, the resonance structure (for the non-protonated form) in which the double bond has shifted from $\text{O}=\text{C}-\text{N}$ to $^-\text{O}-\text{C}=\text{N}^+$ will lead to a relatively large negative charge on the oxygen atom. All water molecules will be protonated by the sulphuric acid, and will therefore have strong interaction with any negative charge present. Obviously, such an interaction will occur with the proton-donating sulphuric acid moiety, but it is also likely to occur with the negatively charged oxygen atom on the amide unit. An example of this is shown in figure 6.18, which is a low-energy frame taken from a geometry optimization (the optimization eventually failed to reach a stable energy minimum). Due to steric constraints, the number of H_3O^+ moieties bonded strongly to an amide unit may well be limited to one. This would explain the observed effect when water is added.

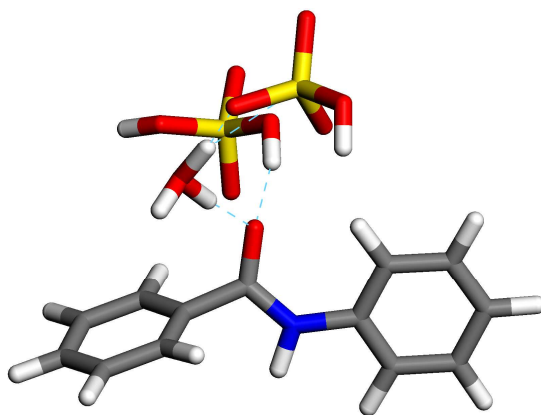


Figure 6.18: *Optimized aromatic amide-sulphuric acid-water complex.*

6.6 Structure of PpPTA dissolved in sulphuric acid

A molecular dynamics simulation was carried out to study the behaviour of PpPTA dissolved in sulphuric acid. As a starting model, a 3-D periodic box was created containing 7 PpPTA chains, of 4 monomers each, surrounded by 64 sulphuric acid molecules. Because the system is periodic in 3 dimensions, the simulation box is surrounded by an infinite number of identical copies of itself. This eliminates surface effects and causes the PpPTA chains to behave as if they were infinitely long. The PpPTA concentration in this system is 35 wt%.

Based on the structural information presented in section 6.2, it was decided to use a model in which all (28) carbonyl oxygens were protonated. To arrive at a consistent model, a random selection of 28 out of the 64 sulphuric acid molecules was modified to HSO_4^- . The PpPTA chains were placed in a geometry taken from the crystal structure of the pure polymer, as shown in 6.19. Cell dimension were 19.0x18.7x25.8 Å, with all angles set to 90°, and were kept fixed during the dynamics simulation. A 2.5 ns MD simulation at 473 K and constant volume was carried out.

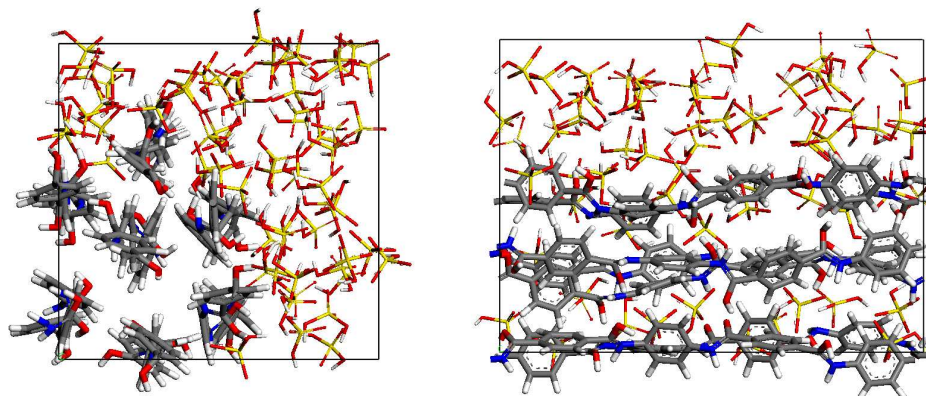


Figure 6.19: *Initial model for the MD simulation of 7 PpPTA chains in sulphuric acid, views along the chain axis (left) and perpendicular to the chain axis (right).*

Within 30 ps after the start of the simulation, the polymer chains have moved apart and solvent molecules and ions have filled the space between them. Obviously, this is due to the high electrostatic energy caused by the interaction between the positively charged chains. After this molecular rearrangement, the structure remains virtually unchanged in the remainder of the simulation. The space between the chains is mostly filled with negatively charged HSO_4^- ions, as is shown in 6.20.

Evidence from both experiments and quantum mechanical calculations

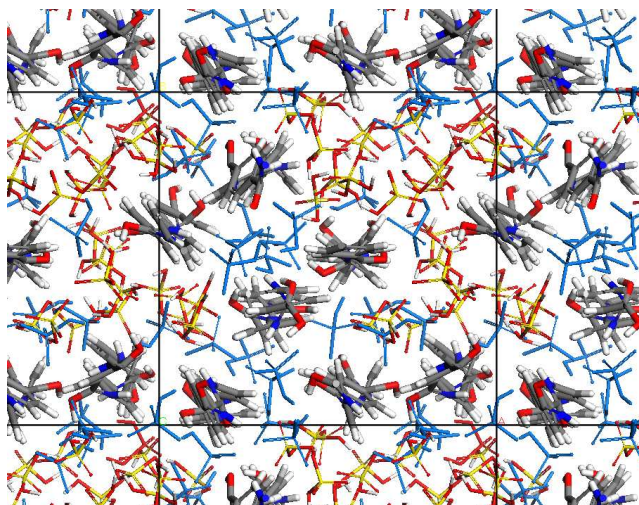


Figure 6.20: The structure of PpPTA dissolved in sulphuric acid after 2000 ps of molecular dynamics. The negatively charged HSO_4^- ions are shown in blue.

shows that the amide unit, if protonated, will accept a proton at the carbonyl oxygen.

The dissolution of PpPTA in sulphuric acid appears to be critically dependent on the protonation of the amide unit by the acid. Therefore the question comes up whether other acids may also protonate the PpPTA amide unit. The possibility of protonation by HCl was examined.

6.6.1 Interaction between HCl and aromatic amides

The interaction between HCl and aromatic amides was studied in a way similar to the approach taken in the earlier study on the protonation of PpPTA by H_2SO_4 . The feasibility of protonation of the carbonyl part of the amide unit was investigated by doing quantum chemical (QM) calculations on amide complexes with HCl, at different values of the dielectric constant ϵ_r . The test molecule used was N,N'-(p-phenylene)dibenzamide (PPDB). As PPDB contains two amide units, geometry optimizations were carried out on PPDB.2HCl complexes, starting from both the non-protonated situation (PPDB.2HCl) and protonated situation ($\text{PPDBH}_2^{2+} \cdot 2\text{Cl}^-$), to take into account the effect of the starting configuration. For the QM calculations, the computer program Turbomole was used, employing a GGA BP functional and a TZVP basis set. Depending on the relative dielectric constant, the optimized structure was either protonated or not, as shown in figure 6.21.

Results are shown in table 6.3. Although for each value of ϵ_r a calculation was done starting from the protonated as well as the non-protonated geometry,

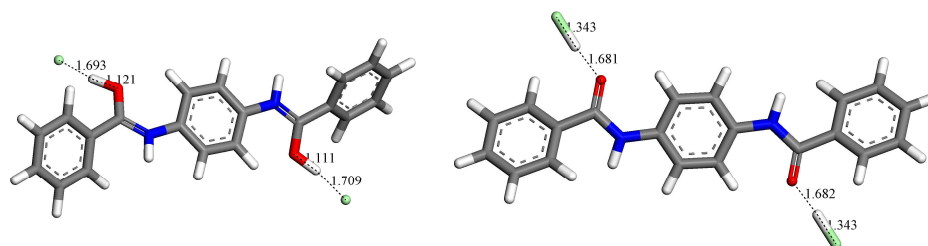


Figure 6.21: Protonated (left) and non-protonated (right) forms of PPDB.2HCl complexes. Relevant atomic distances (Å) are shown.

no effect on the final geometry was found. Apparently, no significant energy barrier for transferring the proton from HCl to PPDB is present. Starting from extreme values of ϵ_r , calculations showed that the transition from non-protonated to protonated forms occurs at a value for the dielectric between 10 and 15.

Table 6.3: Optimized structure of PPDB.2HCl complex depending on ϵ_r .

ϵ_r	optimized complex structure	H-Cl distance (Å)	H-O distance (Å)
1	non-protonated	1.34	1.68
4	non-protonated	1.39	1.50
10	non-protonated	1.48	1.32
15	protonated	1.00	1.19
25	protonated	1.64	1.15
100	protonated	1.70	1.12

The possibility of protonation of PPDB by HCl starting at values for ϵ_r of around 10 may be interesting in view of the relative dielectric constant of liquid HCl itself, which varies between 12 and 4.6 in the temperature range -113°C to 28°C as shown in table 6.4.

Table 6.4: Relative dielectric constant of liquid hydrogenchloride at different temperatures.

Temperature (°C)	ϵ_r HCl (liquid) ²
-113	12.0
-15	6.35
28	4.6

²Source: Handbook of chemistry and physics, 56th edition, 1975-1976, CRC Press Inc., Cleveland Ohio.

6.7 Conclusions

Quantum chemical calculations show that the energy required to protonate the amide group depends on the relative dielectric constant of the surrounding medium, protonation at the carbonyl oxygen is only feasible if the relative dielectric constant is high. The relative dielectric constant of sulphuric acid solutions depends strongly on the concentration and drops rapidly if water is added to 100% sulphuric acid. Thus protonation of the polymer chains in sulphuric acid is only likely to take place if the acid concentration is close to 100%.

A molecular dynamics simulation at 200°C shows that a 35 wt% PpPTA in sulphuric acid system will be a viscous mixture at this temperature. The polymer chains will not pack together due to their net charge, but form a rather immobile structure of polymer chains and solvent molecules, where the solvent provides the negative charge to compensate for the positive charge on the chains. Due to the high PpPTA concentration and the strong electrostatic interactions between the solvent and the polymer chains, the system does not behave as a fluid at 200°C.

Results from electrical conductivity experiments in which controlled amounts of water were added to sulphuric acid could be explained by assuming the binding of water to the amide units of PpPTA, up until molar equivalence. Addition of more water subsequently resulted in the presence of "free" water. This in turn increases the electrical conductivity of the mixture and decreases its relative dielectric constant. The Debye length as a result increases and causes Manning condensation, resulting eventually in neutral chains that precipitate. A quantum chemical calculation showed indeed it is sterically probable that only one hydronium ion can bind at an amide site.

In short: a high relative dielectric constant of the mixture results in protonated chains that repel one another and keep them apart. Once this relative dielectric constant is lowered, e.g. by adding water, the charged chains are neutralized and crystallize. Calculations suggest that protonation of PpPTA by HCl may be possible, although the low dielectric constant of HCl at room temperature hampers protonation energetically.

7. Hairpin Formation

This final chapter introduces the intriguing phenomenon of hairpin formation in PpPTA chains. Unlike often assumed the polymer chains are not completely extended along a common director. They are able to fold back at relative low energy cost. Evidence for the existence of these hairpins is found in measurements of oscillation rheometry on PpPTA of different molecular weight in sulphuric acid.

7.1 Introduction

In the previous chapters the focus was on the possible dissolution of PpPTA in acidic and non-acidic media. The presence of the polymer chains in these media were assumed to be in a stretched configuration due to their intrinsic rigidity. During coagulation the stretched configuration of the polymer chains is "frozen" in and the resulting excellent mechanical properties of aramid fibers are largely contributed to the orientation of the chain molecules in the the direction of the fiber axis. In an article Picken et al. [104] presented experimental evidence of the existence of hairpins in solutions of PPTA in sulphuric acid, based on neutron scattering (SANS) measurements, directly influencing the orientation conformation. They come to this conclusion by comparing the experimentally determined radii of gyration ($\langle R_g \rangle_{\parallel} = 250 \text{ \AA}$, $\langle R_g \rangle_{\perp} = 70 \text{ \AA}$), determined using contrast matching conditions, with predicted values of two models. The first model, by Odijk [105], uses a worm-like chain model in which a deflection length is defined as the characteristic length scale. In this model it is assumed that polymer chains are confined in their statistics by the nematic potential. The nematic potential forces the chains to align parallel to the director. The calculated radii in this model differ substantially from the experimental values ($\langle R_g \rangle_{\parallel} = 455 \text{ \AA}$, $\langle R_g \rangle_{\perp} = 24 \text{ \AA}$). In a second model, assuming an undisturbed chain (similar to a worm-like chain in dilute isotropic environment) and using the persistence length (290 \AA [7]) as the appropriate length scale in the nematic phase, the calculated radii of gyration

and their temperature dependence, based on a modified Maier-Saupe theory [11], are found to agree well with the experimental values ($\langle R_g \rangle_{\parallel} = 300 \text{ \AA}$, $\langle R_g \rangle_{\perp} = 78 \text{ \AA}$). A schematic drawing of the molecular conformation in the nematic phase for both situations is shown in figure 7.1.

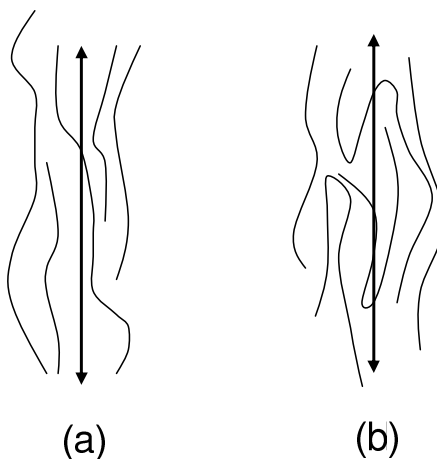


Figure 7.1: *Schematic drawing of molecular conformations of PPTA in the nematic phase for (a) worm-like model with confined chains and (b) worm-like model with hairpins.*

To explain the disagreement with the deflection length concept, it was stated that the description of a quadratic form of the free energy as a function of the molecular curvature is only valid for rather small molecular deformations. In real solutions beyond a certain point the chain may fold back on itself and form a hairpin. This should occur at low energy cost. The article of Picken et al. [104] ends with the intriguing question to whether such conformational back folds can be formed at relatively low energy cost and if this folding back occurs over a single bond length (sharp bend) or is smeared out over several bonds.

In this chapter, the results are presented of quantum chemical (QM) and molecular dynamics (MD) simulations regarding possible geometries of hairpins, and the energy change involved in their formation.

7.2 Simulations of hairpin configurations in PpPTA chains

Manually, hairpin geometries from a PPTA 10-mer and 11-mer were created, using the Materials Studio software¹. It appears that (at least) two geome-

¹Material Studio is available from Accelrys, <http://www.accelrys.com>

tries are possible, shown in figure 7.2. (Both geometries have the same chain lengths after the fold.) Adjusting the torsion angles in a single amide unit can result in a 90° change in the overall chain direction. Thus, it takes two such conformations to obtain a complete reverse of the chain direction. The amide units involved can be attached to the same central phenyl ring, or may have an additional ring in between. Which is the most favourable will most likely depend on how the two ends of the chain fit together when the chain folds back to itself, forming hydrogen bonds between them.

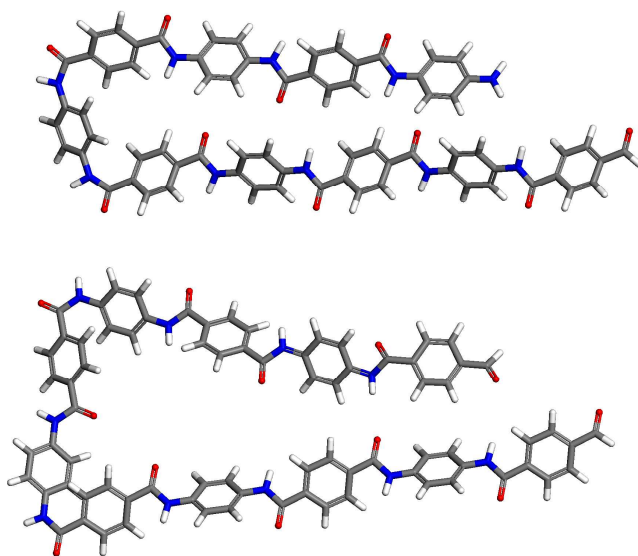


Figure 7.2: Two possible geometries for a hairpin in PpPTA, differing by the number of rings between the rotated amide units (top one, bottom two).

To test the stability of both types of hairpin geometries in practice, Molecular Dynamics (MD) simulations were carried out on a 10-mer (adjacent *cis* conformations) and 11-mer (non-adjacent *cis* conformations) structure, put into a rectangular MD simulation box of $\sim 20 \times 16 \times 40$ Å, together with two (linear) 6-mers and 70 NMP molecules, creating a system of density 1.15 g/ml. Figure 7.3 shows the initial configuration for the 11-mer structure. Simulations were done at constant volume and temperature, using the Compass force field ². A 9.5 Å cut off radius was used for van der Waals interactions and Ewald summation was used for electrostatic interactions.

In contrast to the experiments performed by Picken, in the simulations NMP was used as a solvent instead of sulphuric acid. To show that hairpin formation is mainly a conformational effect, an intra molecular phenomenon,

²COMPASS (Condensed-phase Optimized Molecular Potentials for Atomistic Simulation Studies)

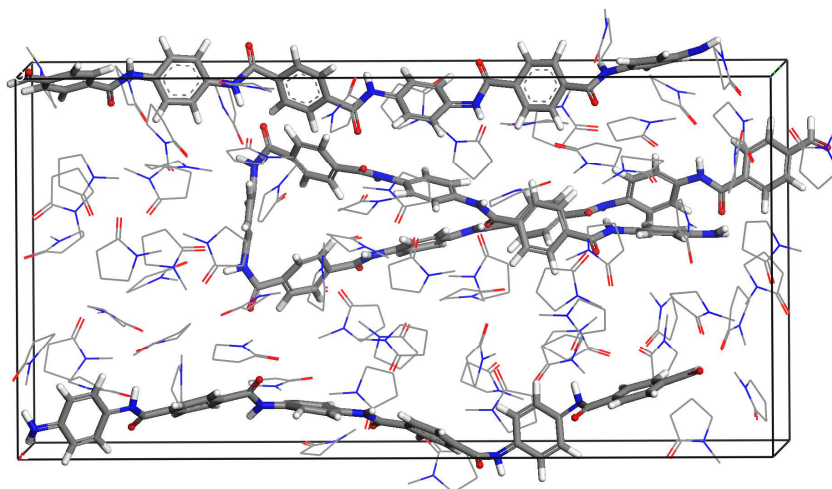


Figure 7.3: *Snapshot from initial MD run configuration of PPTA structures, dissolved in NMP.*

regardless of the solution medium, NMP is a better choice as it lacks the capability to protonate the amide unit.

Simulations at 200°C and 450°C, for 3.5 ns each, showed that in fact a single rotated amide unit (changing the conformation from trans to cis) is sufficient to obtain a hairpin structure. Relative small deviations in amide bond torsions near the cis conformation take care of a complete reversal of chain direction. Several snapshots from one of the MD runs, as shown in figure 7.3, are given in figure 7.4. For clarity the aramid units of interest are indicated bigger than the other units. The end geometry shows a complete reversal of the chain with only one amide unit in cis conformation.

7.3 Energy aspects of the observed hairpin structures

The MD simulations suggest that a single cis amide unit can be sufficient to obtain a hairpin geometry, in combination with a number of energetically small torsion angle adjustments. This implies that the energy difference between linear and hairpin structure can be estimated by simply looking at the relative energy of a cis amide conformation, compared to the trans conformation.

This energy difference has been calculated by QM-calculations. The QM software used here, Turbomole, employs a TZVP basis with polarizing d-set, and a BP DFT functional. The Cosmo approach [90], [91] was used to take into account the surrounding dielectric.

From the energy difference, the ratio trans/cis is estimated using the Boltzmann relation, equation 7.1, results are listed in table 7.1.

$$\frac{n_{trans}}{n_{cis}} = \exp \frac{-(E_{trans}-E_{cis})}{RT} . \quad (7.1)$$

The calculated energy of cis relative to trans is about 17 kJ/mol, and this value is hardly influenced by the dielectric constant of the medium. This is an important result as the dielectric constant of sulphuric acid-water mixtures decreases rapidly upon adding water. It decreases from 100 to 70 when the amount of water is increased from 0 to 0.5 wt% [99] and probably even more upon further addition of water as discussed before. The dielectric constant of NMP is about 32 [79]. Apparently the environment only has a minor influence on the conformational energy difference.

Table 7.1: Conformational energy differences in hairpin formation from quantum chemistry at 298 K. The marked (*) value indicates protonation of the amide unit.

Dielectric constant	Relative energy (cis-trans) (kJ/mol)	ratio trans/cis (25°C)
1	18.2	1540
32	16.6	565
100	16.8	880
100	15.1*	445

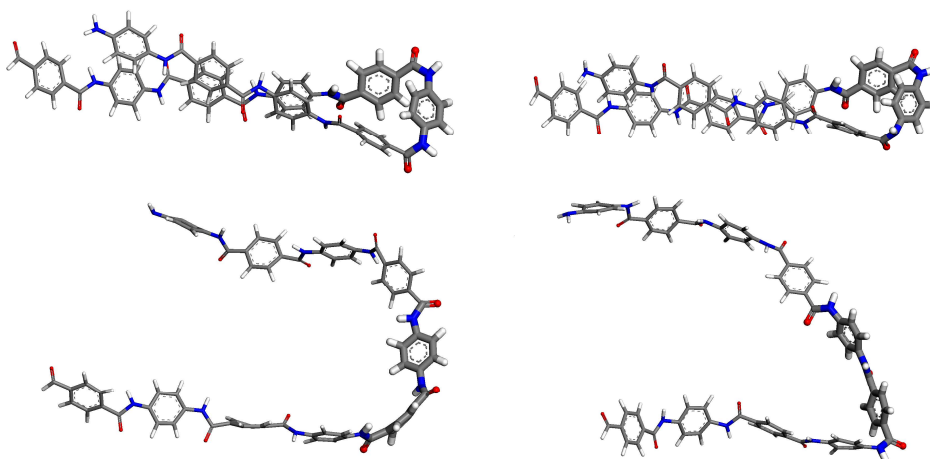


Figure 7.4: Snapshots from a MD run on PpPTA hairpin structures. a) at 25 ps, starting conformation trans-cis-cis b) 35 ps, transition, trans-cis-trans conformation c) 2900 ps, transition, trans-trans-trans conformation d) 3000 ps, transition, trans-trans-cis conformation.

The energy barrier between cis and trans amide geometries was estimated using QM methods (DMol3 software available within Material Studio; GGA BP functional, DNP basis set). The torsion angle of an amide unit of a model component, shown in figure 7.5, was varied from -90° to 180° and back in steps of 5° . The energies of the different conformations, after minimization, keeping the amide torsion fixed is shown in figure 7.6.

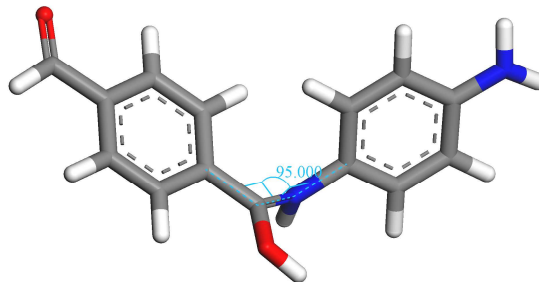


Figure 7.5: One of the conformations used in the calculation of the relative energy as a function of the torsion angle of the amide unit.

Changing the torsion in the amide unit leads to steric hindrance between the adjacent phenyl rings, causing them to reorient. As a consequence intermittencies in the relative energy appear at various angles, depending on the torsion scan direction. The energy barrier in both scans is found to be about 100 kJ/mol.

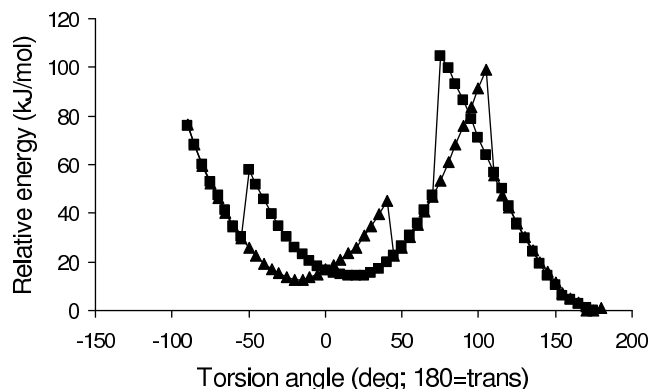


Figure 7.6: Relative energy of various conformations of a PpPTA unit in which the amide torsion angle is varied between -90° and 180° (triangles) and between 175° and -90° (squares). The intermittency seen at various angles is due to steric hindrance and rotation of the phenyl rings.

The values presented in table 7.1 suggest a hairpin conformation every 880 amide units on average at 25°C in an environment with a dielectric constant of 100 (sulphuric acid at 100%). The average molecular weight (M_w) used in

the SANS experiments of Picken [104] is 32000 gr/mol. With the molecular weight of the repeat unit 238 gr/mol (two aramid units) and a length of 12.9 Å, according to Cotts et al. [6] this corresponds to 134 repeat units which is equal to 267 amide units per chain and a contour length of 1750 Å. This gives a result of $267/880 \approx 0.3$ hairpins per chain. Comparing this to the value based on Pickens evaluation $N_{HP} = L_c/4L_p = 1750 \text{ Å} / 4 \cdot 290 \text{ Å} = 1.5$ (number of hairpins equals the ratio of the chain contour length over 4 times the persistence length), this last number is much larger than the modeling result. Dissolved in sulphuric acid though, amide units are (partly) protonated, lowering the relative energy difference between cis and trans from 16.8 to 15.1 kJ/mol, resulting in an increase of the number of hairpins per chain to 0.6, which comes closer. The model results furthermore have a different temperature dependence, as a Boltzmann relation is used while a $1/T$ dependence of the persistence length is applied in the article of Picken [104]. At the isotropic-nematic transition temperature of PPTA in sulphuric acid (at 11 wt% this corresponds to 88°C [56], [57]) the predicted number of hairpins are almost the same. $N_{HP} = L_c/4L_p = 1750 \text{ Å} / 4 \cdot 240 \text{ Å} = 1.8$ and the simulation predicts, using an energy difference of 15.1 kJ/mol, 1.7 hairpins per chain. It is expected that the number of hairpins match at the transition temperature, as the nematic potential is relieved.

7.4 Oscillation rheometry measurements

As a consequence of the existence of hairpins a physical network could be formed if the chain functionality exceeds 2. That is when the number of hairpins per chain exceeds 2. To test this, three samples of PpPTA varying in molecular weight were dissolved in sulphuric acid up to 20 wt% and exposed to an oscillatory rheometer measurement at a temperature of 85°C (Haake RheoStress 600, cone-plate geometry 2°). In table 7.2 the calculated number of hairpins per chain of the samples is presented. In the calculation ($N_{HP} = L_c/4L_p$) the persistence length (290 Å) is the same for all samples and the contour length scales with molecular weight.

Table 7.2: *Molecular weight, contour length and number of hairpins per chain for the three samples measured.*

Molecular Weight (g/mole)	Contour length (Å)	#Hairpins/chain
22000	1200	1.2
32000	1750	1.8
65000	3600	3.6

Based on the number of hairpins per chain network formation would be expected in the samples with molecular weights 32000 and 65000 g/mole. In figure 7.7 the loss and storage moduli are given.

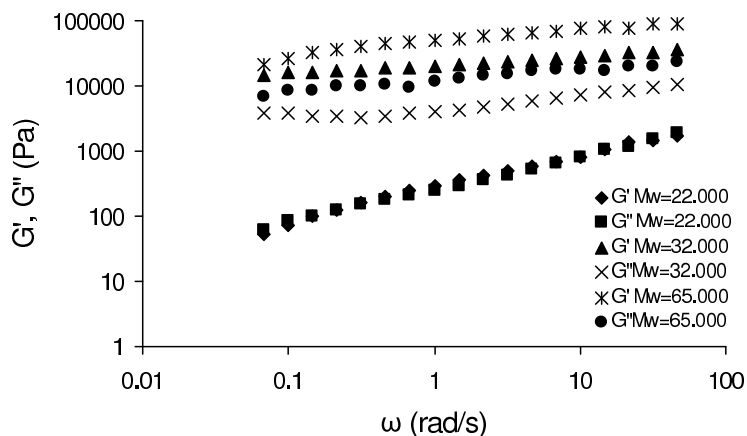


Figure 7.7: Storage (G') and loss (G'') moduli for three samples, PpPTA dissolved in sulphuric acid (20 wt%), of different molecular weight. All measurements are based on stress controlled oscillation (1 Pa for the $M_w=22000$ g/mol sample and 10 Pa for the other molecular weight samples). All experiments were performed in the linear viscoelastic regime.

The 22000 g/mol sample shows a low modulus with storage and loss moduli coinciding. This suggests gel formation, a state between liquid and solid. The other two samples show clearly a higher moduli and a storage modulus exceeding the loss modulus, indicating elastic behaviour and thus network formation. As the molecules themselves are stiff in nature this increase in elastic behaviour can very well be attributed to hairpins. Moreover the network formation, as expected, occurs when the calculated number of hairpins per chain is two or more.

7.5 Conclusions

Molecular dynamics simulations suggest that hairpin formation in PpPTA chains is facilitated when an amide unit adopts the cis-conformation. A single cis conformation appears to be sufficient for the formation of a complete hairpin, even though by itself it does not lead to a complete 180° change of the chain direction. The frequency at which hairpins are to be expected is then directly related to the energy of the cis amide conformation relative to the trans conformation. These numbers directly correspond to the expected chain length (number of amide units) between hairpins.

From QM-calculations an energy difference of about 15-18 kJ/mol is calculated in the range of a dielectric constant of 1-100, with an energy barrier of about 100 kJ/mol. The calculated number of hairpins per chain at 25°C is lower (0.6) than the experimentally observed value from SANS measurements (1.5) [104]. At the isotropic-nematic temperature (88°C) however, both simulation and experimental extrapolation predict roughly the same number of hairpins per chain (1.8). Even if the nematic potential in the high concentrated solution should prevent chain folding, still hairpins may be present as they can very well have been formed during polymerization.

The main conclusion of the calculations in this chapter is that there is a high likeliness for the existence of hairpins in PpPTA chains.

8. Concluding Remarks

In this thesis the dissolution behaviour of Poly(p-phenylene terephthalamide) (PpPTA) and to some extent its isomers PBA, DABT and PmPTA, in acidic and non-acidic media was discussed. Next to experimental evidence also a thermodynamic model to explain the dissolution behaviour of PpPTA was presented. At high PpPTA concentrations e.g. 11 wt%, used in commercial polymerization, mixtures result directly in a crumble product and due to their high viscosity are not suitable for study purposes. Rather low concentrations, up to 5 wt%, result in solid polymer mixtures of which the viscosity can be lowered dramatically by neutralizing the reaction product with CaO. Even mixtures containing polymer with a molecular weight (M_w) in the order of 20000 g/mol are processable. At these concentrations the mixtures are fluid-like after the polymerization process, however were found to solidify and/or phase separate in due time, depending on the concentrations of the components in the mixture and storage conditions. Depending on the polymer concentration, solutions show visual phase separation and the solidifying of one of the phases, or only the formation of a solid phase at higher PpPTA concentration. During the process of phase separation the shear viscosity and structure of the mixture change and a calorimetric transition was observed. After a gradual decrease of the shear viscosity a rather steep increase was seen. This upturn coincided with the disappearance of an enthalpic transition at $\sim 75^\circ\text{C}$ and was sometimes accompanied by the formation of spherulitic particles.

X-ray diffraction experiment showed the formation of large non-crystalline structures, followed in a later stage by Bragg reflections, indicating crystallization. Under the microscope, formation of spherical and needle like particles were seen that in time grew both in number and size. The time frame in which these processes took place varied largely with temperature and PpPTA concentration.

Above 2,5 wt% these solutions show anisotropic behaviour. This is at surprisingly low concentrations, considering the molecular dimensions; in sul-

phuric acid the same polymer shows an isotropic-nematic transition at 8 wt%. This supports the idea of aggregate formation right after polymerization. Further support for the particle formation in solution is the Osager like phase behaviour of PpPTA in NMP-CaCl₂, represented in an a-thermal phase diagram.

During polymerization the presence of CaCl₂ is essential to gain high molecular weight polymer. In pure NMP low molecular weight polymer precipitates immediately. The interaction of PpPTA with CaCl₂ was seen to be key in slowing the phase separation process down. Electrical conductivity measurements in NMP-CaCl₂ showed weak electrolyte behaviour in which only a rather small portion of the CaCl₂ is present in ionic form. Furthermore the cations form clusters of calcium and chloride in NMP and the mixture behaves like a weak electrolyte. The fraction split in ionic form decreases from ~20% to ~6% when the CaCl₂ concentration is raised from 1 wt% to 6 wt%. The presence of PpPTA does not influence the electrical conductivity, although the viscosity rises steeply. Apparently the mixture behaves like a bi-phase system for ion mobility. These findings agree with modeling calculations, showing preferential interaction of the amide unit of PpPTA with chloride ions and aggregate formation of cations.

The observed decrease in viscosity observed when polymer mixtures are neutralized after polymerization could be explained. During polymerization HCl is formed. The proton can interact with the carbonyl-oxygen of the amide unit of PpPTA as well as of NMP. In NMP-HCl mixtures a protonated adduct of NMP was identified by NMR analysis. In case of adding CaO the HCl is neutralized in formation of CaCl₂. As mixtures of CaCl₂ form clustered cations and the electrical conductivity of the mixture decreases due to weak electrolytic behaviour, the amount and strength of ionic interactions decrease with increasing CaCl₂ content. This eventually leads to more neutral chains, hence lower viscosity.

Electrical conductivity measurements in sulphuric acid show strong electrolyte behaviour of PpPTA in the range from 2 to 14 wt%. Also now a bi-phase system is probably responsible for the electrical conductivity behaviour as also now the viscosity increase upon adding PpPTA does not influence electrical conductivity. Further increase of the PpPTA content above 14 wt% results in an electrical conductivity decrease. As the internal structure of the solution carries the bi-phase properties, ion mobility is limited above 14 wt%. Some kind of structure formation between PpPTA and sulphuric acid may very well be responsible for this decrease as the ratio amide units to sulphuric acid molecules approaches 1:4 which is a known ratio in complex formation and hence decreases the ion mobility. It also provides an argument for the max-

imum solubility of 20 wt% PpPTA in sulphuric acid. At this concentration the ratio amide units to sulphuric acid molecules is 1:5 which is close to the 1:4 ratio and no more sulphuric acid is available for interacting with additional PpPTA.

When water was added the electrical conductivity did not change until the molar amount of water exceeded the molar amount of amide units. An explanation may be the binding of water to the amide units in a 1:1 ratio in the form of H_3O^+ up until no more amide units are available. Any additional "free" water reacts with sulphuric acid to produce ions and simultaneously decreases the relative dielectric constant of the mixture. The resulting condensation of ions on the PpPTA chains neutralizes them. This explains the precipitation of PpPTA when water is added. The protonation of the polymer amide units together with the high relative dielectric constant is responsible for the stable dissolution of PpPTA in 100 wt% sulphuric acid. Molecular modeling calculations indeed resulted in partial protonation of the amide units in a high relative dielectric environment and de-protonation in case the relative dielectric constant is lowered in agreement with experiment. Also sterically one hydronium ion could be accommodated by an amide unit as proposed in the addition of water.

To explain the observed instability of PpPTA in NMP- CaCl_2 mixtures a thermodynamical model, based on volume fraction statistics, for the behaviour of liquid mixtures was presented. From this model excess chemical potentials for the participating components are calculated, based on which the mixture stability was determined. In this model an interchange parameter was introduced to describe the change in the partial excess free enthalpy when changing the surrounding of different molecules in a mixture. Due to the definition of this parameter it is symmetrical and has the same numerical value in exchanging a molecule A by a molecule B in a liquid of molecules A and vice versa. The model assumes the components to be present in random distribution and absence of preferential orientation between different components. From ^1H -NMR there appear to be no independent complexes present in the NMP- CaCl_2 (-PpPTA) mixtures but rather a kinetic equilibrium between NMP, CaCl_2 and PpPTA is established. This means there is no lasting interaction between the components. From electrical conductivity measurements of CaCl_2 in NMP it was already concluded that only a small part of the CaCl_2 is present in ionic form and another part forms clusters. Therefore the assumption of neglecting ionic effects and using the non-ionic components as input for the model are not entirely true but seems reasonable in this case.

In a calorimeter heats of dissolution were measured which were used to calculate the interchange terms (-4093 J/cm^3 between CaCl_2 and benzanilide and

-1613 J/cm³ between CaCl₂ and NMP), benzanilide was used as a model compound for PpPTA as PpPTA itself does not dissolve in NMP-CaCl₂. These values were subsequently used as input for the model to calculate the excess chemical potentials of the participating components. It was found that PpPTA-NMP-CaCl₂ mixtures can theoretically form thermodynamically stable solutions only above 22 wt% CaCl₂. This can, in practise, never be achieved as the maximum solubility of CaCl₂ in NMP is about 5.5 wt% at 25°C. Above this concentration solid complexes are formed that precipitate from the solution. As 5.5 wt% is too low to overcome the fusion enthalpy of PpPTA (-340 J/g) in practice NMP-CaCl₂-PpPTA mixtures will always be unstable and phase separate. To express the solvent power of a mixture, the TDP-index was defined as the ratio of the maximum solubility of a given salt in a given mixture over the minimally required concentration of that salt to gain a thermodynamically stable solution. If it exceeds unity it is a potential solvent. For CaCl₂-NMP this is 5.5 wt%/22 wt% = 0.25.

Interactions between other salt-NMP solvents and PpPTA were determined using calorimetry, as well as the maximum solubility of the salt in the respective amides. Just as for CaCl₂ these salts interact strongly with PpPTA and are, in combination with their solubility, mainly responsible for the solvent power.

In the case of NMP-CaCl₂ three different solid complexes are identified which limits the solubility to 10 wt% at 90°C and 5.5 wt% at 25°C. LiCl seems to do better as it has a stronger interaction with benzanilide (PpPTA) (-6123 J/cm³) and a higher solubility (7.8 wt%). The bromine salts LiBr and CaBr₂ have far higher solubilities in NMP (21.1 and 24.7 wt% respectively). Their interactions with benzanilide (PpPTA) are much lower though (-3184 and -2330 J/cm³ respectively). All combinations do not have enough dissolution power to dissolve PpPTA.

To prevent complex formation due to preferred interactions it seems favourable to search for salt-solvent combinations that have high interaction terms and are roughly identical between salt-amide and salt-PpPTA. To gain more insight on the effect of the amide solvent, the influence of various amide solvents on the interactions were determined and expressed in molecular group contributions. That is the influence of different molecular groups on the interactions. Amides containing an NH-group showed the strongest interaction with salts, followed by phenyl groups adjacent to an amide containing an NH-group. For LiCl the difference between NH containing groups and non NH containing groups was large, for LiBr the difference was far less. This might be contributed to the interaction of PpPTA with the small Li ions, that are less sterically hindered and which are more abundantly available in LiBr solvents.

N-methylformamide-LiCl and N-ethylformamide-LiCl were found to be interesting candidates for the dissolution of PpPTA. They possess high interaction terms and also show rather large solubilities resulting in TDP-indices of 1.23 and 1.06 respectively.

As salts have such a strong interaction with PpPTA, their influence on solutions of PpPTA in sulphuric acid were examined. A strong interaction was indeed also found and solubility of PpPTA seems to increase from 20 wt% to 25 wt% at 88°C by adding only 1 wt% CaF_2 (both CaCl_2 and CaBr_2 were found to be unfit as chloride and bromide evaporate in the form of HCl and HBr). This opens the possibility to search for other salt-solvent combinations in which PpPTA might dissolve.

To understand the mechanism of dissolution on a molecular scale, simulations were performed on PpPTA in NMP- CaCl_2 solutions as well as in sulphuric acid solution. CaCl_2 indeed showed aggregate formation agreeing with electrical conductivity measurements. Also the maximum dissolution of CaCl_2 was predicted correctly when these aggregates were assumed. Simulations performed with LiCl and HCl also showed aggregate formation. The chloride ion is found to be more time in the proximity of the PpPTA chain causing it to be negatively charged. This in contrast to simulations in sulphuric acid in which the chain is positively charged due to protonation. The degree of protonation is high in 100 wt% sulphuric acid and much less in 97 wt% sulphuric acid due to a decrease in the dielectric constant. From quantum mechanical simulations it appears that the relative energy of the protonated-compared to the unprotonated state increases due to this decrease of the dielectric constant. This also results, as earlier argued, in ion condensation upon adding water and neutral chains to precipitate.

In all considerations, chains of PpPTA are thought to be present in a linear conformation due to their rigidity. Simulations showed that even one amide unit in the cis conformation might lead to a complete internal reverse in chain conformation and thus the formation of a hairpin. The accompanying cis-trans transition energy was found to be in the order of 17 kJ/mol. In dynamic simulations cis-trans transitions were observed and oscillation rheometer measurements on PpPTA-sulphuric acid solutions revealed network formation. The fact that in real solutions the nematic potential might hinder hairpin formation might well be irrelevant if the hairpins are formed during the polymerization.

In general, charged chains are needed to keep PpPTA in solution. Due to strong hydrogen bonding, neutral PpPTA chains have a strong tendency to crystallize. A possible way to keep them apart are repulsing charges. In the case of 100 wt% sulphuric acid, protonation is numerous enough to overcome the free enthalpy of fusion, however in case of NMP- CaCl_2 the ions are only

able to slow down the crystallization process, but cannot prevent it. The path in trying to find an amide solvent lies in the search for salt-solvent combinations that can overcome the free enthalpy of fusion by strong interactions with PpPTA and that simultaneously do not phase separate or form complexes with either solvent or PpPTA, which prevents a high solubility. In this way maximum use of strong interactions can be made.

The list of possibilities seems endless. In this thesis a selection method was developed to come to a result. So far N-methylformamide and N-ethylformamide are amides that show the necessary large interaction with LiCl and are liquid at room temperature. Bromine salts were shown to have a large solubility in amides but exhibit rather low interaction with PpPTA.

N-ethylformamide-LiCl mixtures were found to exhibit enough dissolution power to overcome the free enthalpy of fusion of PpPTA and thus act as a true solvent for PpPTA. Low crystalline PpPTA was found to (partly) dissolve in this mixture.

Of course other solvent with suitable properties might again produce a whole new class of possibilities, e.g. recently the solubility of Polyamide-4,6 in salt-water systems was investigated by J. Harings [106]. However, for polymerization purposes a non-acidic medium is required limiting the possibilities for the development of a one-step fiber producing process. Amide solvents seem a best first choice as non-acidic media. An alternative could be ionic liquids as the salt-PpPTA interactions are responsible for the dissolution power. The amide solvent acts merely as a carrier to keep the salts in solution. Ionic liquid seem to be perfect for this means as they are already liquid. In literature a number of articles have been published in which PpPTA was polymerized in ionic liquids [107], [108], [109] unfortunately resulting in poor molecular weight. A number of trials have indeed been explored but are not mentioned in this work as they were found unfit to dissolve PpPTA. The main disadvantage of ionic liquids lies in the rather low ion concentration. In order for them to be liquid at low temperature rather large, tail like ions, are required.

References

- [1] Kwolek Hill and Morgan. u.s. pat. (3,006,899), 1961.
- [2] H.H. Yang. *Aromatic High-Strength Fibers*. Wiley-Interscience Publication, 8 1989.
- [3] P. Doty H. Benoit. *J. Phys. Chem*, 57:958, 1953.
- [4] G. Weill H. Benoit M. Arpin, C. Strazielle. *Polymer*, 18:262, 1977.
- [5] F.M. Logulle V.H. Good L.W. Gulrich F.L. Killian J.R. Schaeffgen, V.S. Folid. *Polym. Prepr., Am. Chem. Soc., Div. Polym. Chem.*, 17:69, 1976.
- [6] G. C. Berry P.M. Cotts. *J. Polym. Sci., Polym. Phys. Ed.*, 21:1255, 1983.
- [7] B. Chu Q. Ying. Persistence length of poly(1,4-phenyleneterephthalamide) in concentrated sulfuric acid. *Makromol. Chem., Rapid Commun.*, 5:785–791, 1984.
- [8] K. Nagai. *Polym. J.*, 3:67, 1972.
- [9] M. Doi and S.F.Edwards. *The Theory of Polymer Dynamics*. Oxford science Publications, 1986.
- [10] O. Kratky and G.Porod. *Rec. Trav. Chim.*, 68(1106), 1949.
- [11] S.J. Picken. Orientational order in aramid solutions determined by diamagnetic susceptibility and birefringence measurements. *Macromolecules*, 23:464–470, 1990.
- [12] A.J.J. Hendriks and J.M. Surquin. Non-fibrous polymer solution of para-aramid with high relative viscosity, nov. 2004.
- [13] A.J.J. Hendriks and D. Wilbers. Para-aramid fibrid film, june 2005.

-
- [14] A.J.J. Hendriks and J.D.C. Tiecken. Aramid fibrils, june 2005.
- [15] J.R. Schaefgen S.L. Kwolek, P.W. Morgan and L.W. Gulrich. Synthesis, anisotropic solutions, and fibers of poly(1,4-benzamide). *Macromolecules*, 10(6):1390–1396, 1977.
- [16] P.W. Morgan. *u.s.Patent*, (3,943,110), March 1976.
- [17] E. Mendez W.F. Jager S. Viale, A.S. Best and S.J. Picken. A supramolecular nematic phase in sulphonated polyaramids. *Chem. Comm.*, 2004.
- [18] D.F. Sokolova A.A. Federov and L.B. Sokolov. Solubility of aromatic amides in amide-salt systems. *J. of general Chemisrty*, 40(11):2520–2521, november 1970. This is an abstract of work on deposit at and available from: VINITI, ul. Baltiiskaya, 14, Moscow, A-219, USSR.
- [19] C.N.R. Rao et al. Binding of alkali and alkaline eart cations and of protons to the peptide group. *FEBS letters*, 46(1):192–194, september 1974.
- [20] D. Balasubramanian and B.C. Misra. Effects of metal ions on the structure and spectra of the peptide group. *Biopolymers*, 14(5):1019–1026, 1975.
- [21] D. Balasubramanian and B.C. Misra. Relative affinities of alkali metal ions to the ligands in ionophores. *FEBS Letters*, 41(1):78–80, april 1974.
- [22] B.G. Cox. Salt effects on the rate of protonation of amides. *J.Chem.Soc., Perkin translation II*, 9:942–945, 1975.
- [23] D. Haas J.Bello and H.R.Bello. Interactions of protein-denaturing salts with model amides. *Biochemistry*, 5(8):2539–2548, august 1966.
- [24] S.K. Madan. Amides as ligands. complexes of n-methyl-gamma-butyrolactam with nontransition metals. *Inorganic Chemistry*, 6(2):421–424, februari 1967.
- [25] W.E. Waghorne and A.J.I. Ward. Effect of different cations on the n-co rotation barrier of dma. *J.C.S. Faraday I*, 76:1131–1137, 1980.
- [26] A. Goel D. Balasubramanian and C.N.R. Rao. Interaction of amides with lithium ion. *Chemical Physics Letters*, 17(4):482–485, december 1972.

-
- [27] A. Fukushi K. Shimozaki J. Kawakami, R. Miyamoto and S. Ito. Ab initio molecular orbital study of the complexing behavior of n-ethyl-1-naphthalenecarboxamide as fluorescent chemosensors for alkali and alkaline earth ions. *Journal of photochemistry and photobiology A:Chemisrty*, 146:163–168, 2002.
- [28] V.M. Savinov A.A. Federov and L.B. Sokolov. Synthesis of polyterephthalamides of high molecular weight by polycondensation in amide-salt systems. *Vysokomol. soyed.*, A12(10):2185–2198, 1970.
- [29] L.B. Sokolov V.M. Savinov and A.A. Federov. *Vysokomol. soyed.*, B10:111, 1968. Not translated in polymer Sci. USSR.
- [30] A.A. Grinberg. Introduction to the chemistry of complex compounds. *Izd.Khimiya*, 1966.
- [31] V.Z. Nikonov and L.B. Sokolov. *Vysokomol. soyed.*, 7:1529, 1966. Translated in polymer Sci. USSR 7: 9, 1693, 1965.
- [32] L.B. Sokolov. The polycondensation method of polymer synthesis. *Izd.Khimiya*, page 137, 1966.
- [33] A.J. Parker. *Uspekhi khimii*, (32):1270, 1963.
- [34] J. Bufalini and K.H. Stern. Interactions in ionic solutions. the effect of electrolytes on the infrared spectra of some hydrogen-bonded compounds. *J. Amer. Chem. Soc.*, (83):4362, 1961.
- [35] S.V. Izosimova I.S. Perelygin and Yu. M. Kessler. *Zh. stukt. khim.*, (9):390, 1968.
- [36] Zlatogorskii Grechishkin A.A. Federov, L.B. Sokolov and Proshutinskii. *Vysokomol. soyed.*, B12:205, 1970. Not translated in Polymer Sci. USSR.
- [37] R.C. Paul and B.R. Sreenathan. Dimethylformamide as a polar solvent: Part:iv-solubility, solvate formation and solvolytic reactions of substrates in dimethylformamide. *Indian J.Chemistry*, 4:382–386, April 1965.
- [38] R. Gopal and M.M. Husain. Studies on solutions of high dielectric constant. part iv. solvation of some ions in protic and aprotic solvents from conductance data. *Jour. Indian Chem. Soc.*, 40(12), 1963.

- [39] Lippincott Diorio and Mandelkern. Complex formation of monomeric amides with lithium perchlorate. *Nature*, 195:1296–1297, September 1962.
- [40] L.H. Gan et al. Physicochemical characterization of some fully aromatic polyamides. *Journal of applied polymer science*, 19:69–82, 1975.
- [41] V.B. Glazunov A.K. Dibrova and S.P. Papkov. Interaction in the system polymer-dipolar aprotic solvent-salt. *Fibre Chemistry*, 18(3):180–183, 1986. Translated from *Kimicheskije Volokna* No. 3 pp 21-23 may-june 1986.
- [42] M. Vert and J.Le Bris. H-nmr study of ion-dipole interactions of poly (-) 1,2-diaminopropane sebacamide and its model compound with CaCl_2 in methanol. *Polymer Letters edition*, 15:559–563, 1977.
- [43] I.K. Nekrasov. Determination of some molecular parameters of poly-m-phenyleneisophthalamide by the high-speed sedimentation and viscosity methods. *Vysokomol. soyed.*, A13(8):1707–1715, 1971.
- [44] M. Panar and L.F. Beste. Structure of poly(1,4,-benzamide) solutions. *Macromolecules*, 10(6):1401–1406, 1977.
- [45] J. Calabrese Y.H. Kim and C. McEwen. CaCl_3 - or Ca_2Cl_4 complexing cyclic aromatic amide. template effect on cyclization. *American chemical society*, 118:1545–1546, 1996.
- [46] M.M. Iovleva. Physicochemical aspects of examining the role and mechanism of action of lithium chloride in solutions of fibre-forming polymers. *Fibre chemistry*, 33(3):10–14, may-june 2001.
- [47] M. Panar and L.F. Beste. *Polym.Prepr.*, 17(1):65, 1976.
- [48] Yu.I. Mitchenko and Tsiperman. *Preprints, III International Symposium on Chemical Fibres*, 1:292, 1981. [in Russian].
- [49] L.M. Bronshtein et al. Yu.I. Mitchenko. Nmr study of the molecular state of lyotropic salts in solutions of polyamidohydrazides. *Polymer Science USSR*, 22(10):2605–2614, 1980.
- [50] Black Preston and Hofferbert. *J.Macromol. Sci.-Chem.*, 7(67), 1973.
- [51] Prozorova. PhD thesis, All-Union Scientific-Research Institute of Synthetic Fibres, 1983. Candidate Dissertation p.190.

-
- [52] Polatovskaya et al. Lobanova. *Synthetic Fibres*, page 280, 1969. [in Russian].
- [53] G.R. Luckhurst and G.W. Gray. *The Molecular Physics of Liquid Crystals*. Academic Press, 1997.
- [54] P.G. de Gennes and J. Prost. *The Physics of Liquid Crystals*. Oxford University Press, 2nd ed. edition, 1993. Section 2.2.1.1.
- [55] M.E. Rose. *Elementary Theory of Angular Momentum*. Academic Press, 1979.
- [56] S.J. Picken. Phase transitions and rheology of aramid solutions. *Liquid Crystals*, (5), 1989.
- [57] H. Rommel. *Aramide - Der Einfluss ihrer Struktur auf das Phasenverhalten in binaren und ternaren Mischungen mit Schwefelsaure und Wasser*. PhD thesis, Mathematisch-Naturwissenschaftlich-Technischen Fakultät der Martin-Luther-Universität Halle-Wittenberg, feb. 1995.
- [58] W. Maier and A. Saupe. A simple molecular theory of the nematic crystalline-liquid state. *Zeitschrift fur Naturforschung*, (13a), 1958.
- [59] W. Maier and A. Saupe. A simple molecular statistical theory of the nematic crystalline-liquid phase. i. *Zeitschrift fur Naturforschung*, (14a), 1959.
- [60] W. Maier and A. Saupe. A simple molecular statistical theory of the nematic crystalline-liquid phase. ii. *Zeitschrift fur Naturforschung*, (15a), 1960.
- [61] P. G. James R. L. Humphries and G. R. Luckhurst. Molecular field treatment of nematic liquid crystals. *Journal of the Chemical Society, Faraday Transactions 2: Molecular and Chemical Physics*, 68(6), 1972.
- [62] L. Onsager. The effects of shape on the interaction of colloidal particles. *Annals New York academy of sciences*, (51), Dec. 1949.
- [63] L.D. Landau and E.M. Lifshitz. *Statistical physics*. Pergamon, 1958. Section 71.
- [64] Chu et al. *Aggregation of sulfonated poly(p-phenylene terephthalamide) in dilute solutions.*, 1995.

- [65] O. Santin M. Heinrich E. Mendes, S. Viale and S.J. Picken. A small-angle neutron scattering investigation of rigid polyelectrolytes under shear. *Journal of Applied Crystallography*, 36(4), 2003.
- [66] C. Dell'Erba M. Novi P. Cavalleri, A. Ciferri and B. Purevsuren. Tailored rigid-flexible block copolymers. 3. fate of the flexible block within the mesophase. *Macromolecules*, 30(12), 1997.
- [67] P.W. Atkins. *Physical Chemistry*. Oxford University Press, 1988. page 579.
- [68] R. Mehra. Application of refractive index mixing rules in binary systems of hexadecane with n-alkanols at different temperatures. *Proc. Indian Acad. Sci. (Chem. Sci.)*, 115(2), 2003.
- [69] H. Ito K. Yabuki and T. Ora. Studies on the fine structure and the physical properties of poly(p-phenylene terephthalamide). part 2. consideration on the relation between fine structure and mechanical properties of poly(p-phenyleneterephthalamide) fibers. *Sen'i Gakkaishi*, 32(2), 1976.
- [70] Vollbracht. Process for the preparation of poly-p-phenyleneterephthalamide. *u.s.Patent*, (4,308,374), Dec. 1981.
- [71] A.E. Klausner T.A. Modro P. Wan R.A. Cox, L.M. Druet and K. Yates. Protonation acidity constants for some benzamide, acetamides and lactams. *Can.J.Chem.*, (59):1568, 1981.
- [72] A. El-Kafrawy. Investigation of the cellulose-licl-dimethylacetamide and cellulose-licl-n-methyl-2-pyrrolidinone solutions by ¹³c nmr spectroscopy. *Journal of Applied Polymer Science*, (27):2435–2443, 1982.
- [73] W. Berger B. Morgenstern, H.-W. Kammer and P. Skrabal. Lithium-7 nmr study on cellulose-lithium chloride-n,n-dimethylacetamide solutions. *Acta Polym.*, (43):356, 1992.
- [74] P.A. Callais C.L. McCormick and B.H. Hutchinson Jr. Solution studies of cellulose in lithium chloride and n,n-dimethylacetamide. *Macromolecules*, (18):2394, 1985.
- [75] H. Lee H.J. Lee, J. Won and Y.S. Kanga. Solution properties of poly(amic acid)nmp containing licl and their effects on membrane morphologies. *Journal of Membrane Science*, (196):267–277, 2002.
- [76] C. Lassigne and P. Baine. Solvation studies of lithium salts in dimethylformamide. *J.Phys.Chem.*, (75):3188, 1971.

- [77] D. Balasubramanian and R. Shaikh. Interaction of lithium salts with model amides. *Biopolymers*, (12):1639, 1973.
- [78] P. Balaram Ch.P. Rao and C.N.R. Rao. ^{13}C nuclear magnetic resonance studies of the binding of alkali and alkaline earth metal salts to amides. *Journal of the Chemical Society, Faraday Transactions I*, (76):1008, 1980.
- [79] Kazuhiko Kawamura Takashi Yasuhiro, Uosaki and Moriyoshi. Static relative permittivities of water + 1-methyl-2-pyrrolidinone and water + 1,3-dimethyl-2-imidazolidinone mixtures under pressures up to 300 mpa at 298.15 k. *J. Chem. Eng. Data*, (41):1525–1528, 1996.
- [80] S. Chandrasekhar. *Liquid Crystals*. Cambridge Monographs on Physics, 1977. page 25.
- [81] C.Strazielle M. Arpin and A.Skoulios. Study of nematic phase of a poly (paraphenylene terephthalamide). *Journal de Physique*, 38(3):307–313, 1977.
- [82] S.I. Banduryan et al. S.P. Papkov, M.M. Iovleva. Structure formation in system poly-p-benzamide - sulphuric-acid. *Vysokomolekulyarnye Soedineniya Seriya A*, 20(3):658–..., 1978.
- [83] M.G. Northolt. X-ray diffraction study of poly(p-phenylene terephthalamide) fibres. *European Polymer Journal*, 10:799–804, 1974.
- [84] M.Kobayashi K. Tashiro and H.Tadokoro. Elastic moduli and molecular structures of several crystalline polymers, including aromatic polyamides. *Macromolecules*, 10(2):413–420, March-April 1977.
- [85] L.Penn and F.Larsen. Physicochemical properties of kevlar 49 fiber. *Journal of Applied Polymer Science*, 23:59–73, 1979.
- [86] H.C. Zegers. Uitbreiding van het vloeistof-vloeistof interactie model ii. interchangetermen voor n,n-amide en n-amide groepen, october 1989. Internal report.
- [87] A. Tonelli and R. Kotek. Lewis acid-base complexation of polyamides and the effect of hydrogen bonding on structure development. *National Textile Center Annual Report*, nov. 2001. page 8.
- [88] D.W. Van Krevelen en K. te Nijenhuis. *Properties of Polymers. Their correlation with chemical structure; their numerical estimation and prediction from additive group contributions*. Elsevier, 4rd edition, 2009.

- [89] T. Kajiyama K. Haraguchi and M. Takayanagi. Uniplanar orientation of poly(p-phenylene terephthalamide) crystal in thin film and its effect on mechanical properties. *Journal of Applied Polymer Science*, 23:903–914, 1979.
- [90] F. Eckert and A. Klamt. Fast solvent screening via quantum chemistry: The cosmo-rs approach. *AIChE Journal*, 48:369–385, 2002.
- [91] A. Klamt and F. Eckert. *A novel way from Quantum Chemistry to Free Energy, Solubility and General QSAR-Descriptors for Partitioning*, book chapter in *Rational Approaches to Drug Design*, H.-D. Hltje and W. Sippl. Prous Science, S.A., Barcelona, pp 195 - 205 edition, 2001.
- [92] R.H. Perry and D.W. Green. *Perry's Chemical Engineers Handbook*. McGraw-Hill, 7 edition, 1997.
- [93] J. Marrero and R. Gani. Group-contribution based estimation of pure component properties. *Fluid Phase Equilibria*, 183-184:183–208, 2001.
- [94] P.J. Flory. *Principles of Polymer Chemistry*. Cornell University Press, 10 pp 568-571 edition, 1978.
- [95] B. Delly. *J. Chem. Phys.*, (113):7756, 2000.
- [96] J.C. Calabrese and K.H. Gardner. Structure of 4:1 sulfuric acid-n,n-(p-phenylene)dibenzamide complex. *ACTA Cryst.*, C41:389–392, 1985.
- [97] H.E. Darling. Conductivity of sulphuric acid solutions. *Journal of Chemical Engineering data*, 9(3):421–426, july 1964.
- [98] R.G.H. Record. Determination of the electrical conductivity of sulphuric acid from 90-100 pct. and 20-90c. *Instrument Engineer*, 4(7):131–134, april 1967.
- [99] D.G. Hall and R.H. Cole. Dielectric polarization of sulfuric acid solutions. *J. Chem. Eng. Data*, 85(8):1065–1069, 1981.
- [100] D.G. Baird and J.K. Smith. Dilute solution properties of poly(1,4-phenylene terephthalamide) in sulfuric acid. *Journal of Polymer Science*, 16:61–70, 1978.
- [101] G.S. Manning. Limiting laws and counterion condensation in polyelectrolyte solutions. iii. an analysis based on the mayer ionic solution theory. *Journal of Chemical Physics*, 51(8):3249–3252, 1969.

-
- [102] G.S. Manning. Limiting laws and counterion condensation in polyelectrolyte solutions. i. colligative properties. *Journal of Chemical Physics*, 51(3):924–933, 1969.
- [103] S.D. Samant J. Narayanan S. Mishra, B.K. Mishra and C. Manohar. Charge-induced nematic-isotropic transition in mixed surfactant solutions. *Langmuir*, 9(11):2804–2807, 1993.
- [104] S.J. Picken et al. Molecular conformation of a polyaramid in nematic solution from small angle neutron scattering and comparison with theory. *Journal of Chemical Physics*, 109(17):7612–7617, 1998.
- [105] T. Odijk. Theory of lyotropic polymer liquid crystals. *Macromolecules*, 19(9):2313–2329, 1986.
- [106] J. Harings. *Shielding and mediation of Hydrogen Bonding in Amide-based (Macro)Molecules*. PhD thesis, Technische Universiteit Eindhoven, april 2009.
- [107] A.S. Shaplov E.I. Iozinskaya and Ya.S. Vygodskii. Direct polycondensation in ionic liquids. *European Polymer Journal*, 40:2065–2075, 2004.
- [108] E.I. Iozinskaya Ya.S. Vygodskii and A.S. Shaplov. Ionic liquids as novel reaction media for the synthesis of condensation polymers. *Macromol. Rapid Commun.*, 23:676–680, 2002.
- [109] P. Kubisa. Ionic liquids in the synthesis and modification of polymers. *Journal of polymer science:PartA:Polymer chemistry*, 43:4675–4683, 2005.
- [110] H.C. Zegers. *Structure in liquid mixtures a thermodynamic approach*. PhD thesis, Vrije universiteit Amsterdam, 1988.

A. Thermodynamics of Liquid Mixtures

The thermodynamics of mixtures in the liquid state has been described by many types of models. Most models assume random mixing and in this way disregard preferential orientation, or structure in the mixture due to intermolecular force fields. In order to describe preferential orientation in liquid mixtures the contributing molecules are thought to consist of functional groups. The group interactions are determined by their chemical structure and orientation in the molecule. The interaction between two molecules is now the weighted sum of all possible pair interactions of the two molecules. The chance of interaction between groups can be taken proportional to the number of contact points, the cross sectional surface, the molecular surface or the group volume. The corresponding interactions are expressed in an interaction parameters. In his thesis, H.C. Zegers [110], has developed a theoretical method to describe the mixing behaviour in the liquids state, including interactions between the components in a mixture. He showed that volume fractions of n-alkanes (being neutral, homogeneous components consisting out of one group) correlate best with the enthalpy change upon mixing, expressed in the excess enthalpy of mixing. The change of interaction between components in the mixture is therefore taken proportional to the volume fractions of the participating components/groups. These interactions between components/groups are expressed in so called interchange terms. The interchange terms express the non-ideal behaviour upon mixing of different components and express the excess property per unit of volume at infinite dilution as will become clear later on. It is a value representing the change of a thermodynamic property when the surrounding of molecule/group 1 is changed from molecules/groups 1 to molecules/groups 2 and the surrounding of molecule/group 2 is changed from molecules/groups 2 to molecules/groups 1. By introducing correction factors for non-random mixing and preferential orientation in the mixture, also complex structured liquids can be described. The results are used in chapter 4

to determine the dissolution behaviour of PpPTA in amide-salt mixtures. In this appendix the derivation of excess properties is presented based on volume fraction statistics.

In a mixture composed of C components, indicated by n_1, n_2, \dots, n_C , the number of moles of each component. The relative amounts are given by the mole fractions x_k by,

$$x_k = \frac{n_k}{\sum_{k=1}^C n_k} = \frac{n_k}{n}. \quad (\text{A.1})$$

We define an extensive thermodynamic property Y of the mixture. This can, for instance, be the Gibbs-energy, enthalpy, entropy, heat capacity etc. . . . The change of Y when adding a small amount of component k to a mixture is expressed by the partial molar quantity of Y and is written:

$$\bar{Y}_k = \left(\frac{\partial Y}{\partial n_k} \right)_{n', p, T}. \quad (\text{A.2})$$

The bar above a quantity expresses that it is a molar quantity. The quantity Y is obtained by summation over all components.

$$Y = \sum_{k=1}^C n_k \bar{Y}_k, \quad (\text{A.3})$$

or for the molar quantity, summed over all mole fractions:

$$\bar{Y} = \sum_{k=1}^C x_k \bar{Y}_k. \quad (\text{A.4})$$

The excess molar quantity \bar{Y}_m^E of a mixture is defined as the difference between the real molar quantity \bar{Y}_m and the ideal molar quantity \bar{Y}_m^{id} .

$$\bar{Y}_m^E = \bar{Y}_m - \bar{Y}_m^{id}. \quad (\text{A.5})$$

A quantity that is more directly related to experimentally obtained data is the apparent molar quantity. For component k this is, $\bar{Y}_{k,\phi}$ and is defined as:

$$Y_m = \sum_{l=1}^C \delta_{kl} n_l \bar{Y}_l^* + n_k \bar{Y}_{k,\phi}, \quad (\text{A.6})$$

with $\delta_{kl} = 0$ if $k = l$ and $\delta_{kl} = 1$ if $k \neq l$. The superscript $*$ refers to the pure component. All non-ideal behaviour of the mixture is in this way contributed to component k . From equations A.5 and A.6 the relationship between the excess molar quantity of the mixture and the apparent excess partial molar quantity can be found.

$$\begin{aligned}\bar{Y}_m^E &= \sum_{l=1}^C \delta_{kl} x_l \bar{Y}_l^* + x_k \bar{Y}_{k,\phi} - \sum_{l=1}^C \delta_{kl} x_l \bar{Y}_l^* - x_k \bar{Y}_k^* \\ &= x_k [\bar{Y}_{k,\phi} - \bar{Y}_k^*] = x_k \bar{Y}_{k,\phi}^E,\end{aligned}\quad (\text{A.7})$$

and so:

$$\bar{Y}_{k,\phi}^E = \frac{\bar{Y}_m^E}{x_k} . \quad (\text{A.8})$$

By differentiation of equation A.6 with respect to n_k the partial molar quantity \bar{Y}_k is obtained:

$$\bar{Y}_k = \bar{Y}_{k,\phi} + n_k \left(\frac{\partial \bar{Y}_{k,\phi}}{\partial n_k} \right)_{n',p,T} . \quad (\text{A.9})$$

In order to express the partial molar quantity in terms of the mole fraction x_k the relationship $x_k = \frac{n_k}{n}$ is substituted into equation A.9. After rearrangement it follows that:

$$\bar{Y}_k = \bar{Y}_{k,\phi} + x_k (1 - x_k) \left(\frac{\partial \bar{Y}_{k,\phi}}{\partial x_k} \right)_{n',p,T} . \quad (\text{A.10})$$

Furthermore the volume of the mixture is defined by:

$$V_m = \sum_{k=1}^C n_k \bar{V}_k , \quad (\text{A.11})$$

in which \bar{V}_k represents the partial molar volume of component k . The volume fraction of component k is now defined as:

$$\phi_k = n_k \bar{V}_k / V_m . \quad (\text{A.12})$$

Every component is build up out of a number of groups, each contributing to the volume. The volume itself can be thought of to consist of an intrinsic part (not influenced by interactions with its surrounding) and a configurational part. The intrinsic partial molar volume \bar{V}_k° of a component k can now be written as the summation of the group volumes i of the contributing groups g_k .

$$\bar{V}_k^\circ = \sum_{i=1}^{g_k} V_{k,i}^\circ, \quad (\text{A.13})$$

here $\bar{V}_{k,i}^\circ$ is the contribution of group i of k to \bar{V}_k° . A group volume fraction of the i -th group can now be defined as:

$$\alpha_{k,i} = \bar{V}_{k,i}^\circ / \bar{V}_k^\circ. \quad (\text{A.14})$$

However, the actual partial molar volume of a mixture depends on its composition. This is expressed in the conformational partial molar volume \bar{V}_k^{con} . More general, the partial molar quantity \bar{Y}_k^{con} of a mixture depends on its composition. In pure liquid component k each molecule is surrounded by molecules of the same type. The partial molar quantity is in this case the partial molar quantity for pure k , \bar{Y}_k^* and can also be written as $\bar{Y}_k(k)$. In this way $\bar{Y}_k(l)$ indicates the partial molar quantity of k surrounded by molecules l . So \bar{Y}_k^{con} can be written as:

$$\bar{Y}_k^{con} = \sum_{l=1}^C \phi_l \Phi_l(k) \bar{Y}_k(l), \quad (\text{A.15})$$

$\Phi_l(k)$ is a correction factor in combination with ϕ_l . It represents a local volume fraction of component l in the vicinity of component k . In case of random mixing $\Phi_l(k) = 1$. As molecules of component l are composed of g_l distinct groups j , $\bar{Y}_k(l)$ can be written as:

$$\bar{Y}_k(l) = \sum_{j=1}^{g_l} \alpha_{l,j} A_{l,j}(k) \bar{Y}_k(l, j). \quad (\text{A.16})$$

In this expression $A_{l,j}$ is a correction factor to the fraction $\alpha_{l,j}$. In case of random orientation of molecules l in the vicinity of component k , $A_{l,j} = 1$. The product $\alpha_{l,j} A_{l,j}$ represents the local fraction of \bar{V}_l° that is occupied by the j -th group in the vicinity of component k . $\bar{Y}_k(l, j)$ is the value of \bar{Y}_k of

component k dissolved in a hypothetical solvent of groups j of component l . Combination of equations A.15 and A.16 results in:

$$\bar{Y}_k^{con} = \sum_{l=1}^C \phi_l \Phi_l(k) \sum_{j=1}^{g_l} \alpha_{l,j} A_{l,j}(k) \bar{Y}_k(l, j) . \quad (\text{A.17})$$

This can also be written as:

$$\bar{Y}_k^{con} = \bar{V}_k \sum_{l=1}^C \phi_l \Phi_l(k) \sum_{j=1}^{g_l} \alpha_{l,j} A_{l,j}(k) \frac{\bar{Y}_k(l, j)}{\bar{V}_k} . \quad (\text{A.18})$$

Since molecules of type k constitute out of g_k groups, i , $\bar{Y}_k(l, j)$ is given by:

$$\bar{Y}_k(l, j) = \sum_{i=1}^{g_k} \bar{Y}_{k,i}(l, j) = \bar{V}_k \sum_{i=1}^{g_k} \alpha_{k,i} \frac{\bar{Y}_{k,i}(l, j)}{\alpha_{k,i} \bar{V}_k} \quad (\text{A.19})$$

$\bar{Y}_{k,i}(l, j)$ expresses the contribution of group i of component k to $\bar{Y}_k(l, j)$. Substitution of A.19 in A.18 leads to:

$$\bar{Y}_k^{con} = \bar{V}_k \sum_{l=1}^C \phi_l \Phi_l(k) \sum_{j=1}^{g_l} \alpha_{l,j} A_{l,j}(k) \cdot \sum_{i=1}^{g_k} \alpha_{k,i} \frac{\bar{Y}_{k,i}(l, j)}{\alpha_{k,i} \bar{V}_k} \quad (\text{A.20})$$

Also the volume fractions of groups j in molecule l surrounded by molecules k can be written as:

$$\alpha_{l,j} A_{l,j}(k) = \sum_{i=1}^{g_k} \alpha_{l,j} A_{l,j}(k, i) , \quad (\text{A.21})$$

in which $\alpha_{l,j} A_{l,j}(k, i)$ is $\alpha_{l,j}(k)$ in the vicinity of groups i of molecules k . Therefore,

$$\bar{Y}_k^{con} = \bar{V}_k \sum_{l=1}^C \phi_l \Phi_l(k) \sum_{j=1}^{g_l} \sum_{i=1}^{g_k} \alpha_{l,j} A_{l,j}(k, i) \cdot \alpha_{k,i} \frac{\bar{Y}_{k,i}(l, j)}{\alpha_{k,i} \bar{V}_k} \quad (\text{A.22})$$

By using the relations:

$$x_k \bar{V}_k = \phi_k V_m / n = \phi_k \bar{V}_m \quad (\text{A.23})$$

and

$$\bar{Y}_m^{con} = \sum_{k=1}^C x_k \bar{Y}_k^{con} = \sum_{l=1}^C x_l \bar{Y}_l^{con} \quad (\text{A.24})$$

in which $\bar{V}_m = V/n$ is the molar volume of the mixture, and \bar{Y}_m^{con} is the configurational molar quantity of the mixture, after some rearrangements the following expression for \bar{Y}_m^{con} can be obtained:

$$\bar{Y}_m^{con} = \bar{V}_m \sum_{k=1}^C \sum_{l=1}^C \phi_l \Phi_l(k) \phi_k \sum_{j=1}^{g_l} \sum_{i=1}^{g_k} \alpha_{l,j} A_{l,j}(k, i) \alpha_{k,i} \frac{\bar{Y}_{k,i}(l, j)}{\alpha_{k,i} \bar{V}_k} . \quad (\text{A.25})$$

In expression A.25 use was made of $\bar{Y}_m^{con} = \sum_{k=1}^C x_k \bar{Y}_k^{con}$. A similar expression can be obtained by using $\bar{Y}_m^{con} = \sum_{l=1}^C x_l \bar{Y}_l^{con}$. By taking half of each \bar{Y}_m^{con} can be written in the form:

$$\begin{aligned} \bar{Y}_m^{con} = & \bar{V}_m \left[\frac{1}{2} \sum_{k=1}^C \sum_{l=1}^C \phi_l \Phi_l(k) \phi_k \right. \\ & \sum_{j=1}^{g_l} \sum_{i=1}^{g_k} \alpha_{l,j} A_{l,j}(k, i) \alpha_{k,i} \frac{\bar{Y}_{k,i}(l, j)}{\alpha_{k,i} \bar{V}_k} \\ & + \frac{1}{2} \sum_{l=1}^C \sum_{k=1}^C \phi_k \Phi_k(l) \phi_l \\ & \left. \sum_{i=1}^{g_k} \sum_{j=1}^{g_l} \alpha_{k,i} A_{k,i}(l, j) \alpha_{l,j} \frac{\bar{Y}_{l,j}(k, i)}{\alpha_{l,j} \bar{V}_l} \right] . \quad (\text{A.26}) \end{aligned}$$

This can be rearranged to:

$$\begin{aligned} \bar{Y}_m^{con} = & \frac{1}{2} \bar{V}_m \sum_{k=1}^C \sum_{l=1}^C \phi_l \Phi_l(k) \phi_k \sum_{j=1}^{g_l} \sum_{i=1}^{g_k} \alpha_{l,j} A_{l,j}(k, i) \alpha_{k,i} \\ & \left[\frac{\bar{Y}_{k,i}(l, j) - \bar{Y}_{k,i}(k, i)}{\alpha_{k,i} \bar{V}_k} + \frac{\bar{Y}_{k,i}(k, i)}{\alpha_{k,i} \bar{V}_k} \right] \\ & + \frac{1}{2} \bar{V}_m \sum_{l=1}^C \sum_{k=1}^C \phi_k \Phi_k(l) \phi_l \sum_{i=1}^{g_k} \sum_{j=1}^{g_l} \alpha_{k,i} A_{k,i}(l, j) \alpha_{l,j} \\ & \left[\frac{\bar{Y}_{l,j}(k, i) - \bar{Y}_{l,j}(l, j)}{\alpha_{l,j} \bar{V}_l} + \frac{\bar{Y}_{l,j}(l, j)}{\alpha_{l,j} \bar{V}_l} \right] . \quad (\text{A.27}) \end{aligned}$$

With the notion that $\sum_{l=1}^C \phi_l \Phi_l(k) = 1$ and $\sum_{j=1}^{g_l} \alpha_{l,j} A_{l,j}(k, i) = 1$ this can be rewritten in the form:

$$\begin{aligned} \bar{Y}_m^{con} = & \frac{1}{2} \bar{V}_m \sum_{k=1}^C \sum_{l=1}^C \phi_l \Phi_l(k) \phi_k \sum_{j=1}^{g_l} \sum_{i=1}^{g_k} \alpha_{l,j} A_{l,j}(k, i) \alpha_{k,i} \\ & \left[\frac{\bar{Y}_{k,i}(l, j) - \bar{Y}_{k,i}(k, i)}{\alpha_{k,i} \bar{V}_k} \right] \\ & + \frac{1}{2} \bar{V}_m \sum_{l=1}^C \sum_{k=1}^C \phi_k \Phi_k(l) \phi_l \sum_{i=1}^{g_k} \sum_{j=1}^{g_l} \alpha_{k,i} A_{k,i}(l, j) \alpha_{l,j} \\ & \left[\frac{\bar{Y}_{l,j}(k, i) - \bar{Y}_{l,j}(l, j)}{\alpha_{l,j} \bar{V}_l} \right] \\ & + \frac{1}{2} \bar{V}_m \left[\sum_{k=1}^C \phi_k \sum_{i=1}^{g_k} \alpha_{k,i} \frac{\bar{Y}_{k,i}(k, i)}{\alpha_{k,i} \bar{V}_k} + \sum_{l=1}^C \phi_l \sum_{j=1}^{g_l} \alpha_{l,j} \frac{\bar{Y}_{l,j}(l, j)}{\alpha_{l,j} \bar{V}_l} \right] \quad (\text{A.28}) \end{aligned}$$

We now introduce an interchange term defined as:

$$\sigma_y(k, i; l, j) = \frac{1}{2} \left[\frac{\bar{Y}_{k,i}(l, j) - \bar{Y}_{k,i}(k, i)}{\alpha_{k,i} \bar{V}_k} + \frac{\bar{Y}_{l,j}(k, i) - \bar{Y}_{l,j}(l, j)}{\alpha_{l,j} \bar{V}_l} \right] . \quad (\text{A.29})$$

It holds the property that the interchange term in pure components is set to zero. Only interactions between different components are taken into account. By assuming that $\Phi_k = \Phi_l = \Phi_{k,l}$ and $A_{l,j}(k, i) = A_{k,i}(l, j) = A(k, i; l, j)$ and noting that the last two summations in equation A.28 are the same as they both sum over the pure components it can be written as:

$$\begin{aligned} \bar{Y}_m^{con} = & \bar{V}_m \sum_{k=1}^C \sum_{l=1}^C \phi_k \phi_l \Phi_{k,l} \sum_{i=1}^{g_k} \sum_{j=1}^{g_l} \alpha_{k,i} \alpha_{l,j} A(k, i; l, j) \sigma_y(k, i; l, j) \\ & + \bar{V}_m \sum_{k=1}^C \phi_k \sum_{i=1}^{g_k} \alpha_{k,i} \cdot \frac{\bar{Y}_{k,i}(k, i)}{\alpha_{k,i} \bar{V}_k} \quad (\text{A.30}) \end{aligned}$$

Through the definition of the interchange term equation A.30 holds the property that k and l can be interchanged. In this way a mixture can be described by one parameter, holding all interactions between each combination of groups, in every relative amount. For a pure component the expression for the molar quantity becomes:

$$\begin{aligned}
\bar{Y}_m^{con} &= \bar{V}_k^* \sum_{i=1}^{g_k} \sum_{j=1}^{g_k} \alpha_{k,i} \alpha_{k,j} A^*(k, i; k, j) \sigma_y^*(k, i; k, j) \\
&\quad + \bar{V}_k^* \sum_{i=1}^{g_k} \alpha_{k,i} \frac{\bar{Y}_{k,i}(k, i)}{\alpha_{k,i} \bar{V}_k^*}.
\end{aligned} \tag{A.31}$$

and for an ideal mixture:

$$\begin{aligned}
\bar{Y}_m^{id,con} &= \sum_{k=1}^C x_k Y_k^{*,con} \\
&= \sum_{k=1}^C x_k \bar{V}_k^* \sum_{i=1}^{g_k} \sum_{j=1}^{g_k} \alpha_{k,i} \alpha_{k,j} A^*(k, i; k, j) \sigma_y^*(k, i; k, j) \\
&\quad + \sum_{k=1}^C x_k \bar{V}_k^* \sum_{i=1}^{g_k} \alpha_{k,i} \frac{\bar{Y}_{k,i}(k, i)}{\alpha_{k,i} \bar{V}_k^*}.
\end{aligned} \tag{A.32}$$

The molar excess quantity \bar{Y}_m^E for the mixture is defined as the difference between the actual and the ideal configurational molar quantity. It expresses the pure configurational contribution part in a mixture:

$$\bar{Y}_m^E = \bar{Y}_m^{con} - \bar{Y}_m^{con,id}. \tag{A.33}$$

From this definition and taking $\bar{Y}_{k,i}(k, i)/\alpha_{k,i} \bar{V}_k = \bar{Y}_{k,i}(k, i)/\alpha_{k,i} \bar{V}_k^*$ and $\sigma_y(k, i; l, j) = \sigma_y^*(k, i; k, j)$ based on the assumption that internal degrees of freedom in molecules are independent of composition and separable from other degrees of freedom. The excess molar quantity then becomes:

$$\begin{aligned}
\bar{Y}_m^E &= \bar{V}_m \sum_{k=1}^C \sum_{l=1}^C \phi_k \phi_l \Phi_{k,l} \sum_{i=1}^{g_k} \sum_{j=1}^{g_l} \alpha_{k,i} \alpha_{l,j} A(k, i; l, j) \sigma_y(k, i; l, j) \\
&\quad - \bar{V}_m^{id} \sum_{k=1}^C \sum_{l=1}^C \phi_k^{id} \phi_l^{id} \sum_{i=1}^{g_k} \sum_{j=1}^{g_l} \alpha_{k,i} \alpha_{l,j} A^*(k, i; k, j) \sigma_y(k, i; k, j) \tag{A.34}
\end{aligned}$$

A.1 Binary mixtures

For a binary system expression A.34 becomes:

$$\begin{aligned}
\bar{Y}_m^E = & \bar{V}_m \sum_{k=1}^2 \sum_{l=1}^2 \phi_k \phi_l \Phi_{k,l} \sum_{i=1}^{g_k} \sum_{j=1}^{g_l} \alpha_{k,i} \alpha_{l,j} A(k, i; l, j) \sigma_y(k, i; l, j) \\
& - \bar{V}_m^{id} \sum_{k=1}^2 \sum_{l=1}^2 \phi_k^{id} \phi_l^{id} \sum_{i=1}^{g_k} \sum_{j=1}^{g_l} \alpha_{k,i} \alpha_{l,j} A^*(k, i; k, j) \sigma_y(k, i; k, j) \quad (\text{A.35})
\end{aligned}$$

From equation A.8 the apparent excess molar quantity of component 1, $\bar{Y}_{1,\phi}^E$, is defined as:

$$\bar{Y}_{1,\phi}^E = \bar{Y}_m^E / x_1 . \quad (\text{A.36})$$

At infinite dilution of component 1 in 2, $\phi_1 \approx 0$, $\phi_2 = 1$, values of $\bar{Y}_{1,\phi}^E$ can be obtained by extrapolation and equal the excess partial molar quantity at infinite dilution, $\bar{Y}_1^{E,\infty}$. By further assumption of random mixing $\Phi_{k,l} = 1$, which is true at infinite dilution and no preferential orientation between the components, $A(1, i; 2, j) = A^*(1, i; 1, j) = A^*(2, i; 2, j) = 1$, true when interactions are relatively weak (non-ionic), equation A.35 reduces to:

$$\begin{aligned}
\bar{Y}_1^{E,\infty} = & 2\bar{V}_1^\infty \sum_{i=1}^{g_1} \sum_{j=1}^{g_2} \alpha_{1,i} \alpha_{2,j} \sigma_y(1, i; 2, j) \\
& - \bar{V}_1^* \left[\sum_{i=1}^{g_1} \sum_{j=1}^{g_1} \alpha_{1,i} \alpha_{1,j} \sigma_y(1, i; 1, j) \right. \\
& \left. + \sum_{i=1}^{g_2} \sum_{j=2}^{g_2} \alpha_{2,i} \alpha_{2,j} \sigma_y(2, i; 2, j) \right] . \quad (\text{A.37})
\end{aligned}$$

As changes in volume upon mixing are generally small the excess molar volumes are assumed to be zero. Volumes and group volume fractions can now be approximated by the values of their respective pure components. $\bar{V}_k = \bar{V}_k^*$ and $\alpha_{k,i} = \alpha_{k,i}^*$.

$$\begin{aligned}
\bar{Y}_1^{E,\infty} = & 2\bar{V}_1^* \sum_{i=1}^{g_1} \sum_{j=1}^{g_2} \alpha_{1,i}^* \alpha_{2,j}^* \sigma_y(1, i; 2, j) \\
& - \bar{V}_1^* \left[\sum_{i=1}^{g_1} \sum_{j=1}^{g_1} \alpha_{1,i}^* \alpha_{1,j}^* \sigma_y(1, i; 1, j) \right. \\
& \left. + \sum_{i=1}^{g_2} \sum_{j=2}^{g_2} \alpha_{2,i}^* \alpha_{2,j}^* \sigma_y(2, i; 2, j) \right] . \quad (\text{A.38})
\end{aligned}$$

By neglecting group contributions in molecules and realizing that interactions of components in the pure state are zero by definition, $\alpha_{1,i}^* = \alpha_{2,j}^* = \alpha_{1,i}^* = \alpha_{1,j}^* = \alpha_{2,i}^* = \alpha_{2,j}^* = 1$, $\sigma_y(1; 1) = \sigma_y(2; 2) = 0$ equation A.38 further reduces to:

$$\bar{Y}_1^{E,\infty} = 2\bar{V}_1^* \sigma_{y(1;2)} . \quad (\text{A.39})$$

A similar expression can be obtained for component 2. In this way the interchange parameter $\sigma_{y(1;2)}$ represents the excess molar quantity per unit of volume at infinite dilution.

With the same assumptions as before but not requiring the infinite dissolution of 1 in 2 equation A.35 becomes:

$$\bar{Y}_m^E = 2\bar{V}_m \phi_1 \phi_2 \sigma_{y(1;2)} . \quad (\text{A.40})$$

With equations A.12 for $k = 1$ and A.36 an expression for the apparent excess molar quantity for component 1 becomes:

$$\bar{Y}_{1,\phi}^E = 2\bar{V}_1^* \sigma_{y(1;2)} \phi_2 . \quad (\text{A.41})$$

An expression for the partial excess molar quantity is found after substitution of A.41 in equation A.9 and noticing that $\phi_1 = \frac{x_1 V_1^*}{x_1 V_1^* + x_2 V_2^*} = \frac{x_1 V_1^*}{V_m}$ and $\phi_2 = \frac{x_2 V_2^*}{V_m}$

$$\bar{Y}_1^E = 2\bar{V}_1^* \sigma_{y(1;2)} \phi_2^2 . \quad (\text{A.42})$$